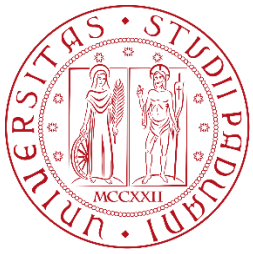

UNIVERSITA' DEGLI STUDI DI PADOVA

DIPARTIMENTO DI SCIENZE CHIMICHE

CORSO DI LAUREA MAGISTRALE IN CHIMICA

TESI DI LAUREA MAGISTRALE

Synthesis of difluoroalkyl-sulfoximines via a light-promoted atom transfer radical addition (ATRA) process

Relatore: Prof. Luca Dell'Amico
Controrelatore: Prof.ssa Donatella Carbonera

LAUREANDO: Baldon Simone

ANNO ACCADEMICO 2022/2023

Table of Contents

1. Preface

Sulfoximines are mono-aza derivatives of sulfones for which there has been an increased interest in the last 20 years, as this moiety is found in numerous biologically active molecules, such as agrochemicals and drugs. For this reason, the synthesis of new molecules bearing this functionality has found growing research in the fields of crop science and in the pharmaceutical industries.

Another growing interest in agrochemical and pharmaceutical research is the development of new compounds that can act as bioisosteres. This strategy deals with the synthesis of molecules structurally similar to the drug of interest, in which some chemical motifs are replaced with other functionality. This substitution allows to tune the physicochemical and biological properties of a drug without changing the specific drug-receptor interactions of molecular recognition. In this context, molecular units containing fluorine are of special interest to use them as bioisosteric replacements. In particular, it has been observed that the difluoromethylene group (-CF_2-) is a bioisostere of carbonyl groups (C=O) or oxygen atoms, with significant improvements in efficacy, selectivity and pharmacokinetics of the drug analogue.

The reasons listed above have triggered increased research into the synthesis and study of fluorinated sulfoximine. Such research has shown over the years how the incorporation of fluorine atoms into sulfoximines allows for a new functionality with electronic properties and reactivity that are completely different from those of classical sulfoximines, sulfones, and fluorinated sulfones. Thanks to these characteristics, this new functional group is widely used in different and varied fields ranging from material science to drug design.

Fluorinated sulfoximines are also used as versatile reagents for the synthesis of fluorinated molecules. For example, they are effectively used in olefination reactions for the synthesis of fluorinated olefins or as fluoromethyl reagents for nucleophiles or unsaturated compounds.

Regarding the functionalization reactions of fluorinated sulfoximines, the protocols present in the literature are mainly focused only on the N-functionalization of nitrogen NH.

However, no protocol focused on a possible functionalization of the fluorinated chain of these sulfoximines, despite the great potential. In fact, the possibility of attaching new functional groups in fluorinated Cα would open the way for easier incorporation of fluorinated sulfoximines into various molecular structures, even complex ones.

In parallel with this, photochemistry and photocatalysis have found increasing popularity in the field of synthetic organic chemistry in the last decade. This is because through the photoexcitation of appropriate reacting molecules it is possible to open the way to a type of radicalic reactivity totally different from the more classic polar reactivity that characterizes the molecules in ground state. These new photochemical or photocatalyzed strategies allow to obtain products, even complex, in a simple way and requiring mild reaction condition, not obtainable in the normal conditions of polar reaction. For this reason, this branch is proving to be a pioneer for a more green and sustainable synthetic chemistry.

With all these considerations, the following thesis project focused on the development of a synthetic method for the introduction of difluoroalkyl sulfoximine moieties in simple and economical molecules such as unactivated olefins. The proposed synthetic strategy is based

on an organophotocatalyzed ATRA (atom transfer radical addition) process using as model substrates the bromodifluoromethyl phenyl sulfoximine (**1**) and 1-hexene (**3**). (Figure 1).

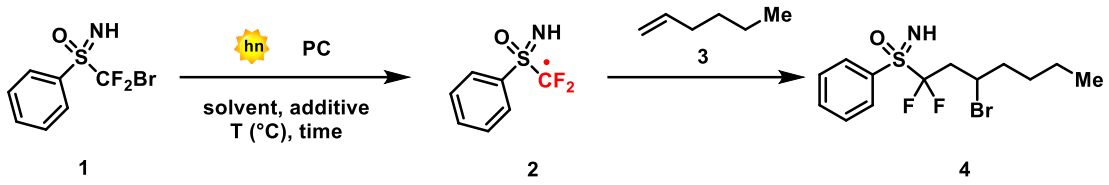

Figure 1. General reaction scheme for the photocatalyzed Cα-alkylation of fluorinated sulfoximines.

The originality of the project consists in the development of the first synthetic photocatalytic protocol that allows the generation of a difluorosulfoximine radical **2**, which has never been generated under other chemical or photochemical means. This intermediate can then be trap using simple molecules such as olefines, with which it is possible to obtain the alkylation of carbon Cα of fluorinated sulfoximine. No one had previously focused on the photochemical functionalization of Cα, since the main functionalization processes of sulfoximine affect N-functionalization. Moreover, the reaction is based on the use of organophotocatalysis which, with the use of totally organic-based photocatalysts, is able to trigger the formation of product **4** under mild reaction conditions and avoiding the use of transition-metals catalysts.

2. Introduction

2.1 Photochemistry and photocatalysis

Photochemistry is *"the branch of chemistry that exploits the properties of light applied to molecules to carry out chemical transformations driven by light irradiation*".[1] The birth of organic photochemistry aimed at synthesis dates to the beginning of the last century, specifically with the work of Ciamician and Silber in 1908 and 1913, which was focused on the study of photoinduced cycloadditions and condensation reactions.[2,3]

After this important discovery, the branch of photochemistry remained a niche field for most of the 20th century, with no application of great practical relevance. This lack of interest can be attributed to several factors, including the fact that many of the organic molecules do not absorb visible light. Therefore, it was necessary for their direct photoexcitation to use highly energetic UV lamps (wavelengths of $\lambda < 350$ nm), which were difficult to obtain at the time. This was compounded by poor technological development, both in terms of spectroscopic techniques for studying photochemical processes and in terms of light sources, with expensive and not particularly efficient lamps, thus hampering the progress in this field. .[4,5]

In the early 21st century, with the advancement of technology (such as the development of lasers and LEDs) and a better understanding of the nature of light and light-matter interaction, there was an intense renaissance of this field that has extended to the present day. This growing interest in photochemical phenomena today is also driven by the need for organic synthesis to move toward greener synthetic protocols. This is with the aim of limiting the impact the chemical sector causes to the environment and curbing its influence on the global warming that is rapidly changing the planet's climate. Indeed, the use of light opens up the possibility of obtaining compounds under mild and safe reaction conditions, generally without the use of heating or high reaction temperatures and with protocols that are operationally simple to implement. Moreover, the ultimate goal of this research is the possibility of directly employing sunlight as an abundant and inexpensive renewable energy resource.

Photochemistry has also found interest because of the peculiar reactivities that can be achieved. Indeed, light irradiation can open reactivity pathways completely different from those pertinent to the classical thermal domain. Under light-irradiation, it is possible to reach high-energy reactive intermediates that make possible the access to new complex structures, that are otherwise not accessible through classical thermal activation.[6,7,8]

The field of organic photochemistry has expanded greatly over the years, to such an extent, that a distinction across different light-promoted reactions is necessary for its comprehensive description (Figure 2).

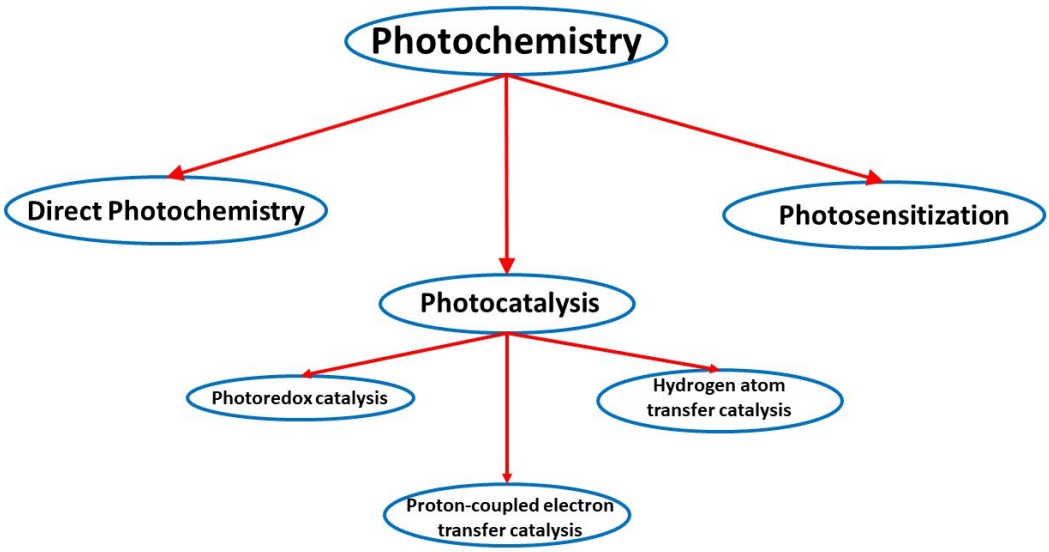

Figure 2. Schematization of the main branches of photochemistry.

Three different classes of photochemical reactions can be defined (Figure 3):[9]

- **Direct photochemistry**: the light is directly absorbed by one or more reaction substrates.
- **Photosensitization:** a physical energy transfer between the sensitizer and one or more non-absorbing reagents is involved.
- **Photocatalysis:** the light is absorbed by an appropriate photocatalyst, which activates the substrate toward, predominantly, radical reactivity.

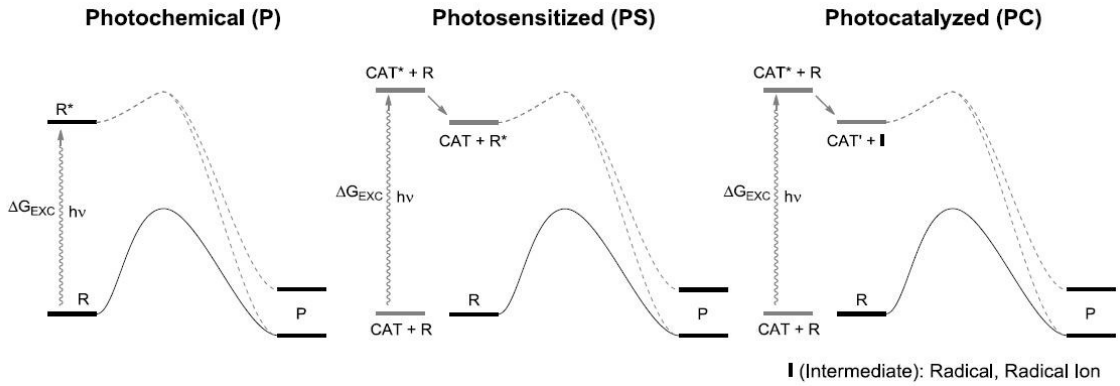

Figure 3. Different light-induced processes. a.): Direct photochemical reaction. b.): Photosensitized reaction. c.): Photocatalyzed reaction.[9]

2.1.1 Direct photochemistry

In direct photochemistry, the light is absorbed directly by one or more reactant molecules without the need to employ an external photocatalyst. The process is particularly sustainable because it is possible to directly convert reactants to products using light as the only energy source in the process (Figure 4).

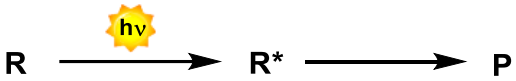

Figure 4. General scheme of direct photochemical reaction. R: reactant; R: reactant in an excited state; P: product.*

To promote the photoexcitation of the substrate, it is necessary to employ light sources with an appropriate wavelength (λ), which corresponds to the value in energy of the substrate's HOMO-LUMO orbital gap (HOMO: highest occupied molecular orbital, LUMO: lowest unoccupied molecular orbital). This value in organic molecules is variable, ranging from wavelengths in the visible region (390-700 nm) for variously conjugated molecules to wavelengths in the UV-region (10-380 nm) for simpler unconjugated molecules.

With the absorption of a photon by the substrate, there is the promotion of an electron from the frontier orbital HOMO to the frontier orbital LUMO with the generation of the photoexcited species. The latter possesses a different electronic distribution and different orbital symmetry in comparison with the same molecule in the fundamental state, and this different distribution causes a substantial change in the chemical properties and reactivity of the compound. The reactant molecule, once excited, is thus on a surface of totally different potential energy from that of the molecule in the fundamental state, and this opens the way for new reaction pathways entirely different from the more classical thermal pathway (Figure 5).[10,11,12]

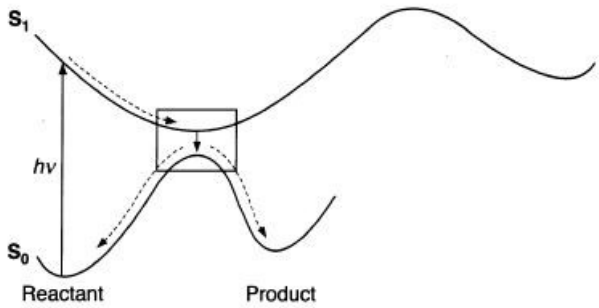

Figure 5. Schematic surface diagram for a photochemical reaction.[10]

Many reactions that are thermally prohibited turn out to be possible under photochemical conditions. The most striking examples of this behavior are found in the case of pericyclic reactions, a reaction in which there is a process of rearranging the electrons of the reactant(s) through a cyclic pattern.[13]

The most famous category of pericyclic reactions are cycloaddition reactions, in which two reactant molecules containing π bonds react with each other to give a cyclic compound as a product, generated by the reorganization of π electrons with formation of two new σ bonds.[14]

According to the theory of symmetry conservation of orbitals, pericyclic reactions require a phase overlap of the reactants' frontier orbitals to take place.

In the specific case of cycloadditions, for the reaction to take place thermally, the total number of π electrons of the reactants diene and dienophile must correspond to the value [4n+2], with n being a positive integer (Woodward-Hoffman rule). In fact, only by complying with this rule the HOMO and LUMO frontier orbitals of the reactants have symmetry suitable for their effective overlap.

An example of how light can be an advantageous tool for triggering new reactions is the case of [2+2] cycloadditions between two olefins (Figure 6).

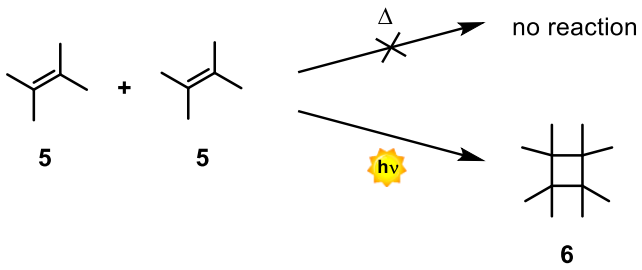

Figure 6. General scheme of a [2+2] cycloaddition.

In this case, the reaction is thermally prohibited because the HOMO and LUMO orbitals of the two reactants do not have the proper symmetry for their phase overlap (Figure 7). Photochemistry helps us with this problem, because through irradiation it is possible to excite an electron of one of the two reactants from the HOMO orbital to the LUMO orbital, changing the symmetry of the new HOMO orbital involved in the process. Thanks to this, now the two frontier orbitals have the right symmetry to overlap in phase, and the reaction can proceed to the cyclobutane product.[14,15]

This explains why cycloaddition [2+2] reactions, normally prohibited by thermal means, are instead allowed by photochemical means.

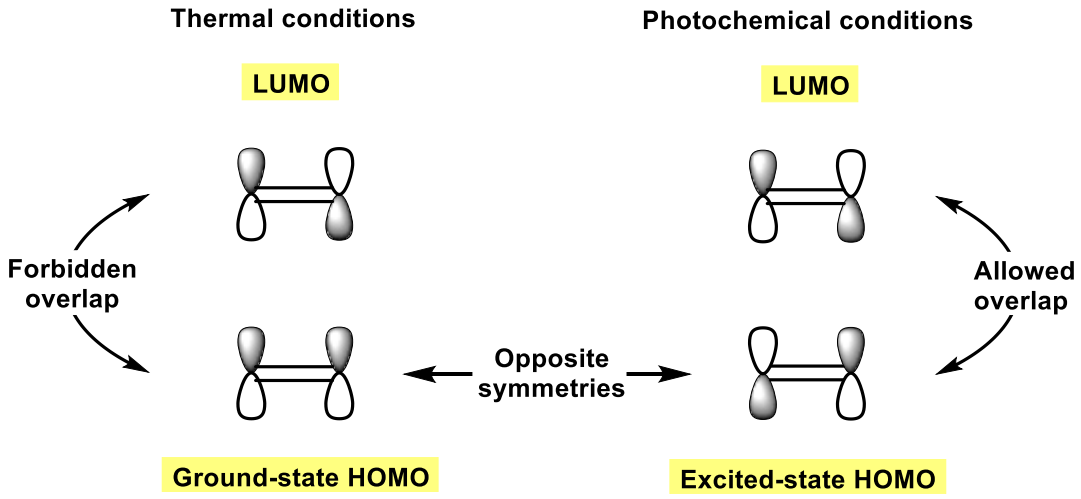

Figure 7. Frontier orbitals involved in cycloaddition [2+2].[15]

2.1.2 Photosensitization

Photosensitization is "*the process by which a photochemical or photophysical alteration occurs in one molecular entity as a result of the initial absorption of radiation by another molecular entity, called a* ***photosensitizer***" (Figure 8).[16]

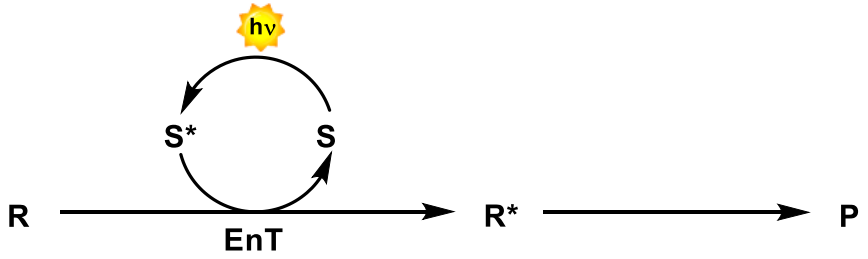

Figure 8. General scheme of a photosensitized reaction. S: photosensitizer; S: photosensitizer in the excited state.*

The main problem with direct photochemistry is that relatively few organic molecules absorb light in the visible wavelength range (λ). In fact, many of the molecules are colorless, with an absorption spectrum shifted to the ultraviolet region, making highly energetic UV light sources necessary for their photoexcitation. The use of UV can be problematic, as there are many chemical species that absorb in this wavelength range, including intermediate species. This fact makes difficult to control the reactivity of the system, promoting undesirable reaction pathways that lead to the formation of numerous byproducts.

Photosensitization represents a solution to the problem, as it allows the generation of species in the excited electronic state of reactant molecules that cannot be photoexcited directly, promoting the photochemical reaction under mild irradiation conditions.[17]
For the generation of the excited species the phenomenon of energy transfer (EnT) occurs, which is defined as "*the photophysical process in which an excited state of one molecular entity is deactivated to a lower-lying state by transferring energy to a second molecular entity, which is thereby raised to a higher energy state*".[18]

In fact, molecules called sensitizers are used for the process. The latter are capable of efficiently absorbing light in the visible range and following that transfer their excited state via EnT to the target molecule. In this way, highly energetic UV-light sources can be avoided, limiting substrate photodegradation and other side-reactions.

In practice, the photosensitizer (**S**) is excited by a photon of appropriate wavelength (λ) from the fundamental electronic state $\mathbf{S_0}$ to the excited singlet state $\mathbf{S_1}$ (Figure 9). After this, several possible relaxation paths to lower-energy energy states follow, most notably the intersystem crossing (ISC) phenomenon, which converts the singlet $\mathbf{S_1}$ state to the triplet $\mathbf{T_1}$ state. Once this $\mathbf{T_1}$ state is reached, the radiative relaxation to the fundamental state is strongly slowed as it turns out to be a spin-forbidden process. This, combined with slow non-radiative relaxation processes, means that the photosensitizer can live long enough in the $\mathbf{T_1}$ state to the point where it can transfer its excited state to the reactant molecule through an EnT process. This generates the reactant species in the excited state, which can now take part in the various reaction pathways defined in the excited-state potential energy surface. All this is achieved by employing light sources to which the reactant of interest does not absorb.[19]

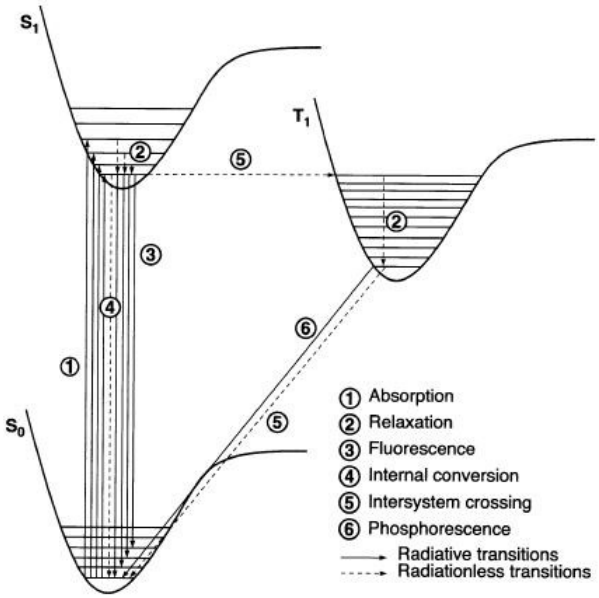

Figure 9. Jablonski diagram.[10]

2.1.3 Photocatalysis

Photocatalysis is defined as "*the change in the rate of a chemical reaction or its initiation under the action of ultraviolet, visible or infrared radiation in the presence of a substance, the photocatalyst, that absorbs light and it is involved in the chemical transformation of the reaction partners*" (Figure 10).[20]

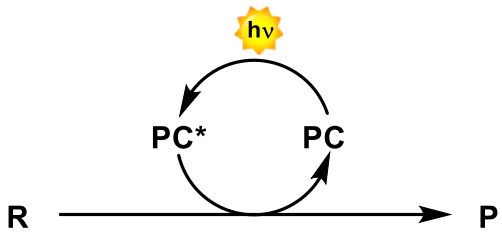

Figure 10. General scheme of a photocatalyzed reaction. PC: photocatalyst; PC: photocatalyst in the excited state.*

The photocatalyst (**PC**) is a molecular species (metal-based or a purely organic compound) that, once it absorbs light of the appropriate λ and reaches an electronically excited state, is capable of chemically modifying, at least, one of the reactants. Therefore, specific intermediates are formed that evolve towards the products through reaction pathways that are different from classical ground-state reactivity. The overall process finishes with the regeneration of the PC, which can start a new catalytic cycle with the absorption of another photon.[21,22]

What distinguishes and makes advantageous a photocatalyzed process from a thermal-catalyzed one is the different thermodynamics of the processes. In fact, a classical thermally catalyzed reaction allows the speed of the process to be increased by lowering the activation energy. This is possible by going through alternative reaction mechanisms, but without changing the thermodynamics of the process. All this implies that only exergonic processes with Gibbs free energy of the reaction $\Delta_r G<0$, can take place thermally. In the case of

photocatalysis, on the other hand, photocatalyzed processes can take place even if they are endoergonic ($\Delta_r G>0$), since the energy needed to carry out the reaction is provided precisely by light through the intermediation of the PC.[9]

The field of photocatalysis can be divided into several subcategories, considering the type of interaction between PC* and the substrate. They are: photo-induced electron transfer (**PET**) catalysis, proton-coupled electron transfer (**PCET**) catalysis and hydrogen-atom transfer (**HAT**) catalysis.

- ## Photo-induced electron transfer (PET) catalysis

In this process (also known as photoredox catalysis) the photocatalyst (**PC**), once photoexcited, can reduce or oxidize the substrate of interest through a single electron transfer (**SET**) event. The transition from the ground to the excited state leads to a substantial change in the electronic distribution of the PC for which the reduction/oxidation potentials in the excited state are totally different from the same potentials in the ground-state. Therefore, the excitation of the PC increases its reducing or oxidizing power.[22,23]

Once a photon is absorbed by the PC and an electron is promoted to the excited electronic state, the latter can be quenched through two possible routes of interaction with the substrate: oxidative quenching and reductive quenching (Figure 11).[24]

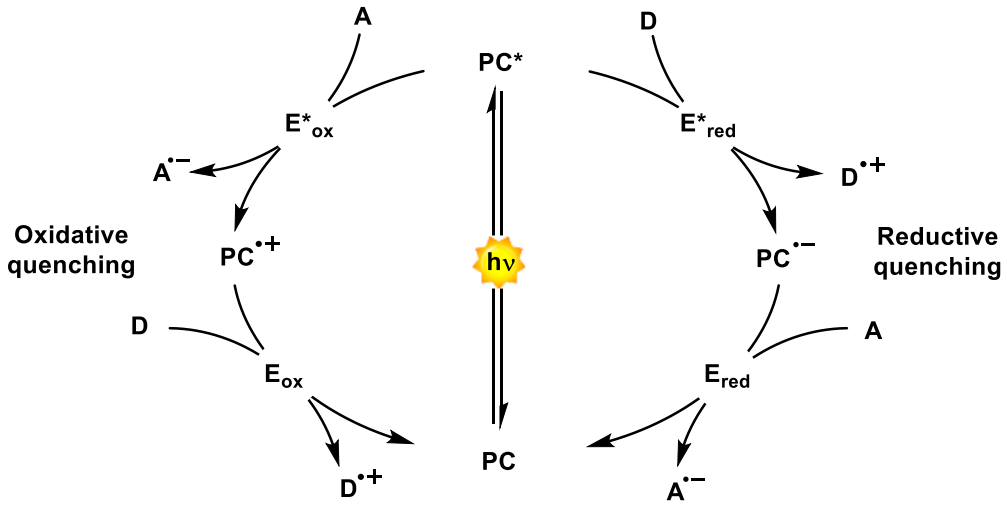

Figure 11. General mechanism of oxidative and reductive quenching. D = donor, A = acceptor, PC = photocatalyst.

In oxidative quenching, the excited photocatalyst (**PC***) gives an electron to the acceptor substrate (**A**) by reducing it and generating the oxidized species $\mathbf{PC}^{\bullet+}$. This is followed by restoration of the ground-state photocatalyst (**PC**) through a second SET process with a donor molecule (**D**). Conversely, in reductive quenching, the **PC*** extracts an electron from the **D** by oxidizing it and generating the reduced species $\mathbf{PC}^{\bullet-}$. This species then converts to the ground-state **PC** via SET with an acceptor molecule (**A**). Thus, via this catalytic cycle, intermediate radical species $\mathbf{A}^{\bullet-}$ and $\mathbf{D}^{\bullet+}$ are generated, which can react in different ways leading to product formation.

In order to act as an oxidant or reductant, the PC must possess oxidation and reduction potentials in the excited state (E^*_{ox} and E^*_{red}) suitable against the target substrate potentials.

Specifically, for oxidative quenching the E^*_{ox} potential of the **PC** must be lower than the reduction potential of substrate **A**, while in reductive quenching the E^*_{red} potential of the **PC** must be bigger than the oxidation potential of substrate **D**.[24]

Photocatalysts can be molecular species of different natures, such as metal complexes or highly conjugated organic molecules.[25,26] For both species, it is possible to modulate E^*_{ox} and E^*_{red} potentials through structural modifications of the molecule. In this way, new PCs can be synthesized with the excited-state potentials of interest through appropriate rational design and a study of the structure-property relationship.[27]

- ## Proton-coupled electron transfer (PCET) catalysis

In the case of multisite PCET, an electron and a proton arising from a single molecule are transferred to two different and independent acceptors, a Bronsted base and an oxidant (which may be an excited state PC), often through a concerted mechanism (Figure 12).[28-31]

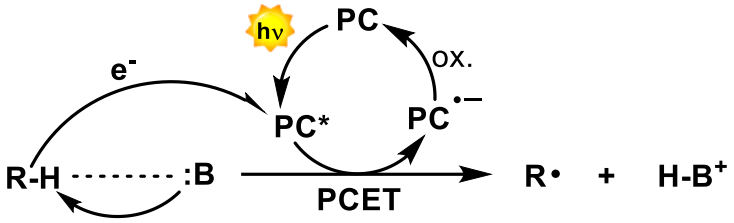

Figure 12. General scheme of a photocatalyzed concerted proton-coupled electron transfer (PCET) reaction. B: base.

In this way, C-H and X-H bonds (X = N, O, S) can be easily activated with several advantages. The main one is the ability to independently modulate the potential of the oxidant and the strength of the Bronsted base, thus being able to vary the binding dissociation free energy (BDFE) of the target species. With this, it is possible to make react substrates that cannot be activated through hydrogen atom transfer (HAT).

Moreover, when proton and electron transfer occur in a concerted manner, it goes for the formation of more stable neutral intermediate species than the charged intermediates generated through an oxidation/deprotection step process. An advantage of this is that this passage for lower-energy intermediates decreases the activation barrier of the process, consequently increasing the speed of the reaction compared to the slower step process (Figure 13).[28-31]

For a concerted PCET to occur, the base must first be pre-associated with the proton through a hydrogen bonding interaction.

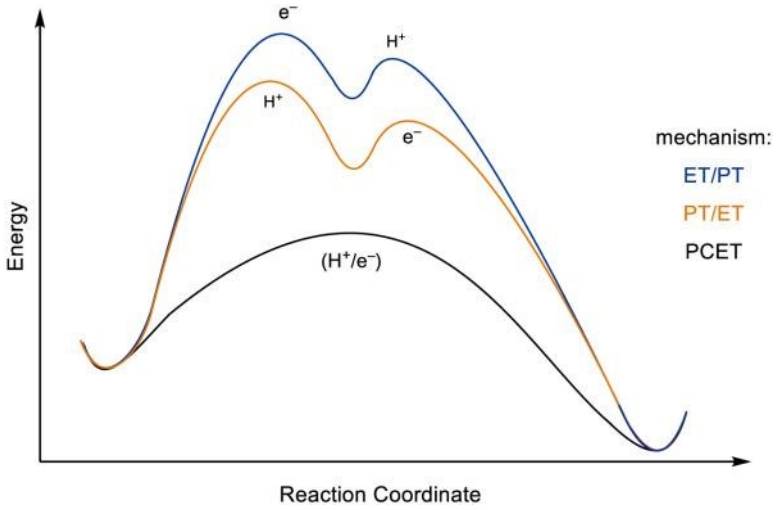

Figure 13. Reaction coordinate diagram comparing the activation barriers of the concerted PCET process and the proton transfer (PT) and electron transfer (ET) step processes. [32]

- **Hydrogen atom transfer (HAT) catalysis**

HAT is a process involving the transfer of a formal hydrogen atom H• ($H^+ + e^-$) from a donor substrate to an acceptor substrate through a single kinetic step (Figure 14).

Figure 14. General scheme of a HAT process.

Conceptually, a HAT process can be defined as a subcategory of PCET, in which there is a concerted transfer of a proton and an electron described by the same initial and final orbital.[32]

In the context of photocatalyzed HAT, this process can occur through two possible mechanisms, termed direct and indirect, respectively (Figure 15).[33]

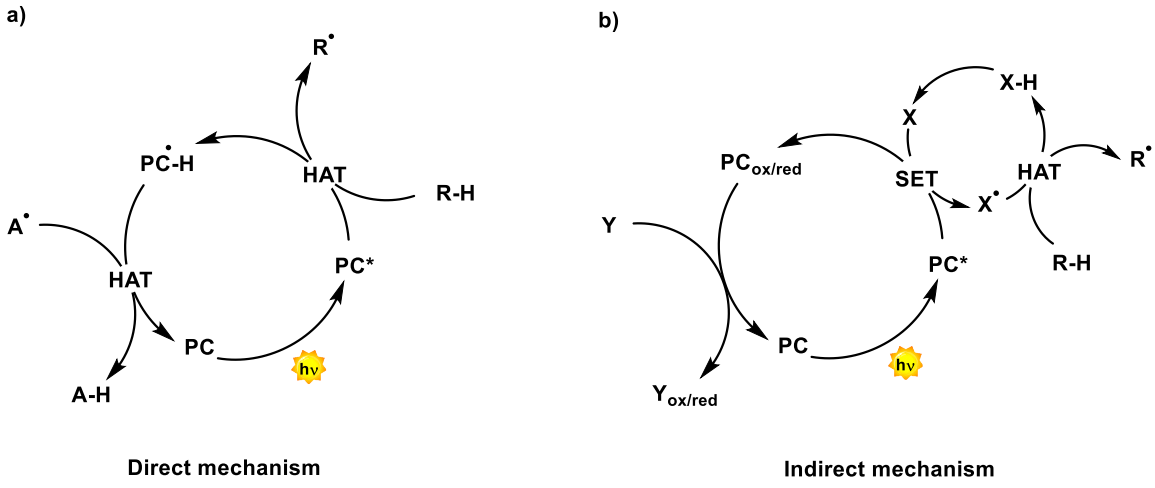

*Figure 15. General scheme for (**a**) a direct HAT mechanism, and (**b**) an indirect HAT mechanism.*

In the direct mechanism, the photocatalyst (**PC**), once photoexcited, directly abstracts a hydrogen atom (H•) from a specific C-H bond of the target substrate (**R-H**). Once the

abstraction is done, the PC can close the catalytic cycle by supplying the hydrogen atom to the product via a back-HAT, or it can give the H• to some other acceptor species (**A**) present in the system.

In the indirect mechanism, the **PC**, once photoexcited, activates a suitable species (**X**) added in the system through a SET process, forming **X•.** Then, this radical (**X•**) carries out the HAT process with the target **R-H** substrate. The key species **X** can be employed in either stoichiometric or catalytic amounts (through its cyclic restoration within the system).[33]

- ## Atom transfer radical addition (ATRA) process

In photocatalysis, numerous are the possible reaction pathways that the reactant can take once activated by the photocatalyst. Among these, one mechanism that frequently occurs in the field of photoredox catalysis is the ATRA mechanism (atom transfer radical addition).

The ATRA mechanism consists of the addition of a free radical species on a π-bond of an alkene or alkyne thus allowing the difunctionalization of the multiple bond with the formation of two new σ-bonds C-C and C-X. This process is capable of self-sustaining by being able to continue through a radical chain process. For this reason, the reaction requires only an initiator to start (Figure 16).[34]

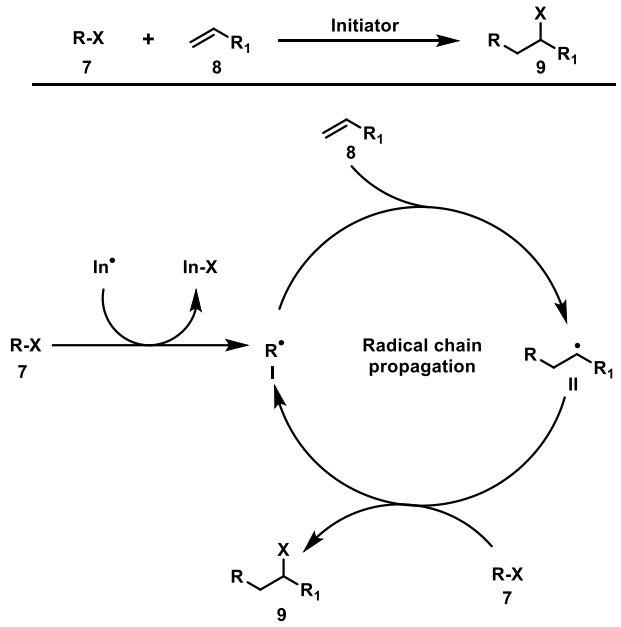

Figure 16. General mechanism of an ATRA process.

In fact, the **In•** initiator leads to the generation of the first radical species **I**, following the breaking of the R-X bond of the reactant (**7**). This intermediate radical species **I** can now be added to the double bond of olefin **8**, with the formation of the new carbon radical intermediate **II**. The latter can convert to product **9** by radical abstraction of substituent X from a new molecule of reagent **7**, which is thereby converted to the radical intermediate **I**. Species **I** can then begin a new ATRA cycle. In this way, the process is self-sustaining since the final step of product **9** formation is the same step that triggers the process.

Historically, the ATRA process was triggered by employing stoichiometric initiators, the most common of which were organic peroxides, organotin reagents and organoboranes, which

turn out to be dangerous and toxic species that require heating of the reaction mixture for their operation.[35]

Instead, with the advent of photoredox catalysis, it is possible to employ a photocatalyst as the initiator of the process, which allows the radical chain reaction to be triggered by SET from the PC in an excited state to the R-X substrate. Advantage of using photocatalysis is the possibility of working under mild reaction conditions, replacing the high temperature required to initiate the process with simple irradiation of the reactant mixture at room temperature. With this, undesirable high temperature reaction pathways are limited, allowing the formation of byproducts to be minimized and thus making the purification process easier. In addition, the PC can be regenerated, and consequently, more radical cycles can be triggered, increasing the turnover of the process.[34,36]

An example of difunctionalization of olefins with diethyl bromomalonate is shown in Figure 17, proceeding through a photocatalyzed ATRA mechanism.[36]

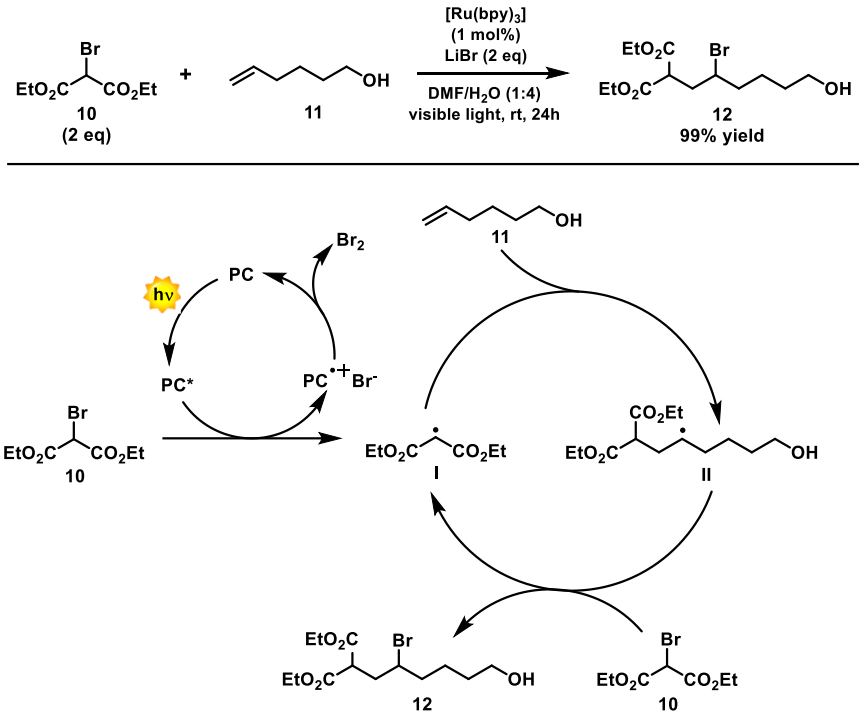

*Figure 17. Proposed mechanism for the photocatalyzed addition of diethyl bromomalonate **10** into double bond of olefins (**11**).*

2.2. Sulfoximines: structure and applications

Sulfoximines (Figure 18) are mono-aza derivatives of sulfones, which have found an increased interest in recent decades, as this moiety is found in numerous biologically active molecules, such as agrochemicals and drugs.[37]

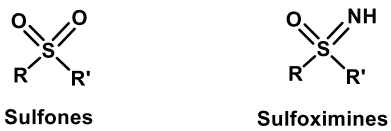

Figure 18. Structure of sulfones and sulfoximines.

Sulfoximines, which are isoelectronic with sulfones, are configurationally and constitutionally stable molecules. The substitution of an oxygen atom for a nitrogen atom causes the tetragonal sulfur center to be stereogenic (if the two carbon substituents are different).
In general, these molecules are stable and can be handled without special care, being able to even store them without the use of inert atmospheres or low temperatures.
The presence of the nitrogen atom allows their use as Lewis bases, being able to be easily employed in coordination with Lewis acids such as metallic species. Also, in the case of unsubstituted sulfoximines, the free NH can act as weak Bronsted bases, being able to easily form salts with mineral acids.
The two double bonds S=O and S=NH are excellent hydrogen-bond acceptor/donor, where in the case of free N-H the latter can act as both donor and acceptor.
Sulfoximine is a more electron-withdrawing substituent than the sulfone group, and also results readily soluble in protic solvents, such as alcohols and, in case of small molecule, also water.
Unlike sulfone, the presence of the labile N-H group constitutes an additional substitution site, thanks to which it is possible to introduce different functional groups into the molecule (e.g., synthesize cyclic sulfoximines). Taking advantage of the latter feature it possible to modulate and fine-tune the physicochemical properties with N-substituents, such as the acid/base behavior of the compound. [38,39,40]

The substitution of an oxygen atom for a nitrogen atom provides this functional group with advantageous properties and reactivity, never observed in the case of the sulfone analogue, which have led sulfoximines to be widely used in medicinal chemistry (Figure 19).

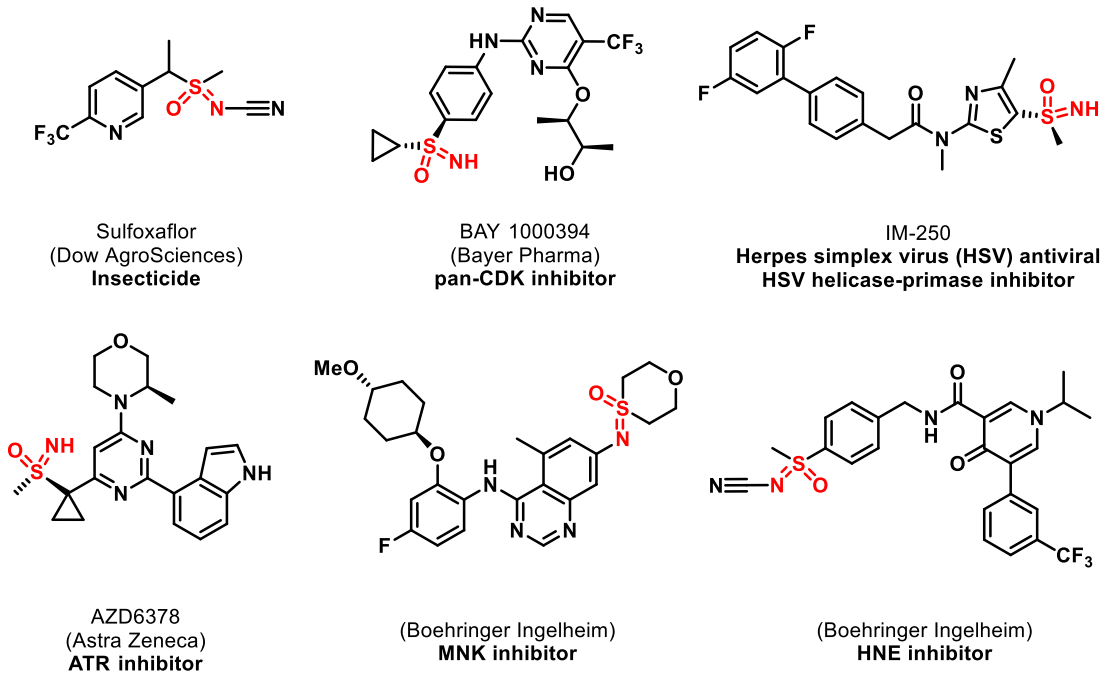

Figure 19. Bioactive sulfoximines.[37,41]

The discovery of this functionality dates back to the 1950s by Bentley and Whitehead, with the synthesis and study of the biologically active molecule L-methionine (S)-Sulfoximine (MSO), an inhibitor of GSH tripeptide biosynthesis (Figure 20). Subsequently, one of its derivatives, buthionine sulfoximine (BSO), was found to be a potent and specific inhibitor of γ-glutamylcysteine synthetase, for which clinical trials have also been performed for its

possible application in the treatment of tumors involving GSH overexpression (e.g., hepatocarcinoma).[38]

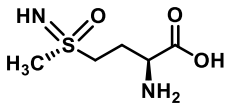

L-Methionine (S)-Sulfoximine (MSO)

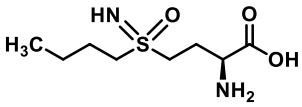

L-Buthionine Sulfoximine (BSO)

Figure 20. Structure of biologically active sulfoximine MSO and BSO.

After the discovery of sulfoximines, the latter were no longer used in the pharmaceutical sector, finding in the past mainly synthetic applications. For example, sulfoximines have been widely used as chiral auxiliaries and useful ligands in asymmetric synthesis.[42,43]

2.2.1 Synthesis of sulfoximines

Several strategies are available for the synthesis of sulfoximines **16** starting from different possible substrates. Typically, the synthesis consists of two reaction steps (Figure 21): an initial oxidation process starting with sulfide **13** to form the sulfoxide intermediate **14**, followed by an imination process. Alternatively, sulfoximine **16** can be accessed through an initial imination process from **13** to give the sulfilimine **15**, followed by an oxidation process. Nowadays, however, there are also new one-pot synthesis strategies in which oxidation and imination occur in the same reaction system, without going through the isolation of the intermediates **14** and **15**. Typically, most of these procedures result in the formation of the N-protected product sulfoximine **16**, which then requires a subsequent deprotection step to obtain the NH product sulfoximine. [39,40]

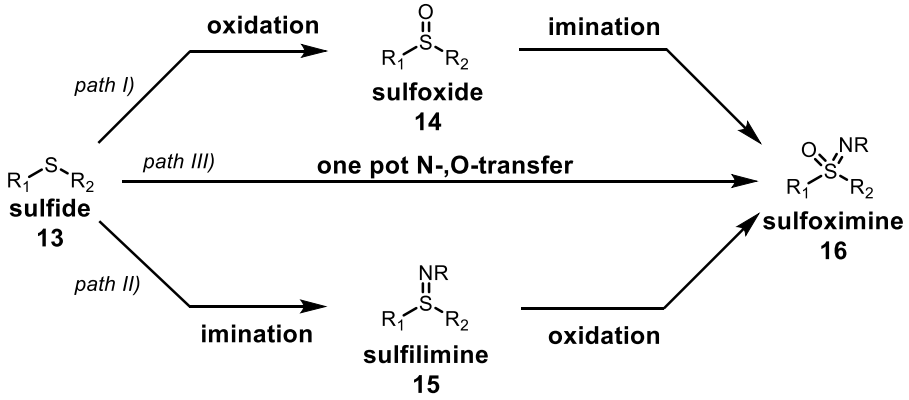

*Figure 21. Synthetic routes to access sulfoximines **16**.*

Numerous examples for the synthesis of sulfoximines **16** are reported, proceeding through different strategies, such as metal catalysis, metal-free stoichiometric processes, etc.
The following are some of them:

- **Path I): sulfoximine synthesis via initial imination and final oxidation**

A good imination reagent for the conversion of sulfide **13** to sulfilimine **15** found to be chloramine-T **(17)** (i.e., N-chloro tosylamide sodium salt). By working under anhydrous

conditions at pH = 5 in methanol, it is possible to obtain the corresponding N-tosyl sulfilimine **15** in good to excellent reaction yields (58-95%).

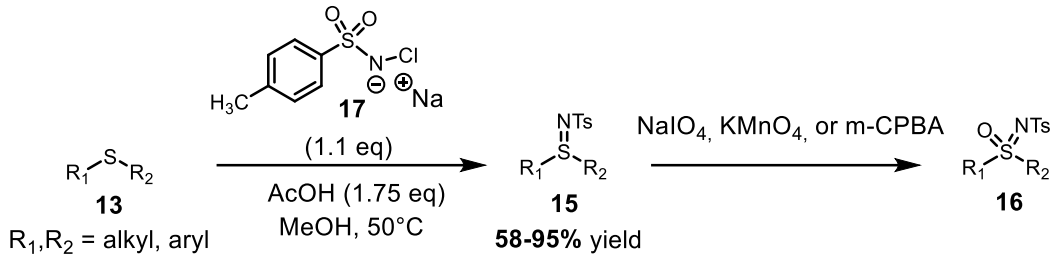

*Figure 22. Synthesis of sulfoximine **16** via imination/oxidation.*

This process proves to be diasteroselective in the case of cyclic or aromatic sulfides, succeeding in obtaining the desired product with a diasteroselective ratio of 9:1, by transferring the N-Ts fragment to the less-hindered face of the sulfide.[44] Once this intermediate has been obtained, a subsequent oxidation step with common oxidizing agents, such as $NaIO_4$, $KMnO_4$ or m-CPBA, leads to the formation of the desired sulfoximine product **16**.[39]

- **Path II): sulfoximine synthesis via initial oxidation and final imination**

For the synthesis of sulfoxide **14** from sulfide **13**, an excellent strategy is the use of dimethyl dioxirane (DMDO) **18** in DCM at -78°C, which allows the corresponding intermediate product to be obtained in high yields (Figure 23). Working at low temperatures, high diastero and chemoselectivity of the product from chiral sulfoxides can be achieved.[45]

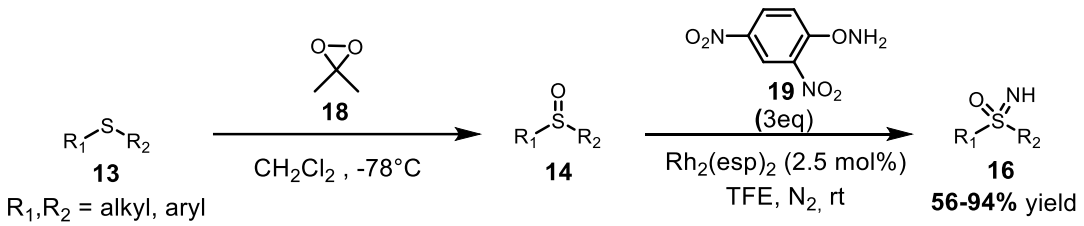

*Figure 23. Synthesis of sulfoximine **16** via oxidation/imination.*

For the subsequent sulfoxide imination step, an example of a mild metal-catalyzed reaction process is represented by the use of $Rh_2(esp)_2$ as catalyst in the presence of O-(2,4-dinitrophenyl)hydroxylamine **19** (DPH) as nitrogen source in trifluoroethanol (TFE) at room temperature for 22h. With these conditions the NH sulfoximine **16** product can be obtained without going through any deprotection process, in moderate to excellent reaction yields (56-94%). This process demonstrates excellent tolerance toward numerous functional groups, such as halogen, acyl group, aryl, heteroaryl and alkyl group (cyclic and acyclic).[46]

- **Path III): one-pot sulfoximines synthesis**

Until now, we have seen examples of a two-step reaction, with the formation and isolation of sulfilimines **15** or sulfoxides **14** as intermediate species. However, there are more recent strategies in which it is possible to directly obtain the sulfoximine product **16** from sulfide **13**

by going through only one reaction step, via a one-pot NH- and O- transfer process (Figure 24).

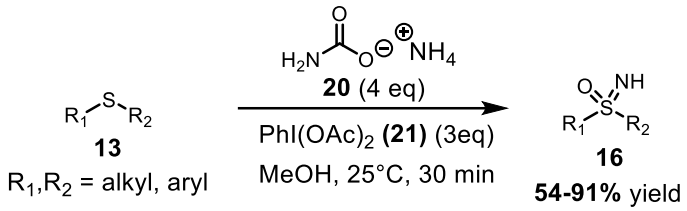

*Figure 24. Synthesis of sulfoximine **16** via a one-pot process.*

An advantageous metal-free example corresponds to the use of ammonium carbamate **20** as an inexpensive and safe source of nitrogen together with the oxidizer (diacetoxyiodo)benzene (PIDA) **21** in methanol, allowing the NH-sulfoximine product **16** to be easily obtained in 30 minutes of reaction at room temperature and under air. This process also demonstrates good tolerance toward several functional groups, with moderate to high yields (54-91%), while also avoiding the subsequent nitrogen substituent deprotection step.[47]

2.2.2 Chiral sulfoximines synthesis

The preceding examples are effective synthetic strategies that, nevertheless, allow the sulfoximine product to be obtained without any stereoselectivity, thus resulting in a racemic mixture.
In the case of biologically active molecules with pharmaceutical application, however, it is of paramount importance to obtain this functional group in enantiopure form.
Examples of enantioselective sulfoximine synthesis strategies are based, as in the previous cases, in two reaction steps in which there is an initial enantioselective oxidation or imination step of sulfides, followed by the final stereospecific imination or oxidation process that yields the sulfoximine in an enantiopure form.
The majority of asymmetric synthesis strategies for the conversion of sulfides to sulfoxide or sulfilimines rely on the use of metal catalysis, employing appropriate chiral ligands. In these reaction systems, the enantioselectivity is high when the two carbon substituents of the sulfide are different in size, as in the case of aryl alkyl sulfides. This is because in this manner it is possible to discriminate more effectively the less-hindered face of the sulfide.
An example of sulfide to sulfoxide oxidation is using a Ti catalyst in the presence of an appropriate chiral ligand **22** and an organic peroxide, such as tert-butyl hydroperoxide (TBHP) (Figure 25). With this reaction system, it is possible to convert aryl alkyl sulfides **13** to chiral sulfoxides **14** with good yields and high enantioselection (70% with 90% ee).[48]

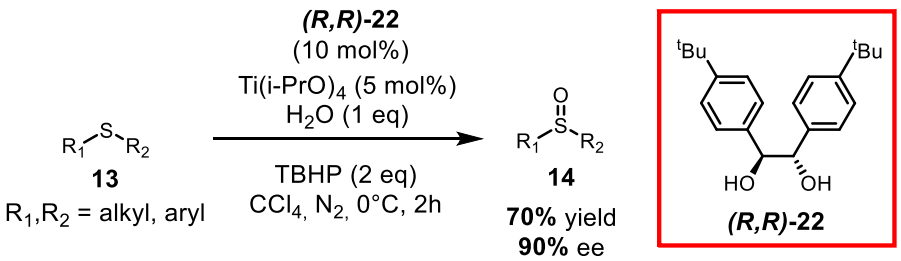

*Figure 25. Example of enantioselective oxidation of sulfide **13** to sulfoxide **14**.*

An example of enantioselective imination of sulfides **13** is the use of a Ruthenium catalyst **24** employing a chiral version of the salen ligand in the presence of an organic azide **23** as a nitrogen source (Figure 26).

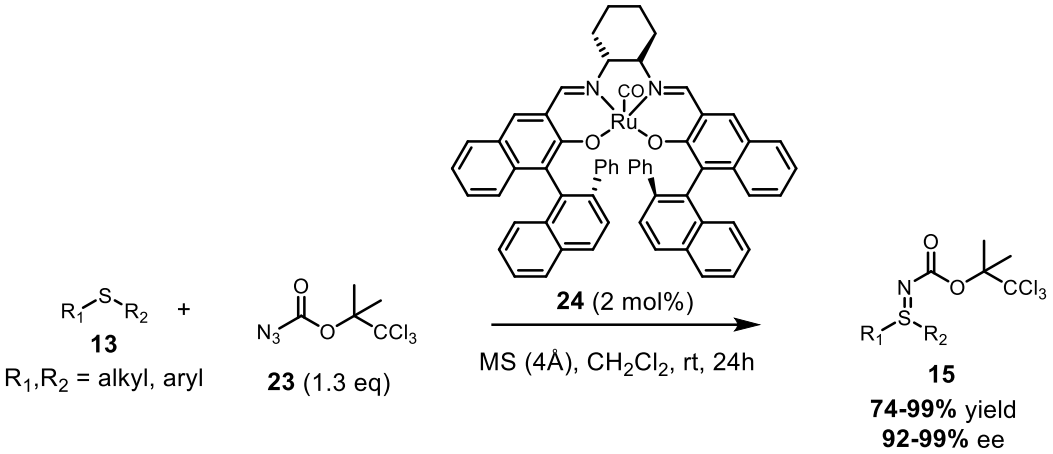

*Figure 26. Example of enantioselective imination of sulfide **13** to sulfilimines **15**.*

With this catalytic system it is possible to obtain in the case of alkyl aryl sulfides the corresponding chiral sulfilimine **15** in high yields and excellent enantioselectivity (yield: 74-99%, ee: 92-99%).[44,49]
A disadvantage of this process, however, is the use of an organic azide, which is toxic and explosive, especially on a large scale.

2.2.3 Reactivity of sulfoximines under photocatalytic conditions

The reactivity of sulfoximines is very diverse due to the many different substituents bound to the sulfur center, making this functional group very useful and versatile in the field of organic synthesis. Some reactivities are common to those of the analogue sulfones (Figure 27).

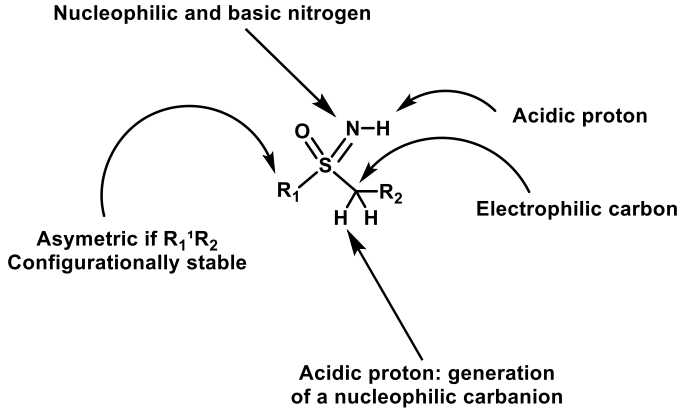

Figure 27. Schematization of possible reactivity of sulfoximines.

Specifically, sulfoximines can behave as a nucleophile to the carbon after abstraction of the acid proton in alpha carbon Cα relative to the sulphur centre. They can also behave as an electrophile to the sulfur center; and also, due to the electron-withdrawing nature of the sulfoximine substituent, it can make Cα a good electrophile.[50]

The main reactivity of sulfoximines (indeed, reactivity that distinguishes it from sulfones) is that to the imine substituent (C=NH) that can be easily functionalized with species of different nature.
N-H functionalization strategies are very diverse and can be carried out by stoichiometric reaction, metal catalysis, organocatalysis, etc. [51]
Although such processes are mainly dominated by metal catalysis, in the recent years there has been a growing number of publications that exploit the innovative branch of photocatalysis in the functionalization of sulfoximine derivatives. These new protocols proceed under mild and sustainable reaction conditions, thus being more attractive from a synthetic point of view.
The next sections will be focused on discussing examples of photocatalytic functionalization strategies.

- **N-Arylation**

N-arylation processes are the most widely reported examples for N-H functionalization of sulfoximines. This is due to the high interest in pharmaceuticals, as many bioactive sulfoximines are functionalized with imine nitrogen aryls.
There are also numerous photocatalyzed examples.

The first example exploits a metallaphotoredox strategy in which dual nickel photocatalysis is used to obtain an N-C cross-coupling between an NH-sulfoximine **25** and a bromine arene **26**, allowing the N-arylated product **27** to be obtained under mild reaction conditions (Figure 28).

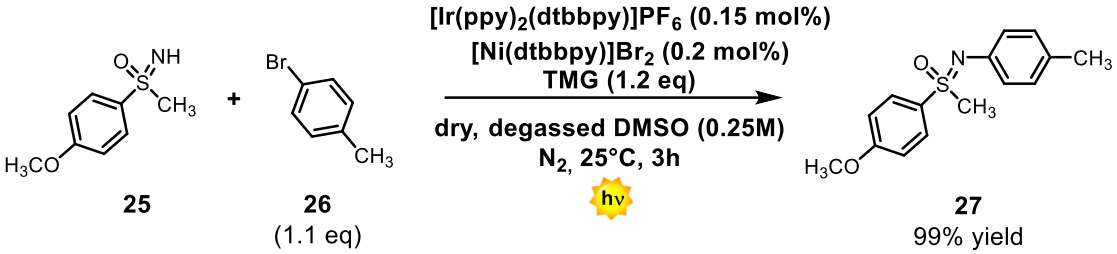

Figure 28. N-arylation of NH-sulfoximines via dual nickel photocatalysis.

The reaction uses $[Ir(ppy)_2(dtbbpy)]PF_6$ as the PC, $NiBr_2$ with di-tert-butyl-bipyridine (dtbbpy) as the ligand (added separately) and 1,1,3,3-tetramethylguanidine (TMG) as the base in dry and degassed DMSO. The process, carried out under nitrogen atmosphere with the irradiation of a blue LED (455 nm) for 3h at 25°C, yields the corresponding N-arylated product **27** in good to excellent yields (59-99%).
The reaction also shows great tolerance toward various arene functional groups, with excellent yields for both electron-rich and electron-poor arenes, and moderate to good yields even for the use of heteroarenes (25-99%).
The reaction is also tolerant to the different nature of the sulfoximine, achieving good results with both differently substituted alkyl and aryl substrates (47-99%). This demonstrates the great generality of the process.
Moreover, starting from an enantiopure chiral sulfoximine **25** the reaction does not lead to racemization of the substrate, being able to obtain the corresponding N-arylated product while preserving its optical purity.[52]

The second process is an example of organophotocatalysis, through the use of a strongly oxidizing photoredox organocatalyst for N-H arylation of sulfoximine **28** with electron-rich arenes **29** (Figure 29).

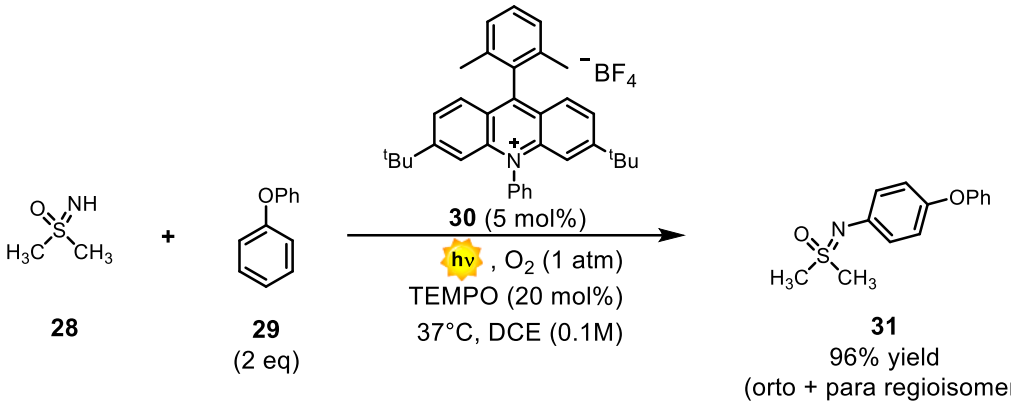

Figure 29. Late-stage sulfoximidation of electron-rich arenes by photoredox catalysis.

The process employs a strongly oxidizing acridinium photocatalyst **30** (E^*_{red} = 2,15 V vs SCE) in the presence of TEMPO as a co-catalyst, under oxygen atmosphere (for PC regeneration) in dichloroethane (DCE). By irradiating with blue LED at 460 nm, the corresponding N-arylated product **31** can be obtained in moderate to good yields (41-96%).
This reaction shows several advantages from a synthetic point of view: (i) the possibility of using arenes **29** that do not have to be previously functionalized; (ii) the possibility of carrying out the reaction in an aerobic atmosphere; and (iii) the absence of metal species, which make this process mild and more sustainable in comparison with metallaphotoredox catalysis.
A disadvantage of this process is that the reaction is limited only to the use of electron-rich arenes, and furthermore, the process leads to the formation of a mixture of regioisomers, with the possibility of both *ortho*- and *para*-substitution in the aromatic ring. The reaction is found to be tolerant to the nature of the sulfoximine substituents, achieving good results with both alkyl and aryl substituents.[53]

- **N-Acylation**

This functionalization allows different acyl groups to be introduced on the NH substituent, which are excellent functional groups for further synthetic manipulations.
The protocol below is an example of a direct photochemical process, in which the light-absorbing species are directly the reactants of the reaction, and therefore, there is no need to use external PCs.

In this example, the N-Acylated product **35** can be obtained through the photo-induced reaction between diazoketones **32** and sulfoximines **34** (Figure 30).

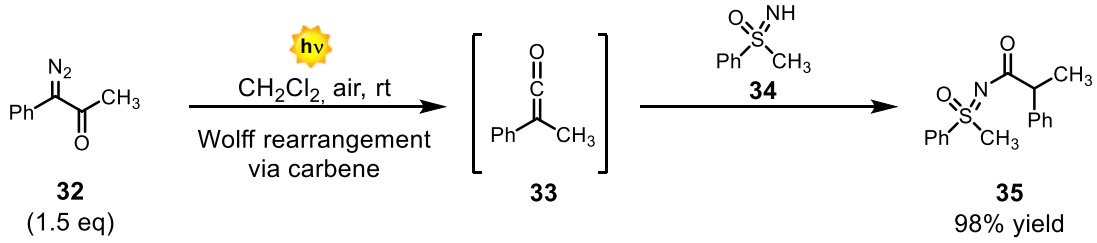

Figure 30. Matching carbenes and sulfoximines via ketenes generated from α-diazoketones by blue light.

In this case, the light-absorbing species is diazoketone **32**, which, once in an excited state, quickly converts to the ketene intermediate **33** through a Wolff rearrangement (via carbene species) which then reacts in situ with sulfoximine **34** to generate the desired product **35**.
This process works under very mild reaction conditions and is easy to prepare, as it only needs to irradiate the two reactants in DCM solution with blue LED, without the need for additional additives (such as base), catalysts or oxidants and being able to work freely in air at room temperature.
This process is also very tolerant of both sulfoximine substituents (64-98% yield) and diazoketone substituents (44-97% yield), yielding the corresponding N-acylated products with moderate to excellent reaction yields with both alkyl and aryl groups.
Another advantage is the possibility of subsequently reducing the carbonyl group so that the corresponding N-alkylated sulfoximine **36** can be obtained in good yields from N-acylated sulfoximine **35** (Figure 31).[54]

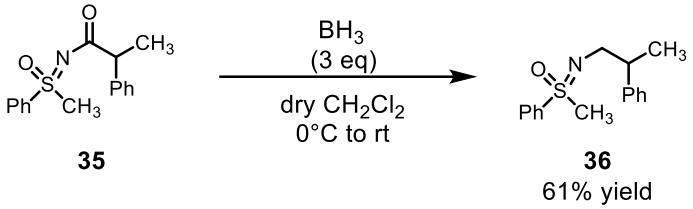

Figure 31. Example of reduction of N-acylated sulfoximine to N-alkylated sulfoximine.

- **N-Alkylation**

In the area of photocatalyzed N-alkylation, the main examples are based on the addition of N-halogen or N-pseudohalogen sulfoximine on olefin double bonds.

This process consists on the photocatalyzed addition reaction of N-SCN sulfoximine **37** on olefins **38**, through the generation via single electron transfer (SET) of the sulfoximidoyl radical intermediate via homolytic breaking of the N-SCN bond (Figure 32).

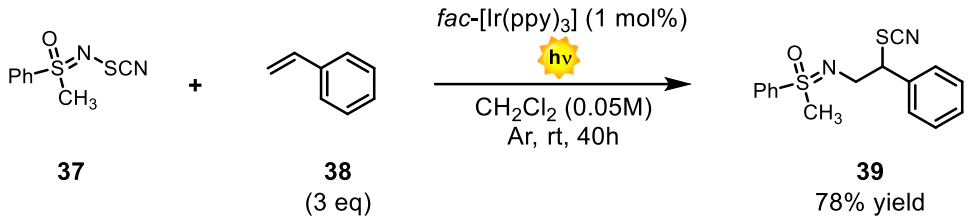

Figure 32. Photocatalytic difunctionalisations of alkenes with N-SCN sulfoximines

fac-[Ir(ppy)$_3$] is employed as the PC, which reduces the N-SCN sulfoximine **37**, while generating the nitrogen radical that is then added to the double bond of **38**. This allows the di-functionalization of olefin **38** with the generation of two new bonds, C-N and C-SCN respectively. By working in DCM under argon atmosphere for 40 h with blue-LED irradiation (455 nm), it is possible to obtain the N-alkylated product **39** in good yields (33-80%). The scope of the reaction focused only on the use of variously substituted styrene species (model substrate **38**), demonstrating that the reaction can tolerate well many electron-attracting and electron-donating substituents in different positions of the aromatic ring (33-80% yield). The reaction also shows good tolerance toward several aryl and alkyl substituents of sulfoximine **37** (40-71% yield).[55]

2.3. Bioisosterism in medicinal chemistry

The concept of bioisosterism originated in the 1950s is an evolution of the phenomenon of isosterism, which was extensively studied by Irving Langmuir at the beginning of the last century.[56]

Isosterism refers to the ability whereby compounds with the same number of atoms and the same number of electrons possess similar physical properties, indicating that their electrons are arranged in the same manner.[57]

A typical example of this phenomenon is the comparison between CO_2 and N_2O, molecules consisting of 3 atoms and both containing 22 total electrons. Such characteristics leads to have similar physical properties, such as critical pressure and temperature, density, refractive index, dielectric constant, solubility, etc. (Table 1).

Physical property	N_2O	CO_2
Critical pressure (atm)	75	77
Critical temperature (°C)	35.4	31.9
Density of liquid at +10°C	0.856	0.858
Refractive index of liquid, D line, 16°C	1.193	1.190
Dielectric constant of liquid at 0°C	1.598	1.582
Solubility in alcohol at 15°C	3.25	3.13

Table 1. Experimental physical data for nitrous oxide (N_2O) and carbon dioxide (CO_2).[57]

Instead, the term of bioisosterism is developed primarily by Friedman and Thornber, who give two definitions for this phenomenon similar to what is understood today. The first definition is introduced with Friedman:

"Bioisosteres are structural moieties which fit the broadest definition of isosteres and have the same type of biological activity".[58]

What is defined, however, only goes to encompass the biological phenomenon of molecular recognition but does not go to consider all the other physicochemical properties that are studied in the field of medicinal chemistry.

The second definition, introduced by Thornber, is more general in nature and fully summarizes the modern concept of bioisosterism:

"Bioisosteres are groups or molecules which have chemical and physical similarities producing broadly similar biological properties".[59]

As anticipated, the phenomenon of bioisosterism is of relevant interest in medicinal chemistry, finding an increased application in agrochemical and pharmaceutical research for the development of new drug candidates. Specifically, this strategy deals with the synthesis of molecules structurally similar to the drug of interest, in which some chemical motifs are replaced with other functionality. This substitution allows to tune the physicochemical and biological properties of a drug without changing the specific drug-receptor interactions of molecular recognition, with significant improvements in efficacy, selectivity and pharmacokinetics of the drug analogue.[60]

The parameters of interest for a drug that can be adjusted through this strategy are different in nature:[57]

- Size
- Shape: bond angles and hybridization state
- Electronic distribution: polarizability, inductive effects, charge and dipoles
- Lipid solubility
- Water solubility
- pK_a
- Chemical reactivity and metabolic stability
- Hydrogen bonding capacity.

In the context of drug optimization, several molecular motifs have been shown to be very efficient in their use as bioisosteric replacements, and prominent among them are fluorine-containing molecular units.

In fact, fluorine is of relevant interest in medicinal chemistry due to its peculiar and versatile properties, which enable it to effectively mimic several functional groups, such as carbonyl and sulfonyl functionalities, the nitrile and the C-H bond.[61]
Fluorine is approximately 20% larger than hydrogen (in terms of van der Waals radii), while the length and size of a C−F bond is similar to the value of a C=O bond.
The electronegativity of fluorine is closer to that of oxygen, for which there is consequently a dipole moment value closer to that of a C-OH bond.
Moreover, fluorine is significantly more lipophilic than the hydroxyl (-OH), carbonyl (-C=O) or nitrile groups (-CN). Unlike other halogens, fluorine does not participate in halogen bonding and is non-polarizable. The latter property allows this atom to take part in strong electrostatic interactions, which can be attractive or repulsive.[61,62]

Among several possible examples of fluorinated functional groups, it has been observed that the difluoromethylene group ($-CF_2-$) is an efficient bioisostere of carbonyl groups (C=O) or oxygen atoms. The following are two literature examples of the use of the $-CF_2-$ group as a bioisostere in drug design.

- **Difluoromethylene group ($-CF_2-$) as bioisostere of carbonyl groups (C=O)**

The example reported concerns the bioisosteric replacement of the drug candidate **41**, a molecule with the same biological activity of the FK506-binding protein inhibitor **40**. This molecule, known as tacrolimus (**40**), is an immunosuppressive drug used to treat certain autoimmune diseases and to prevent organ rejection after transplantation (Figure 33).

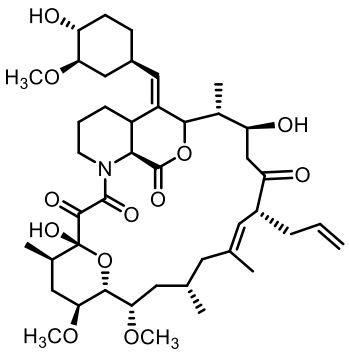

40
Tacrolimus

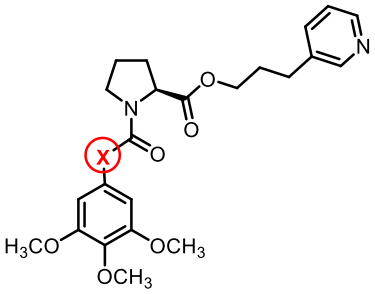

41
a) **X**: C=O Ki = 4.0 mM
b) **X**: CF_2 Ki = 0.87 mM
c) **X**: CH_2 inactive

*Figure 33. Structure of the immunosuppressant drug Tacrolimus (**40**) and the drug candidate **41 (a-c)**.*

In this example, substitution of a ketone carbonyl for the -CF_2- group leads to an increase in the inhibitory ability of the drug **41b** against the target enzyme, observable by the value of the inhibitor binding affinity constant for the enzyme (Ki). The smaller the Ki, the greater the binding affinity and the smaller amount of drug needed to inhibit the activity of that enzyme. Comparing these values (0.87 µM for **41b** vs 4.0 µM for **41a**) it can be deduced how the potency of the drug is increased with this substitution. The importance of the -CF_2- group is also demonstrated by the compound **41c**, in which the substitution of -CF_2- for -CH_2- leads to the complete nullification of the molecule's inhibitory capacity. Considering the similarity in size between H and F, this large difference in behavior goes to indicate that the fluorine atoms in -CF_2- not only play a steric role in molecular recognition but also take part in specific interactions within the active site of the enzyme.

Another advantage of this bioisosteric replacement is the increase in chemical stability by switching from molecule **41a** to **41b**. In fact, molecule **41b** demonstrated excellent hydrolytic stability, being stable for more than 27 hours in a 9:1 mixture of phosphate buffered saline/DMSO containing bovine serum albumin at pH 7.4 and at room temperature. [63]

- **Difluoromethylene group (-CF_2-) as bioisostere of an oxygen atom**

The -CF_2- group is also widely used for the substitution of oxygen atoms (generally ethers) within molecular structures, as the fluorine atoms in the C-F bonds mimic the lone pairs of the oxygen atom.

This replacement was performed in the cannabinoid drug candidates **42** (**a-b**), employed as selective CB2-enzyme agonists for the treatment of inflammatory pain (Figure 34).

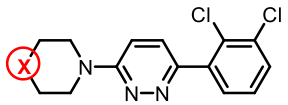

42
a) **X**: O Ki = 75 nM
b) **X**: CF_2 Ki = 15 nM

*Figure 34. Structure of candidate cannabinoid drugs **42 (a-b)**.*

In this example, it is observed that the replacement of the ether oxygen with the -CF_2- group leads to an increase in the lipophilicity of the molecule and a consequent increase in the potency of the drug. Indeed, the comparison of the Ki of both compounds (75 nM for **42a** vs 15 nM for **42b**), suggests that this bioisosteric replacement leads to increased affinity of the molecule toward the lipophilic receptor binding site of the target enzyme.[64]

2.4. Fluorinated sulfoximines: structures and applications

The selective incorporation of fluorine atoms into organic compounds has become an area of research of great interest in organic chemistry. This is because fluorine possesses peculiar characteristics, such as high electronegativity, small atomic radius and almost no polarizability, giving to fluorinated organic molecules unique and advantageous properties of practical interest. For this reason, these compounds are finding increasing use in various fields, including materials science and medicinal chemistry.[65]

The incorporation of fluorine atoms into sulfoximines (Figure 35) allows for a new functionality with electronic properties and reactivity that are completely different from those of classical sulfoximines, sulfones, and fluorinated sulfones.

R_F = CF_3, CF_2H, CF_2R, CH_2F, CHFR, etc.

Figure 35. Structure of fluorinated sulfoximines.

In particular, fluorinated sulfoximines have been shown to be strong electron-withdrawing substituents, even more than their fluorinated sulfone analogs. Moreover, there is the possibility of modulating the electronic properties of this functionality through a judicious choice of the nitrogen substituent.[65.66]

A practical example of this high electron-withdrawing character can be seen in Figure 36, comparing the effect of the trifluoromethyl N-triflated sulfoximine and trifluoromethyl sulfone substituent in the aromatic nucleophilic substitution reaction (S_NAr) of species **43**-**44**.

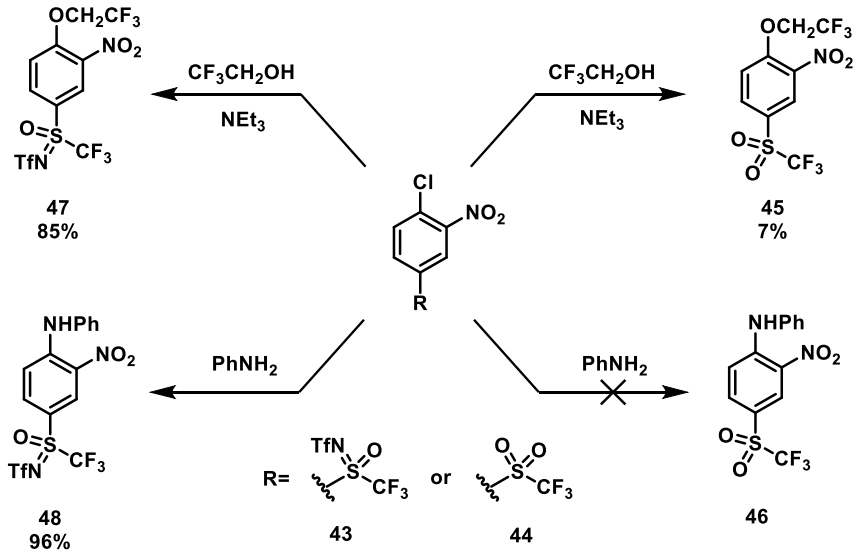

*Figure 36. S_NAr with fluorinated sulfoximine substituent **43** and sulfone **45**.*

In this case, the fluorinated sulfone **45** is not found to be sufficiently electron-withdrawing to trigger an S_NAr reaction, leading to poor yields of product **45**, or remaining unreactive to form **46**. In contrast, the high electron-withdrawing character of the fluorinated sulfoximine **43** makes the arene sufficiently electron-poor to trigger the S_NAr reaction with high yields for the products **47** and **48**.

These characteristics, together with high dielectric anisotropy (Δε), high dipole moment, intense absorption band in near UV/blue visible, and good fluorescence emission capabilities, make fluorinated sulfoximines attractive functional groups for materials science research (e.g. generation of OLEDs, OFETs, LCDs, etc.).[66]

Fluorinated sulfoximines also find interesting applications in the field of medicinal chemistry. As discussed extensively in chapter **2.3**, the fluorine atom plays a special role in this field because it can act as bioisostere of different functional groups such as carbonyl groups (-CO), hydrogens (-H) or the nitrile group (-CN), among others.[61] There are numerous examples of biologically active molecules containing the fluorinated sulfoximine moiety with applications in the pharmaceutical and agrochemical sectors (Figure 37).

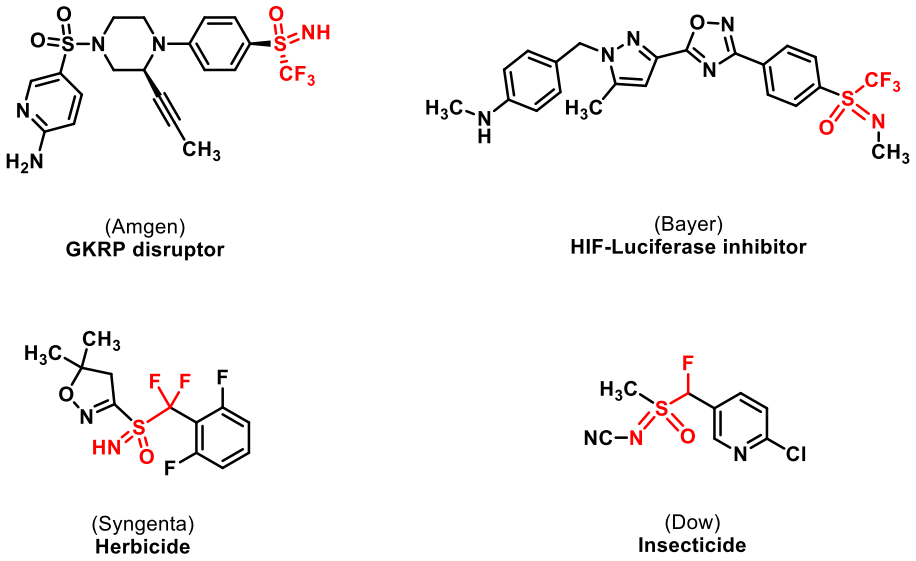

Figure 37. Bioactive fluorinated sulfoximines.[37,66]

2.4.1. Synthesis of fluorinated sulfoximines

Regarding the synthesis of fluorinated sulfoximines, the current strategies are similar to those already reported for the synthesis of classical sulfoximines, with some variations to take into account the reactivity variation of starting materials due to the presence of fluorine atoms. As discussed in Section **2.2.1**, the synthesis can start from the corresponding fluorinated sulfoxide or sulfilimine, or from a fluorinated sulfide with a two-step or one-pot process.[65]

The following is an example of one-pot synthesis of fluorinated NH-sulfoximine **50** (Figure 38):

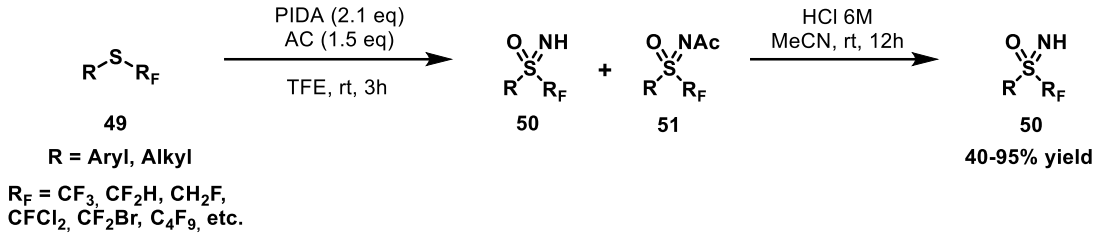

*Figure 38. One-pot synthesis of aryl- and alkyl S-perfluoroalkylated NH-sulfoximines **50** from sulfides **49.***

This one-pot process is a safe, general and metal-free strategy for the preparation of fluorinated NH sulfoximines **50** from the corresponding sulfide **49**. The reaction proceeds under mild reaction conditions, using the oxidant phenyliodine diacetate (**PIDA**) and ammonium carbamate (**AC**), and using trifluoroethanol (**TFE**) as solvent.

After the oxidation step a mixture of NH-sulfoximine (**50**) and N-Ac sulfoximine (**51**) are obtained. The final NH-sulfoximine (**50**) is obtained under acidic hydrolysis conditions, using 6M HCl in MeCN, under stirring at room temperature for 12 h (40-89% yields).

This reaction demonstrates excellent tolerance to many different fluorinated chains and can be carried out from both alkyl and aryl sulfides, demonstrating the excellent generality of the process.[67]

2.4.2. Reactivity of fluorinated sulfoximines

The presence of fluorine atoms in the structure of sulfoximines confers to these species peculiar reactivities not observed in the case of their non-fluorinated analogues. In addition, the presence of fluorine modifies the N-H acidity and facilitates the deprotonation in the alfa carbon Cα to generate the corresponding carbanion.[65,66]

The main reaction pathways characteristic of fluorinated sulfoximines are summarized in the next sections.

- **N-Functionalization**

Also in the case of fluorinated sulfoximines, there are several examples in the literature of N-functionalization. In most cases, these strategies exploit the high N-H acidity (caused by the presence of electron-withdrawing fluorine substituents) for the generation of the nucleophilic nitrogen anion, which can then be functionalized with electrophiles or though cross-coupling reactions (Figure 39).[65]

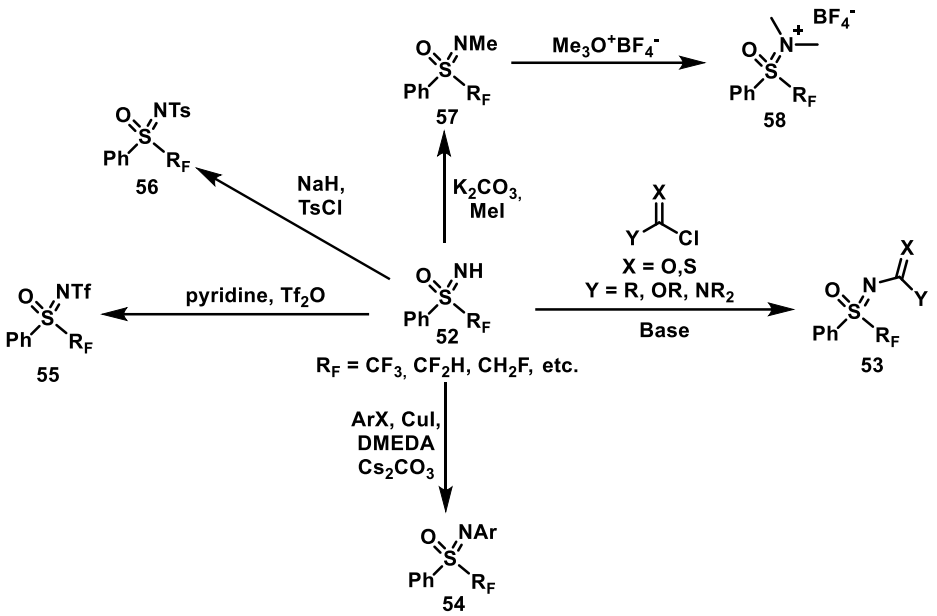

*Figure 39. Different N-functionalization pathways for fluorinated NH-sulfoximines **52**.*

The branch of photocatalysis emerges as a new and advantageous strategy, allowing the easy N-functionalization of sulfoximines under mild reaction conditions.

Figure 40 shows an example of an N-alkylation reaction using a photocatalytic method.

This process consists of the photocatalyzed addition reaction of fluorinated N-Cl sulfoximine **59** on olefins **8.** The process occurs through the generation of a sulfoximidoyl radical intermediate via the homolytic cleavage of the N-Cl bond in **59**.

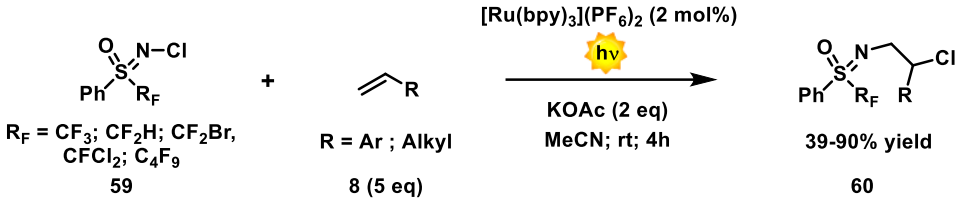

*Figure 40. Photoredox-initiated 1,2-difunctionalization of alkenes **8** with N-chloro S-fluoroalkyl sulfoximines **59**.*

$[Ru(bpy)_3](PF_6)_2$ is employed as the PC, which reduces the N-Cl sulfoximine **59**, while generating the nitrogen radical that is then added to the double bond of **8**. Addition generates a carbon radical which converts to a product by abstraction of a chlorine atom from the starting material (**59**). This allows the di-functionalization of olefin **8** with the generation of two new bonds, C-N and C-Cl respectively. By carrying the reaction in MeCN under argon atmosphere for 4 h with blue-LED irradiation, it is possible to obtain the N-alkylated product **60** in good to excellent yields (39-90%).

The reaction demonstrates good tolerance to the different nature of the olefin **8,** obtaining good yields with alkyl and aryl olefins bearing different functional groups (53-83% yield). Finally, this process also demonstrates good tolerance to the different nature of the fluorinated alkyl chain, with moderate to excellent yields (39-90%).[68]

- **Fluorinated sulfoximines as nucleophilic fluoroalkylating agents**

Fluorinated sulfoximines can be used as efficient nucleophiles, since due to the presence of electron-withdrawing fluorine substituents it is very easy to deprotonate the acidic proton of the Cα-H bond of sulfoximine. In this manner, a carbanionic species is generated, which is stabilized by the presence of the fluorine substituents.

These intermediate species can be used for various functionalizations that include generic attack on electrophiles. The most prominent application of fluorinated sulfoximines as nucleophiles is as fluoroalkylating agents in olefination processes (Figure 41).

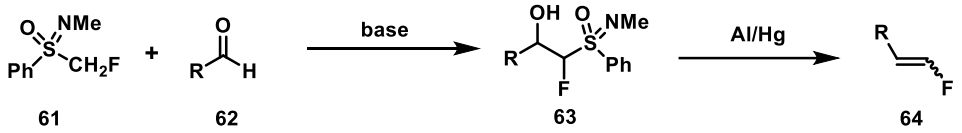

*Figure 41. Example of olefination with fluorinated sulfoximine **61** for the generation of monofluoroalkenes **64**.*

Indeed, as with the sulfone analogs in Julia's reaction, sulfoximines can be employed for olefination of carbonyl compounds **62**. In addition, in the case of fluorinated sulfoximines **61** such reactivity allows the incorporation of fluorine atoms into the product structure, allowing the generation of fluorine-containing olefins **64**.[69]

Working with more reactive species such as nitrones **67** and taking advantage of the good leaving-group capabilities of sulfoximines, the olefination process can also be carried out without the need for the final reduction step with Al/Hg (Figure 42).[70]

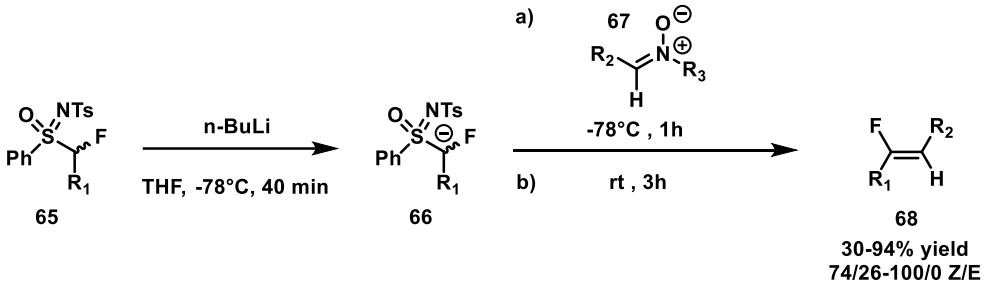

*Figure 42. Example of olefination with fluorinated sulfoximine **65** and nitrone **67** for the generation of monofluoroalkenes **68**.*

- **Fluorinated sulfoximines as electrophilic fluoroalkylating agents**

Since their discovery, sulfoximines have been employed as electrophilic carbon species due to the electron-withdrawing character of the sulfur center. In particular, the Johnson's reagent **69** is employed in organic synthesis as an efficient methyl-transfer reagent by attachment with nucleophiles (Figure 43).[71]

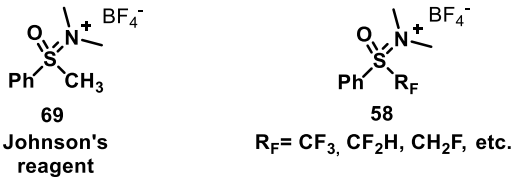

*Figure 43. Structure of Johnson's reagent **69** and fluorinated version of Johnson's reagent **58**.*

Over the past decade, there has been an increased development in the synthesis and use of fluorinated versions of Johnson's reagent for the transfer of variously fluorinated methyls. The process consists of a simple bimolecular nucleophilic substitution (S_N2) with the attachment of an appropriate nucleophile on the electrophilic methyl, resulting in the escape of the optimal N,N-dimethyl benzenesulfinamide **71** leaving group and the generation of the fluorinated species **70** (Figure 44).[65,66]

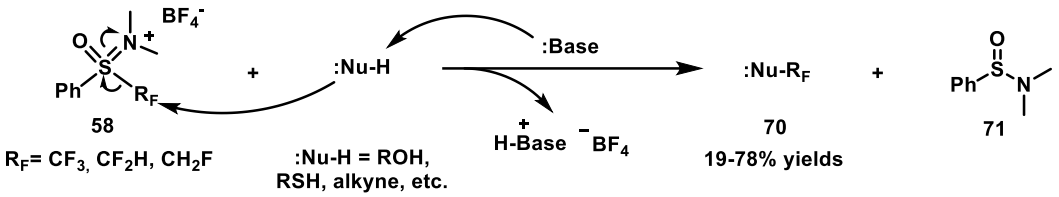

*Figure 44. Example of reactivity of fluorinated Johnson's reagent **58**.*

- **Fluorinated sulfoximines as radical fluoroalkylating agents**

In addition to electrophilic and nucleophilic-type reactivity, fluorinated sulfoximine exhibits extensive and useful radical-type reactivity, which can be triggered under mild reaction conditions through the use of photocatalysis. Using appropriate PCs, it is possible to reduce the fluorinated sulfoximine precursor **72** via single electron transfer (**SET**), promoting mesolytic S-C bond breaking and generating the fluoroalkyl radical **73** (Figure 45).

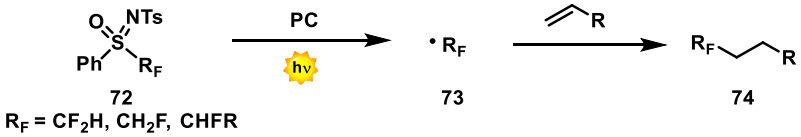

*Figure 45. Radical reactivity of fluorinated sulfoximines **72**.*

The open-shell intermediate **73** can react with different types of radical traps, such as double bonds of olefins, forming products of type **74** [72]

Olefins can be functionalized by inserting other functional groups along with fluoroalkyl substituents. Three examples of possible synthesis strategies are given below.

The first example allows mono- and di-fluoroalkylation of double bonds with additional incorporation of nucleophilic oxygen species (Figure 46).

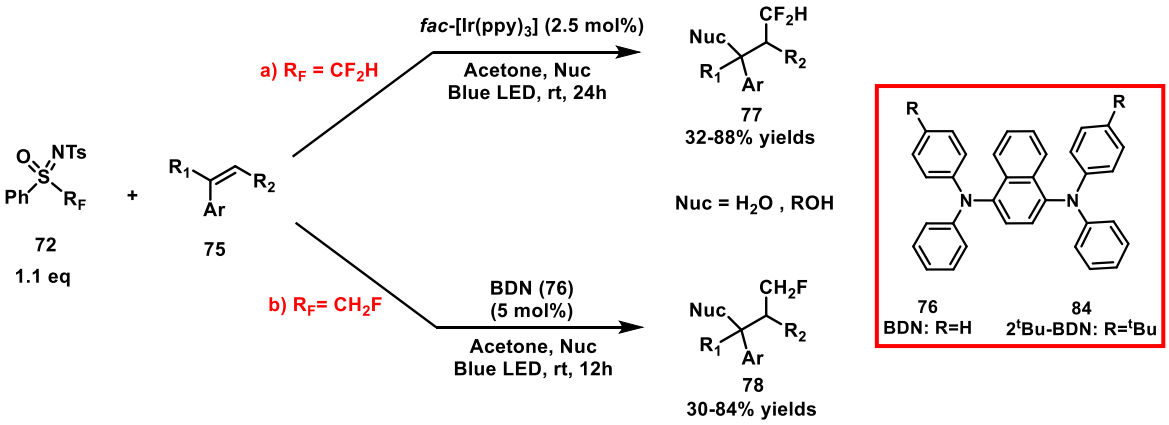

Figure 46. Oxy-mono and oxy-difluoromethylation of aromatic alkenes.

This process allows for simple fluoromethylation of olefins by mixing the two reagents **72** and **75** together with an appropriate PC, respectively *fac*-[Ir(ppy)$_3$] for pathway **a)** and BDN (**76**) for pathway **b).**

The nucleophiles that can be incorporated into the structure are H_2O or alcohols (MeOH, EtOH, etc.) that are used in a mixture with acetone as reaction solvents. Thus, by irradiating with Blue LED for 12/24h it is possible to obtain as products fluorinated alcohols or ethers **77-78** in good to excellent yields (30-88%). When $\mathbf{R_F}$= -CF_2H, the reaction shows good tolerance to variously substituted alkyl and aryl olefins, while in the case of $\mathbf{R_F}$= -CH_2F the process proceeds only with aryl olefins.[72]

With the appropriate choice of nucleophilic species, various fluorinated species of interest can be obtained. In the example above, alcohols and ethers could be obtained, but ketones can also be synthesized (Figure 47).

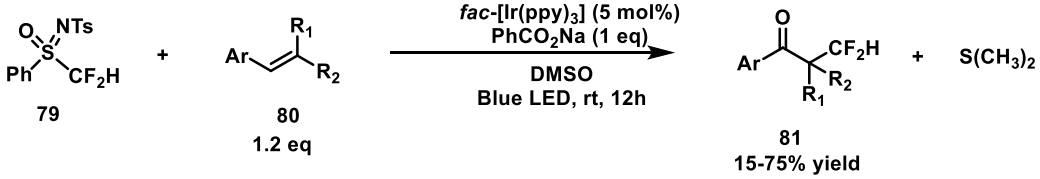

Figure 47. Keto-difluoromethylation of aromatic alkenes **80**.

In fact, by employing dimethyl sulfoxide (DMSO) as the process nucleophile, it is possible to obtain, via a Swern-type reaction mechanism, the corresponding fluorinated ketone **81** in moderate to good yields (15-75%). The reaction, however, tolerates only the use of aryl olefins **80**, but these can be variously substituted in the aromatic ring with simple electron-withdrawing and electron-donating group.[72]

Finally, functionalization of olefins with fluorinated chains is not only restricted to methyl substituents but can also be extended to longer -CHFR alkyl chains.

An example is the α-monofluoroethylation of alkenyl acetates **83** with sulfoximines **82**, in which the monofluoroethyl fragment can be transferred onto the double bond of **83** to form as products fluorinated ketones **85** (Figure 48).

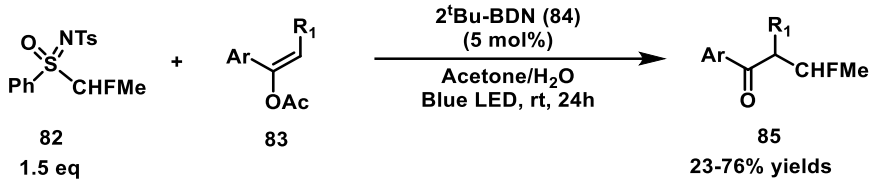

*Figure 48. α-monofluoroethylation of alkenyl acetates **83**, using sulfoximines **82**.*

The reaction tolerates different functional groups on substrate **83**, as long as it is an aryl alkenyl acetate, with moderate to good reaction yields (23-76%).[72]

3. Results and discussions

3.1 Aim of the study

Sulfoximines are of high interest because of their promising applications in diverse fields of research, including medicinal chemistry and material science. Of special importance are fluorinated sulfoximines, whose interesting uses and properties have already been discussed in the previous chapter (Section **2.4**).

So far, it has been seen that fluorinated sulfoximines are mainly used as reagents for the introduction of fluorine-containing motifs in organic compounds. For example, the Johnson's reagent **58** is employed for the fluoromethylation of various nucleophilic species.[65,66]

Nevertheless, due to their unique physicochemical characteristics and relevant biological activity, an increased effort has been observed in recent years in designing new synthetic protocols for introducing fluorinated sulfoximine moieties into molecular structures.[68,73,74] Among these methods, photocatalysis is a suitable approach to develop more sustainable synthetic protocols.

Until now, almost all of the functionalization processes of fluorinated sulfoximines occur in the nitrogen atom (N-functionalization), while no reports are found to perform a Cα functionalization of the fluorinated chain (Figure 49).

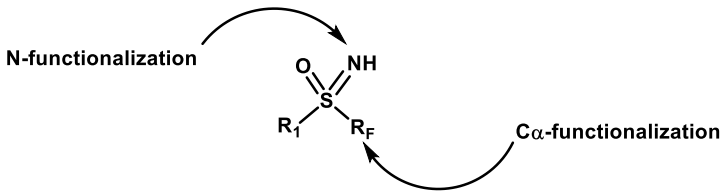

Figure 49. Generic scheme on possible functionalization of fluorinated sulfoximine.

A starting point for the development of new synthetic protocols can be the comparison of the reactivity of sulfoximines analogs: the sulfones.

In that regard, the group of Prof. Dell'Amico has recently developed two strategies for the introduction of sulfones and CF_2-sulfones in organic molecules, specifically in double bonds and in propellanes.[60,75]

The first example concerns a photocatalyzed process for the iodosulfonylation of terminal olefins (**8**), employing α-iodosulfones **86** as the initial substrate and the phenolate derivative **87** as the reducing PC (Figure 50).

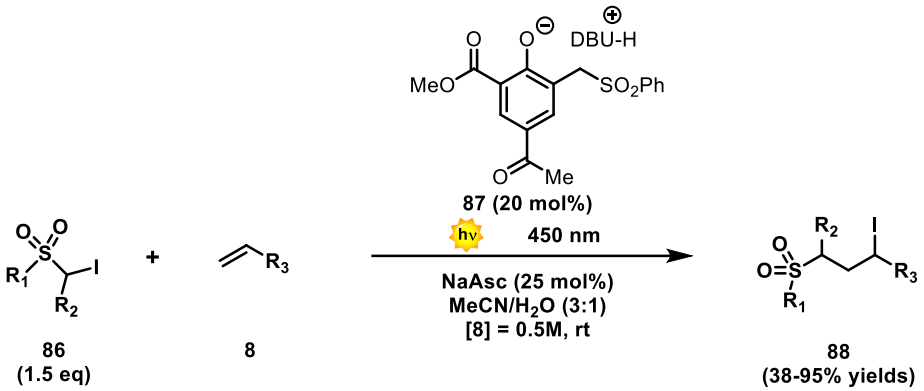

Figure 50. Example of iodosulfonylation of olefins, under photocatalytic conditions.

Under irradiation with visible light at 450 nm, in MeCN/H_2O solvent (3:1) and at room temperature, product **88** can be obtained in good to high yields (38-95%), with the generation of two new σ C-C and C-I bonds. The base 1,5-diazabicyclo(5.4.0)undec-7-ene (**DBU**) and sodium ascorbate (**NaAsc**) are required for the deprotonation of the corresponding pre-catalyst phenol, thus forming the phenolate **87**. The reaction consists of an ATRA process, in which the excited PC **87** reduces the C-I bond of iodosulfone **86** generating the carbon radical Cα, which can then add to the double bond of olefin **8** and thus trigger the radical chain process. The reaction shows good tolerance toward both different functional groups on the olefin **8** reagent (43-85% yields) and toward different aryl and alkyl substituents on the α-iodosulfones **86** substrate (38-95% yields).[75]

This demonstrates how in the case of sulfones it is possible to generate radicals at the Cα carbon, which can then be trapped by alkenes.

The second example concerns a strategy for the synthesis of difluorobicycloalkanes (CF_2-BCAs) via a photocatalyzed ATRA process between the highly strained species [1.1.1]-propellane **90** and molecules containing a difluorobromomethyl substituent (Figure 51). The reaction shows excellent process generality, being able to successfully obtain numerous products of different natures in good to high yields (27-87%).

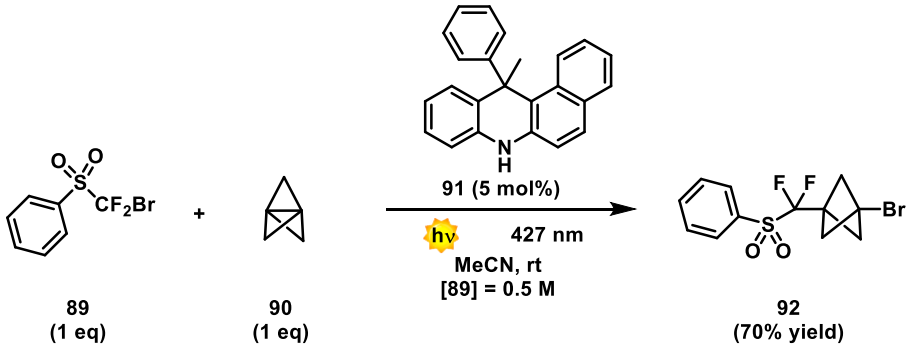

Figure 51. Reaction scheme for the bromo-difluorosulfoximination of [1.1.1]-propellane.

By mixing species **89** and **90** in the presence of the PC **91**, in MeCN solvent at room temperature, the corresponding product **92** could be obtained with a good yield of 70%. This product was obtained through the generation of a new C-C bond on the Cα difluorinated carbon of the sulfone.[60]

This demonstrates how radical-type reactivity can be triggered even for species such as difluorinated sulfones **89**, generating Cα-carbon radical intermediates that, although highly reactive, can be effectively trapped by appropriate radical traps.

Considering the radical reactivity characteristics of α-halogenated sulfones, it was thought to test this type of reactivity in the case of fluorinated sulfoximines.

Specifically, the purpose of this study is to design a photochemical method for the generation of difluorosulfoximine radicals **2**, which can be used in different reaction pathways (ATRA process, strain-release process, etc.). In this specific case of study, difluorosulfoximine radicals **2**, once generated via photoredox catalysis, are reacting with double bonds **8** through an ATRA mechanism. Throughout this process is possible to obtain the di-functionalized products of type **93** (Figure 52). For this purpose, the study of this reactivity is carried out using as model substrate the (bromodifluoromethyl)phenylsulfoximine **1.**

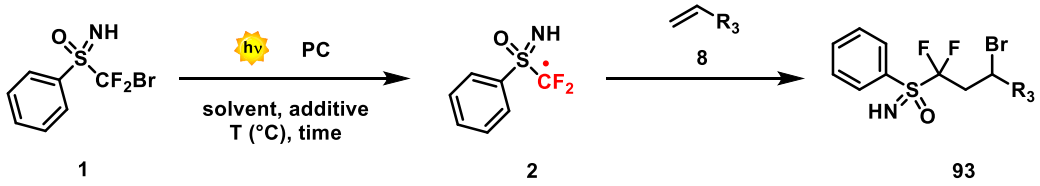

*Figure 52. Proposed reaction scheme for the synthesis of difluoroalkyl-sulfoximines **93**.*

The working hypothesis is shown in Figure 53:

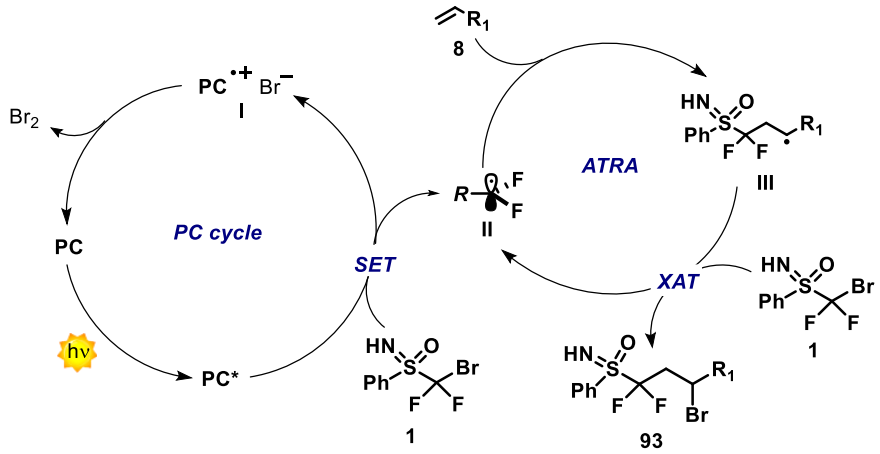

*Figure 53. Proposed ATRA mechanism for the synthesis of difluoroalkyl-sulfoximines **93**.*

The proposed synthetic strategy is based on a photocatalyzed ATRA process. The light-excitation of the reaction system allows the generation, *via* single electron transfer (**SET**) from the PC, of a difluoromethylene radical **II** which is able to undergo an addition process to the double bond of olefins **8** to form intermediate **III**. This intermediate **III**, latter engages in an ATRA mechanism, thus forming the product **93**, while generating another molecule of reactive difluoromethylene radical **II**.

3.2 Preliminary study

The first step in studying the process is to know the value of the reduction potential of the substrate (bromodifluoromethyl)phenylsulfoximine **1**, since only by knowing this value it is

possible to choose the most appropriate PC on the basis of the oxidation potential in the excited state E^*_{ox}.

As follows is a plot of the cyclic voltammetry (CV) measurement for substrate **1**, considering only the reduction potential. This is because a mechanism that proceeds via oxidative quenching of the PC is proposed for the process (Figure 54).

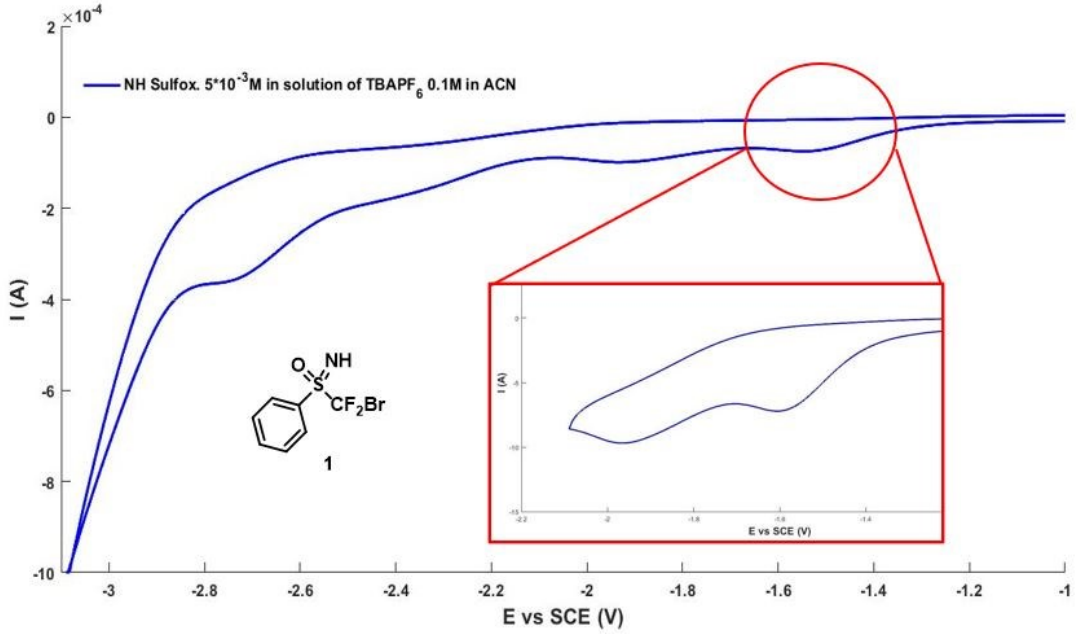

Figure 54. Cyclic voltammetry (CV) of substrate (bromodifluoromethyl)phenylsulfoximine **1.** The CV is reported using the IUPAC convention, in which the oxidative potential sweep runs from left (negative values) to right (positive values) along the x-axis. The anodic peak, on the y-axis, is positive and the cathodic peak is negative.

The experimental value of the reduction potential of species **1** was derived from the measurement, which corresponds to a value of E_{red}= **-1.57 V** vs SCE.
From this data, the photocatalyzed ATRA reaction was performed, testing two possible olefins to find the model substrate for the optimization step: 1-hexene **3** and styrene **38** (Table 2). As the first photocatalyst, the species 12-methyl-12-phenyl-7,12-dihydrobenzo[a]acridine (**PC1**) was employed, characterized by a value of E^*_{ox}= -2.37 V vs SCE.[34]
The reaction was carried out by working in acetonitrile (MeCN), at room temperature and under irradiation with a 427 nm LED lamp (Kessil lamp). This value of λ falls within the tail of the absorption of **PC1**. Once the reaction was carried out, the crude obtained was analyzed by ^{19}F-NMR, evaluating the presence of the product and any by-products and calculating the NMR yield and conversion using the ^{1}H-NMR technique.
If the obtained ^{1}H-NMR yields are promising, the reaction crude is purified by flash chromatography (eluent: hexane/ethyl acetate with increasing polar phase gradient) in order to get the isolated yield value.

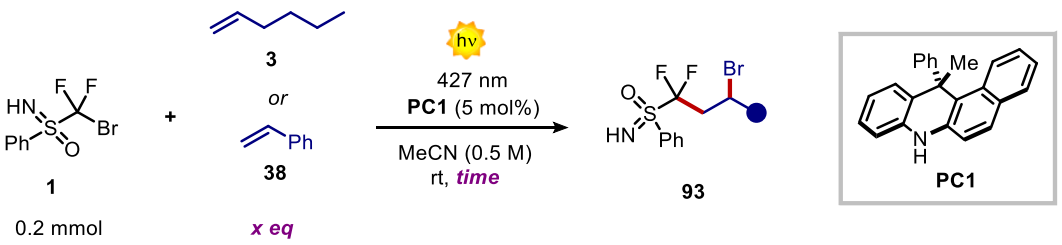

Entry	Olefin	Eq of 12	Time (h)	Yield[a] (%)
1	3	1,5	6	0
2	38	1,5	6	0
3	3	3,0	16	20
4	38	3,0	16	0
5	3	3,0	16	28

[a] All Yield are ^{1}H-NMR Yield with Trichloroethylene as Internal Standard.

*Table 2. Test of 1-hexene **3** and styrene **38** as model substrate for the process.*

The first tests performed (Entry 1-2) with a reaction time of 6 h and 1.5 eq of the olefin reagent resulted in no observable products via ^{19}F-NMR and ^{1}H-NMR. A first promising result was observed only after increasing the reaction time from 6 h to 16 h and doubling the olefin equivalents (Entry 3-4). However, this result is only visible in the case of the substrate 1-hexene (**3**), with a ^{1}H-NMR yield of 20%. In the case of styrene (**38**), no product formation was observed in both attempts (Entry 2-4). For this reason, as the model substrate for the process optimization it was chosen 1-hexene (**3**).

The reaction was then repeated with 1-hexene (Entry 5) to evaluate the reproducibility of the data, obtaining a yield value of 28%. This confirms the reproducibility of the reaction, allowing the study to continue.

3.3 Reaction optimization

3.3.1 First photocatalyst screening

At first, a screening of photocatalysts (PCs) was performed, looking for the species that leads to the greatest increase in the reaction yield. The choice of PCs to be tested was mainly based on their value of oxidation potential in the excited state, which must be higher against the reduction potential of the substrate sulfoximine **1**. The PCs were evaluated at different values of reaction wavelengths (λ), which always located on the tail of the UV-Visible absorption band of the molecule.

The results obtained are shown below (Table 3). The yield values are given below the structure of each molecule, along with the wavelength value (λ) employed. The value in parentheses corresponds to the conversion of the reaction, that is the amount of limiting reagent (substrate **1**) that reacted in the process. Yield and conversion may not match, as the reactant may also take part in other secondary reactions, leading to other species that are different from the desired product.

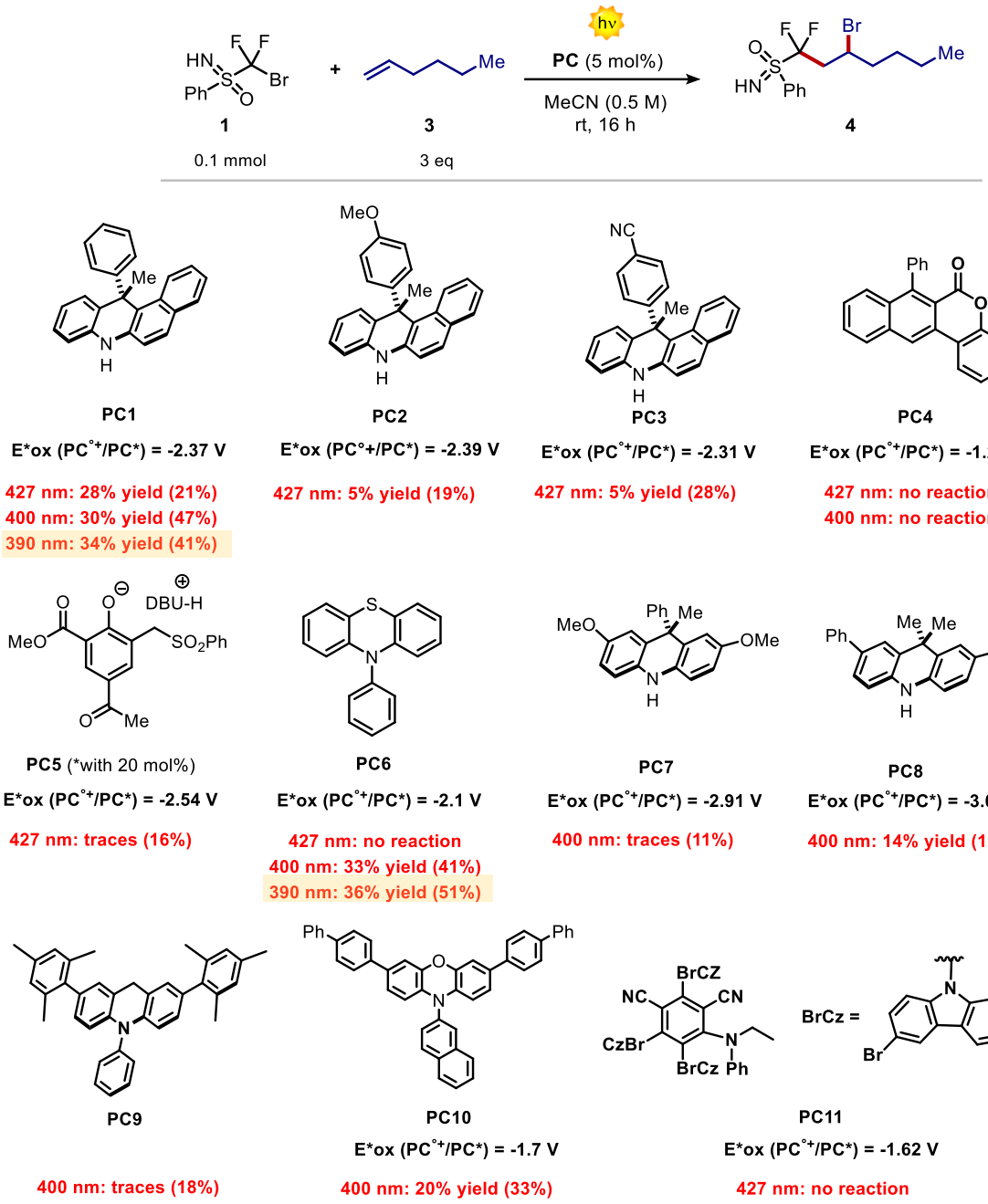

Table 3. First screening of photocatalysts. Results scheme as "λ: yield (conversion)". All Yield and Conversion are ^{1}H-NMR Yield and ^{1}H-NMR Conversion with Trichloroethylene as Internal Standard. NOTE: ***PC9-10-11*** *are insoluble in MeCN.*

What emerges from this initial screening is that there are two best PCs for the process: **i)** the species 12-methyl-12-phenyl-7,12-dihydrobenzo[a]acridine (**PC1**), with a yield of 34%, and **ii)** the 10-phenyl-10H-phenothiazine (**PC6**), with a yield of 36%. Both results were obtained at a working wavelength (λ) of 390 nm.

3.3.2 Screening of the base

As seen above, the two best PCs tested are **PC1** and **PC6**. In the case of the **PC1**, it is reported how it can be used together with an external base in proton-coupled electron transfer (**PCET**) processes (Figure 55).[31]

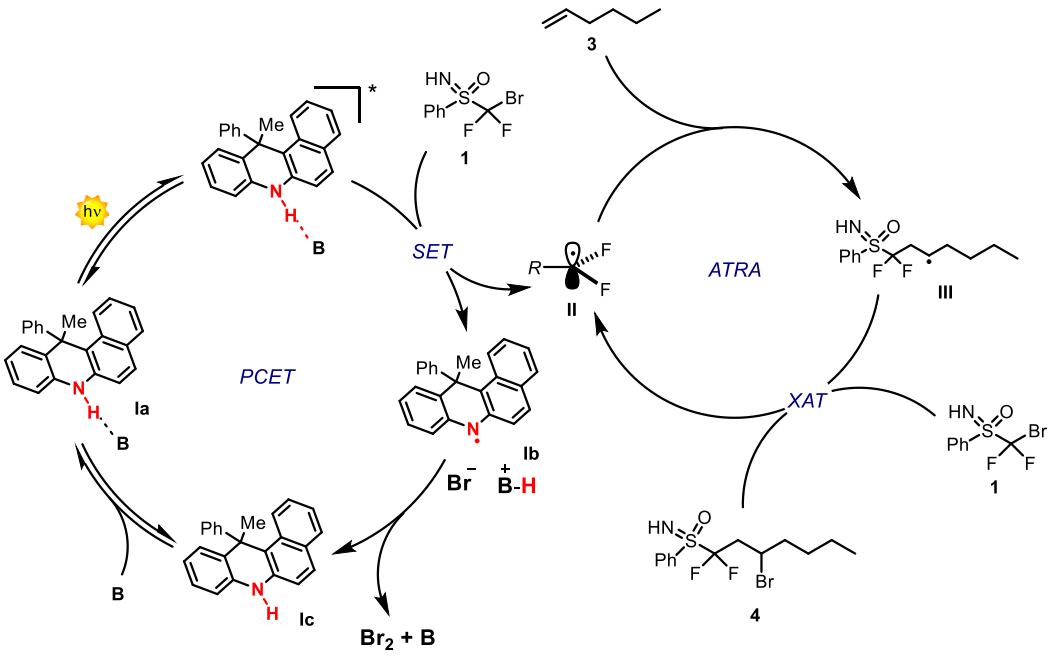

Figure 55. Proposed PCET mechanism for the ATRA process. B: base.

In this phenomenon, the simultaneous deprotonation of the base and the oxidation process of **PC1** leads to the formation of a neutral radical species (**Ib**) that is more stable than the analogous radical cation species. For this reason, the addition of a base can promote the substrate reduction process, as via PCET a more stable intermediate is formed with a consequent lowering of the activation barrier of the reduction process.

With these considerations, several bases were tested to observe whether the reaction can proceed through a PCET mechanism (Table 4).

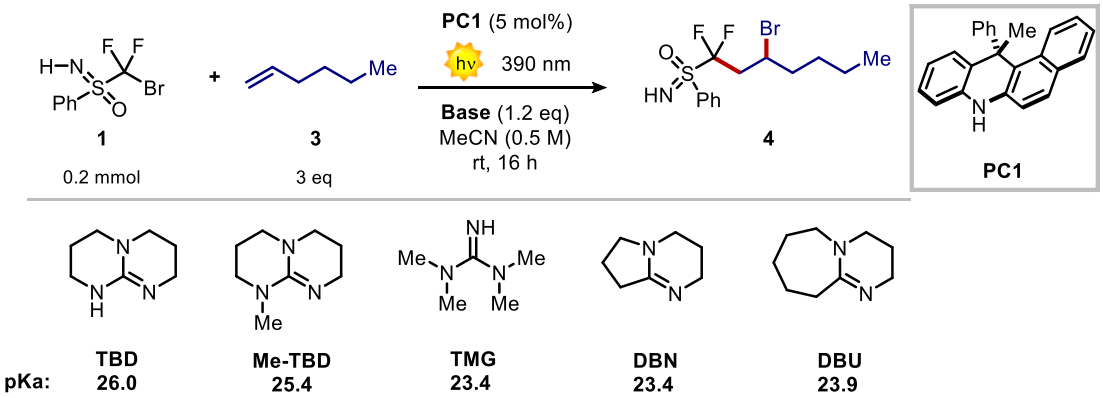

Entry	Base	Conversion[a] (%)	Yield[a] (%)
6	/	41	34
7	TBD	75	23
8	Me-TBD	87	34
9	TMG	76	17
10	DBN	83	28
11	DBU	80	20

[a] All Yield and Conversion are ^{1}H-NMR Yield and ^{1}H-NMR Conversion with Trichloroethylene as Internal Standard.

Table 4. Screening of Base.

From the results, no increase in the reaction yield is observed, but rather in most cases the values obtained were lower than the reaction in the absence of base (entry 6). This indicates that probably the reaction does not proceed through PCET mechanism. Furthermore, what is observed is that the reaction is very sensitive to the various molecular species in the system, due to the formation during the process of highly energetic and reactive intermediates. Therefore, any added molecular species can interfere with the reaction mechanism, reacting with the highly energetic radical intermediates and forming undesirable species as byproducts.

3.3.3 Reaction with N-Ts sulfoximine

Further test was to employ an N-protected sulfoximine as starting materials, specifically an N-Ts (bromodifluoromethyl)phenylsulfoximine **94**. The reduction potential via cyclic voltammetry (CV) was also measured for this substrate, reporting a value of E_{red} = **-1.24 V** vs SCE. The motivation in wanting to test this new substrate (**94**) is that a radical-type reactivity such as that in this reaction can be a problem for the NH-sulfoximine reagent (**1**). In fact, the free N-H group can easily go through hydrogen atom transfer (**HAT**) processes with radical species, thus opening the way for other types of parasitic reactivities leading to the formation of undesirable species. With nitrogen protection, the aim is to limit the formation of byproducts. (Table 5)

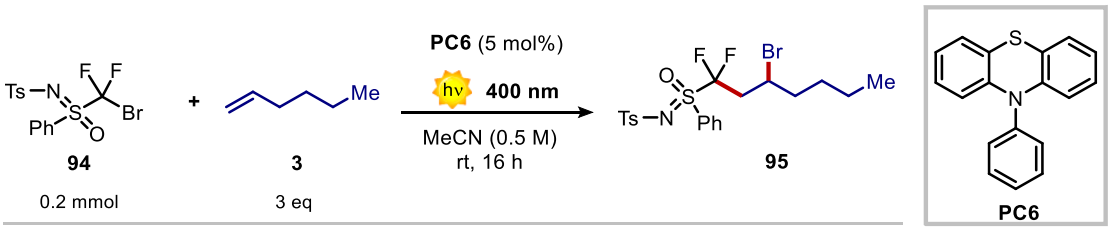

Entry	Solvent	Conversion[a] (%)	Yield[a] (%)	Comments
12	MeCN	22	traces	N-TS Insoluble
13	DCM	67	18	N-Ts soluble
14	Toluene	72	12	N-TS Insoluble
15	Dichlorobenzene	61	14	N-TS Insoluble

[a] All Yield and Conversion are ^{1}H-NMR Yield and ^{1}H-NMR Conversion with Trichloroethylene as Internal Standard.

*Table 5. Text with N-Ts (bromodifluoromethyl)phenylsulfoximine **94**.*

The reaction in MeCN did not lead to results (entry 12), probably due to the insolubility of species **94** in that solvent. Therefore, a small solvent screening was carried out to find the one that leads to a result. The only one in which **94** is soluble is dichloromethane (DCM, entry 13), and in that solvent product formation is observed, albeit in low yield. Such a low value agrees with the peculiar reactivity of fluorinated N-TS sulfoximines. In fact, as described in chapter **2.4**, these sulfoximines are used as reagents for the photocatalyzed process of radical fluromethylation of olefins. This is because once reduced these species undergo mesolytic breaking of the S-C bond, generating the fluoromethyl radical, which then continues with the process. This is reported only in the case of N-protected sulfoximines, particularly N-Ts, probably due to a higher stability of the sulfur anion formed after bond breaking.

As mentioned above, the formation of product **95** in higher yield corresponds to the reaction in DCM (entry 13), but with that we also observe a high conversion that is much higher than the yield. Connected to this event is the observation at ^{19}F-NMR of a new intense doublet at about -43 ppm, which corresponds to neither the product nor the reagent. This indicates how in the case of N-Ts the breaking of the S-C bond to give the •CF_2Br radical is prevalent, as opposed to the breaking of the C-Br bond to give the desired S-CF_2• radical. Testifying to this is precisely this new doublet observed at ^{19}F-NMR, which is probably attributable to some by-product resulting from the generation of the •CF_2Br radical.[65,66]

In the case of NH sulfoximines, the presence of this doublet at -43 ppm is also observed at the end of the reaction, but in less quantity than in the formation of the desired product **4**. Probably the absence of the protecting group leads to less stabilization of the sulfur anion, thus limiting the mesolytic breaking of the C-S bond.

3.3.4 External reductant screening

It has been discussed that the reaction should proceed through an ATRA mechanism (Figure 56), in which the formation of product **4** allows the formation of intermediate **II**, enabling the process to be self-sustaining. In parallel with this, the reaction is also cyclically triggered by the catalytic cycle of the photocatalyst. What has been observed so far is that the reaction proceeds to a certain point and then stops. This can be attributed to the difficulty for the PC to close the catalytic cycle, more precisely to restore the PC to a ground state through the reduction of intermediate **I** (reaction circled in red).

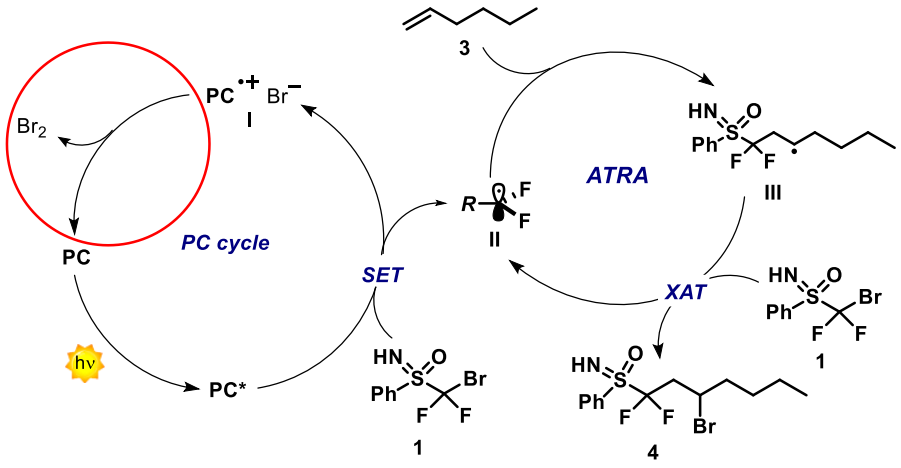

*Figure 56. Proposed ATRA mechanism. The step circled in red is the photocatalyst restoration step via reduction of the intermediate **I**.*

In fact, if the PC is not restored, fewer reaction cycles are triggered and the process eventually blocks. For this reason, reducing species were added to the reaction mixture in order to help and force the reduction step of intermediate **I**. These species should allow a more efficient closing of the catalytic cycle, which can then resume with the reaction and trigger more ATRA processes.

Three different reducing agents were tested: Sodium Ascorbate, DIPEA and Hantzsch ester (Table 6). These species are commonly used to close catalytic cycles in photocatalyzed reactions.[26]

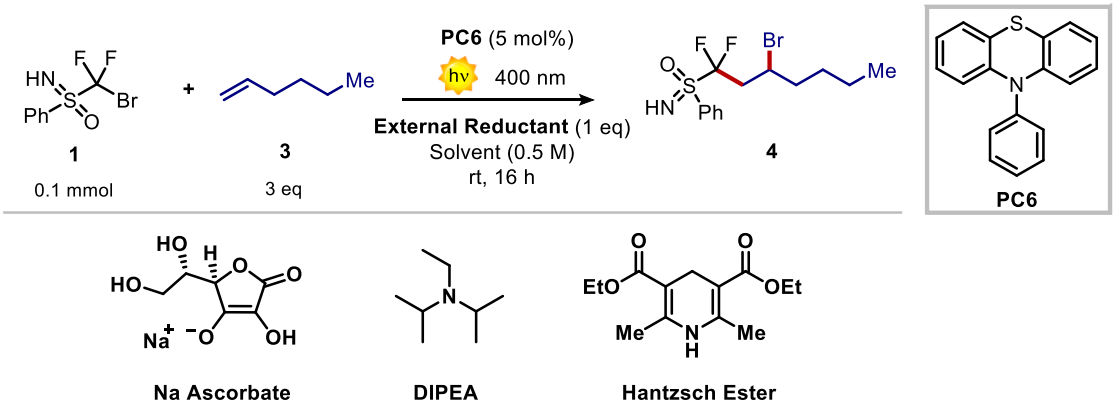

Entry	External reductant	Solvent	Conversion[a] (%)	Isolated Yield (%)	Comments
16	/	MeCN	41	21	/
17	Na Ascorbate	MeCN	81	10	Insoluble
18	DIPEA	MeCN	66	traces	/
19	Hantzsch ester	MeCN	88	43	Insoluble
20	Na Ascorbate	MeCN:H_2O 3:1	85	traces	Soluble
21	Hantzsch ester	MeCN:H_2O 3:1	100	48	Partially soluble

[a] All Conversion are ^{1}H-NMR Conversion with Trichloroethylene as Internal Standard.

Table 6. External reductant screening.

The ^{1}H-NMR analysis of the reaction crudes was particularly difficult, thus leading to the need to derive the isolated reaction yield instead of the ^{1}H-NMR yield.

What was observed was that the addition of DIPEA completely quenched the reaction, yielding only traces of product observable **4** at ^{19}F-NMR.

In the case of Sodium Ascorbate, an isolated yield of 10% was obtained, initially attributed to the insolubility of sodium ascorbate in organic solvent. For this reason, the reaction was repeated using a 3:1 MeCN:H_2O mixture as solvent, but the presence of water combined with the reducing agent quenched the reaction, obtaining only traces of product **4** observable at ^{19}F-NMR.

In the case of the Hantzsch ester, a good isolated yield of 43 and 48% was obtained in both cases (entry 19 and 21), respectively. However, the obtained species does not correspond to the desired product **4** but corresponds to its de-brominated analogue. What was obtained will be discussed in detail in Chapter **3.7**.

3.3.5 Photocatalyst loading screening

Next step was to increase the photocatalyst equivalents in the process from the initial 5 mol% to 10, 15, 20 mol%. Both the two best photocatalysts **PC1** and **PC6** were tested, in the case of **PC1** at two different wavelengths (Table 7).

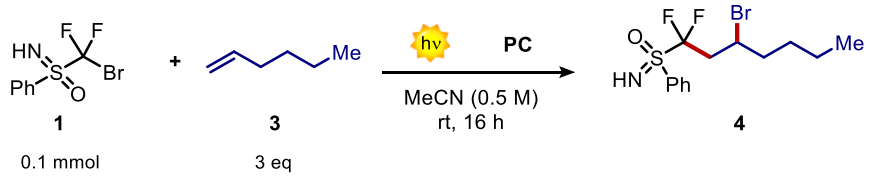

Entry	PC	λ (nm)	% mol of PC	Conversion[a] (%)	Yield[a] (%)	Isolated Yield (%)
16	PC6	400	5	41	33	21
22	PC6	400	10	75	51	/
23	PC6	400	15	100	60	40
24	PC6	400	20	100	54	/
6	PC1	390	5	41	34	/
25	PC1	390	10	62	34	/
26	PC1	390	15	78	48	/
27	PC1	390	20	98	22	/
28	PC1	427	5	21	28	/
29	PC1	427	15	62	47	/

[a] All Yield and Conversion are ^{1}H-NMR Yield and ^{1}H-NMR Conversion with Trichloroethylene as Internal Standard.

Table 7. PC loading screening at different wavelength.

The results obtained show for both **PC1** and **PC6** a yield trend that reaches a maximum value by employing 15 mol% of PC (entries 23-26-29), while moving to 20 mol% the yield starts to drop to lower values (entries 24-27). The best result is that given by **PC6** with 15 mol%, in which a ^{1}H-NMR yield of 60% and an isolated yield of 40% were obtained. This discrepancy can be attributed to the difficulty of calculating the ^{1}H-NMR yield, since there are numerous signals at chemical shift values similar to that of the signal used for the calculation. This creates a baseline of the spectrum that is not perfectly flat, thus lead to an overestimation of the yield.

Good results are also obtained in the case of **PC1** at 15 mol%, with a ^{1}H-NMR yield value of 47%. This good result was obtained by employing a wavelength of 427 nm, which is not far from the 48% yield obtained at 390 nm. This leads us to the conclusion that a less energetic wavelength can be employed for the reaction with **PC1**, such as that at 427 nm.

3.3.6 Second photocatalyst screening

After the results obtained with the two photocatalysts **PC1** and **PC6**, new PCs similar in structure (except PC17-18) were synthesized, that then were tested at different wavelengths (λ). Again, the λ values are located on the tail of the UV-Visible absorption band of the molecule under investigation (Table 8).

The design and characterization of these new PCs will be discussed in detail in Chapter **3.4**.

The yield values are given below the structure of each molecule, along with the wavelength value λ employed. The value in parentheses corresponds to the conversion of the reaction, that is the amount of limiting reactant (substrate **1**) that reacted in the process.

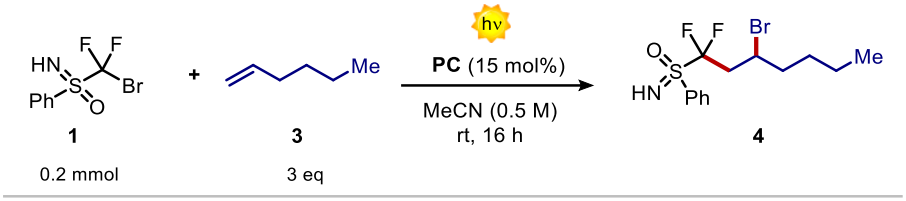

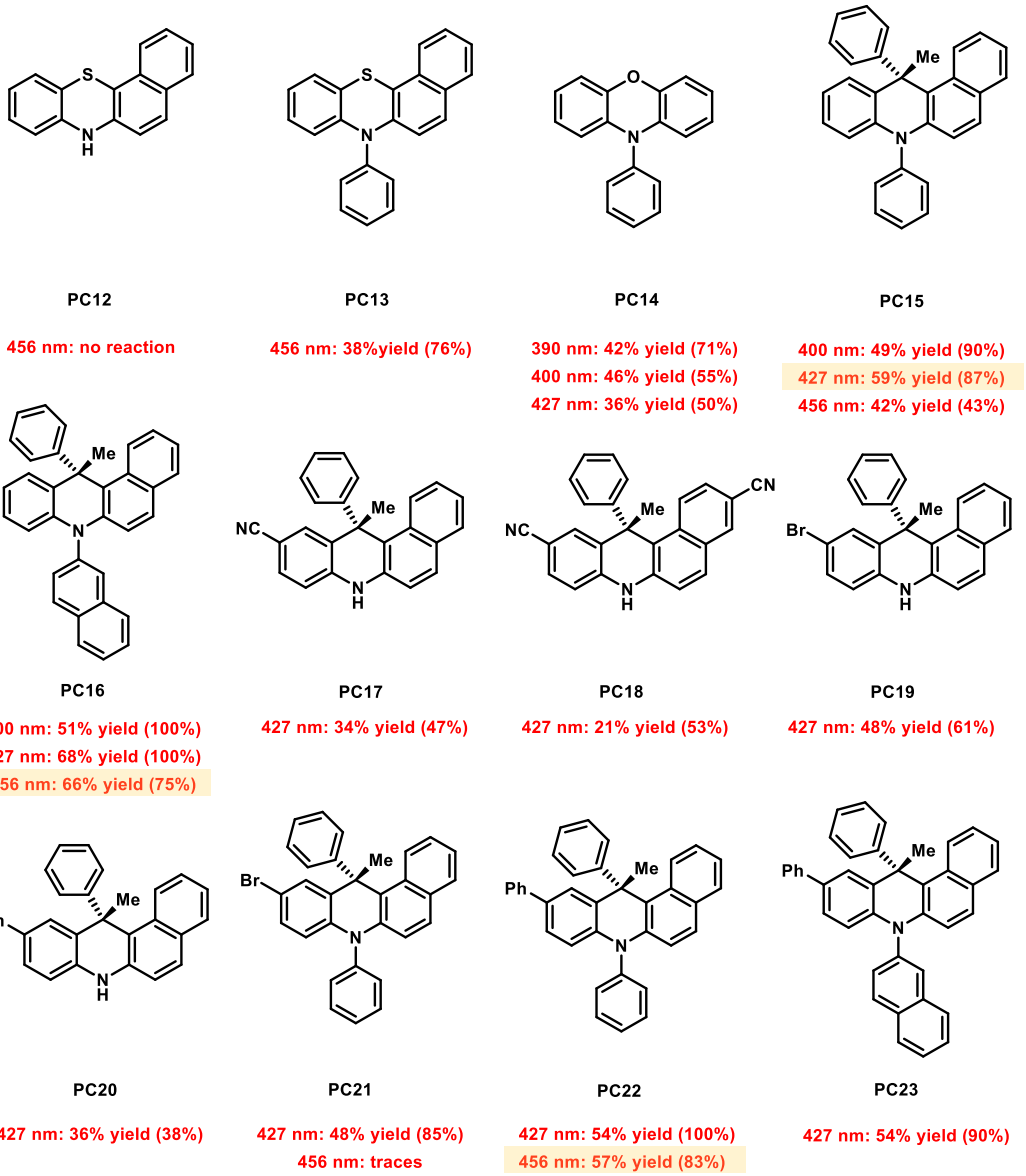

Table 8. Second screening of photocatalysts. Results scheme as "λ: yield (conversion)". All Yield and Conversion are ^{1}H-NMR Yield and ^{1}H-NMR Conversion with Trichloroethylene as Internal Standard.

From the results obtained, it appears that the best ^{1}H-NMR yield results were obtained in the case of **PC15**, **PC16** and **PC22**. For these, the ^{1}H-NMR yield is compared with the isolated yield value obtained after purification by flash chromatography (Table 9).

Entry	PC	λ (nm)	Conversion[a] (%)	Yield[a] (%)	Isolated Yield (%)
30	PC15	427	87	59	49
31	PC16	427	100	68	50
32	PC22	456	83	57	42

[a] All Yield and Conversion are ^{1}H-NMR Yield and ^{1}H-NMR Conversion with Trichloroethylene as Internal Standard.

Table 9. ^{1}H-NMR yield and isolated yield compared.

These results show that the best photocatalyst in terms of highest isolated yield and ^{1}H-NMR yield/isolated yield congruence is **PC15** ((S)-12-methyl-7,12-diphenyl-7,12-dihydrobenzo[a]acridine). In the case of the **PC16** and **PC22**, the difference between the two yield values is too high to consider their possible use in further optimization, since it is uncertain how high this discrepancy might be in subsequent cases.

3.3.7 Decreasing the reaction time

As will be discussed in Chapter **3.8**, the kinetics of the reaction was followed, which showed that the reaction reaches the maximum yield after 8h of reaction, and then no longer increases in value until the reaction is stopped. Therefore, the reaction was repeated under the best reaction conditions so far but decreasing the reaction time from 16h to 8h (Table 10).

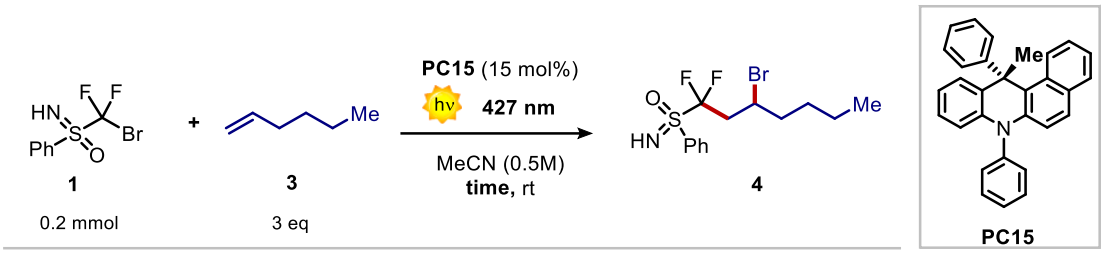

Entry	Time (h)	Conversion[a] (%)	Yield[a] (%)	Isolated Yield (%)
33	24	100	50	/
30	16	87	59	49
34	8	100	59	50

[a] All Yield and Conversion are ^{1}H-NMR Yield and ^{1}H-NMR Conversion with Trichloroethylene as Internal Standard.

Table 10. Decreasing of the reaction time.

What emerges is that after 8h of reaction the same result is obtained as in the past with 16h of reaction. For this reason, from now the reaction can be safely stopped after 8h, thus going to limit the formation of by-products that could be generated during the classic 16h of previous reactions. Moreover, with this decrease in reaction time, the over-irradiation of the reaction mixture is also limited. The latter in fact can lead to degradation of the product through undesirable reaction pathways.

3.3.8 Best results of the reaction optimization

Other reaction parameters were evaluated during the optimization process, including: solvent screening, stoichiometry test, reaction temperature test, concentration screening and light source intensity screening (Kessil lamp).

At the end of the optimization process, it was possible to increase the reaction yield from an initial value of 20% via ^{1}H-NMR to a final result of 59% via ^{1}H-NMR, with isolated yield of 50%. This value is obtained by mixing substrates **1** and **3** in molar ratio of 1:3, in the presence of 15 mol% of **PC15**, irradiating at 427 nm (25% intensity) for 8h in MeCN solvent (0.5M) at room temperature (Figure 57).

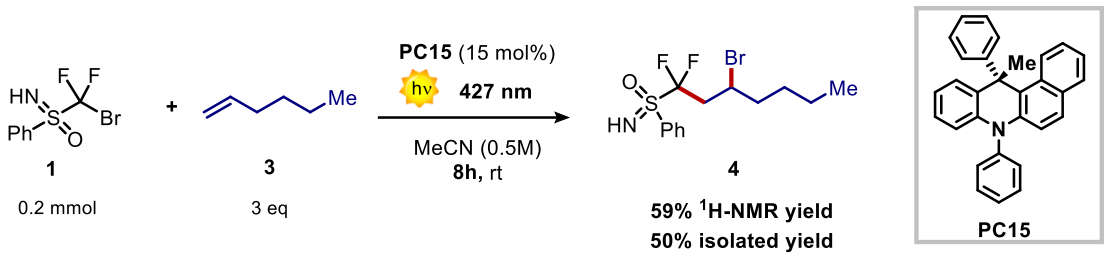

Figure 57. Best result of the reaction.

3.4 Photocatalysts synthesis and design

From the first screening of photocatalysts performed in the optimization phase (Section **3.3.1**), the **PC1** (12-methyl-12-phenyl-7,12-dihydrobenzo[a]acridine) and **PC6** (10-phenyl-10H-phenothiazine) species emerged as the best PCs. Considering this, it was decided to synthesize new PCs analogous in structure to **PC1** and **PC6**, with the aim of optimizing the structures in order to increase the reaction yield. In particular, the synthesis of these new PCs is aimed at solving some problems for **PC1** and improving some photophysical properties in **PC6** (Figure 58).

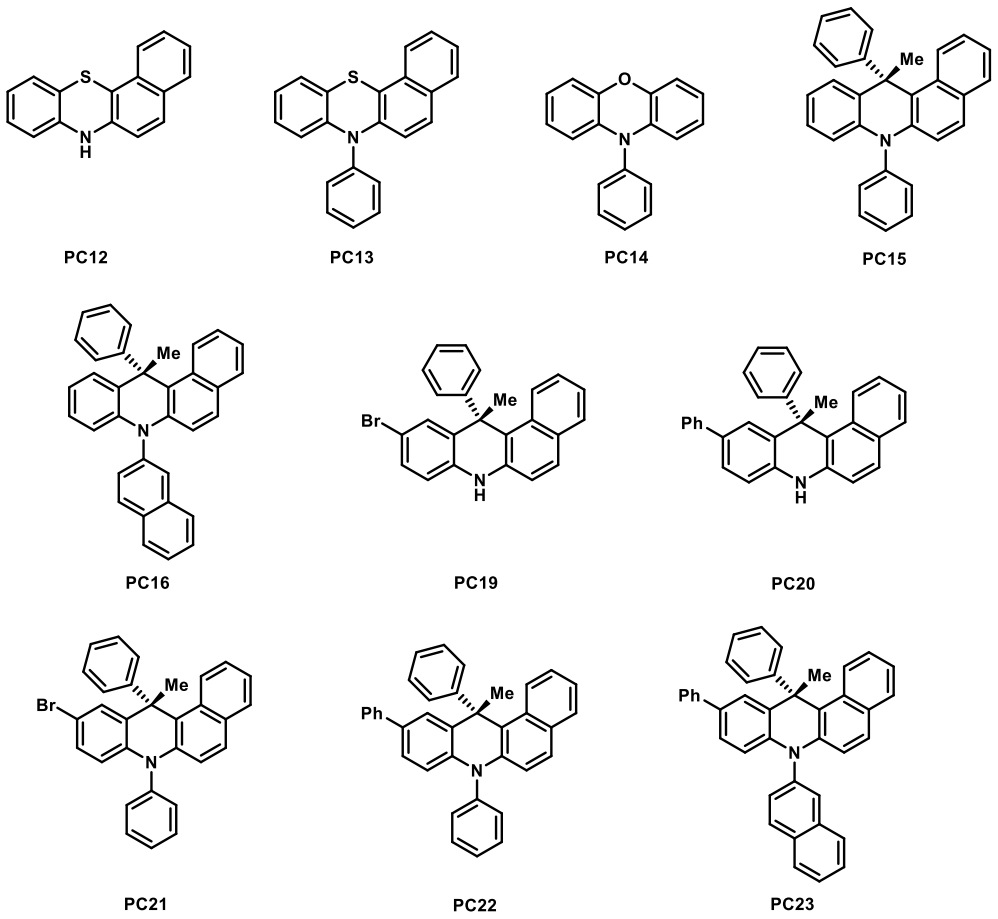

Figure 58. New synthesized photocatalysts.

Specifically, with the **PC6**, one is limited in using light sources with wavelengths no greater than 400 nm, as above this threshold the PC is no longer able to absorb. This turns out to be a major limitation, since if possible one wants to avoid using light sources at low wavelength values, tending toward the near UV. This is because in that range more molecular species, including reaction intermediates, can absorb light thereby opening other reaction pathways with the formation of byproducts. Therefore, optimization of the **PC6** focused on expanding the wavelength range in which it is capable of absorbing, moving more toward absorption in the visible. To do this, inspired by the structure of **PC1**, it was decided to add a benzene ring by condensing it to the phenothiazine core.

The synthesis of this new **PC12** (7H-benzo[c]phenothiazine) molecule consists of a cyclization of the starting material N-phenylnaphthalen-2-amine (**96**) in the presence of sulfur and iodine, via condensation of a sulfur atom on the amine (Figure 59).[76]

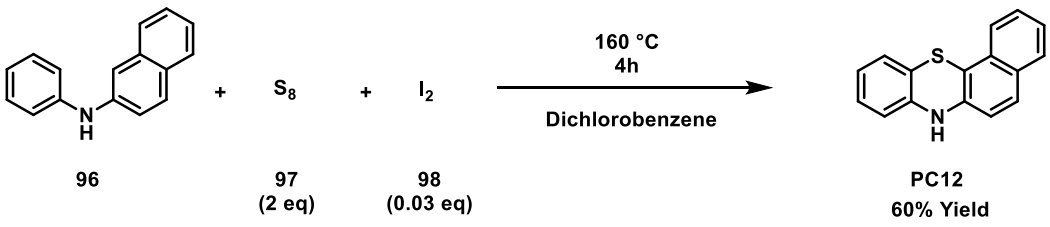

*Figure 59. Synthesis of 7H-benzo[c]phenothiazine (**PC12**).*

After that, a Buchwald-Hartwig reaction was performed for the synthesis of the photocatalyst 7-phenyl-7H-benzo[c]phenothiazine (**PC13**), which consists of a cross-coupling between an amine and an aryl halide (ArX) catalyzed by Palladium.[77] In this way, the reaction effectively allows the generation of a new N-C bond. As follows is the general procedure employed (Figure 60):

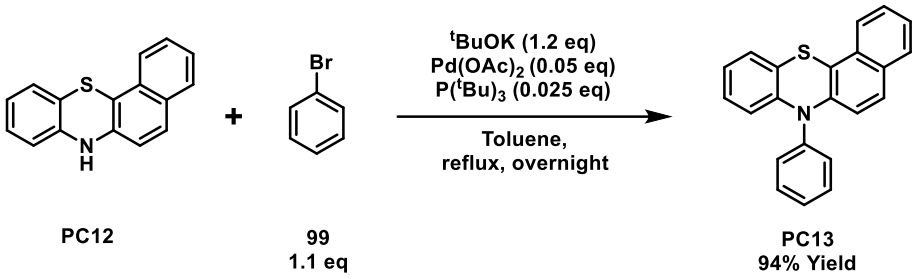

*Figure 60. Synthesis of 7-phenyl-7H-benzo[c]phenothiazine (**PC13**).*

In addition to the shift toward the visible of the absorption spectrum of the PC, the addition of a condensed aromatic ring should lead to increased stability of the cation radical that is generated after the single elctron tranfer (**SET**) process of the PC in the excited state. This increase in stability should also lead to a change in the oxidation potential in the excited state of the PC.

In addition to the expansion of the PC core, I tried to synthesize an analog of **PC6** in which I replaced the sulfur heteroatom with an oxygen atom, the smallest analog of group 16 in the periodic table. This was to see if changing the heteroatom resulted in a change in the reducing power of the PC and thus a change in reactivity toward sulfoximine **1**.[78]

The synthesis of the **PC14** (10-phenyl-10H-phenoxazine) consists of a Buchwald-Hartwig reaction, with similar reaction conditions as the general procedure in Figure 60. In this way, starting from the phenoxazine substrate, it was possible to obtain the **PC14** product with a yield of 89%.

In the case of the **PC1**, structural optimization focused on the free NH group of the molecule. In fact, as already reported, the **PC1** is normally employed in the presence of a base in order to carry out PCET processes, which was seen not to be the case in our reaction (Section **3.3.2**). Therefore, since there is no need to exploit the free NH group, it was preferred to protect it with phenyl or naphthyl groups to avoid PC degradation processes. In fact, a free NH group in a radical-type process such as the reaction under consideration can react with intermediate radical species through hydrogen atom abstraction (**HAT**) processes. With this, a radical nitrogen species is generated that can no longer close the catalytic cycle and restore the PC, leading to its deactivation and shutdown of the catalytic process.

Through NH protection, all HAT-type processes on nitrogen are blocked, safeguarding the PC from possible degradation processes. Among the various possible substituents that can be installed on nitrogen, the phenyl group (**PC15**) and 2-naphthyl group (**PC16**) were chosen, with the aim of observing whether it is possible to extend the absorption spectrum of the PC into the visible. In addition, with the installation of aromatic substituents, I want to understand whether it is possible to stabilize the cation radical **I** of the PC (generated after the single electron transfer process) and whether this has an influence on the oxidation potential in the excited state of the PC.

In addition to this, there is a reaction protocol in the literature for selectively installing a bromine substituent at the para position of phenylamines.[79] This bromination reaction requires only $CuBr_2$ and the oxidizing species oxone (Potassium peroxymonosulfate). This reactivity proves to be particularly selective for the para position and, more importantly, proves to be selective for bromination of phenyl substituents even in amines containing other aromatic substituents, such as naphthyl groups (Figure 61):

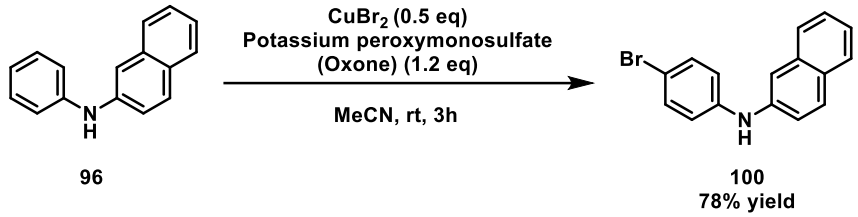

Figure 61. General reaction scheme for the regioselective and controllable bromination of aromatic amines.

With these considerations, this protocol was tested on the **PC1** to install a bromine atom at position 10 of the acridine core (Figures 62). This opens the way for new possible functionalization of the molecule with the possibility of tune its physicochemical properties.

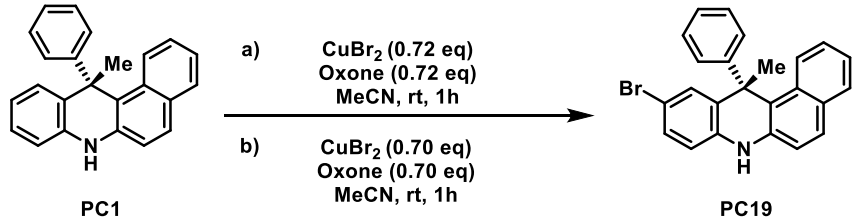

Figure 62. Bromination of **PC1**.

Once the brominated derivative **PC19** was obtained, several functionalization followed, among which the most promising appears to be the installation of a phenyl group (**PC20**). The synthesis of **PC20** consists of a Suzuki-Miyaura reaction, which allows the formation of new C-C bonds through coupling between an aryl halide and an aryl boronic acid.[80] The reaction is catalyzed by Palladium (Figure 63):

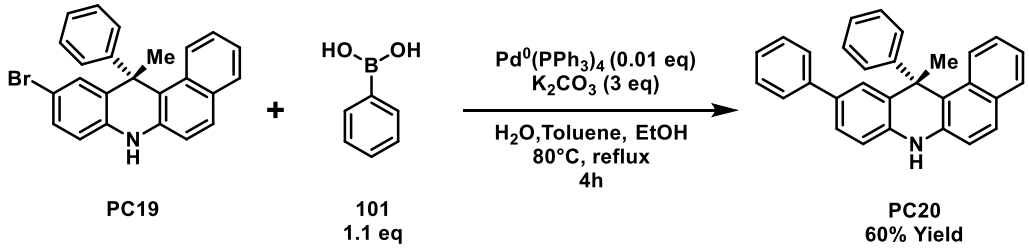

*Figure 63. Reaction scheme for the synthesis of **PC20** via Suzuki-Miyaura reaction.*

I wanted to focus on the synthesis of **PC19** and **PC20** because, as already seen in Section **3.3.6**, these two PCs showed promising structures for PC optimization. In fact, **PC19** showed an excellent ^{1}H-NMR yield of 48% while in the case of **PC20**, despite a lower yield of 36%, the reaction was particularly clean at ^{19}F-NMR, with little by-product presence. This suggested that in the case of **PC20** there is greater photocatalyst stability, making it an excellent starting point for PC optimization.

Therefore, **PC19** and **PC20** were used for the synthesis of additional structures through the installation of phenyl or naphthyl groups.

The installation of these substituents was based on a Buchwald-Hartwig reaction. The generic procedure is given below (Figure 64):

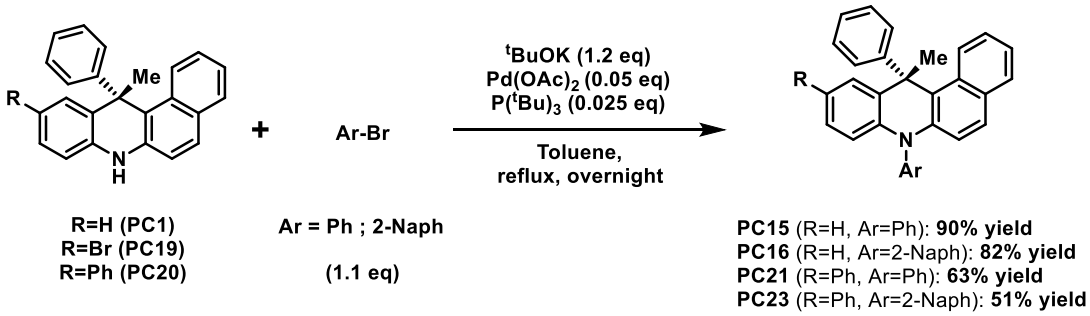

Figure 64. General procedure for the Buchwald-Hartwig reaction.

This generic procedure allows the synthesis of **PC15**-**16** and **PC22**-**23**.[81] In the case of **PC21**, however, this protocol is not suitable because it does not tolerate the presence of the bromine substituent in the reactant molecule. In fact, this bromine could take part in the Buchwald-Hartwig reaction leading to the generation of unwanted species that are difficult to purify and also lower the yield of the process. For this reason, a new protocol with the following modifications was used in the case of **PC21** (Figure 65):

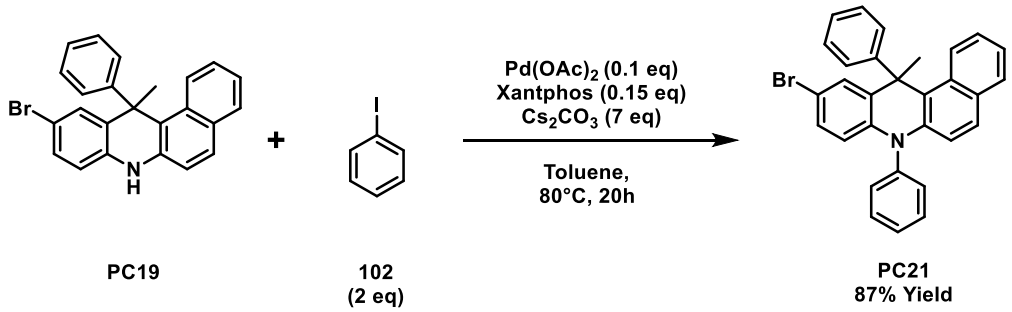

*Figure 65. Reaction scheme for the synthesis of 10-bromo-12-methyl-7,12-diphenyl-7,12-dihydrobenzo[a]acridine (**PC21**).*

First change is the replacement of the $P(^tBu)_3$ ligand with a more deactivated ligand known as Xantphos. Added to this is the use of iodobenzene **102** instead of bromobenzene **99**, a reagent that is more active toward cross-coupling. Finally, last change is the increase of the species equivalents from 1.2eq to 2eq, to force Palladium attachment on iodobenzene **102** instead of on the C-Br bond of **PC19**.[82]

3.5 Photophysical characterization

3.5.1 UV-Visibile absorption spectra

The UV-Visible absorption spectra of the ten synthesized PCs are shown below. Each spectrum was measured in acetonitrile solution with a concentration of 0.015M, where each photocatalyst showed good solubility. Each spectrum is reported by plotting absorbance against wavelength. For a better understanding of the data obtained, the spectra of the PCs

were divided into two groups: class of analogous photocatalysts in **PC6** structure (Figure 66) and class of analogous photocatalysts in **PC1** structure (Figure 67):

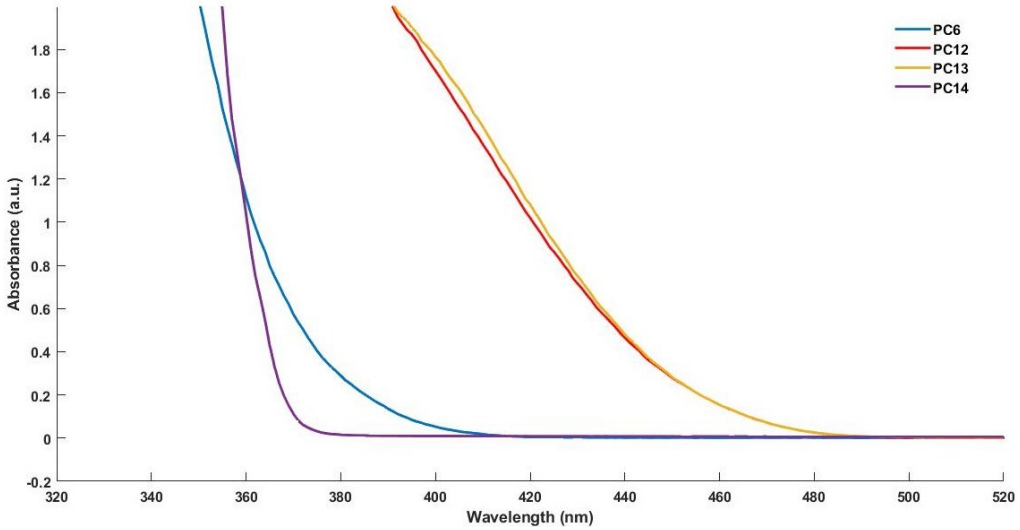

*Figure 66. UV-Visible Absorption spectra of **PC6**, **PC12-14**. PCs were in 0.015M solutions in MeCN.*

What is observed in Figure 66 is that the addition of the condensed benzene ring in the **PC6** structure has led to greatly extending the ability of the new **PC12-13** to absorb light in the visible wavelength range. In fact, initially **PC6** absorption was extinguished above 400 nm, whereas now **PC12-13** are capable of absorbing up to a wavelength of nearly 480 nm. The addition of the phenyl substituent in **PC13** did not lead to any change in the absorption capacity of the photocatalyst.

As for **PC14**, the replacement of a large, polarizable heteroatom such as sulfur with a small, polarizing atom such as oxygen led to a decrease in the absorbance capacity of the PC, which is capable of absorbing up to a wavelength maximum of 370 nm.

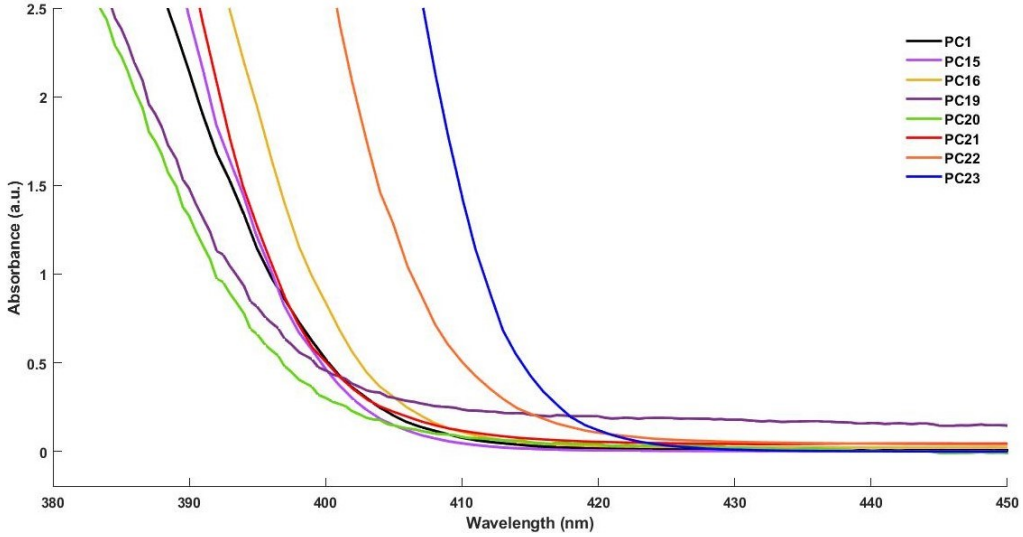

*Figure 67. UV-Visible Absorption spectra of **PC1**, **PC19-23**. PCs were in 0.015M solutions in MeCN.*

What is observed in Figure 67 is that the addition of a phenyl substituent in **PC15** does not go to change the range of light absorption by the photocatalyst. In contrast in **PC16**, the addition of the 2-naphthyl substituent slightly increases the absorption range toward wavelengths in the visible. Counterintuitively, however, in the case of **PC19-20**, the addition of the bromine-phenyl substituent at position 10 of the acridine core decreases the extent of absorption by the photocatalyst, with a shift of the absorption maximum to shorter wavelengths. In the case of **PC22** and **PC23**, the two phenyl substituents in **PC22** and phenyl-naphthyl in **PC23** increase the absorption range in the visible, with a limit extending above 420 nm for both PCs.

3.5.2 EDA complex formation

EDA complex is a molecular aggregate that originates in the ground state when an acceptor molecule **A** (Lewis acid) and a donor molecule **D** (Lewis base) associate with each other (Figure 68). This aggregate is of interest because its light absorption properties differ substantially from those of the two isolated **A** and **D** molecules. In fact, typically an EDA complex is characterized by the presence of new charge transfer bands that exhibit red-shifted absorption in the visible spectrum. These bands are absent in the two isolated **A** and **D** molecules, which may also be unable to absorb in the visible. In addition, absorption of light by the EDA complex can trigger an intramolecular single electron transfer process, which can occur kinetically faster than the same intermolecular process. With this, it is possible to generate radical species under mild condition.[83]

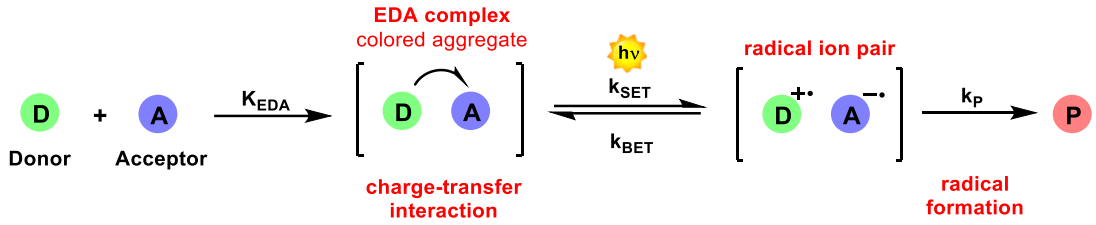

Figure 68. EDA complex theory. K_{EDA}: EDA association constant; k_{SET}: kinetic constant for direct-single electron transfer (SET); k_{BET}: kinetic constant for back-single electron transfer (BET); K_P: kinetic constant for the formation of the products.

The formation of EDA complexes is of considerable interest in photochemistry, although there are several complications to take into account. The main one is that many EDA complexes are not productive from a synthetic point of view because it is difficult to avoid the fast process of unproductive back-electron-transfer (BET) from the radical ion pair, which restores the ground-state EDA complex without triggering any kind of reactivity.

A possible resolution to the problem turns out to be the presence in the aggregate of an appropriate leaving group which, once the radical anion **$[D^{\bullet+}A^{\bullet-}]$** is generated, triggers irreversible fragmentation of the leaving group that can compete kinetically with the BET. This blocks the BET process, being able to exploit the EDA complex for synthetic purposes.[83]

This strategy can also be applied for our ATRA addition reaction on olefins, as after the SET process on sulfoximine **1** there is irreversible fragmentation of the C-Br bond with the generation of the carbon radical **II** and bromide Br-.

With these considerations, the ability to form a donor-acceptor complex (EDA complex) with the substrate (bromodifluoromethyl)phenylsulfoximine **1** was investigated for each photocatalyst synthesized**.**

The investigation was followed by UV-Visible spectroscopy, comparing the spectra of three different solutions: isolated substrate solution, isolated PC solution and substrate + PC solution in the same molar ratio used for the reaction. All solutions are at the same concentrations of the species in the reaction mixture. Once the various spectra are recorded, these three are compared. If the spectrum of the substrate+PC solution shows new absorption bands or a red-shift in absorption then there is an EDA complex.

Considering the numerosity of the spectra, only one example is given below, specifically that of **PC14**. (Figure 69). The remaining spectra will be reported in Chapter **5** "Supporting information" at the end of this thesis.

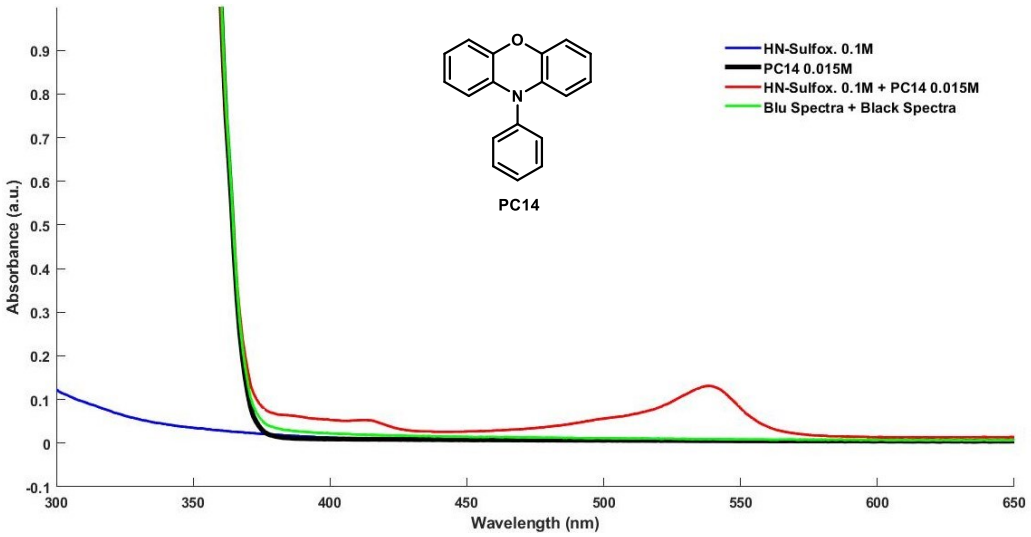

*Figure 69. Search for the formation of an EDA complex for the **PC14**. Solutions in MeCN.*

What is particularly interesting is that in the case of **PC6**-like catalysts (**PC12-14**), the formation of a band centered at about 500-550 nm for **PC6** and **PC14** and a band centered at about 600-650 nm for **PC12** and **PC13** is observed. This is interesting since this aggregate could absorb light at the wavelength of the new band and trigger a **SET** process on the sulfoximine substrate **1**. This would be a huge advantage since it would be possible to carry out the reaction by irradiating with wavelengths in the visible, making this process extremely sustainable and suppressing much of the parasitic reactivities related to the absorption of intermediate species. For this reason, all of these four PCs were tested by carrying out the reaction with light of wavelengths of 525 nm (Table 11).

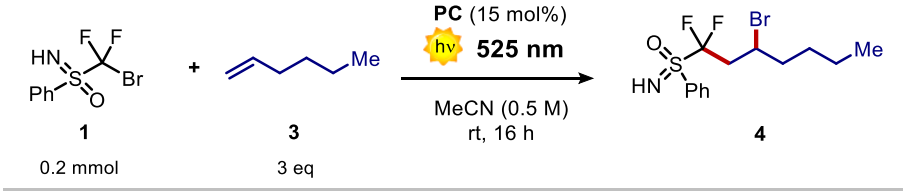

Entry	PC	λ (nm)	Conversion[a] (%)	Yield[a] (%)
35	PC6	525	0	no reaction
36	PC12	525	0	no reaction
37	PC13	525	0	no reaction
38	PC14	525	0	no reaction

[a] All Yield and Conversion are ^{1}H-NMR Yield and ^{1}H-NMR Conversion with Trichloroethylene as Internal Standard.

Table 11. Reaction test at 525 nm.

Unfortunately, product formation was observed for none of the four PCs. In good probability, the back-electron transfer (BET) process is too kinetically fast even for the irreversible fragmentation of the C-Br bond of the reduced sulfoximine.

3.5.3 Fluorescence emission

The emission spectra of the PCs were recorded in acetonitrile (MeCN) solvent, irradiating the solutions at the λ_{max} of the corresponding absorption spectra. Considering the numerosity of the measured spectra, the spectra are grouped into two different graphs to make them easier to read (Figure 70 a-b).

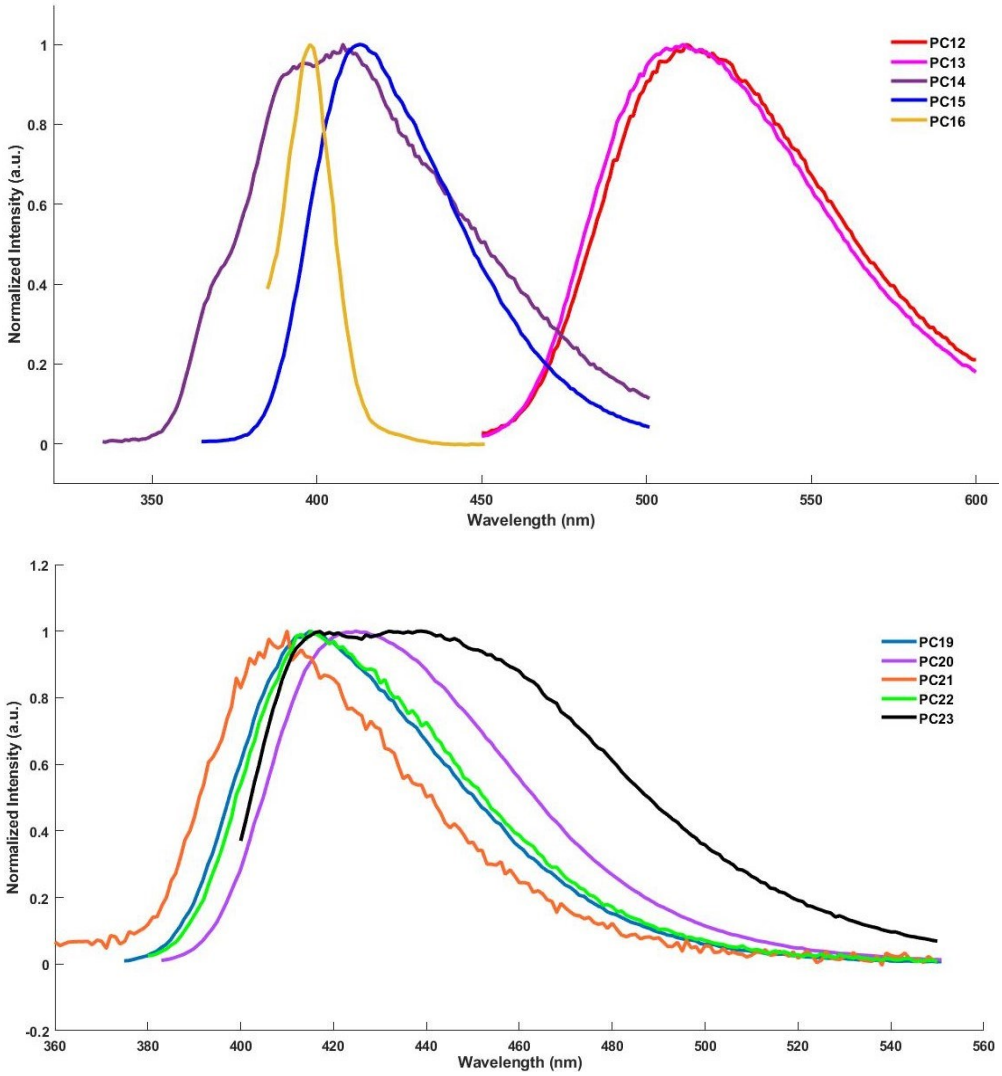

*Figure 70. a) Emission spectra of **PC12-16**. b) Emission spectra of **PC19-23**.*

For each PC, the experimental value of $E_{0,0}$ was derived. This spectroscopic parameter can be obtained experimentally by superimposing the absorption spectrum of the photocatalyst together with its emission spectrum. The wavelength value at which there is the intersection of its spectra corresponds, once converted to eV, to the value of $E_{0,0}$.[84,85,86]

3.5.4 Cyclic voltammetry measurement

Cyclic voltammetry measurements of the various synthesized PCs are reported below. Since in the reaction under analysis the PC reacts through a mechanism via oxidative quenching, only the potentials under oxidation were measured. Again, because of the large number of spectra measured, these spectra are grouped into two different graphs to make them easier to read (Figure 71 a-b).

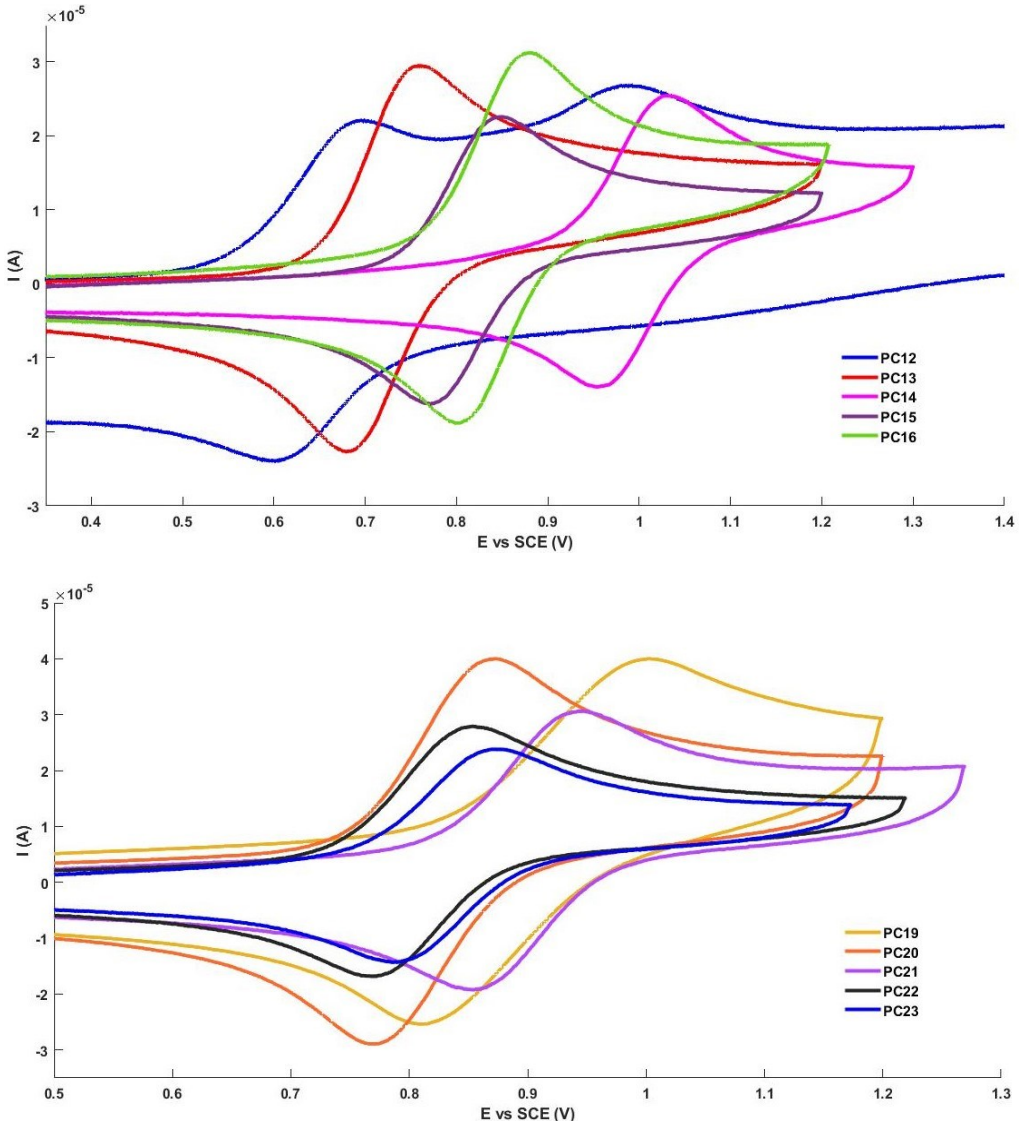

*Figure 71a-b. Photocatalysts Cyclic voltammetry (CV). CV were performed on 5*10^{-3}M PCs samples in TBAPF$_6$ 0.1M solution in MeCN. The CVs are reported using the IUPAC convention, in which the oxidative potential sweep runs from left (negative values) to right (positive values) along the x-axis. The anodic peak, on the y-axis, is positive and the cathodic peak is negative.*

What is observed in cyclic voltammetries is that in the case of **PC6** derivatives (E_{ox} = 0.68 V vs SCE) the addition of the condensed ring in **PC12** shifts the oxidation potential to smaller values. In **PC13** the addition of the phenyl substituent leads to a slight increase in the potential, which still remains lower at the **PC6** value. In **PC14** the substitution of the sulfur atom for oxygen does not lead to a substantial change in potential compared with **PC6**.

In the case of **PC1** analogs (E_{ox} = 0.76 V vs SCE), the addition of the N-aryl substituents leads to an increase in oxidation potential compared with **PC1**. In contrast, the presence of the phenyl substituent at position 10 of the acridine core in **PC20** does not lead to substantial changes in the oxidation potential compared to the unsubstituted analogs. In the case of **PC19**, the presence of the Bromine substituent leads to a discrete increase in the oxidation potential. This increase, however, is partly lost in **PC21** with the addition of the N-phenyl substituent, with the E_{ox} value being closer to the potential values of the unsubstituted analogues.

3.5.5 Calculation of oxidation potential in excited state

Once the UV-Vis absorption, fluorescence emission and cyclic voltammetry spectra were measured, it was possible to derive from these the values of the parameters $E_{0,0}$ and oxidation potential E_{ox} (as $E_{1/2}$). These data are useful because they make it easy to calculate the value of the oxidation potential of a molecular species in the excited state, such as a photocatalyst.

In fact, it has been shown how it is possible to estimate this parameter through the simple formula:[87]

$$\mathbf{E^*_{ox}(PC^+/PC^*)\ [V] = E_{ox}(PC^+/PC)\ [V] - E_{0,0}\ [eV]}$$

Where E^*_{ox} (PC^+/PC^*) is the oxidation potential in excited state (V), E_{ox} (PC^+/PC) is the oxidation potential in ground state (V), $E_{0,0}$ is the transition energy from the ground electronic state S_0 in ground vibrational state to the first excited singlet state S_1 in ground vibrational state (eV).

In this way, it is possible to have an experimental estimation of the oxidation potential in the excited state of the photocatalyst through the experimental measurement of the two parameters $E_{0,0}$ and E_{ox}.

Below is a table with the values of E_{ox}, $E_{0,0}$ and E^*_{ox} calculated for the synthesized **PC12**-**PC23** (Table 12):

PC	E_{ox} [a] (V)	$E_{0,0}$ (eV)	E^*_{ox} [a] (V)
PC1	0,76	3,13	-2,37
PC6	0,68	2,78	-2,10
PC12	0,51	2,67	-2,16
PC13	0,58	2,68	-2,09
PC14	0,67	3,43	-2,92
PC15	0,85	3,16	-2,30
PC16	0,84	3,03	-2,19
PC19	0,91	3,16	-2,25
PC20	0,82	3,1	-2,28
PC21	0,90	3,19	-2,29
PC22	0,81	3,12	-2,31
PC23	0,83	3,09	-2,26

[a] **Potential vs SCE in MeCN**

*Table 12. Experimental values of E_{ox}, $E_{0,0}$ and E^*_{ox} for the synthesized **PC12-23**. **PC1** and **PC6** data are derived from the literature and have been reported in the table for comparison.*[31,88]

What is observed is that in the case of **PC12-13** there is no substantial change in the potential in the excited E^*_{ox} state compared with that of the analog **PC6**. Surprisingly, however, for **PC14** the E^*_{ox} potential is highly reducing, much higher than **PC6**.

In the case of **PC1** analogs, on the other hand, what is observed is that the various N-substitutions and substitutions at position 10 of the acridine core led to a slight decrease in the E^*_{ox} value compared to **PC1**. In addition, the potential values were similar to each other, with little influence of substituents in the diversification of potentials.

3.6. Scope of the reaction

Considering the optimal conditions obtained at the end of the optimization process (Section **3.3.8**), the generality of the alkylation reaction of difluorosulfoximine was tested (Figure 72).

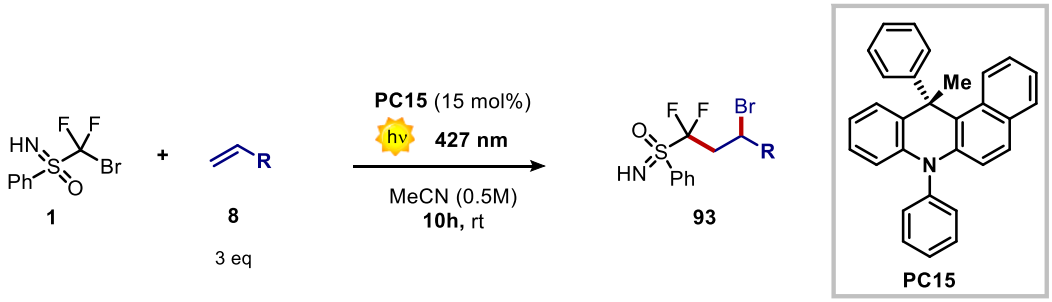

Figure 72. Optimized reaction conditions.

This first reaction scope focused on testing different olefin derivatives in order to demonstrate the good tolerance for the reaction toward different substituents and functional groups present in the reactant olefin structure. Considering that the addition of these substituents may change the reaction rate, it was decided to extend the reaction time from 8 h to 10 h, to allow time for all substrates to react to completeness.

Several functional groups were tested demonstrating a generality of the reaction ranging from good to excellent. The products obtained from the reaction scope are shown below

(Table 13). The percentages shown below each molecule are the isolated yield and, in parentheses, the ^{1}H-NMR yield.

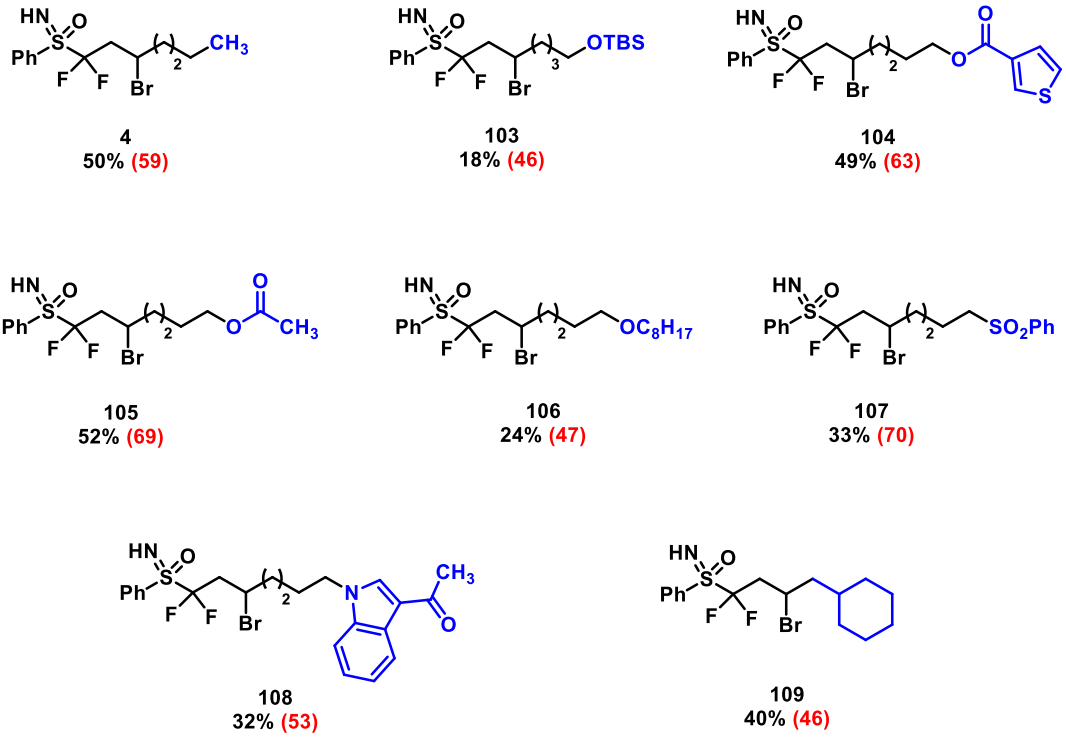

Table 13. Target products in the scope of olefins. Results scheme as "isolated yield (^{1}H-NMR yield)".

One difficulty with the procedure was the purification step, as it is difficult to separate the product from the various byproducts of the process. Despite purification via flash chromatography with very slow gradients the separation was not always optimal, leading to loss of product during the procedure.

The reaction showed good tolerance in the case of alcohol substituents with protecting groups such as acetate groups (**105**) and TBS (**103**). With TBS, the lower yield probably results from the presence of fluorine atoms in the reaction mixture. In fact, Si-F bonds are known to be among the strongest known chemical bonds and for that reason their formation is highly favored. Not surprisingly, generally for the de-protection of -OTBS groups, fluorides F^- are to be used, which are able to easily break the Si-O bond to form the stronger Si-F bond.[89] In the radical alkylation reaction of difluorosulfoximine it is possible that some secondary process could occur that would lead to the liberation of either fluorine radicals or fluorides F^-. If this happened these would then be able to de-protect the OTBS alcohol group leading to the loss of the product **103**.

The reaction demonstrated excellent tolerance toward heteroaromatic substituents, such as thiophene (**104**) and indole (**108**), substituents of great synthetic relevance because they are chemical motifs present in numerous biologically active molecules. Moderate yields were obtained in alkylation with long-chain ethers (**106**) and cyclic alkyl chains (**109**). Good results were also observed in alkylation with sulfonic derivatives (**107**), which is an excellent building block to be used for further functionalization and rearrangements.

3.7. Reaction with Hantzsch ester: new reactivity of difluoro-sulfoximine

3.7.1 Preliminary considerations

In Section **3.3.4**, a small screening of external reducing agents was performed, including the reactive Hantzsch ester. What was seen is that employing this reagent results in the formation of a molecular species that does not correspond with the desired product **4** resulting from the ATRA mechanism. This species was characterized by ^{1}H-NMR, ^{13}C-NMR, ^{19}F-NMR and UPLC-MS techniques, which confirmed the nature of the isolated species as the de-brominated analog of the ATRA product (Figure 73).

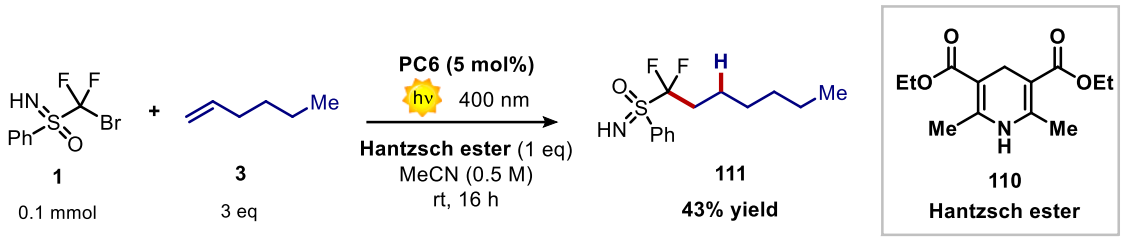

*Figure 73. Synthesis of de-bromurated product **111**.*

Particularly helpful was mass spectrometry analysis, as it easily elucidated the nature of product **111** (Figure 74). In fact, the brominated species **4** is visible at mass with two peaks of **M** (354 m/z) and **M+2** (356 m/z) mass at equal intensity. This pattern is characteristic of organic species containing a bromine atom. In the case of the de-brominated product, the disappearance of these two peaks was observed, and only the **M**-mass peak (276 m/z) could be observed.

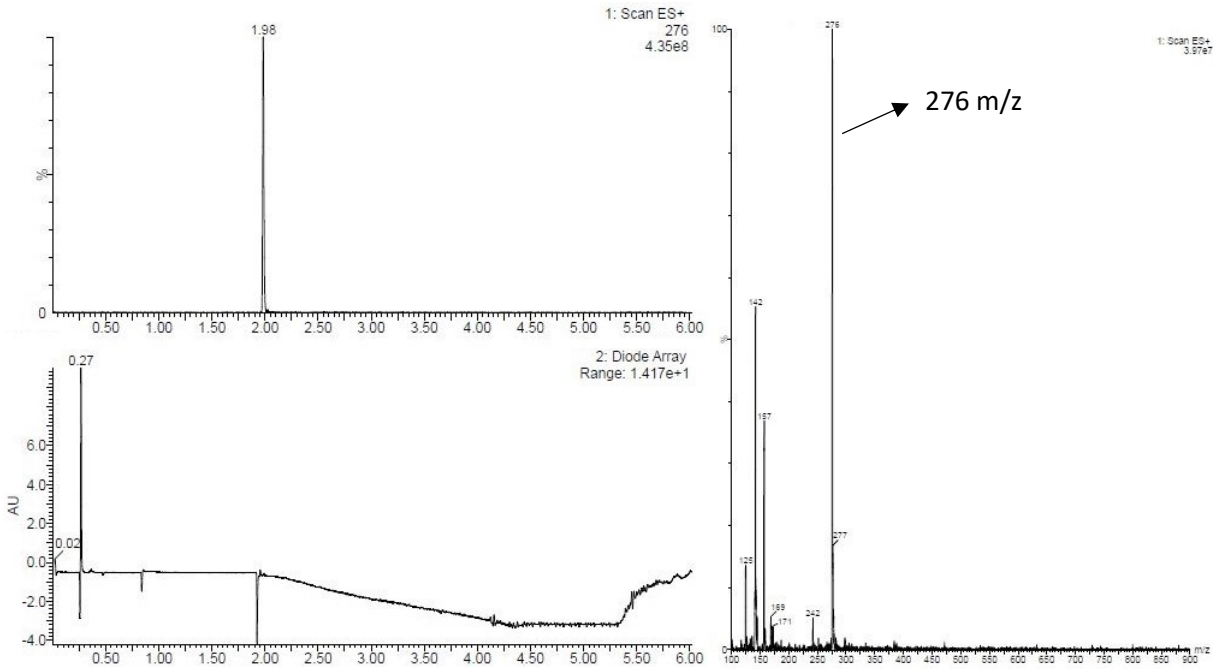

*Figure 74. a) Chromatographic profile of the de-brominated product **111**. b) mass spectrum of the de-brominated product **111** in which the presence of a single molecular peak at 276 m/z is evident. This emphasizes the absence of brominated species in the sample.*

The different nature of the product also corresponds to a different reaction mechanism. In fact, the reaction with Hantzsch ester **110** is no longer an ATRA-type radical chain mechanism, but is a simple photocatalyzed mechanism (Figure 75):

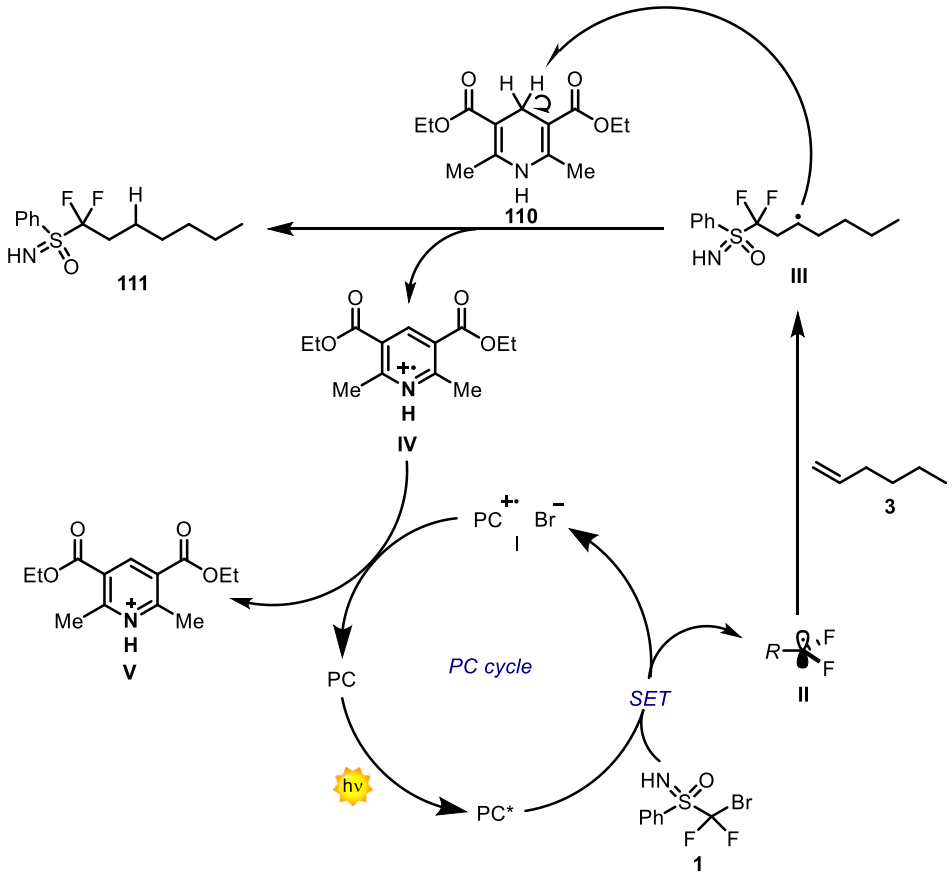

Figure 75. Proposed mechanism for the reaction with Hantzsch ester.

In this mechanism, the first part consisting of the generation of radical species **II** and its addition on olefin **3** is analogous to the ATRA-type mechanism (Figures 53). Diversification begins with the generation of intermediate species **III**, which takes part in a hydrogen atom tranfer (**HAT**) process with Hantzsch ester **110**, thus converting to the de-brominated product **111**. Abstraction of a hydrogen atom on the ring of Hantzsch ester **110** triggers an aromatization process that converts the latter into the radical cation intermediate **IV**. This intermediate finally takes part in the reduction process of radical cation **I**, leading to the restoration of the PC in the ground state through the oxidation of intermediate **IV** to pyridinium cation **V**. From this there is no radical chain mechanism, with no self-sustaining reaction, but rather the process corresponds to a closed photocatalyzed cycle in which Hantzsch ester **110** takes part in both product formation and restoration of the PC.

This process is of particular interest because it does not lead to the formation of any new stereocenter. Starting with a racemic solution of difluorosulfoximine **1**, a racemic mixture of two enantiomers **111** is obtained from this reaction. This is particularly important when compared with the ATRA process, which instead leads to the formation of a new stereocenter without stereoselection, resulting in the formation of product **4** as a mixture of four diasteroisomers. This turns out to be a non-negligible issue, as the separation of four diasteroisomers can be particularly difficult and ineffective. In the case of the de-brominated

product **111** only two enantiomers are obtained, the separation of which, although difficult, is more feasible than the separation of four diasteroisomers. Furthermore, although to be verified, starting from a difluorosulfoximine **1** in enantiopure form should yield as the product of the reaction with Hantzsch ester only one enantiomer, avoiding the challenging process of solving two enantiomers.

Considering the potential of this process, the study of this reaction was continued with a small optimization step.

3.7.2 Reaction optimization

3.7.2.1 Photocatalysts screening

As the first step in the optimization process, a small screening of photocatalysts was performed (Table 14). More specifically, the three PCs that proved to be the best in the similar ATRA process were tested: **PC1**, **PC6** and **PC15**. The reaction conditions used were the optimal ones of the ATRA process reported in section **3.3.8**.

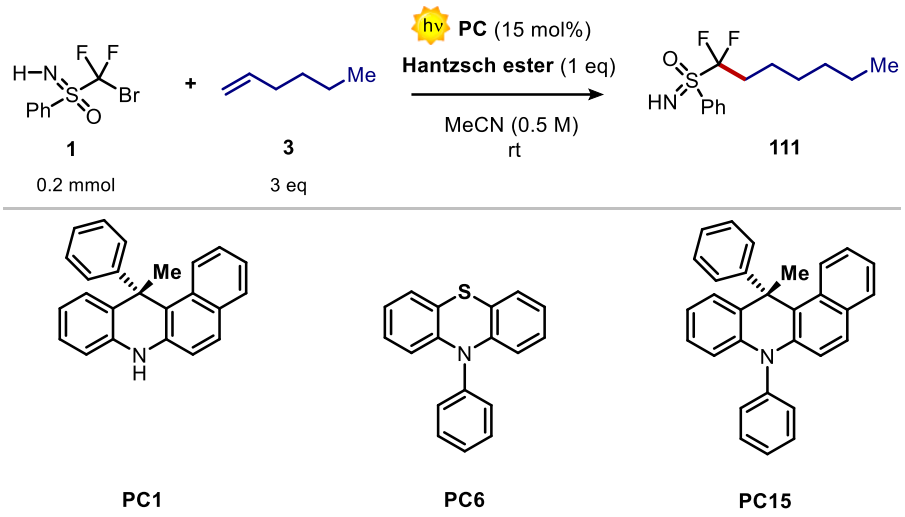

Entry	PC	λ (nm)	Time (h)	Conversion[a] (%)	Yield[a] (%)	Correct Yield[a] (%)	Comments
39	PC15	427	16	86	63	43	Not pure product
40	PC1	427	16	83	54	/	Messy product mixture
41	PC6	400	16	100	54	57	Not pure product
42	PC15	427	24	100	72	33	Not pure product

[a] All Yield and Conversion are ^{1}H-NMR Yield and ^{1}H-NMR Conversion with Trichloroethylene as Internal Standard.

Table 14. Photocatalysts screening.

What emerged was that working under the optimal conditions it is possible to obtain product **111** in yields that were very close to the 50% isolated yield of product **4**.

Among the three PCs, the best was **PC15**, with a corrected yield of 43% (entry 39). In fact, in the case of **PC6** (entry 41), despite the remarkable 57% corrected yield, the reaction crude is at ^{19}F-NMR particularly full of byproducts, making it difficult to purify.

In the case of **PC15** (entry 39), after 16 h of reaction there is still no complete conversion of sulfoximine reagent **1**. Therefore, the duration of the process was extended from 16h to 24h

(entry 42). Unfortunately, after 24h the corrected yield obtained is only around 33%, probably due to the larger number of secondary reactions in which product **111** can take part during the long reaction time.

In all the analyzed entries it was noted that after purification via flash chromatography the product is still not pure. In fact, what was observed at ^{1}H-NMR is that product **111** after purification still turns out to be contaminated by the byproduct **V** resulting from the Hantzsch ester aromatization process.

3.7.2.2 Hantzsch ester loading screening

Once a yield of 43% was obtained with **PC15**, optimization was then continued by screening the Hantzsch ester equivalents. The reaction was then repeated using 15 mol% of **PC15** and varying the Hantzsch ester equivalents from 1, to 1.5 eq up to 2 eq (Table 15).

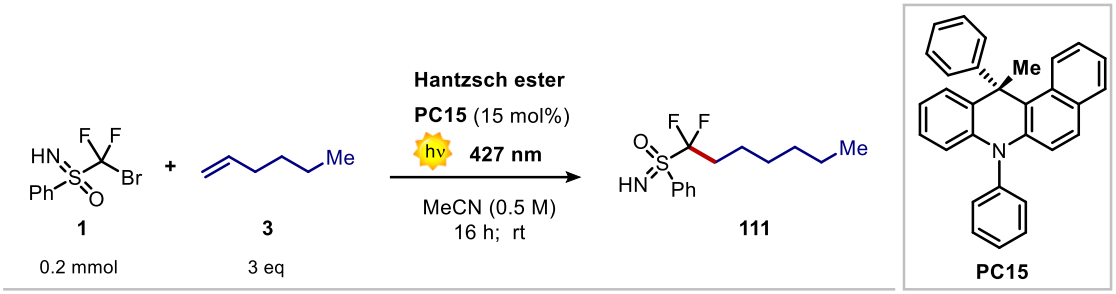

Entry	Equivalent of Hantzsch ester	Conversion[a] (%)	Yield[a] (%)	Isolated Yield (%)	Comments
39	1	86	63	43[a]	Not pure product
43	1.5	100	93	47	Pure product
44	2	100	79	45[a]	Not pure product

[a] All Yield and Conversion are ^{1}H-NMR Yield and ^{1}H-NMR Conversion with Trichloroethylene as Internal Standard.

Table 15. Hantzsch ester loading screening.

In the case of entries 43 and 44, an acid work-up was performed after the reaction by washing the reaction crude three times with a 1 M HCl aqueous solution. In this way it is possible to protonate the pyridine by-product **V** resulting from the Hantzsch ester, which in protonated form can pass into the aqueous phase and thus be easily separated from the organic phase containing the product. What has been observed is that by working with 1.5 eq of Hantzsch ester (entry 43) it is possible to obtain the product in pure form, with an isolated yield of 47%. Working with 2 eq (entry 44), on the other hand, was not able to effectively separate with acid work-up the product **111** from the pyridine by-product **V**, which was still found as contamination of the product after purification via flash chromatography. Probably the amount of 2 eq of Hantzsch ester is too high to be able to separate it all effectively by acid work-up. Moreover, the corrected yield obtained with 2 eq is slightly lower than the process with 1.5 eq, indicating no benefit in using larger amounts of Hantzsch ester.

3.7.2.3 HAT donor screening

In addition to Hantzsch ester, there are also other molecular species that are used in photocatalysis as effective HAT donors. As previously reported, the key process in the mechanism of the following reaction is the hydrogen atom transfer (**HAT**) process that converts intermediate **III** into product **111**. For this reason, a screening of the main known HAT donors was carried out in order to see if there are more efficient species than Hantzsch ester (Table 16):

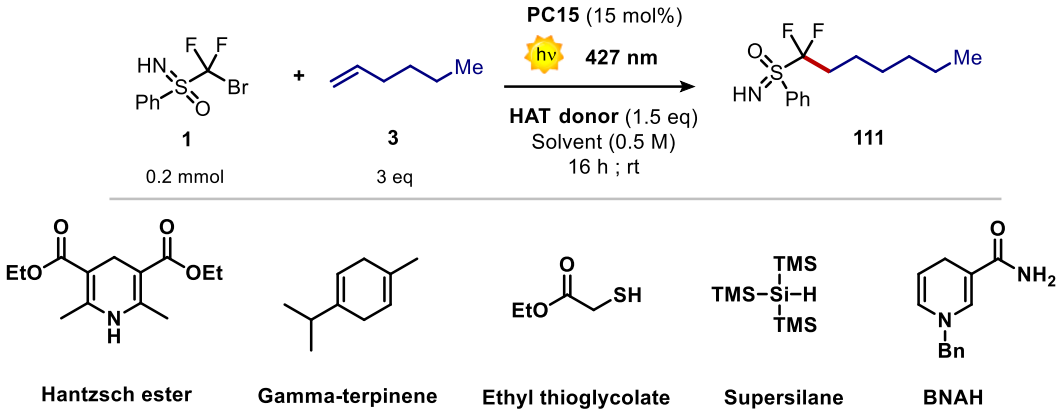

Entry	HAT donor	Solvent	Conversion[a] (%)	Yield[a] (%)	Comments
43	Hantzsch ester	MeCN	100	93	47% isolated yield
45	γ-terpinene	MeCN	100	36	Messy product mixture
46	Ethyl thioglycolate	MeCN	100	51	ATRA product
47	Supersilane	MeCN	100	29	/
48	NADH	DMSO	100	40	Partially soluble
49	BNAH	MeCN	100	37	Messy product mixture

[a] All Yield and Conversion are ^{1}H-NMR Yield and ^{1}H-NMR Conversion with Trichloroethylene as Internal Standard.

Table 16. HAT donor screening.

What was observed was that none of the species tested led to better results than Hantzsch ester (entry 43), which therefore remains the best HAT donor for this process.

3.7.2.4 Best results of the reaction optimization

At the end of the process optimization step, an isolated yield of de-brominated product **111** of 47% was achieved. This was by mixing substrates **1** and **3** in a 1:3 molar ratio, in the presence of 15 mol% of PC15 and 1.5 eq of Hantzsch ester **110**, irradiating at 427 nm (25% intensity) for 16h in MeCN solvent (0.5M) at room temperature. In addition, it is necessary for good purification of the product to perform an acid work-up by washing the reaction crude three times with an aqueous solution of 1M HCl (Figure 76).

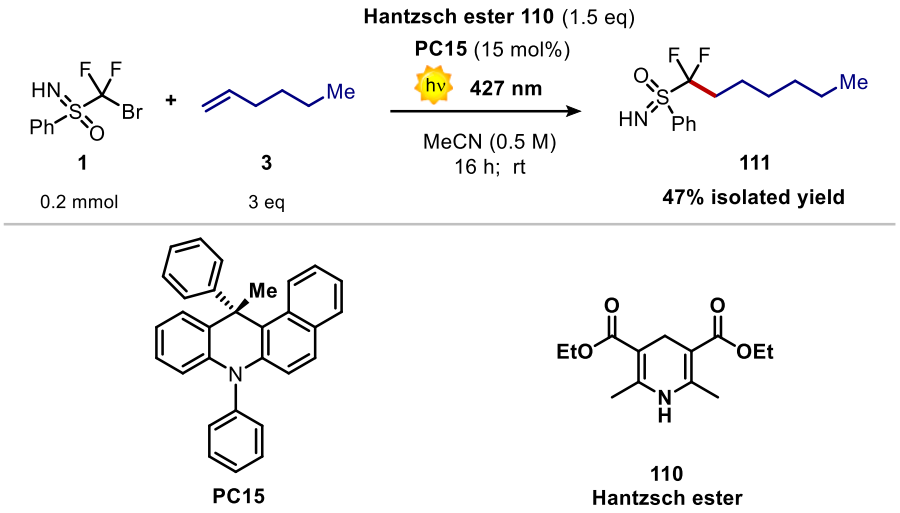

*Figure 76. Best result for the synthesis of de-bromurated product **111**.*

3.8. Mechanistic studies

The following are some experiments performed in order to obtain information on the reaction mechanism of both difluorosulfoximine alkylation processes: ATRA mechanism for the synthesis of product **4** and reaction with Hantzsch ester for the synthesis of the de-brominated product **111**. These studies mainly focused on evaluating the stability of products **4** and **111** under the reaction conditions and possible strategies employed to limit their degradation.

3.8.1 Control experiments

In the study of photochemical reactions two main control experiments are carried out to assess the nature of the reaction under investigation. The first experiment is to carry out the photochemical reaction by irradiating the prepared reagent sample in the absence of the PC. This is to investigate whether the process can take place in the absence of the PC and to what extent. In addition, it is to assess whether the direct photochemical reactivity triggered by irradiation leads to the desired product or opens the way for undesirable processes with by-product formation. The second experiment is to let the reaction mixture (with PC) go under stirring for the stipulated time but in the absence of irradiation. This is to understand whether the desired reactivity is triggered in the absence of light or not, and more importantly to assess whether there are any possible competitive polar reactions that may take part between the reactants or between the latter and the photocatalyst (resulting in its degradation).

That said, these two control experiments were carried out for both the synthesis processes of product **4** (Table 17) and product **111** (Table 18).

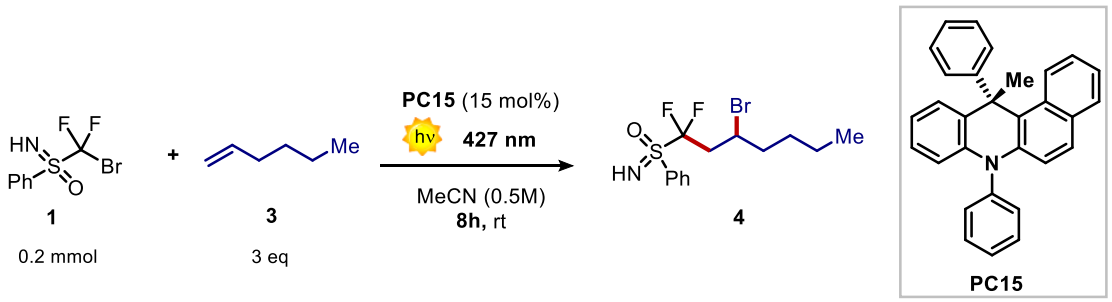

Entry	PC	Irradiation	Conversion[a] (%)	Yield[a] (%)
50	Yes	No	/	no reaction
51	No	Yes	/	no reaction

[a] All Yield and Conversion are ^{1}H-NMR Yield and ^{1}H-NMR Conversion with Trichloroethylene as Internal Standard.

Table 17. Control experiments of the ATRA process.

What is observed in the case of the ATRA process is that there is no reactivity in the absence of irradiation (entry 50) or even in the absence of the PC (entry 51). This shows that this reactivity is photochemical in nature and requires the presence of a photocatalyst for its initiation. In fact, a photochemical reactivity resulting from a direct photoexcitation of sulfoximine **1** is to be ruled out because this species does not absorb at the working wavelength of 427 nm.

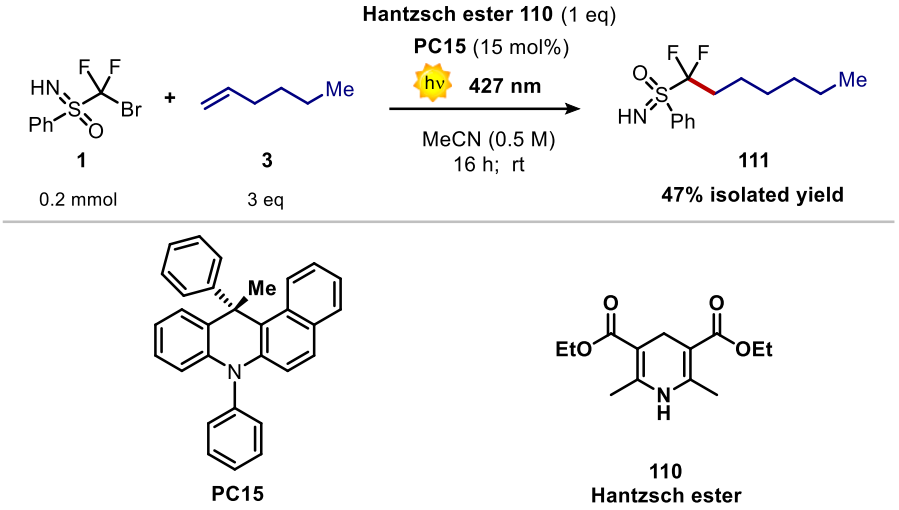

Entry	PC	Irradiation	Conversion[a] (%)	Yield[a] (%)
52	Yes	No	/	no reaction
53	No	Yes	20	<15%

[a] All Yield and Conversion are ^{1}H-NMR Yield and ^{1}H-NMR Conversion with Trichloroethylene as Internal Standard.

*Table 18. Control experiments for the synthesis of the de-brominated product **111**.*

What is observed in the case of the de-brominated product **111** synthesis process is that there is no reactivity in the absence of irradiation. This shows how this reactivity is photochemical in nature, thus needing photoexcitation to trigger the radical-type reactivity. Of interest,

however, is the result obtained in the sample irradiated at 427 nm in the absence of the photocatalyst. In fact, low amounts of product are observed at ^{19}F-NMR even in the absence of **PC15**. This may suggest how such reactivity may be triggered by a direct photoexcitation of the Hantzsch ester **110**, which is capable of absorbing light in the visible up to a maximum of 400-435 nm, being able to initiate the reaction.[90] This reactivity, however, is not optimized, as a significantly lower yield value at ^{1}H-NMR is observed compared to the optimized reaction with **PC15** (47% isolated yield). This confirms that the use of a photocatalyst is necessary to achieve an optimal product yield.

3.8.2 Photostability of the products

By analyzing the optimization data for both alkylation processes (Chapter **3.3** and **3.7**), it has been observed that optimal reaction yields never exceed 50% of isolated yield (entry 30 section **3.3.6** and entry 43 section **3.7.2.2**). These results are obtained by working with a reaction time of 16h. What is observed is that, if the reaction is allowed to continue for longer times such as 24h, the reaction yields are always lower in comparison with the same 16h reaction (entry 33 section **3.3.7** and entry 42 section **3.7.2.1**). This suggests that for both processes there may be a certain degree of photochemical instability of the product that leads to its degradation when exposed to radiation for too long, resulting in a decrease in reaction yield. For this reason, the photostability of products **4** and **111** was tested, irradiating for 16 h separate solutions of these two products under the same optimized conditions used in section **3.3.8** and **3.7.2.4**.

In the specific case of the ATRA process, two samples were tested: a sample in which only the product **4** is present and a sample in which the product **4** and **PC15** are mixed in a molar ratio as close as possible to the reaction conditions. This is done in order to discriminate what is the direct photostability of the product **4** against radiation and what is the stability of the product **4** against a possible reactivity triggered by the photocatalyst (Table 19).

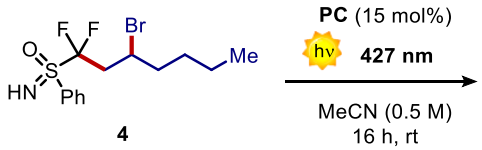

4

Entry	mmol of 4	PC	Degradation of 4	Conversion[a] (%)
54	0,06	/	No	/
55	0,07	PC15	Yes	40

[a] Conversion is ^{1}H-NMR Conversion with Trichloroethylene as Internal Standard.

*Table 19. Photostability of product **4**.*

What has been observed is that product **4** is completely stable to direct radiation in the absence of the PC (entry 54), without any visible degradation to ^{19}F-NMR. In the presence of the **PC15** (entry 55), however, after 16 h of irradiation, the presence of new by-products resulting from the degradation of the product is visible at ^{19}F-NMR. An estimate at ^{1}H-NMR showed that almost 40% of product **4** was converted into several by-products at the end of 16 h.

In the case of the de-brominated product **111**, its photostability was also assessed by irradiating two samples under the same reaction conditions for 16 h: a sample containing

only product **111** and Hantzsch ester and a sample in which product **111** is mixed together with Hantzsch ester and PC. The various reagents are mixed in a molar ratio as close as possible to the reaction conditions (Table 20).

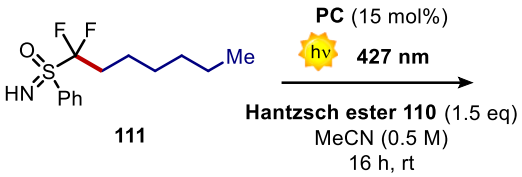

Entry	mmol of 111	PC	Degradation of 111	Conversion[a] (%)
56	0,07	/	No	/
57	0,07	PC15	Yes	46

[a] Conversion is ^{1}H-NMR Conversion with Trichloroethylene as Internal Standard.

*Table 20. Photostability of product **111**.*

In this case what is observed is that product **111** is completely stable to the direct irradiation in the absence of the photocatalyst (entry 56), without any degradation visible at ^{19}F-NMR. On the other hand, in the presence of the **PC15** (entry 57), after 16 h of irradiation, it is visible at ^{19}F-NMR the presence of new by-products deriving from the degradation of product **111**, with an estimated ^{1}H-NMR conversion around 46%. The higher value compared to the ATRA process (entry 55) can be attributed to the presence of a third molecular species in the mixture, Hantzsch ester, which can help the photocatalyst in the degradation of product **111**.

This shows that both product **4** and product **111** are not very stable in the reaction conditions and in this instability the photocatalyst plays a fundamental role. However, it should be noted that this experiment does not reproduce the reaction conditions perfectly. In fact, the product is obtained at the end of the 16 h reaction, whereas in this experiment a quantity of the product already formed was irradiated for 16 h. In the real reaction mixture the product is in contact with the PC for a shorter reaction time and with an increasing molar ratio. Moreover, in the 16 h of reaction, the ATRA process is the main reaction in which the photocatalyst takes part, a reaction that is completely prevalent in solution compared to the degradation of the product.

However, this experiment emphasizes that the product can degrade in the reaction environment and that it is necessary to study a strategy to limit this loss.

3.8.3 Cyclic voltammetry studies

Once the ability of the **PC15** to degrade products **4** and **111** was demonstrated, it was decided to confirm what was observed by analyzing the reduction potentials of products **4** and **111**. This has been done through cyclic voltammetry (CV) analysis, of which the graphs obtained are shown below (Figure 77 a-b):

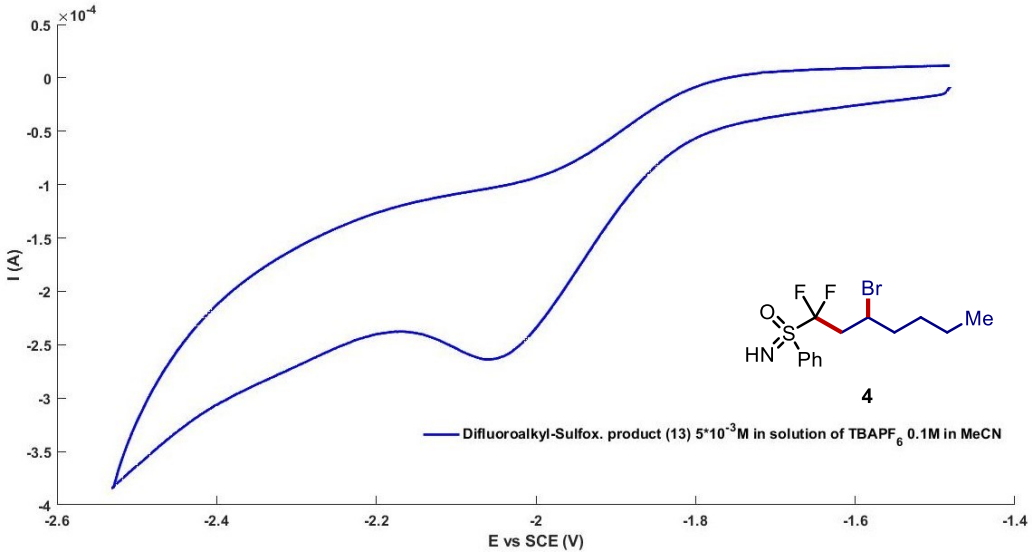

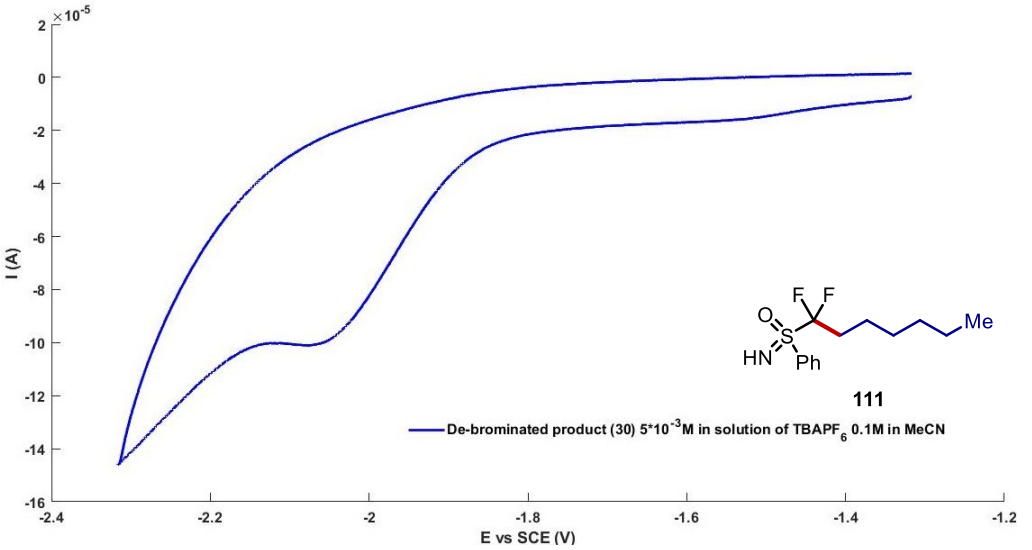

	E_{red} vs SCE
Product **13**	-2,07 V
Product **30**	-2,08 V

*Figure 77. a) Cyclic voltammetry of product **4**. b) Cyclic voltammetry of product **111**.*

From the two measurements it emerges that the potentials of the two products **4** and **111** are totally equal, within the experimental error. This is interesting because it allows to understand what is the portion of the molecule that is reduced during the process. In fact, initially it was thought that the poor stability of product **4** in the presence of **PC15** was due to the possibility of reducing the C-Br bond of the product, with the generation of a carbon radical species that reacted in different degradation processes. However, the value of the product reduction potential **111** contradicts what has been said, as a similar value is observed even though in the structure there is no longer such C-Br bond. With these considerations the instability of products **4** and **111** can be attribute to the possibility of reducing the

sulfoxymine group. Indeed, this group is common in both products and would therefore explain such a similar value of the reduction potential.

Considering the values of the reduction potentials of products **4** and **111** and considering the oxidation potential in excited state calculated for **PC15** (E^*_{ox} = -2.30 V vs SCE), it can be confirmed that the **PC15** is able to reduce and degrade products **4** and **111**.

3.8.4 EDA complex formation for the ATRA product

In the case of product **4**, the formation of a donor-acceptor complex (EDA complex) was investigated with the **PC15**, which can have considerable consequences on the success of the reaction. In fact, with the generation of an EDA complex the product degradation process can be triggered no longer by a reduction process via intermolecular single electron transfer (SET), but by an intramolecular SET process. The possibility of passing through the intramolecular pathway can lead to a significant acceleration of the degradation process.

Moreover, if the association constant between product **4** and **PC15** was higher than the association constant between reagent **1** and **PC15**, then the formation of the EDA complex would be favored in the case of product **4**. This implies that dissociation of product **4** from the photocatalyst to allow association with reagent **1** would be considerably slowed and disadvantaged. This would favor more the degradation process of product **4** than triggering a new ATRA cycle by reducing reagent **1**.

With these considerations, the formation of an EDA complex between the product **4** and the **PC15** was evaluated through UV-Visible spectroscopy (Figure 78). The procedure is the same as described in section **3.5.2**, which reproduces the molar ratio of the two species in the reaction mixture.

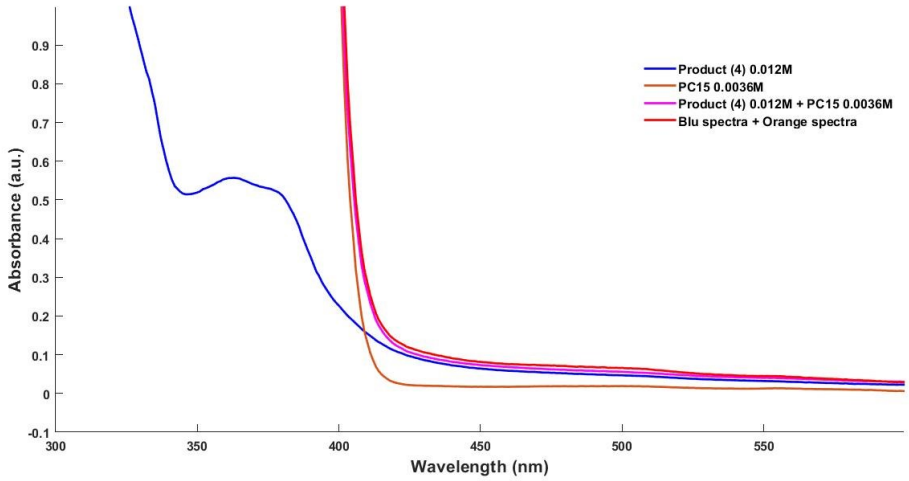

*Figure 78. Research of the formation of an EDA complex between product **4** and **PC15**. Solutions in MeCN.*

What is observed by the UV-Visible spectra is the absence of the formation of an EDA complex between the product **4** and the **PC15**. In fact, if such a complex had been observed it would be visible the formation of new absorption bands or anyway a red-shift of the absorption. This is not observed in the spectra, as the absorption profile of the product+PC

solution is almost overlapping with the red spectrum resulting from the sum of the spectrum of the **PC15** alone and the product **4**.

3.8.5 Reaction kinetics for the ATRA process

Considering the photochemical instability of the product **4** and the fact that extending the reaction time beyond 16h does not bring any benefit, the yield and conversion of the process were followed through the measurement of the reaction kinetics. Kinetics were followed by ^{1}H-NMR and ^{19}F-NMR, evaluating ^{1}H-NMR yield and ^{1}H-NMR conversion of irradiated reaction samples for a preset time of 4, 6, 8, 10, 12, 14 and 16 hours. The data obtained are shown in Table 21 and are also visible in the graph (Figure 79):

Entry	Time (h)	Conversion[a] (%)	Yield[a] (%)
58	4	52	24
59	6	67	32
60	8	100	48
61	10	100	46
62	12	100	44
63	14	100	42
64	16	100	40

[a] All Yield and Conversion are ^{1}H-NMR Yield and ^{1}H-NMR Conversion with Trichloroethylene as Internal Standard.

Table 21. Kinetic of the ATRA process.

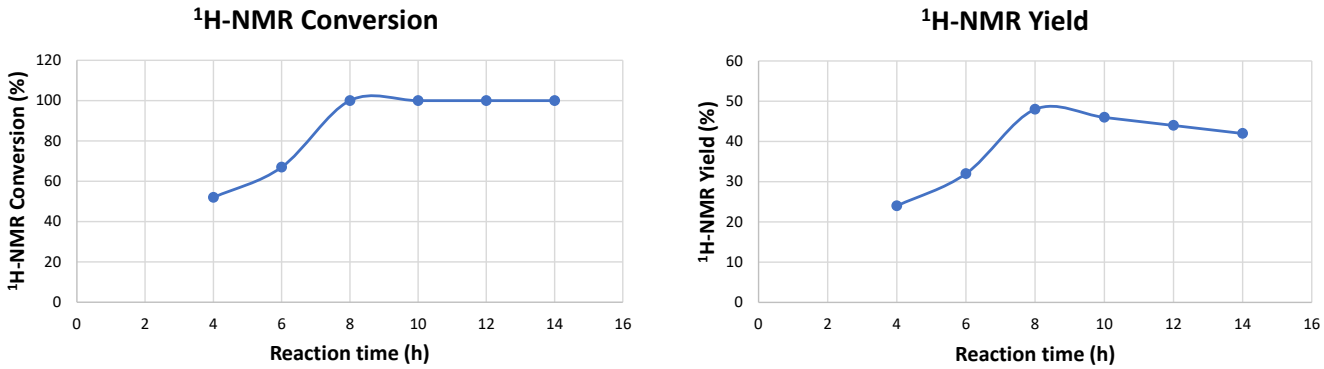

Figure 79. a) ^{1}H-NMR conversion kinetic profile. b) ^{1}H-NMR yield kinetic profile

What is observed by the kinetics of the reaction is that the process stops after 8 hours, as all the starting materials are totally consumed after this time. After 8 hours, the maximum reaction yield is reached, which then decreases in a linear way with a decrease in yield of a value equal to 1% every hour. This is due to the ability of the photocatalyst to degrade product **4**, leading to a constant decrease in yield.

With these considerations it was decided in the optimization process to stop the reaction after 8 h, thus managing to obtain product **4** in its maximum isolated yield of 50% (Section **3.3.7**).

4. Conclusions and future perspectives

In this thesis a new synthetic protocol for the alkylation in Cα of difluoro-sulfoximine was discussed. This process consists of a photocatalyzed reaction that proceeds through an ATRA-type mechanism, leading to the di-functionalization of olefins with an atom economy of 100%, as all the atoms of the reagents are incorporated into the product.

The reaction has been optimized by focusing on the photocatalyst structure, which has proven to be the most efficient parameter in process optimization. A long process of tuning and optimization of the photocatalyst, including the photophysical characterization of the various synthesized species, has allowed to obtain an optimized yield of 50% on the model substrate, going to use as photocatalyst the species (S)-12-methyl-7,12-diphenyl-7,12-dihydrobenzo[a]acridine (**PC15**).

The generality of the reaction was then demonstrated by testing several olefins variously replaced, evaluating the tolerance of the reaction to these new functional groups.

During the optimization process, a new alkylation reaction of difluoro-sulfoximine was encountered, which allows the de-brominated analogue of the ATRA process to be obtained as a product.

This process was then studied and optimized, managing to obtain the de-brominated product with an optimal yield of 47%.

At the end of the thesis project, a small mechanism study was initiated, evaluating the photochemical stability of the reaction products and evaluating the reaction kinetics of the ATRA process.

Still different analysis must be performed in the study of this process, including:

- Conclude the reaction scope focusing on screening the olefinic derivatives.
- Perform the reaction scope by evaluating the generality of the process against fluorinated sulfoximine derivatives.
- Carry out the reaction scope for the synthesis of de-brominated analogues with Hantzsch ester, by screening both olefinic derivatives and fluorinated sulfoximine derivatives.
- Conclude the photophysical characterization of the photocatalysts, also using DFT calculations.
- Conclude the mechanism study, focusing on the measurement of the quantum yield of the two reactions, Stern-Volmer analysis and DFT calculations.

5. Supporting information

5.1 General information

NMR spectra were recorded on Bruker AVANCE Neo 400 Nanobay equipped with a BBFOATM-z grad probehead and Bruker 500 AVANCE III equipped with a BBI-ATM-z grad probe head 5mm. The chemical shifts (δ) for ^{1}H and ^{13}C are given in ppm relative to residual signals of the solvents ($CHCl_3$ @7.29 ppm ^{1}HNMR, 77.16 ppm ^{13}C NMR, CH_2Cl_2 @5,32 ppm ^{1}H-NMR, 53,84 ppm ^{13}C, $(CH_3)_2CO$ @2,05 ppm ^{1}H-NMR, 29,84 ppm ^{13}C NMR). Coupling constants are given in Hz. The following abbreviations are used to indicate the multiplicity: **s**, singlet; **d**, doublet; **t**, triplet; **q**, quartet; **m**, multiplet; **br**, broad signal. NMR yields were calculated by using trichloroethylene as internal standard.

UPLC-MS analysis was performed on a Waters ACQUITY® UPC^2-MS instrument, with single quadrupole ESI mass spectrometer. The column used for UPLC is a Virdis BEH with 2.5 µm silica functionalized, 100% supercritical CO_2 to CO_2/MeOH 60% eluent. Pressure 2500 psi, flow 1.5 mL/min, temperature 55.

Absorption spectroscopy studies have been performed on a Varian Cary 50 UV-Vis double beam spectrophotometer (more info at: www.varianinc.com). All the spectra were recorded at room temperature using a 1 mm or 1 cm path length Hellma Analytics quartz cuvettes. Steady-state fluorescence spectra were recorded on a Varian Cary Eclipse Fluorescence spectrophotometer, using 10 mm path length Hellma Analytics quartz cuvettes.

All the cyclic voltammograms were recorded with a scan rate of 0.1 V/s. A typical three electrode cell was employed, which was composed of a glassy carbon (GC) working electrode (3 mm diameter), a platinum wire as counter electrode and Ag/AgCl (3M NaCl) as reference electrode. The glass electrochemical cell was kept closed with a stopper annexed to the potentiostat. Oxygen was removed by purging the solvent with high-purity nitrogen (N_2), introduced from a line into the cell by means of a glass pipe. The potential of ferrocenium/ferrocene (Fc^+/Fc) couple was used as internal reference system to calibrate the potentiostat. All the results are subsequently converted in V vs SCE, in agreement with the value reported in literature [$E_{1/2}(Fc^+/Fc)$ = +0.38 V vs SCE].[91]

5.2 Materials

Commercial grade reagents and solvents were purchased at the highest commercial quality from Sigma Aldrich or FluoroChem and used as received, unless otherwise stated. 390 nm (52W), 400 nm, 427 nm (45W), 456 nm (50W) and 525 nm (40W) Kessil LED PR160L lights were purchased from Kessil Science: https://kessil.com/products/science_main.php.

5.3 Light source emission spectra

Below are the emission spectra of the Kessil LED PR160L (Figure S1) lamps. These spectra are reported in the Kessil website (more info at: www.kessil.com/science/PR160L.php).
The wavelengths used were 390 nm, 400 nm, 427 nm, 456 nm and 525 nm. The average intensity of a Kessil lamp PR160L is 399 mW/cm^2 measured from 1 cm distance.

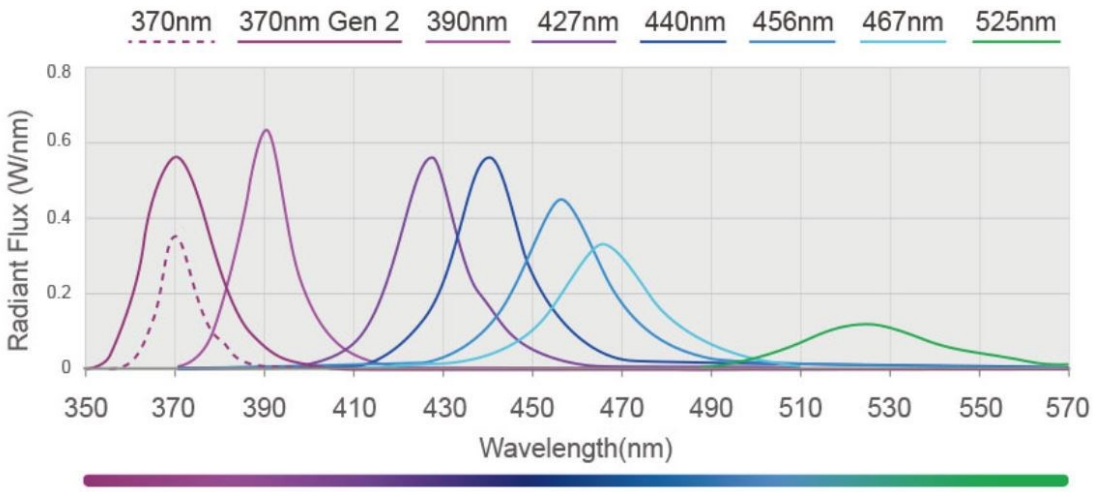

Figure S1. Emission spectra of PR160L Kessil lamp.

5.4 Batch photoreactor setup

The setup used for batch photochemical reactions is shown in Figure S2. The reaction mixture (0.4 ml for a 0.2 mmol scale reaction) is contained in a 4 ml vial (1 cm in diameter), maintained under vigorous agitation through a magnetic stirrer (IKA® Topolino). The reaction mixture is degassed with nitrogen and closed through a cap with septum, which is then covered with parafilm® to limit the infiltration of air into the vial. A Kessil PR160L LED lamp is used as a light source, positioned at a fixed distance of 3 cm from the vial and at an angle of about 30°. A maximum of three reaction was irradiated with the same Kessil lamp. To maintain a stable room-like reaction temperature one fan was placed on top of the irradiated vials.

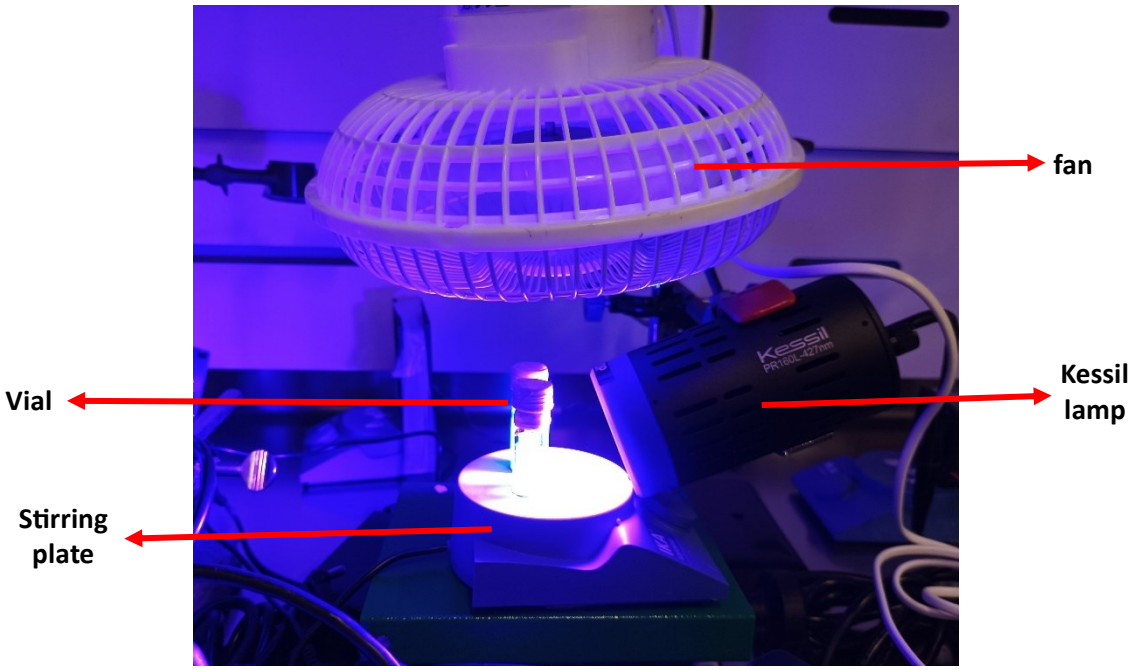

Figure S2. Reaction setup using Kessil lamp.

Due to the high temperatures reached during the summer periods of work, the reaction began to give problems of reproducibility, with a sharp decrease in the reaction yield. For this reason, the reaction was no longer performed with the traditional setup but some

changes were necessary (Figure S3). To maintain a room-like reaction temperature as much as possible the fan was replaced with a chiller. A new type of 4 ml vial was used, surrounded by a glass sleeve, inside which water is thermostated at a temperature of 20 °C by the chiller. All other setup parameters have been kept unchanged. In this way the reaction started again to be reproducible, with a reaction yield returned to the traditional values. With this new reaction setup, the last optimization step (section **3.3.7**) has been completed and the whole purpose of the reaction has been carried out (chapter **3.6**).

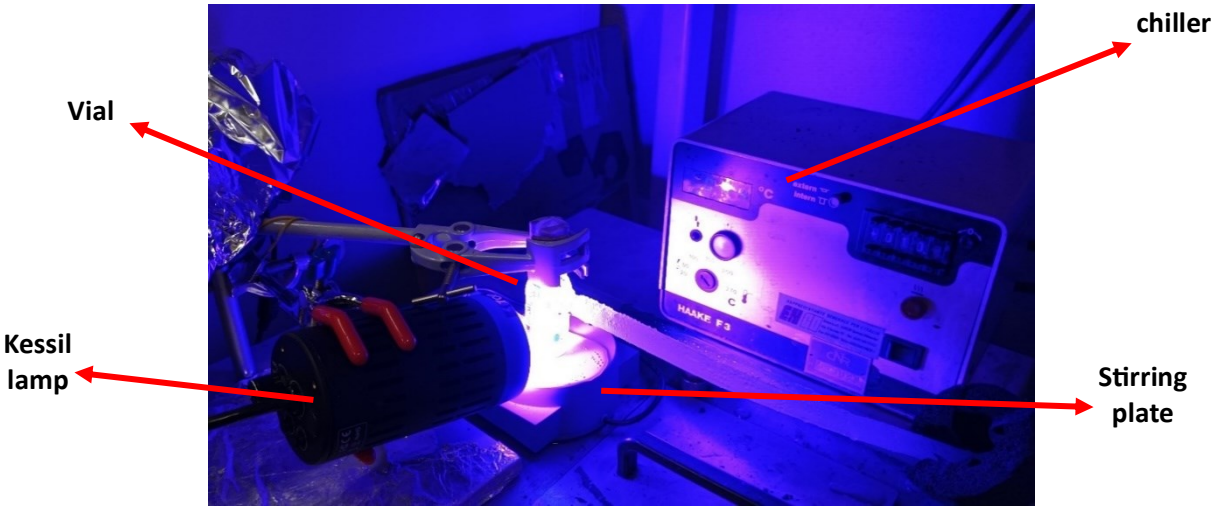

Figure S3. Figure S2. Reaction setup using chiller.

5.5 Experimental procedures for the synthesis of photocatalysts (PCs)

5.5.1 Synthesis of 7H-benzo[c]phenothiazine (PC12)

Under nitrogen atmosphere, in a two-neck round-bottomed flask equipped with a magnetic stir bar, compound N-phenylnaphthalen-2-amine **96** (2.19 g, 10 mmol, 1 eq), sulfur **97** (0.64 g, 20 mmol, 2 eq) and iodine **98** (76 mg, 0.3 mmol, 0.03 eq) were added. After that, 6 mL of dichloromethane solvent (DCM) is added and the system is attached to a refrigerator connected to a trap with a basic solution of NaOH 10%. The solution is stirred for 4h at 160 °C under nitrogen atmosphere. The reaction mixture is then extracted with aqueous basic solution of NaOH 10% (3 x 10 mL), dried over magnesium sulfate and the solvent was removed by distillation under reduced pressure. The reaction crude was purified by flash column chromatography (hexane/DCM 5:1) to give the product 7H-benzo[c]phenothiazine (**PC12**) as a yellow solid (1.5 g, 60% yield).

Note I: This protocol was prepared following a reported procedure, with modifications (D.-G. Chen et al., Angew. Chem. Int. Ed., 2019, 58, 13297–13301. Supporting information).[76]

^{1}H NMR (400 MHz, Acetone-d_6) δ 8.02 (s, 1H), 7.83 (dd, *J* = 8.5, 1.0 Hz, 1H), 7.80 – 7.71 (m, 1H), 7.61 (d, *J* = 8.7 Hz, 1H), 7.50 (ddd, *J* = 8.4, 6.8, 1.3 Hz, 1H), 7.32 (ddd, *J* = 8.1, 6.8, 1.1 Hz, 1H), 7.12 – 7.01 (m, 3H), 6.84 (td, *J* = 7.5, 1.3 Hz, 1H), 6.86 (dd, *J* = 7.9, 1.3 Hz, 1H).

^{13}C NMR (101 MHz, Acetone-d_6) δ 143.8, 140.9, 131.5, 131.2, 129.2, 128.6, 128.3, 127.7, 127.6, 124.2, 123.4, 122.7, 118.0, 117.6, 115.5, 109.3.

5.5.2 Synthesis of 10-phenyl-10H-phenoxazine (PC14)

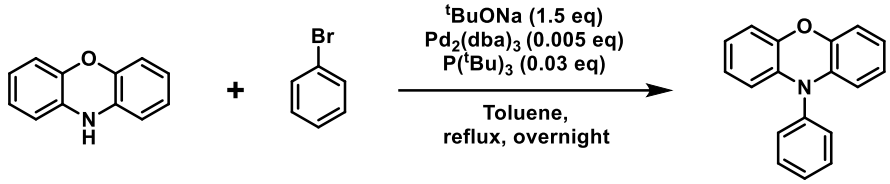

A two-neck round bottom flask, equipped with a magnetic stir bar, was dried with three vacuum/nitrogen cycles. Under nitrogen atmosphere, compounds phenoxazine **112** (183 mg, 1 mmol, 1 eq), phenyl bromide **99** (188 mg, 1.2 mmol, 1.2 eq), $Pd_2(dba)_3$ (4.58 mg, 0.005 mmol, 0.05 eq) and ^{t}BuONa (144 mg, 1.5 mmol, 1.5 eq) were added sequentially, followed by 2 mL of degassed solvent Toluene. After that, $P(^tBu)_3$ (7.3 µL, 0.03 mmol, 0.03 eq) was added and a refrigerator was connected. The reaction was heated at reflux (120°C) under stirring for 6h. The reaction mixture was then extracted with ethyl acetate (3 x 10 mL). The organic phases were combined and washed with brine (20 mL) and then dried over magnesium sulfate. The solvent was removed by distillation under reduced pressure and residue was purified by flash column chromatography (hexane/DCM 98:2) to give the corresponding product 10-phenyl-10H-phenoxazine (PC14) as a white solid (230 mg, 89% yield).

^{1}H NMR (400 MHz, CD_2Cl_2) δ 7.63 (t, *J* = 7.7 Hz, 2H), 7.57 – 7.45 (m, 2H), 7.44 – 7.33 (m, 2H), 6.85 – 6.53 (m, 6H), 5.93 (dd, *J* = 7.8, 1.7 Hz, 2H).

^{13}C NMR (101 MHz, CD_2Cl_2) δ 144.3, 139.4, 134.9, 131.5, 131.1, 128.9, 123.7, 121.6, 115.6, 113.7.

5.5.3 Synthesis of (S)-10-bromo-12-methyl-12-phenyl-7,12-dihydrobenzo[a]acridine (PC19)

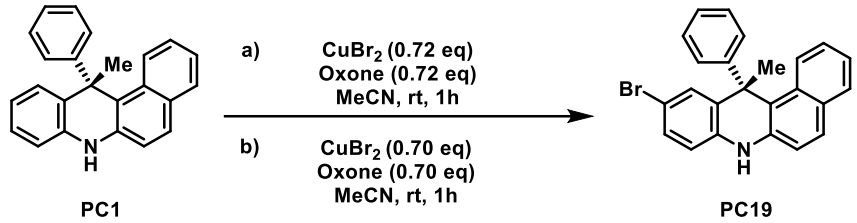

Under air, a round bottom flask equipped with a magnetic stir bar was charged with **PC1** (160.7 mg, 0.50 mmol, 1 eq.) and 5 mL of CH_3CN. Then, $CuBr_2$ (82 mg, 0.36 mmol, 0.72 eq.) and Oxone® (220 mg, 0.36 mmol, 0.72 eq.) were added sequentially in one portion. After 1 hour, more $CuBr_2$ (78 mg, 0.35 mmol, 0.7 eq.) and Oxone® (213 mg, 0.35 mmol, 0.7 eq.)

were added and the reaction was stirred for further 1 hour. After the reaction was completed (controlled by ^{1}H NMR), 40 mL of EtOAc were added. The organic phase was washed with H_2O (2 x 20 mL), the solvent was dried over magnesium sulfate and removed by distillation under reduced pressure. The reaction crude was purified by flash column chromatography (hexane/EtOAc 7:3) to give the product (S)-10-bromo-12-methyl-12-phenyl-7,12-dihydrobenzo[a]acridine (**PC19**) as a white solid (135.5 mg, 68% yield).

*Note I: This protocol was prepared following reported procedure with modifications (Lian-Ming Yang, L. M. RSC Advances **2013**, 3, 12091).[79] Note II: In principle, 1 eq. of Oxone® should be enough for the reaction, but it decomposes over time. The reaction progress cannot be controlled by TLC because both **PC19** and **PC1** runs equally, therefore ^{1}H NMR using CD_3CN was employed instead.*

^{1}H NMR (400 MHz, Acetone-d_6) δ 8.51 (s, 1H), 7.74 – 7.58 (m, 4H), 7.49 (d, J = 8.8 Hz, 1H), 7.32 (t, J = 7.6 Hz, 2H), 7.20 – 7.02 (m, 4H), 6.96 (ddd, J = 8.5, 6.8, 1.6 Hz, 1H), 6.89 (d, J = 2.2 Hz, 1H), 6.76 (d, J = 8.5 Hz, 1H), 2.24 (s, 3H).

^{13}C NMR (101 MHz, Acetone-d_6) δ 152.5, 136.7, 136.3, 133.2, 132.9, 132.7, 131.8, 130.3, 130.3, 129.9, 129.2, 128.9, 126.5, 126.2, 126.1, 122.5, 118.0, 117.2, 116.1, 111.9, 46.6, 30.5.

5.5.4 Synthesis of (S)-12-methyl-10,12-diphenyl-7,12-dihydrobenzo[a]acridine (PC20)

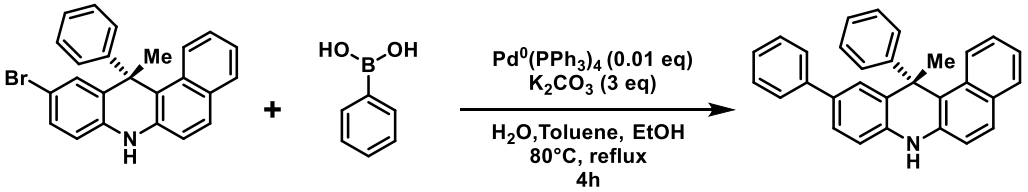

A round bottom flask, equipped with a magnetic stir bar, was dried with three vacuum/nitrogen cycles. Under nitrogen atmosphere, compound **PC19** (186.5 mg, 0.47 mmol, 1 eq), phenylboronic acid **101** (62.79 mg, 0.52 mmol, 1.1 eq) and tetrakis(triphenylphosphine)palladium(0) (5.39 mg, 0.0047 mmol, 0.01 eq) were added sequentially, followed by 2 mL of degassed solvent. The solvent corresponds with a mixture of EtOH (0.35 mL), an aqueous solution of K_2CO_3 (193.4 mg in 0.7 mL, 1.4 mmol, 3 eq, 2M) and toluene (0.95 mL), in ratio 1 : 2 : 2.7. The reaction was heated at reflux (80°C) under stirring for 4 h. After that, the crude was filtered on celite, washed with EtOAc (10 mL) and DCM (10 mL) and the solvent was dried over magnesium sulfate and removed by distillation under reduced pressure. The residue was purified by flash column chromatography (gradient from 100:0 to 9:1 hexane/EtOAc) to give the product (S)-12-methyl-10,12-diphenyl-7,12-dihydrobenzo[a]acridine (**PC20**) as a white solid (110.5 mg, 60% yield).

Note: This procedure was modified from a patent.[80]

Current Patent Assignee: CHANGCHUN HAIPU RUNSI TECHNOLOGY CO LTD - CN111205272, 2020, A. Location in patent: Paragraph 0103-0105

^{1}H NMR (400 MHz, Acetone-d_6) δ 8.48 (s, 1H), 7.73 – 7.62 (m, 4H), 7.59 – 7.53 (m, 1H), 7.46 – 7.25 (m, 7H), 7.23 – 7.10 (m, 4H), 7.00 (dddd, J = 28.2, 8.5, 6.8, 1.4 Hz, 2H), 6.88 (d, J = 8.3 Hz, 1H), 2.32 (s, 3H).

^{13}C NMR (101 MHz, Acetone-d_6) δ 153.1, 142.0, 137.0, 136.4, 133.5, 133.1, 131.7, 130.8, 130.1, 129.8, 129.5, 129.4, 129.0, 128.9, 127.0, 126.7, 126.2, 126.2, 126.1, 126.0, 122.3, 118.1, 117.5, 114.7, 54.9, 46.6.

5.5.5 Synthesis of 10-bromo-12-methyl-7,12-diphenyl-7,12-dihydrobenzo[a]acridine (PC21)

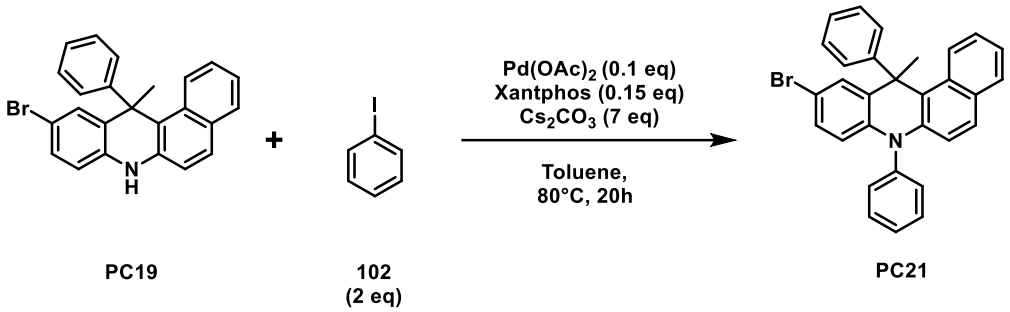

PC19 | **102 (2 eq)** | **PC21**

A round bottom flask, equipped with a magnetic stir bar, was dried with three vacuum/nitrogen cycles. Under nitrogen atmosphere, compound (S)-10-bromo-12-methyl-12-phenyl-7,12-dihydrobenzo[a]acridine **PC19** (80 mg, 0.2 mmol, 1 eq), phenyl iodide **102** (45µL, 0.4 mmol, 2 eq), Palladium (II) acetate (4.5 mg, 0.02 mmol, 0.1 eq), Xantphos (17 mg, 0.03 mmol, 0.15 eq) and Cs_2CO_3 (456 mg, 1.4 mmol, 7 eq) were added sequentially. After that 1 mL of degassed solvent Toluene was added and a refrigerator was connected. The reaction was heated at 80°C under stirring for 20h. The crude was then filtered on celite with washes of EtOAc and the solvent was removed by distillation under reduced pressure. The reaction crude was purified by flash column chromatography (hexane/DCM 9:1) to afford compound **PC21** as a white solid (83 mg, 87% yield).

*Note I: This protocol was prepared following a reported procedure, with modifications (G. Goti et al., Eur. J. Org. Chem., **2021**, 2655–2664. Supporting information)*.[82]

^{1}H NMR (400 MHz, CD_2Cl_2) δ 7.74 – 7.55 (m, 7H), 7.49 – 7.33 (m, 5H), 7.27 – 7.20 (m, 1H), 7.08 (ddd, *J* = 7.9, 6.7, 1.1 Hz, 1H), 7.01 (ddd, *J* = 8.5, 6.8, 1.6 Hz, 1H), 6.96 (d, *J* = 2.3 Hz, 1H), 6.90 (dd, *J* = 8.9, 2.3 Hz, 1H), 6.60 (d, *J* = 9.2 Hz, 1H), 6.06 (d, *J* = 8.8 Hz, 1H), 2.36 (s, 3H).

^{13}C NMR (101 MHz, CD_2Cl_2) δ 152.2, 142.0, 138.2, 138.0, 133.0, 132.9, 131.9, 131.7, 131.7, 130.9, 129.4, 129.2, 129.0, 129.0, 128.9, 128.4, 126.3, 126.2, 125.8, 122.7, 119.2, 117.4, 116.7, 112.8, 45.9, 31.1.

5.5.6 General Buchwald-Hartwig reaction procedure for N-Arylation of Photocatalysts

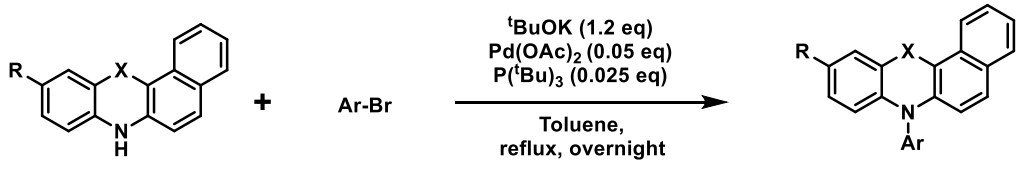

PC1-PC12 PC19-PC20 | **Ar = Ph ; 2-Naph (1.1 eq)** | **PC13-PC15-PC16 PC22-PC23**

A two-neck round bottom flask, equipped with a magnetic stir bar, was dried with three vacuum/nitrogen cycles. Under nitrogen atmosphere, the photocatalyst precursor **PC1-12-19-20** (1 eq), aryl bromide **Ar-Br** (1.1 eq), Palladium (II) acetate (0.05 eq) and ^{t}BuOK (1.2 eq) were added sequentially, followed by degassed solvent Toluene. After that, P(^{t}Bu)$_3$ (0.025 eq) was added and a refrigerator was connected. The reaction was heated at reflux (120°C) under stirring overnight. The crude was then filtered on celite with washes of EtOAc and the solvent was removed by distillation under reduced pressure. The reaction crude was purified by flash column chromatography (hexane/DCM) to give the products **PC13-15-16-22-23** in the stated yield.

Note I: This protocol was prepared following a reported procedure, with modifications (Y. Tian et al., Angew. Chem. Int. Ed., 2021,60, 20259 –20263. Supporting information).[77]

7-phenyl-7H-benzo[c]phenothiazine (PC13)

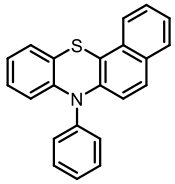

PC13

Compound **PC13** was synthesized according to the general procedure **5.5.6** using 7H-benzo[c]phenothiazine **PC12** (700 mg, 2.8 mmol, 1 eq), phenyl bromide **99** (487 mg, 3.1 mmol, 1.1 equiv), Palladium (II) acetate (31 mg, 0.14 mmol, 0.05 eq), ^{t}BuOK (382 mg, 3.4 mmol, 1.2 eq) and P(^{t}Bu)$_3$ (17 µL, 0.07 mmol, 0.025 eq) in 17 mL of Toluene. The crude was purified by flash column chromatography (hexane/DCM 9:1) to afford compound **PC13** as a yellow solid (858 mg, 94% yield).

^{1}H NMR (400 MHz, Acetone-d$_6$) δ 8.05 – 7.99 (m, 1H), 7.80 – 7.73 (m, 1H), 7.69 (t, *J* = 7.7 Hz, 2H), 7.60 – 7.45 (m, 5H), 7.38 (ddd, *J* = 8.1, 6.8, 1.1 Hz, 1H), 7.19 (dd, *J* = 7.5, 1.7 Hz, 1H), 7.04 – 6.86 (m, 2H), 6.66 (d, *J* = 9.0 Hz, 1H), 6.39 (dd, *J* = 8.1, 1.3 Hz, 1H).
^{13}C NMR (101 MHz, Acetone-d$_6$) δ 145.8, 142.5, 142.4, 131.7, 131.4, 131.2, 129.1, 129.0, 128.2, 128.0, 127.9, 127.7, 125.2, 124.1, 123.3, 121.5, 118.7, 117.8, 114.3.

12-methyl-7,12-diphenyl-7,12-dihydrobenzo[a]acridine (PC15)

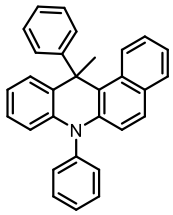

PC15

Compound **PC15** was synthesized according to the general procedure **5.5.6** using 12-methyl-12-phenyl-7,12-dihydrobenzo[a]acridine **PC1** (161 mg, 0.5 mmol, 1 eq), phenyl bromide **99** (86 mg, 0.55 mmol, 1.1 equiv), Palladium (II) acetate (5.6 mg, 0.025 mmol, 0.05 eq), ^{t}BuOK (67 mg, 0.6 mmol, 1.2 eq) and P(^{t}Bu)$_3$ (3 µL, 0.0125 mmol, 0.025 eq) in 2.7 mL of Toluene. The crude was purified by flash column chromatography (hexane/DCM 9:1) to afford compound **PC15** as a white solid (180 mg, 90% yield).

^{1}H NMR (400 MHz, Acetone-d$_6$) δ 7.86 (dd, *J* = 8.4, 7.1 Hz, 2H), 7.73 – 7.66 (m, 3H), 7.67 – 7.58 (m, 2H), 7.53 (d, *J* = 9.1 Hz, 1H), 7.53 – 7.44 (m, 2H), 7.33 (dd, *J* = 8.4, 7.3 Hz, 2H), 7.16 (tt, *J* = 7.3, 1.2 Hz, 1H), 7.06 (ddd, *J* = 8.0, 6.8, 1.1 Hz, 1H), 7.03 – 6.96 (m, 1H), 6.92 (dd, *J* = 7.9, 1.6 Hz, 1H), 6.81 (ddd, *J* = 8.5, 7.1, 1.6 Hz, 1H), 6.67 (ddd, *J* = 8.2, 7.1, 1.3 Hz, 1H), 6.61 (d, *J* = 9.2 Hz, 1H), 6.12 (dd, *J* = 8.3, 1.2 Hz, 1H), 2.37 (s, 3H).

^{13}C NMR (101 MHz, Acetone-d$_6$) δ 153.4, 143.1, 139.2, 139.1, 132.7, 132.3, 132.2, 131.5, 131.3, 131.0, 129.7, 129.4, 129.1, 129.0, 127.0, 126.9, 126.2, 126.1, 122.9, 121.4, 119.9, 117.8, 115.1, 46.2, 31.3.

12-methyl-7-(naphthalen-2-yl)-12-phenyl-7,12-dihydrobenzo[a]acridine (PC16)

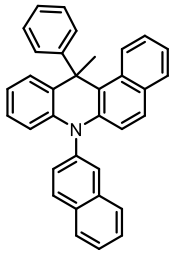

PC16

Compound **PC16** was synthesized according to the general procedure **5.5.6** using 12-methyl-12-phenyl-7,12-dihydrobenzo[a]acridine **PC1** (161 mg, 0.5 mmol, 1 eq) 2-bromonaphthalene (114 mg, 0.55 mmol, 1.1 equiv), Palladium (II) acetate (5.6 mg, 0.025 mmol, 0.05 eq), ^{t}BuOK (67 mg, 0.6 mmol, 1.2 eq) and P(^{t}Bu)$_3$ (3 µL, 0.0125 mmol, 0.025 eq) in 2.7 mL of Toulene. The crude was purified by flash column chromatography (hexane/DCM 9:1) to afford compound **PC16** as a white solid (183 mg, 82% yield).

^{1}H NMR (400 MHz, CD_2Cl_2) δ 8.19 (d, *J* = 8.6 Hz, 1H), 8.03 (d, *J* = 8.2 Hz, 1H), 8.01 – 7.90 (m, 2H), 7.77 – 7.53 (m, 6H), 7.49 (dd, *J* = 8.6, 2.1 Hz, 1H), 7.44 – 7.32 (m, 3H), 7.28 – 7.15 (m, 1H), 7.12 – 6.97 (m, 2H), 6.92 (dd, *J* = 7.8, 1.6 Hz, 1H), 6.77 (ddd, *J* = 8.4, 7.1, 1.6 Hz, 1H), 6.67 (dd, *J* = 16.3, 8.4 Hz, 2H), 6.19 (d, *J* = 8.3 Hz, 1H), 2.41 (s, 3H).

^{13}C NMR (126 MHz, CD_2Cl_2) δ 153.0, 139.8, 138.8, 135.4, 133.4, 132.2, 131.8, 130.9, 130.9, 130.6, 129.3, 129.2, 128.8, 128.7, 128.4, 128.3, 127.3, 127.0, 126.5, 126.5, 125.8, 125.7, 122.5, 121.0, 119.5, 117.7, 115.0, 46.0, 31.1.

12-methyl-7,10,12-triphenyl-7,12-dihydrobenzo[a]acridine (PC22)

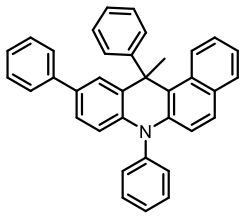

PC22

Compound **PC22** was synthesized according to the general procedure **5.5.6** using (S)-12-methyl-10,12-diphenyl-7,12-dihydrobenzo[a]acridine **PC20** (72 mg, 0.18 mmol, 1 eq), phenyl bromide **99** (31 mg, 0.2 mmol, 1.1 equiv), Palladium (II) acetate (2 mg, 0.009 mmol, 0.05 eq), ^{t}BuOK (24 mg, 0.216 mmol, 1.2 eq) and P(^{t}Bu)$_3$ (1.1 µL, 4.5*10^{-3} mmol, 0.025 eq) in 1 mL of Toluene. The crude was purified by flash column chromatography (hexane/DCM 9:1) to afford compound **PC22** as a white solid (55 mg, 63% yield).

^{1}H NMR (400 MHz, Acetone-d_6) δ 7.85 – 7.72 (m, 5H), 7.64 (ddt, *J* = 9.2, 7.8, 1.5 Hz, 2H), 7.57 – 7.47 (m, 3H), 7.41 – 7.29 (m, 6H), 7.26 (d, *J* = 2.2 Hz, 1H), 7.23 – 7.18 (m, 1H), 7.19 – 7.12 (m, 2H), 7.08 (ddd, *J* = 8.0, 6.7, 1.1 Hz, 1H), 7.01 (ddd, *J* = 8.5, 6.7, 1.6 Hz, 1H), 6.64 (d, *J* = 9.1 Hz, 1H), 6.23 (d, *J* = 8.6 Hz, 1H), 2.46 (s, 3H).

^{13}C NMR (101 MHz, Acetone-d_6) δ 153.4, 142.9, 141.5, 139.0, 138.7, 133.9, 132.7, 132.3, 131.7, 131.6, 129.7, 129.6, 129.5, 129.5, 129.5, 129.2, 129.0, 127.3, 127.0, 126.8, 126.3, 126.2, 125.6, 123.0, 119.9, 117.8, 115.7, 46.4, 31.4.

12-methyl-7-(naphthalen-2-yl)-10,12-diphenyl-7,12-dihydrobenzo[a]acridine (PC23)

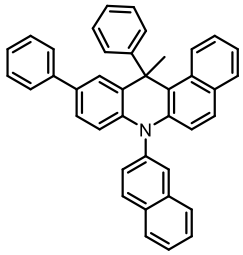

PC23

Compound **PC23** was synthesized according to the general procedure **5.5.6** using (S)-12-methyl-10,12-diphenyl-7,12-dihydrobenzo[a]acridine **PC20** (100 mg, 0.25 mmol, 1 eq), 2-bromonaphthalene (57 mg, 0.275 mmol, 1.1 equiv), Palladium (II) acetate (2.8 mg, 0.0125 mmol, 0.05 eq), ^{t}BuOK (34 mg, 0.3 mmol, 1.2 eq) and P(^{t}Bu)$_3$ (1.6 µL, 6.25*10^{-3} mmol, 0.025 eq) in 1.35 mL of Toluene. The crude was purified by flash column chromatography (hexane/DCM 9:1) to afford compound **PC23** as a white solid (68 mg, 51% yield).

^{1}H NMR (400 MHz, CD_2Cl_2) δ 8.23 (d, *J* = 8.6 Hz, 1H), 8.10 – 8.03 (m, 2H), 7.99 (dd, *J* = 7.7, 1.6 Hz, 1H), 7.79 (dd, *J* = 15.3, 8.3 Hz, 3H), 7.65 (dddd, *J* = 15.5, 14.1, 7.4, 1.6 Hz, 3H), 7.57 (dd, *J* = 8.6, 2.1 Hz, 1H), 7.43 (q, *J* = 8.4, 7.6 Hz, 3H), 7.39 – 7.32 (m, 4H), 7.30 – 7.21 (m, 3H), 7.17 – 7.03 (m, 3H), 6.73 (d, *J* = 9.2 Hz, 1H), 6.34 (d, *J* = 8.6 Hz, 1H), 2.53 (s, 3H).

^{13}C NMR (101 MHz, CD_2Cl_2) δ 152.8, 141.1, 139.6, 138.6, 138.3, 135.3, 133.6, 133.4, 132.2, 131.9, 131.3, 131.0, 130.8, 129.3, 129.2, 129.2, 129.0, 128.9, 128.8, 128.5, 128.3, 127.4, 127.1, 126.9, 126.5, 126.5, 126.0, 125.8, 125.2, 122.7, 119.6, 117.7, 115.5, 46.1, 31.3.

5.6 Experimental procedures for the synthesis of starting materials

Tert-butyl(hex-5-en-1-yloxy)dimethylsilane (114)

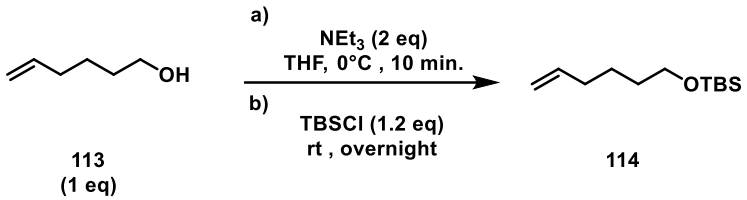

Compound **114** was synthesized following a literature procedure.[75] The characterization data matched with the reported one.

hex-5-en-1-yl thiophene-3-carboxylate (116)

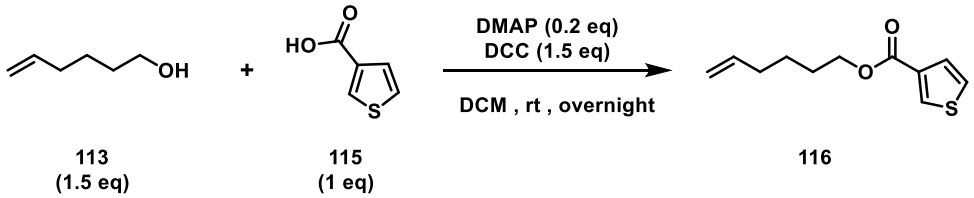

Compound **116** was synthesized following a literature procedure.[92] The characterization data matched with the reported one.

Hex-5-en-1-yl acetate (117)

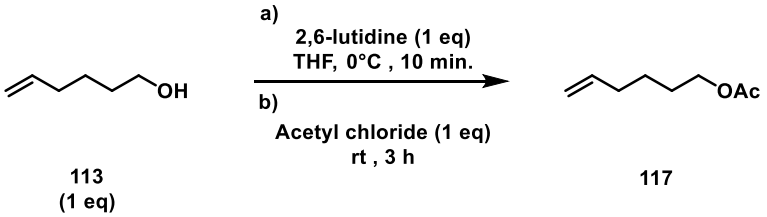

Compound **117** was synthesized following a literature procedure.[75] The characterization data matched with the reported one.[93]

1-(hex-5-en-1-yloxy)octane (119)

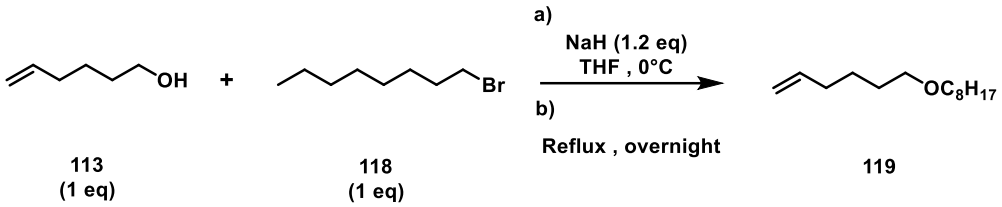

Compound **119** was synthesized following a literature procedure.[75] The characterization data matched with the reported one.[94]

(Hex-5-en-1-ylsulfonyl)benzene (121)

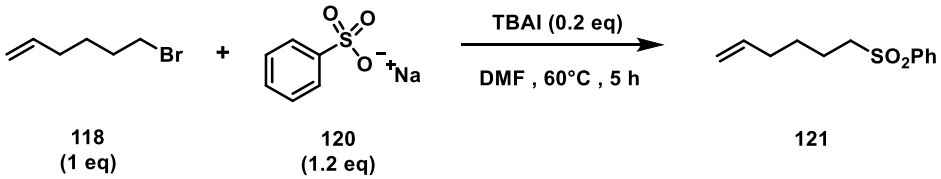

Compound **121** was synthesized following a literature procedure.[75] The characterization data matched with the reported one.[95]

1-(1-(hex-5-en-1-yl)-1H-indol-3-yl)ethan-1-one (123)

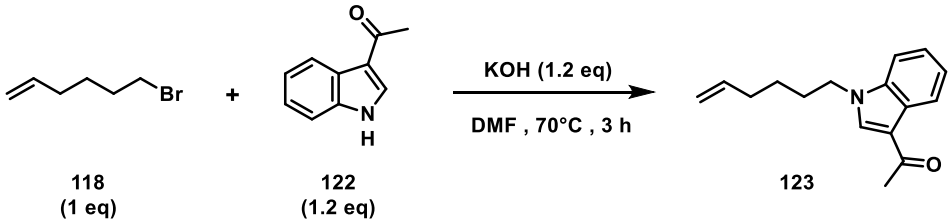

Compound **123** was synthesized following a literature procedure.[75] The characterization data matched with the reported one.

5.7 General procedure for the photocatalyzed synthesis of Difluoroalkyl-Sulfoximines

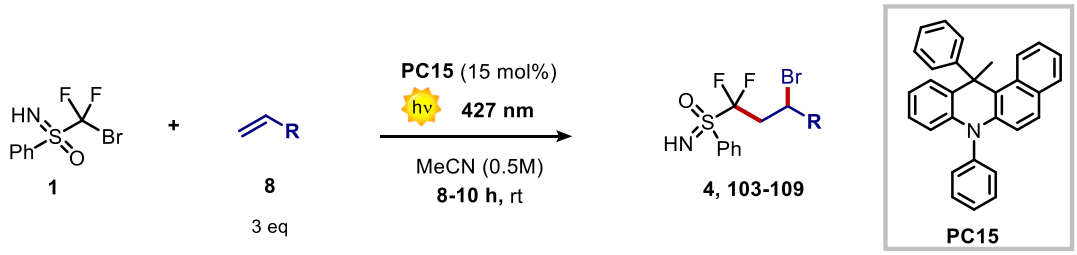

A 4 mL screw cap septum vial was charged with **PC15** (0.15 eq), (bromodifluoromethyl)phenylsulfoximine **1** (1 eq)**,** the olefin substrate **8** (3 eq) and degassed acetonitrile (0.5M). The solution was degassed with nitrogen for 1 minute. The vial was sealed with parafilm, and the reaction mixture was stirred for 8-10 h under the irradiation of a Kessil Lamp PR160L (427 nm, 45W, 25% intensity). After the set time, the solvent was removed by distillation under reduced pressure and the crude product was

directly purified by flash column chromatography on silica gel (hexane:EtOAc) to afford the difluorosulfoximine product in the stated yield.

(3-bromo-1,1-difluoroheptyl)(imino)(phenyl)-λ^6-sulfanone (4)

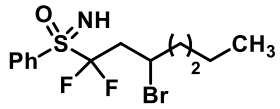

4

Compound **4** was synthesized according to the general procedure **5.7** using (bromodifluoromethyl)phenylsulfoximine **1** (54 mg, 0.2 mmol, 1 eq), **PC15** (11.92 mg, 0.03 mmol, 0.15 eq) and 1-hexene **3** (75 µL, 0.6 mmol, 3 eq) Reaction time: 8 h. The crude was purified by flash column chromatography (gradient from 100:0 to 9:1 hexane/EtOAc) to afford compound **4** as a yellowish oil (35.4 mg, 50% yield). The product is a mixture of four diasteroisomers.

^{1}H NMR (400 MHz, $CDCl_3$) δ 8.06 (d, J = 7.5 Hz, 2H), 7.76 – 7.70 (m, 1H), 7.60 (dd, J = 8.5, 7.2 Hz, 2H), 4.26 (dddd, J = 10.6, 8.1, 6.6, 3.9 Hz, 1H), 3.16 – 2.63 (m, 3H), 2.02 – 1.71 (m, 2H), 1.50 (ddddd, J = 11.4, 9.2, 7.0, 4.5, 2.4 Hz, 1H), 1.45 – 1.21 (m, 3H), 0.90 (td, J = 7.2, 3.0 Hz, 3H).

^{19}F NMR decoupled ^{1}H (377 MHz, $CDCl_3$) δ -102.0, -102.5, -103.4, -103.7 (four doublet, AB system, J_{AB} = 223.0 Hz)

^{13}C NMR (101 MHz, $CDCl_3$) δ 134.9 (d, J = 2.3 Hz), 133.6, 130.8, 129.4 (d, J = 1.9 Hz), 123.6 (t, J = 289.3 Hz), 45.8 (t, J = 2.2 Hz), 45.7 (t, J = 2.3 Hz), 39.1 (m), 38.9 (d, J = 1.4 Hz), 38.8, 29.3, 22.0, 14.0.

(3-bromo-6-((tert-butyldimethylsilyl)oxy)-1,1-difluoroheptyl)(imino)(phenyl)-λ^6-sulfanone (103)

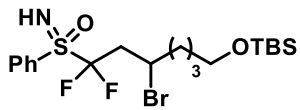

103

Compound **103** was synthesized according to the general procedure **5.7** using (bromodifluoromethyl)phenylsulfoximine **1** (54 mg, 0.2 mmol, 1 eq), **PC15** (11.92 mg, 0.03 mmol, 0.15 eq) and compound **114** (75 µL, 0.6 mmol, 3 eq) Reaction time: 10 h. The crude was purified by flash column chromatography (gradient from 100:0 to 9:1 hexane/EtOAc) to afford compound **103** as a yellowish oil (17.5 mg, 18% yield). The product is a mixture of four diasteroisomers.

^{1}H NMR (400 MHz, $CDCl_3$) δ 8.06 (d, *J* = 7.8 Hz, 4H), 7.73 (t, *J* = 7.4 Hz, 2H), 7.61 (t, *J* = 7.8 Hz, 4H), 4.26 (tdt, *J* = 10.9, 7.6, 3.9 Hz, 2H), 3.60 (dt, *J* = 6.1, 3.0 Hz, 4H), 3.23 (s, 2H), 3.14 – 2.71 (m, 4H), 1.86 (dqd, *J* = 18.7, 9.7, 8.7, 4.1 Hz, 4H), 1.65 – 1.53 (m, 4H), 1.53 – 1.43 (m, 4H), 0.89 (d, *J* = 1.5 Hz, 18H), 0.04 (d, *J* = 1.8 Hz, 12H).

^{19}F NMR decoupled ^{1}H (377 MHz, $CDCl_3$) δ -101.9, -102.5, -103.4, -103.8 (four doublet, AB system, J_{AB} = 223.0 Hz)

^{13}C NMR (101 MHz, $CDCl_3$) δ 134.9, 134.9, 133.6, 133.6, 130.8, 129.4, 129.4, 123.6 (t, *J* = 290.3 Hz), 62.8, 45.7 (t, *J* = 2.2 Hz), 45.6 (t, *J* = 2.3 Hz), 39.3 (t, *J* = 19.3 Hz), 39.1 (t, *J* = 19.3 Hz), 39.0, 38.9, 32.0, 26.1, 23.8, 18.5, -5.2.

5-bromo-7,7-difluoro-6-(phenylsulfonimidoyl)heptyl thiophene-3-carboxylate (104)

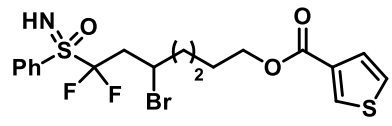

104

Compound **104** was synthesized according to the general procedure **5.7** using (bromodifluoromethyl)phenylsulfoximine **1** (54 mg, 0.2 mmol, 1 eq), **PC15** (11.92 mg, 0.03 mmol, 0.15 eq) and compound **116** (75 µL, 0.6 mmol, 3 eq) Reaction time: 10 h. The crude was purified by flash column chromatography (gradient from 100:0 to 9:1 hexane/EtOAc) to afford compound **104** as a yellowish oil (47.2 mg, 49% yield). The product is a mixture of four diasteroisomers.

^{1}H NMR (400 MHz, $CDCl_3$) δ 8.10 (dt, *J* = 3.0, 1.5 Hz, 2H), 8.05 (d, *J* = 7.4 Hz, 4H), 7.73 (t, *J* = 7.4 Hz, 2H), 7.60 (t, *J* = 7.7 Hz, 4H), 7.52 (dt, *J* = 5.1, 1.2 Hz, 2H), 7.30 (dd, *J* = 5.1, 3.0 Hz, 2H), 4.28 (dtt, *J* = 10.2, 3.7, 2.1 Hz, 6H), 3.17 – 2.69 (m, 6H), 2.04 – 1.84 (m, 4H), 1.83 – 1.65 (m, 4H), 1.65 – 1.52 (m, 4H).

^{19}F NMR decoupled ^{1}H (377 MHz, $CDCl_3$) δ -101.8, -102.4, -103.0, -103.7 (four doublet, AB system, J_{AB} = 222.5 Hz)

^{13}C NMR (101 MHz, $CDCl_3$) δ 162.9, 134.9, 134.9, 133.8, 133.6, 132.8, 130.8, 129.4, 129.4, 128.0, 126.1, 123.5 (t, *J* = 290.1 Hz), 64.3, 45.4 (t, *J* = 2.2 Hz), 45.3 (t, *J* = 2.3 Hz), 39.2 (t, *J* = 19.5 Hz), 39.1 (t, *J* = 19.5 Hz), 38.6, 38.5, 28.0, 23.9.

5-bromo-7,7-difluoro-7-(phenylsulfonimidoyl)heptyl acetate (105)

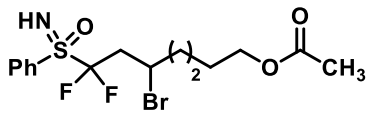

105

Compound **105** was synthesized according to the general procedure **5.7** using (bromodifluoromethyl)phenylsulfoximine **1** (54 mg, 0.2 mmol, 1 eq), **PC15** (11.92 mg, 0.03 mmol, 0.15 eq) and compound **117** (75 µL, 0.6 mmol, 3 eq) Reaction time: 10 h. The crude was purified by flash column chromatography (gradient from 100:0 to 9:1 hexane/EtOAc) to afford compound **105** as a yellowish oil (42.3 mg, 52% yield). The product is a mixture of four diasteroisomers.

^{1}H NMR (400 MHz, $CDCl_3$) δ 8.05 (d, J = 7.8 Hz, 2H), 7.73 (t, J = 7.4 Hz, 1H), 7.61 (t, J = 7.9 Hz, 2H), 4.27 (dtt, J = 9.6, 6.6, 3.2 Hz, 1H), 4.05 (td, J = 6.1, 2.9 Hz, 2H), 3.21 – 2.73 (m, 2H), 2.62 (s, 1H), 2.04 (s, 13H), 2.01 – 1.77 (m, 2H), 1.63 (dddd, J = 16.0, 12.5, 5.8, 3.0 Hz, 2H), 1.55 – 1.44 (m, 2H).

^{19}F NMR decoupled ^{1}H (377 MHz, $CDCl_3$) δ -101.8, -102.3, -103.4, -103.7 (four doublet, AB system, J_{AB} = 222.5 Hz)

^{13}C NMR (126 MHz, $CDCl_3$) δ 134.9, 134.9, 133.6, 130.8, 129.4, 129.4, 123.5 (t, J = 291.3 Hz), 64.1, 45.4 (t, J = 2.3 Hz), 45.3 (t, J = 2.3 Hz), 39.1 (m), 38.6, 38.5, 27.8, 23.9, 21.1.

(3-bromo-1,1-difluoro-7-(octyloxy)heptyl)(imino)(phenyl)-λ^6-sulfanone (106)

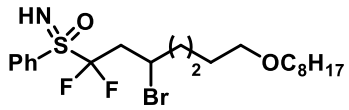

106

Compound **106** was synthesized according to the general procedure **5.7** using (bromodifluoromethyl)phenylsulfoximine **1** (54 mg, 0.2 mmol, 1 eq), **PC15** (11.92 mg, 0.03 mmol, 0.15 eq) and compound **119** (75 µL, 0.6 mmol, 3 eq) Reaction time: 10 h. The crude was purified by flash column chromatography (gradient from 100:0 to 9:1 hexane/EtOAc) to afford compound **106** as a yellowish oil (23.4 mg, 24% yield). The product is a mixture of four diasteroisomers.

^{1}H NMR (400 MHz, $CDCl_3$) δ 8.16 (d, J = 7.8 Hz, 2H), 7.73 (t, J = 7.5 Hz, 1H), 7.61 (t, J = 7.7 Hz, 2H), 4.27 (dddd, J = 10.6, 8.1, 6.6, 3.9 Hz, 1H), 3.38 (dq, J = 6.7, 2.9, 1.9 Hz, 4H), 3.12 – 2.71 (m, 2H), 2.07 – 1.77 (m, 2H), 1.56 (m, 8H), 1.40 – 1.18 (m, 12H).

^{19}F NMR decoupled ^{1}H (377 MHz, $CDCl_3$) δ -101.9, -102.5, -103.3, -103.7 (four doublet, AB system, J_{AB} = 223.0 Hz)

^{13}C NMR (101 MHz, $CDCl_3$) δ 134.9, 134.9, 130.8, 129.4, 129.4, 123.6 (t, J = 290.4 Hz), 71.2, 70.5, 45.6 (t, J = 2.2 Hz), 45.5 (t, J = 2.3 Hz), 39.3 (m), 39.0, 38.9, 32.0, 29.9, 29.6, 29.4, 29.0, 26.3, 24.2, 22.8, 14.2.

(3-bromo-1,1-difluoro-7-(phenylsulfonyl)heptyl)(imino)(phenyl)-λ^6-sulfanone (107)

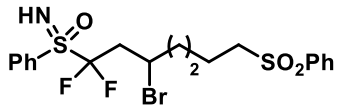

107

Compound **107** was synthesized according to the general procedure **5.7** using (bromodifluoromethyl)phenylsulfoximine **1** (54 mg, 0.2 mmol, 1 eq), **PC15** (11.92 mg, 0.03 mmol, 0.15 eq) and compound **121** (75 µL, 0.6 mmol, 3 eq) Reaction time: 10 h. The crude was purified by flash column chromatography (gradient from 100:0 to 8:2 hexane/EtOAc) to afford compound **107** as a yellowish oil (32.6 mg, 33% yield). The product is a mixture of four diasteroisomers.

^{1}H NMR (400 MHz, $CDCl_3$) δ 8.03 (d, J = 7.9 Hz, 2H), 7.90 (dd, J = 7.6, 2.2 Hz, 2H), 7.73 (t, J = 7.5 Hz, 1H), 7.61 (dp, J = 22.7, 7.5 Hz, 6H), 4.21 (dtt, J = 9.7, 6.4, 3.1 Hz, 1H), 3.24 – 3.03 (m, 2H), 3.03 – 2.62 (m, 2H), 1.93 – 1.83 (m, 2H), 1.82 – 1.57 (m, 2H), 1.52 (dtd, J = 15.7, 8.9, 8.2, 4.2 Hz, 2H).

^{19}F NMR decoupled ^{1}H (377 MHz, $CDCl_3$) δ -102.0, -102.5, -103.3, -103.7 (four doublet, AB system, J_{AB} = 222.5 Hz)

^{13}C NMR (101 MHz, $CDCl_3$) δ 139.1, 134.9, 133.9, 133.6, 130.8, 129.5, 129.4, 128.1, 123.4 (t, J = 290.0 Hz), 56.0, 44.9 (t, J = 2.4 Hz), 44.8 (t, J = 2.3 Hz), 39.1 (m), 38.3, 38.2, 26.0, 22.0, 8.8.

(7-(3-acetyl-1H-indol-1-yl)-3-bromo-1,1-difluoroheptyl)(imino)(phenyl)-λ^6-sulfanone (108)

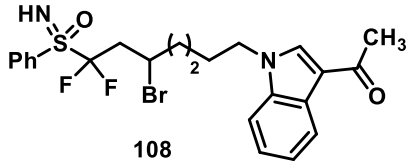

108

Compound **108** was synthesized according to the general procedure **5.7** using (bromodifluoromethyl)phenylsulfoximine **1** (54 mg, 0.2 mmol, 1 eq), **PC15** (11.92 mg, 0.03 mmol, 0.15 eq) and compound **123** (75 µL, 0.6 mmol, 3 eq) Reaction time: 10

h. The crude was purified by flash column chromatography (gradient from 100:0 to 8:2 hexane/EtOAc) to afford compound **108** as a brownish oil (33.1 mg, 32% yield). The product is a mixture of four diasteroisomers.

^{1}H NMR (400 MHz, $CDCl_3$) δ 8.40 – 8.34 (m, 1H), 8.03 (d, J = 7.8 Hz, 2H), 7.75 – 7.68 (m, 2H), 7.59 (t, J = 7.7 Hz, 2H), 7.30 (ddd, J = 9.4, 6.0, 2.8 Hz, 3H), 4.26 (dq, J = 10.3, 3.3 Hz, 1H), 4.16 (td, J = 7.2, 2.3 Hz, 2H), 3.21 – 2.73 (m, 2H), 2.52 (s, 3H), 1.99 – 1.77 (m, 4H), 1.64 (dtt, J = 15.1, 10.2, 5.2 Hz, 1H), 1.51 (ddt, J = 13.2, 6.5, 3.3 Hz, 1H).

^{19}F NMR decoupled ^{1}H (377 MHz, $CDCl_3$) δ -101.6, -102.1, -102.8, -103.3 (four doublet, AB system, J_{AB} = 223.0 Hz)

^{13}C NMR (101 MHz, $CDCl_3$) δ 193.1, 136.8, 135.0, 135.0, 134.8, 133.6, 130.8, 129.4, 126.5, 123.4 (t, J = 290.0 Hz), 122.9, 122.7, 117.2, 109.8, 60.5, 46.9, 45.2 (t, J = 2.3 Hz), 45.1 (t, J = 2.6 Hz), 39.2 (m), 38.4, 38.2, 29.0, 27.8, 24.7, 14.3.

(3-bromo-4-cyclohexyl-1,1-difluorobutyl)(imino)(phenyl)-λ^{6}-sulfanone (109)

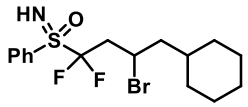

109

Compound **109** was synthesized according to the general procedure **5.7** using (bromodifluoromethyl)phenylsulfoximine **1** (54 mg, 0.2 mmol, 1 eq), **PC15** (11.92 mg, 0.03 mmol, 0.15 eq) and compound **allylcyclohexane** (75 µL, 0.6 mmol, 3 eq) Reaction time: 10 h. The crude was purified by flash column chromatography (gradient from 100:0 to 9:1 hexane/EtOAc) to afford compound **109** as a yellowish oil (31.3 mg, 40% yield). The product is a mixture of four diasteroisomers.

^{1}H NMR (400 MHz, $CDCl_3$) δ 8.06 (d, J = 7.9 Hz, 2H), 7.73 (t, J = 7.5 Hz, 1H), 7.60 (t, J = 7.8 Hz, 2H), 4.31 (tdd, J = 10.3, 6.7, 3.8 Hz, 1H), 3.25 (s, 1H), 3.12 – 2.72 (m, 2H), 1.83 – 1.47 (m, 10H), 1.22 – 1.03 (m, 2H).

^{19}F NMR decoupled ^{1}H (377 MHz, $CDCl_3$) δ -101.5, -102.2 -102.9, -103.5 (four doublet, AB system, J_{AB} = 223.0 Hz)

^{13}C NMR (101 MHz, $CDCl_3$) δ 134.9, 134.8, 133.6, 130.8, 129.4, 129.4, 123.6 (t, J = 290.1 Hz), 47.0, 46.9, 43.5 (t, J = 2.3 Hz), 43.4 (t, J = 2.3 Hz), 39.8 (m), 35.8, 33.7, 33.6, 31.6, 31.5, 26.5, 26.2, 25.9.

5.7.1 Synthesis of (1,1-difluoroheptyl)(imino)(phenyl)-λ^6-sulfanone (111)

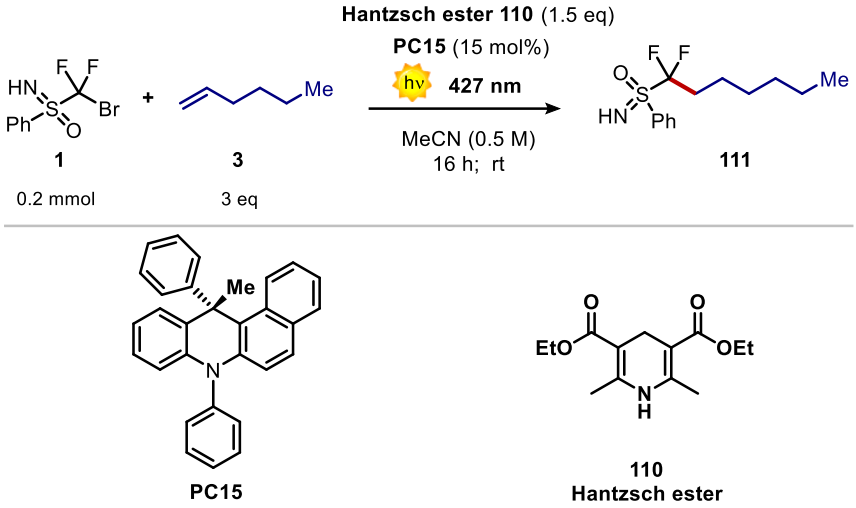

A 4 mL screw cap septum vial was charged with (bromodifluoromethyl)phenylsulfoximine **1** (54 mg, 0.2 mmol, 1 eq)**, PC15** (11.92 mg, 0.03 mmol, 0.15 eq), 1-hexene **3** (75 µL, 0.6 mmol, 3 eq), Hantzsch ester **110** (76 mg, 0.3 mmol, 1.5 eq) and degassed acetonitrile (0.5M). The solution was degassed with nitrogen for 1 minute. The vial was sealed with parafilm, and the reaction mixture was stirred for 8-10 h under the irradiation of a Kessil Lamp PR160L (427 nm, 45W, 25% intensity). After the set time, the reaction mixture was washed with an acid solution of HCl 1M (3 x 10 mL) and then dried over magnesium sulfate. The solvent was removed under reduced pressure and the crude product was purified by flash column chromatography on silica gel (gradient from 100:0 to 9:1 hexane/EtOAc) to afford compound **111** as a yellowish oil (25.7 mg, 47% yield). The product is a mixture of two enantiomers.

^{1}H NMR (400 MHz, $CDCl_3$) δ 8.12 – 7.92 (m, 2H), 7.70 (t, J = 7.5 Hz, 1H), 7.58 (t, J = 7.8 Hz, 2H), 2.77 (s, 1H), 2.62 – 2.00 (m, 2H), 1.77 – 1.50 (m, 2H), 1.42 – 1.30 (m, 2H), 1.34 – 1.22 (m, 4H), 0.87 (t, J = 6.7 Hz, 3H).

^{19}F NMR decoupled ^{1}H (377 MHz, $CDCl_3$) δ -108.9 (d, J = 220.7 Hz), -109.9 (d, J = 220.9 Hz). AB system

^{13}C NMR (101 MHz, $CDCl_3$) δ 134.5, 134.2, 130.8, 129.2, 125.3 (t, J = 287.2 Hz), 31.5, 30.0 (t, J = 20.9 Hz), 29.8, 28.9, 22.5, 21.1, 14.1.

5.8 NMR spectra

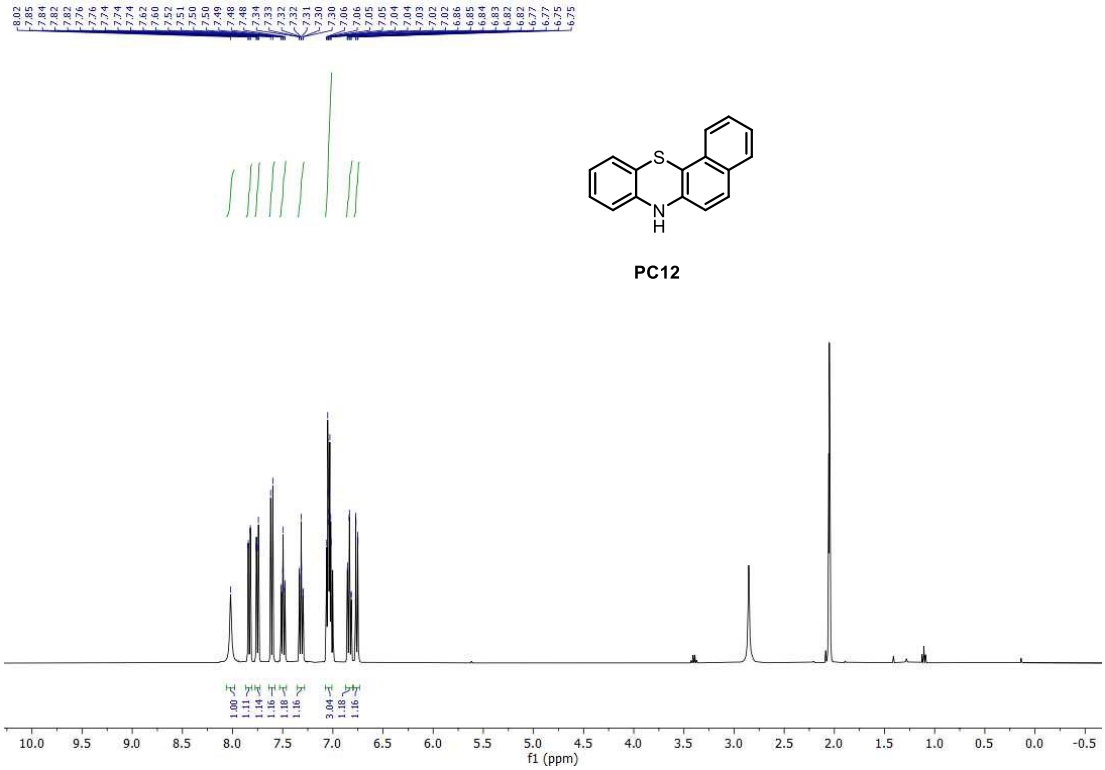

Figure S4. ^{1}H-NMR spectrum of PC12 in Acetone-d^{6}.

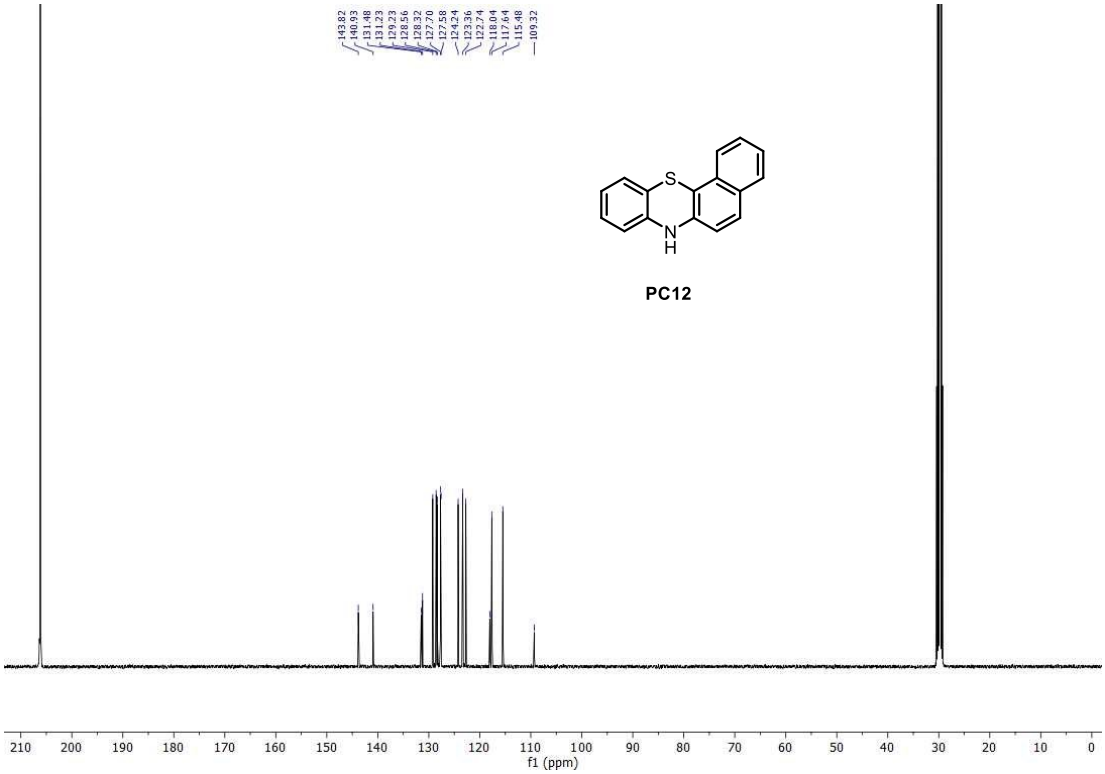

Figure S5. ^{13}C-NMR spectrum of PC12 in Acetone-d$_{6}$.

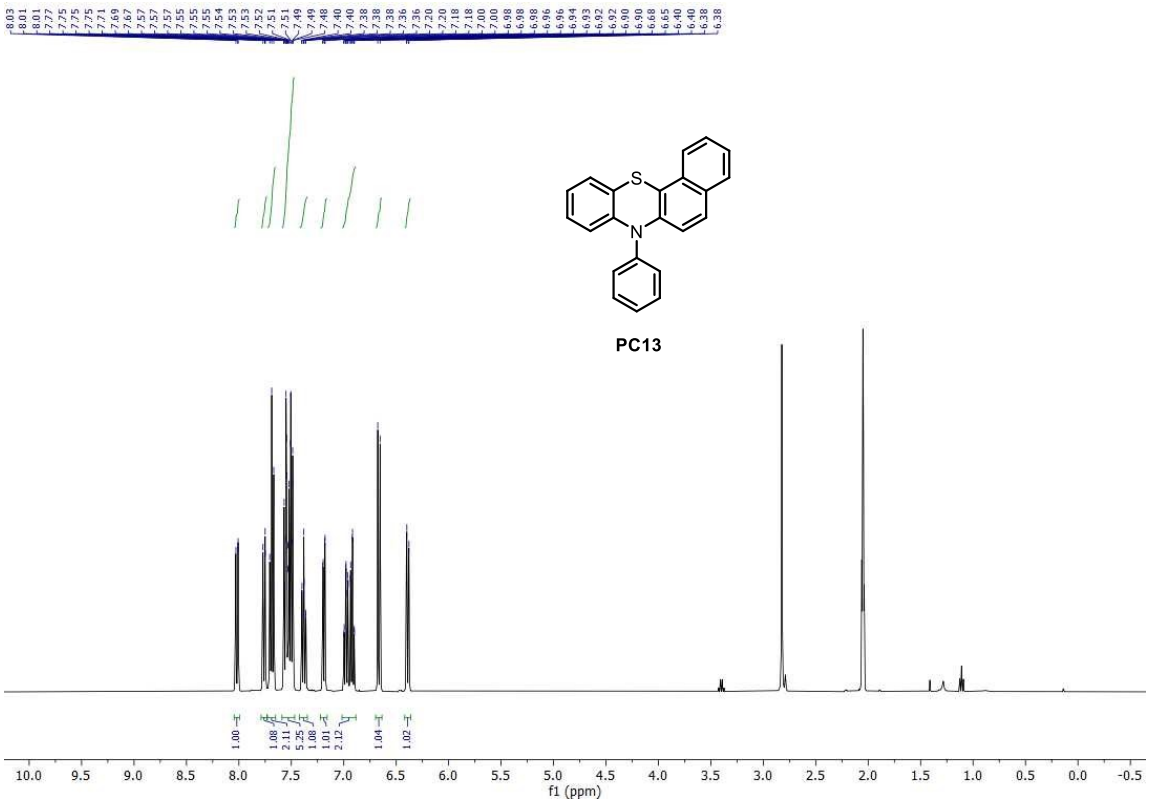

Figure S6. ^{1}H-NMR spectrum of PC13 in Acetone-d_6.

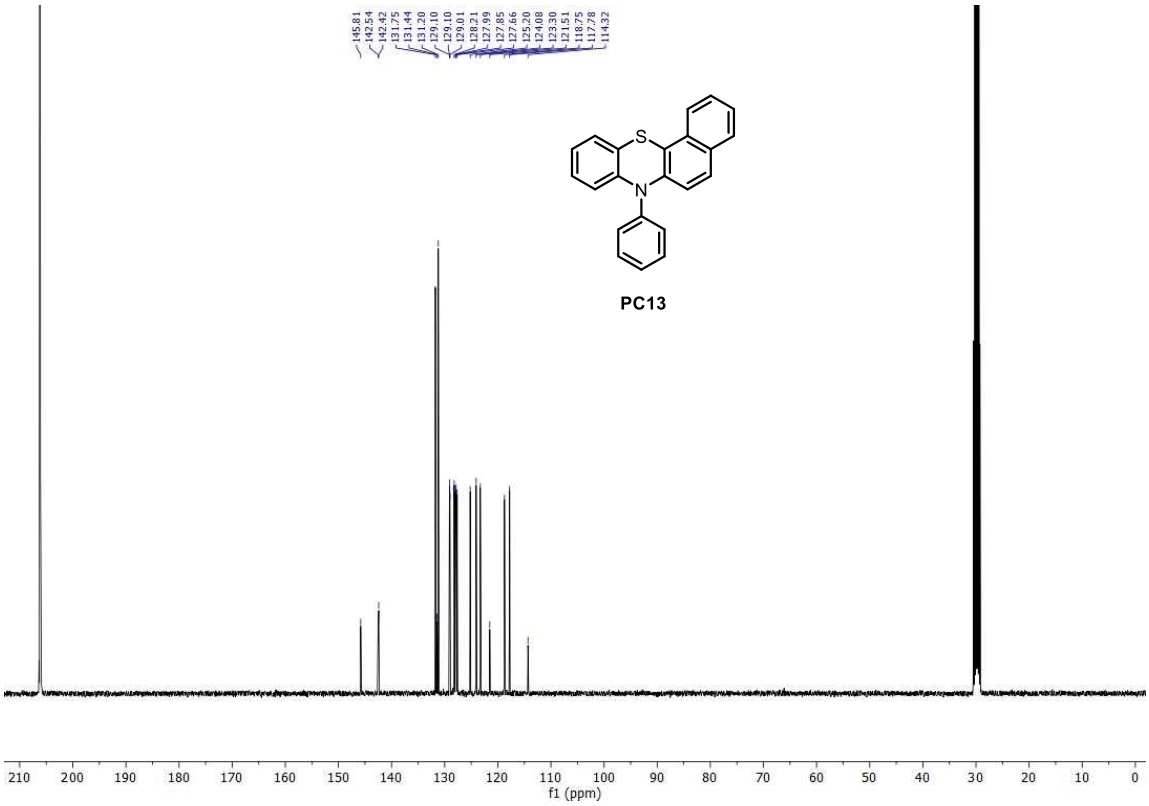

Figure S7. ^{13}C-NMR spectrum of PC13 in Acetone-d_6.

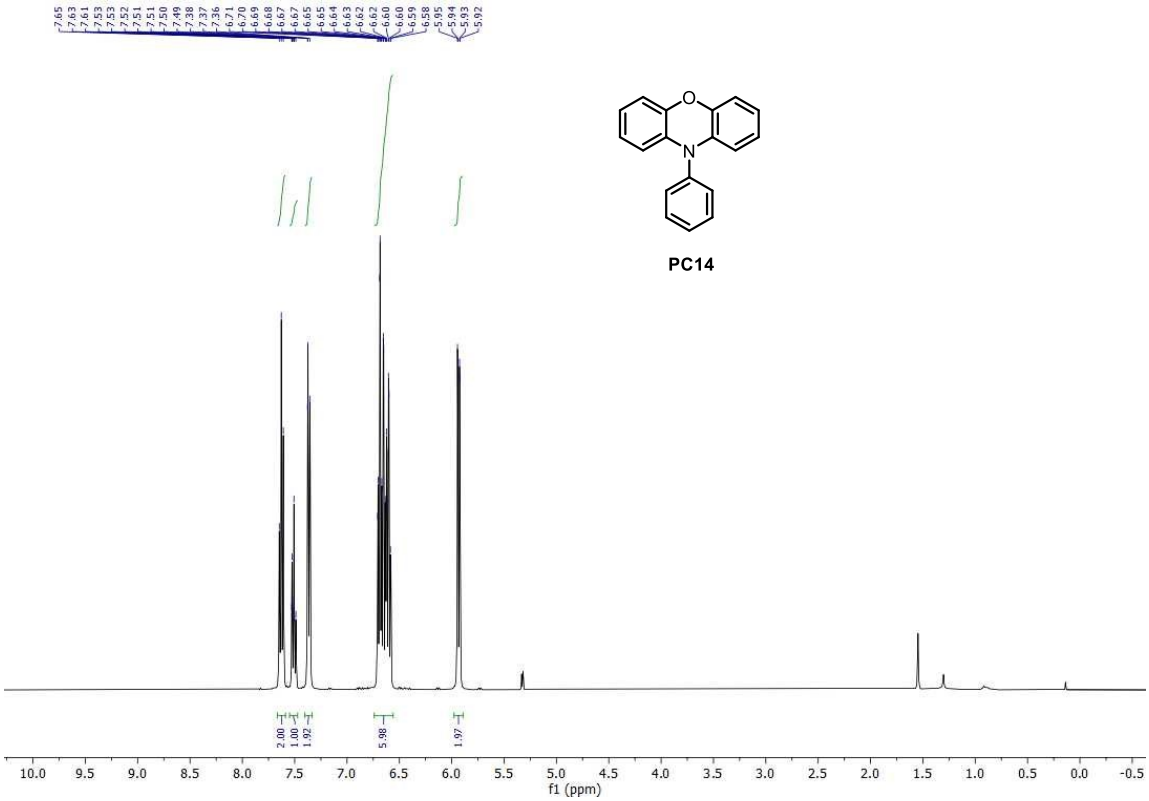

Figure S8. ^{1}H-NMR spectrum of PC14 in CD_2Cl_2.

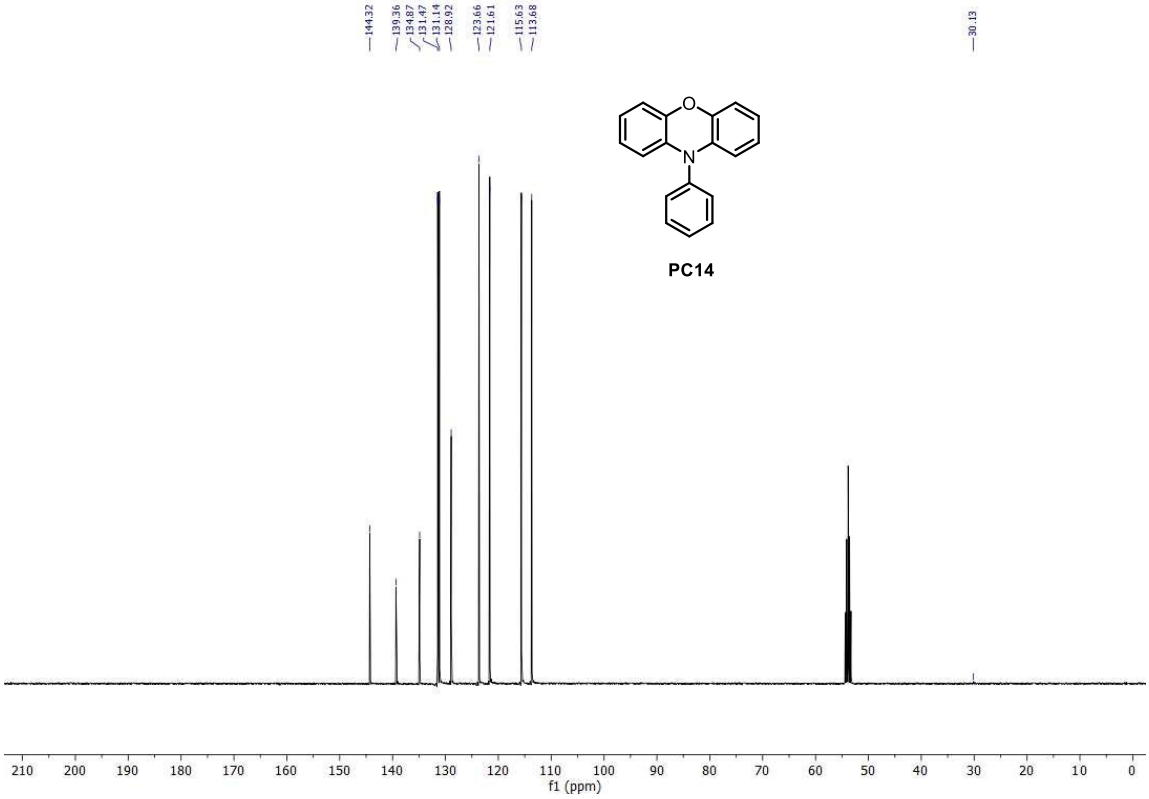

Figure S9. ^{13}C-NMR spectrum of PC14 in CD_2Cl_2.

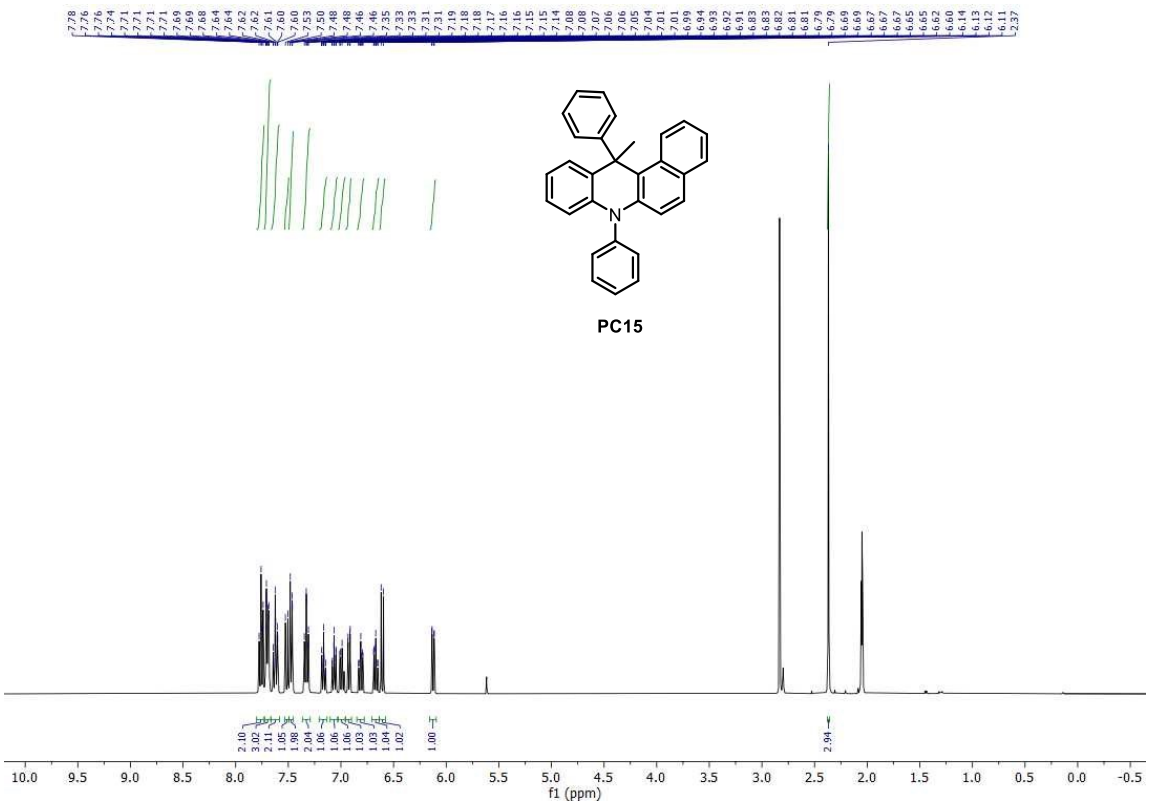

Figure S10. ^{1}H-NMR spectrum of PC15 in Acetone-d_6.

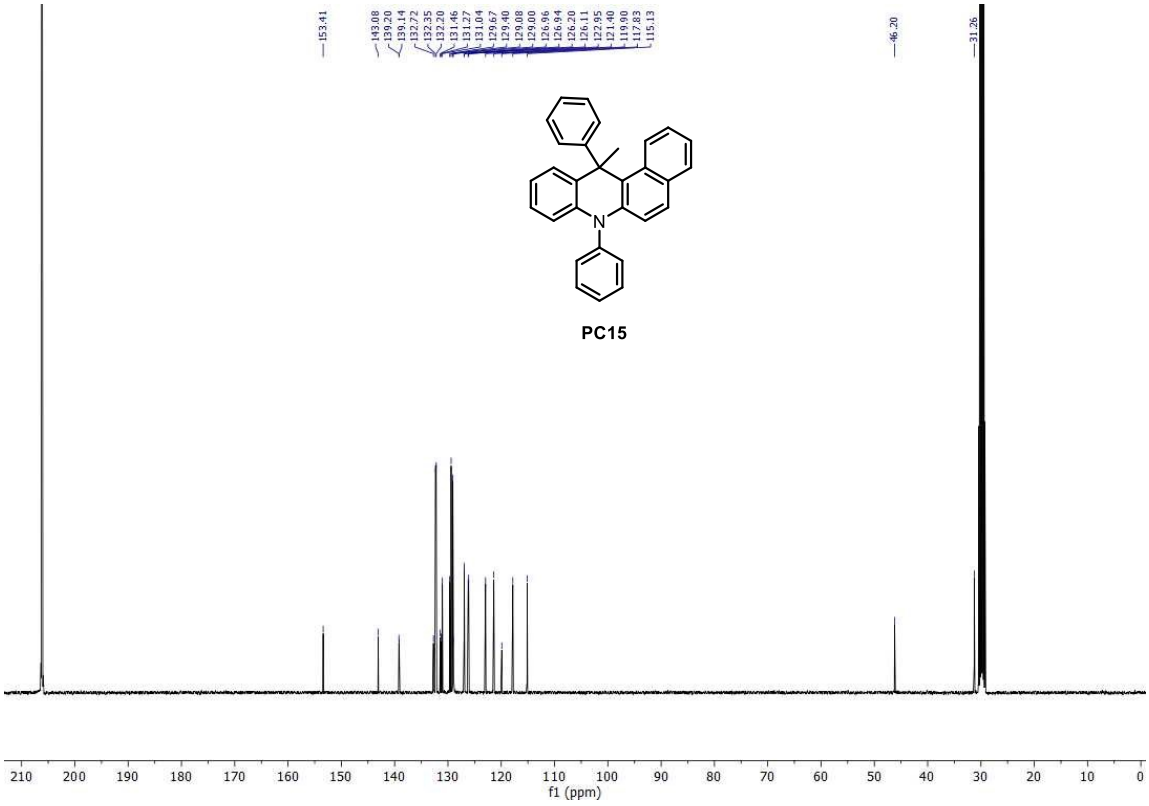

Figure S11. ^{13}C-NMR spectrum of PC15 in Acetone-d_6.

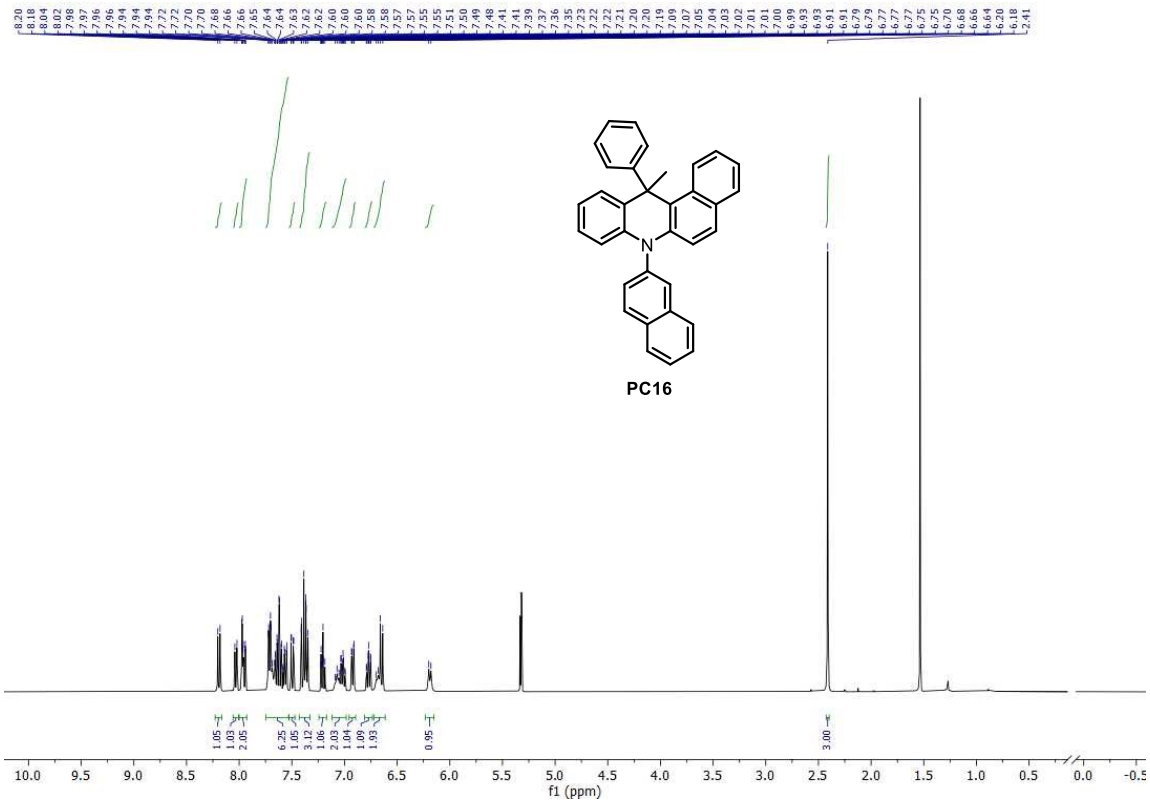

Figure S12. ^{1}H-NMR spectrum of PC16 in CD_2Cl_2.

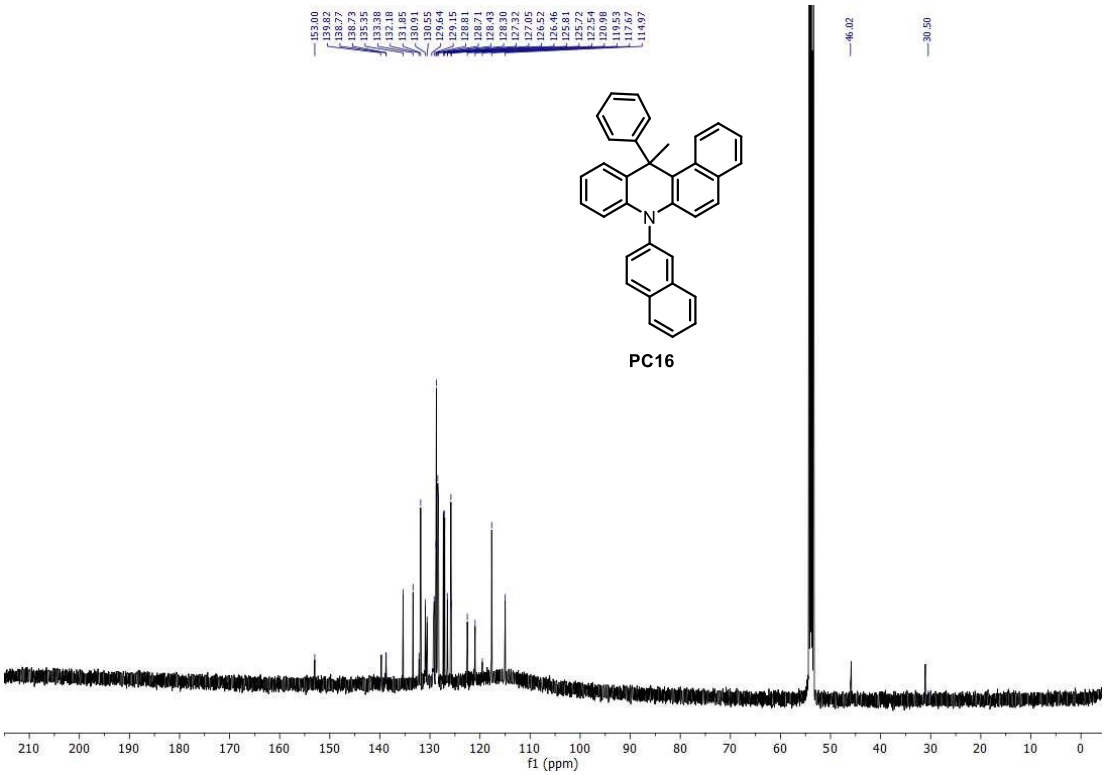

Figure S13. ^{13}C-NMR spectrum of PC16 in CD_2Cl_2.

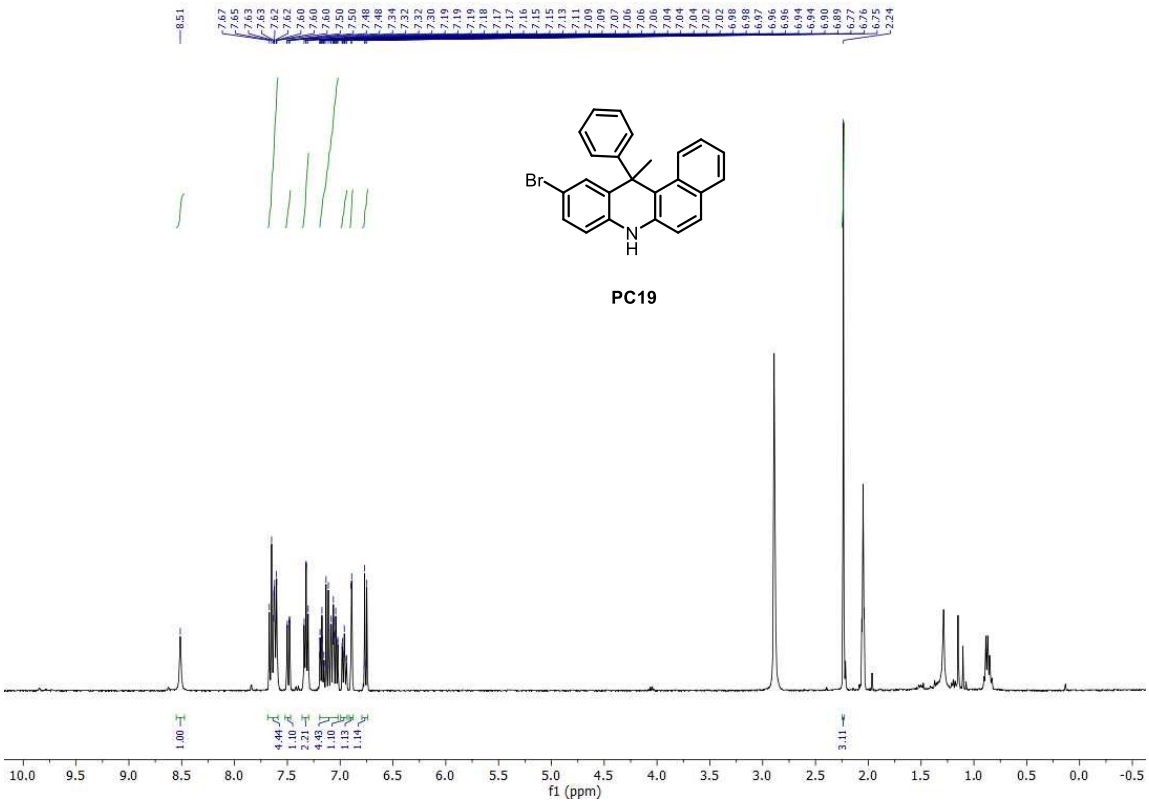

Figure S14. ^{1}H-NMR spectrum of PC19 in Acetone-d_6.

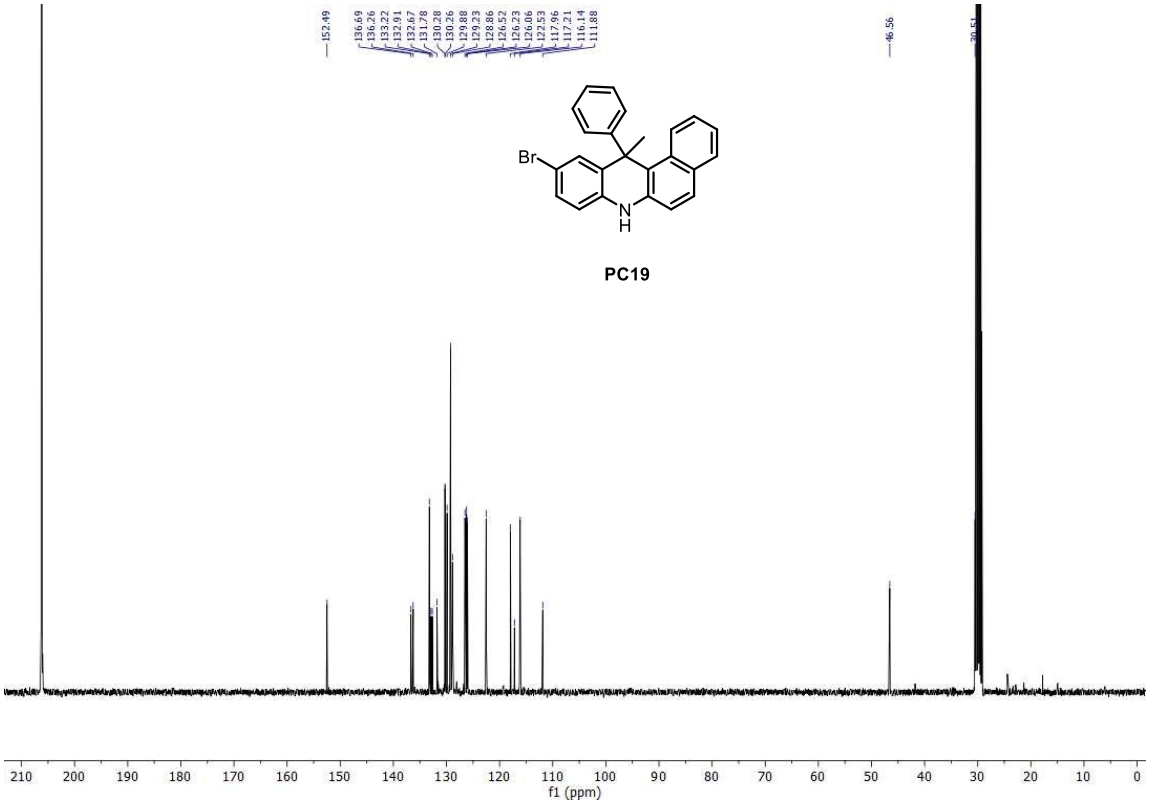

Figure S15. ^{13}C-NMR spectrum of PC19 in Acetone-d_6.

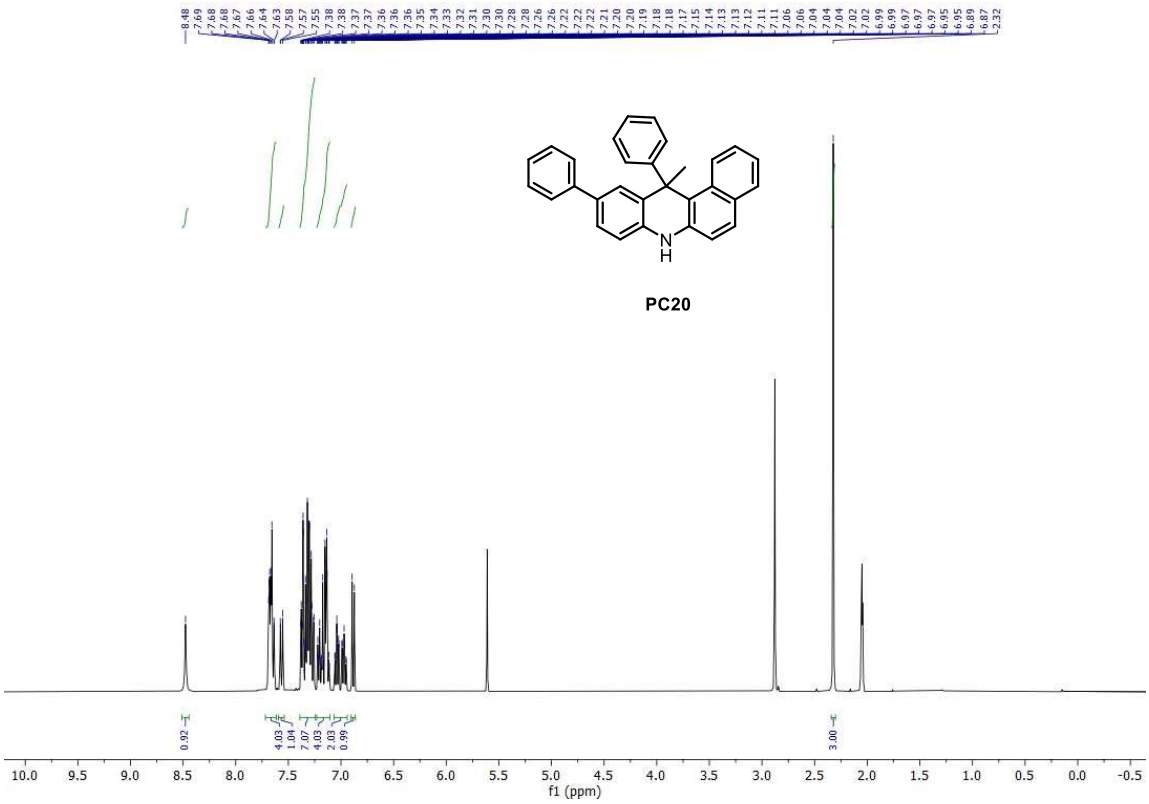

Figure S16. ^{1}H-NMR spectrum of PC20 in Acetone-d_6.

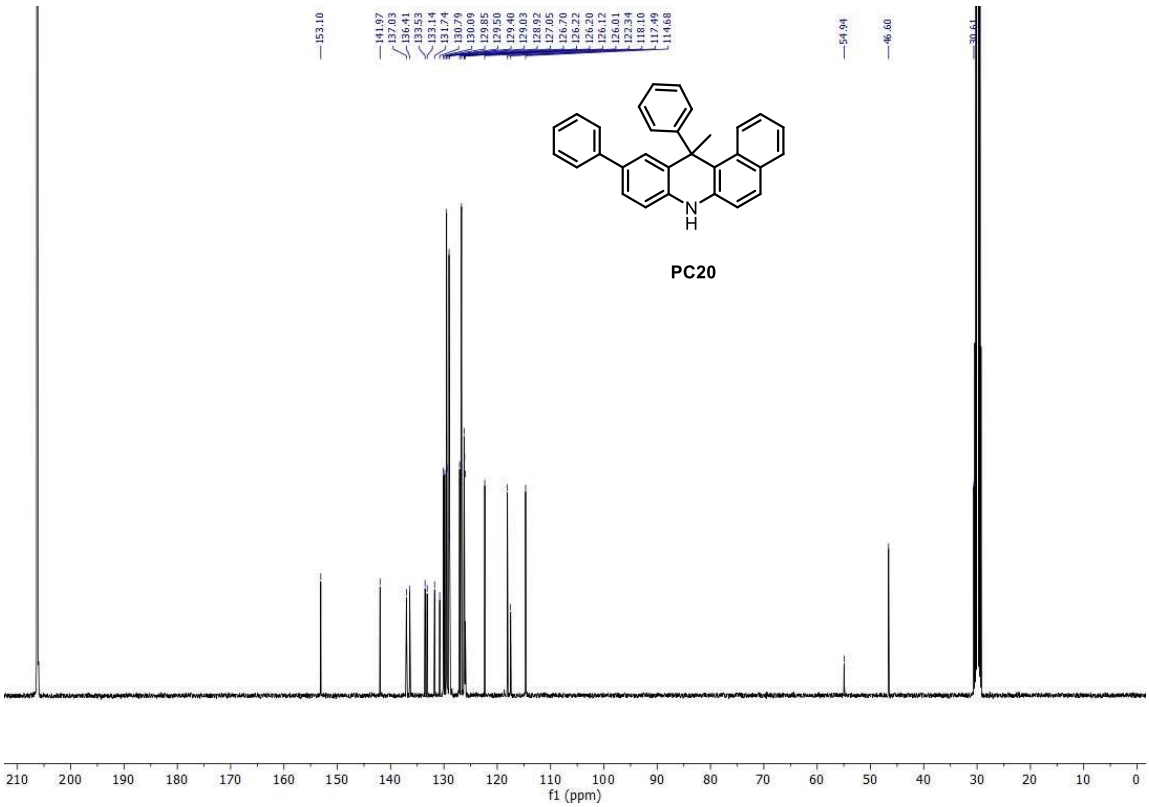

Figure S17. ^{13}C-NMR spectrum of PC20 in Acetone-d_6.

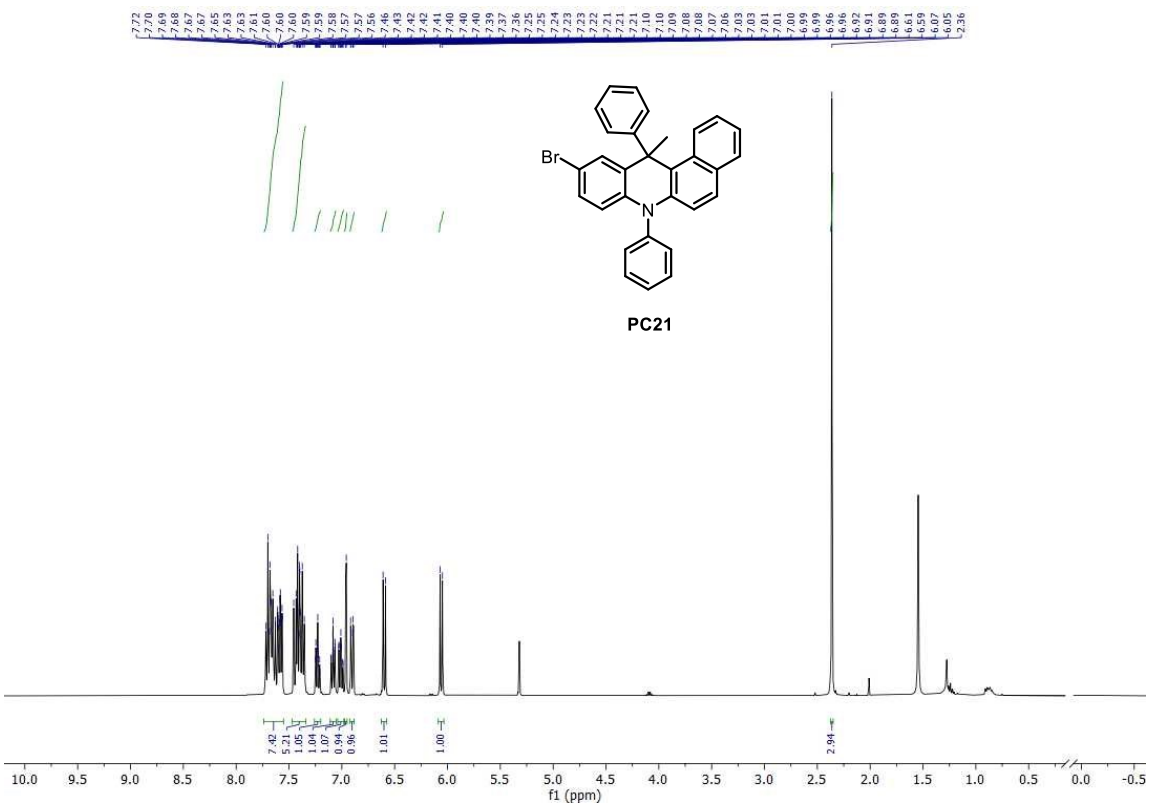

Figure S18. ^{1}H-NMR spectrum of PC21 in CD_2Cl_2.

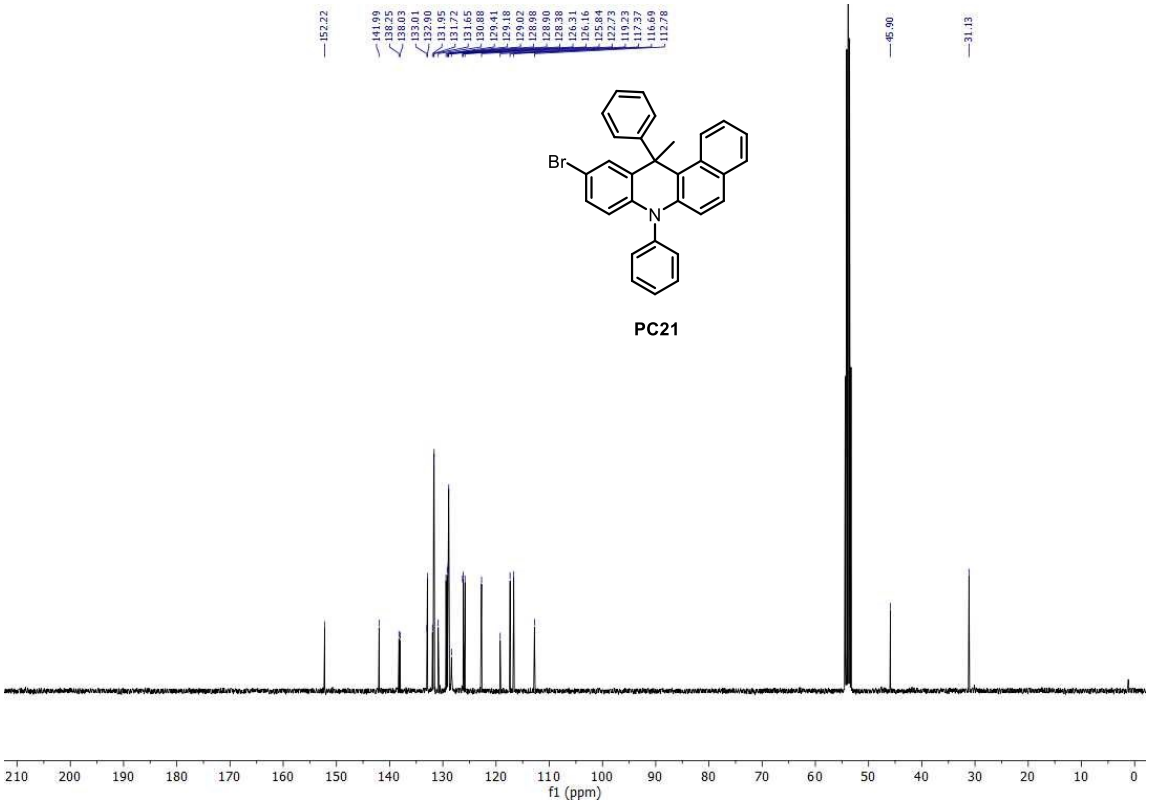

Figure S19. ^{13}C-NMR spectrum of PC21 in CD_2Cl_2.

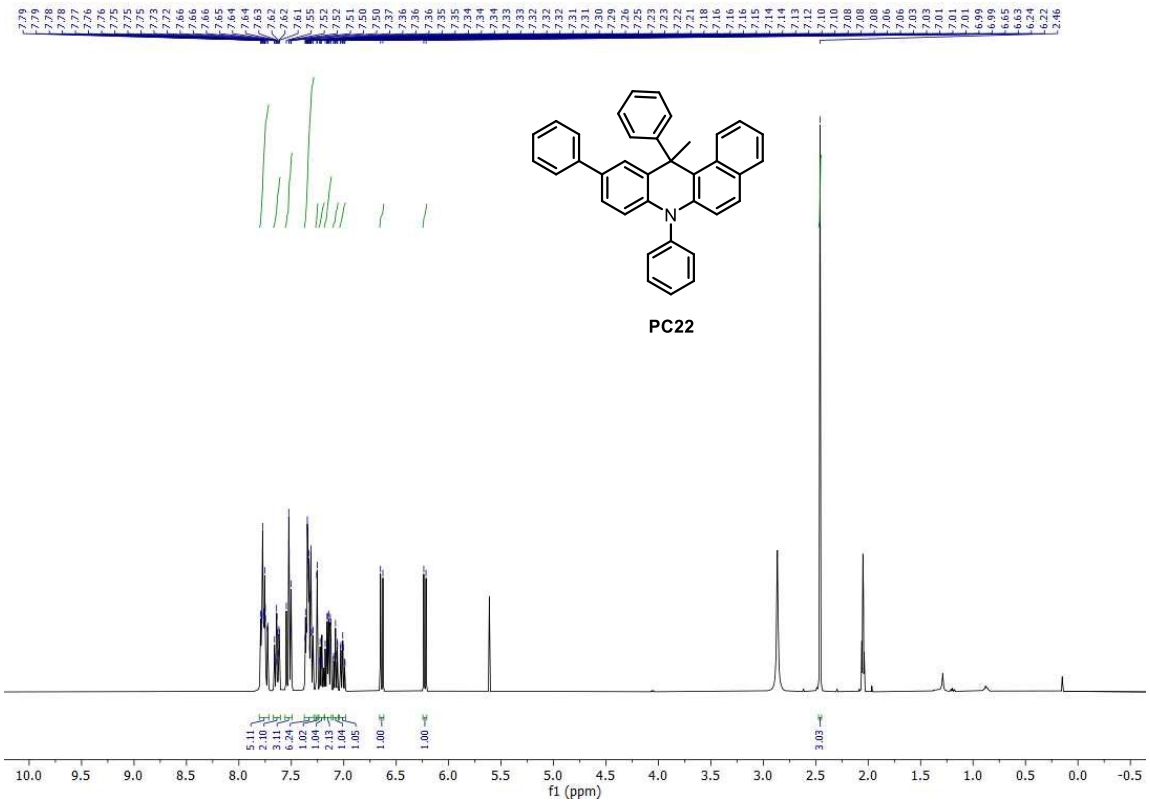

Figure S20. ^{1}H-NMR spectrum of PC22 in Acetone-d_6.

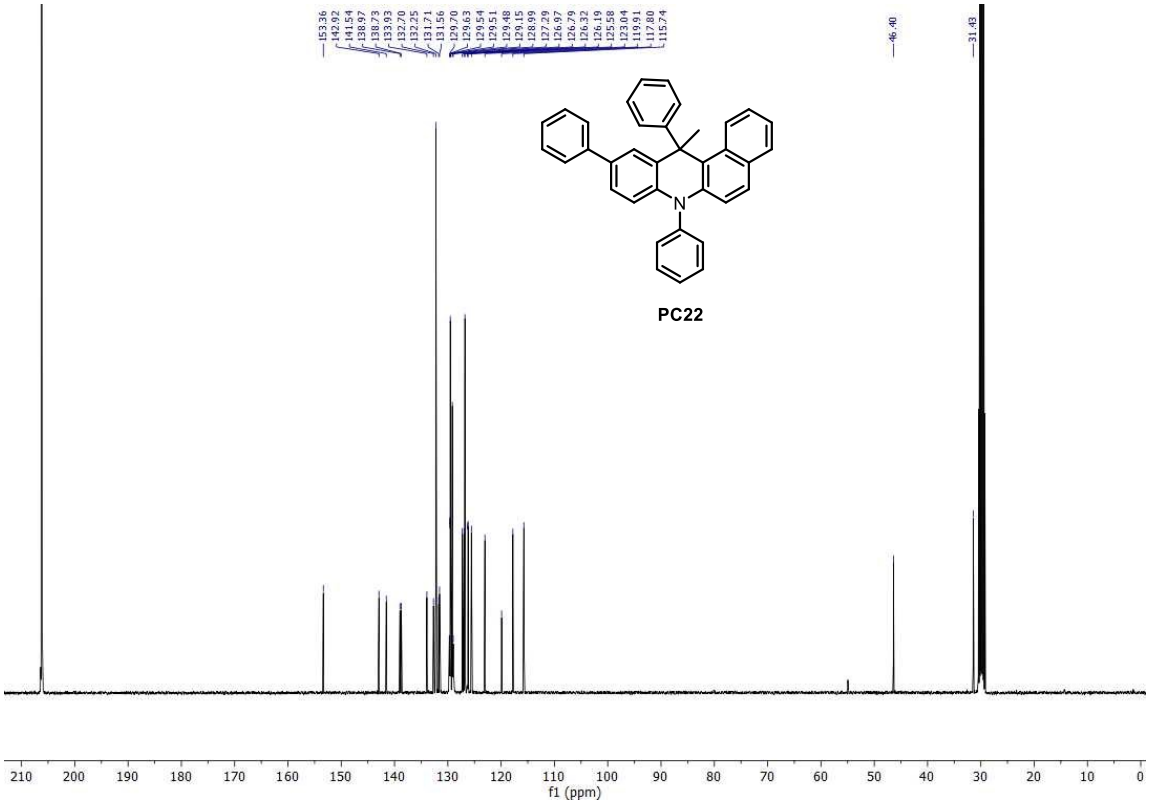

Figure S21. ^{13}C-NMR spectrum of PC22 in Acetone-d_6.

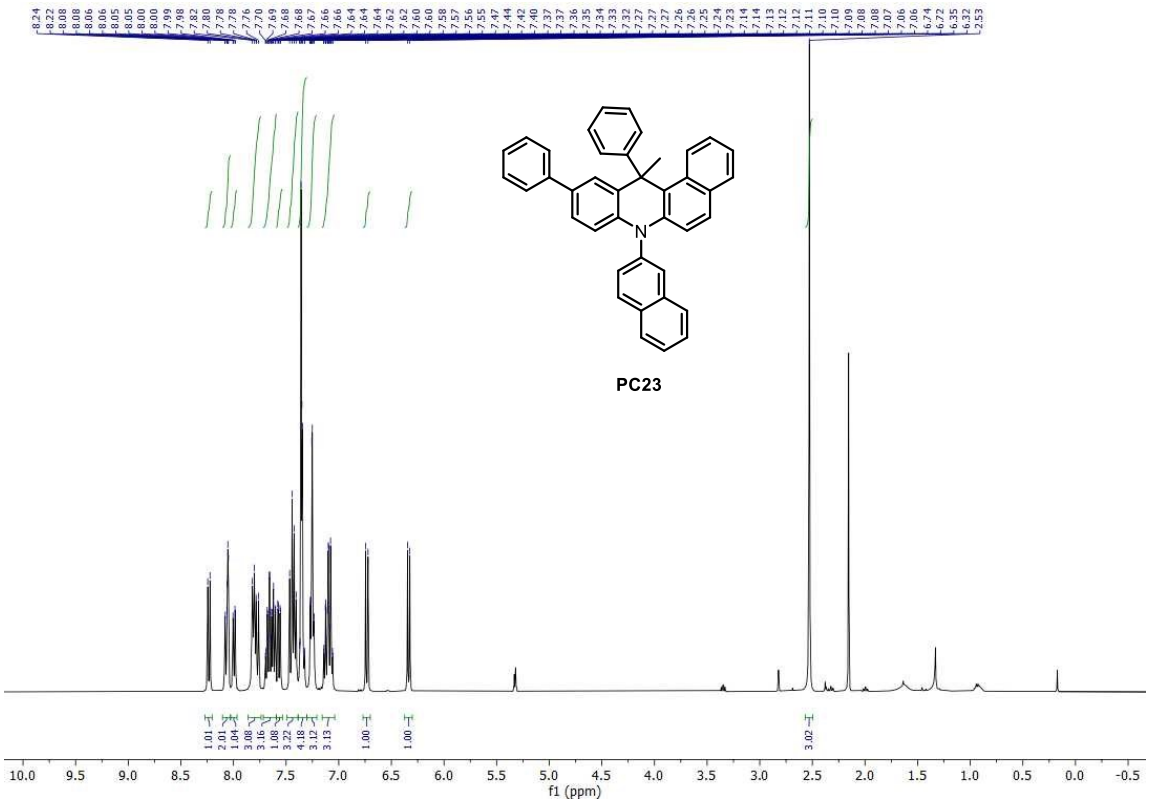

Figure S22. ^{1}H-NMR spectrum of PC23 in CD_2Cl_2.

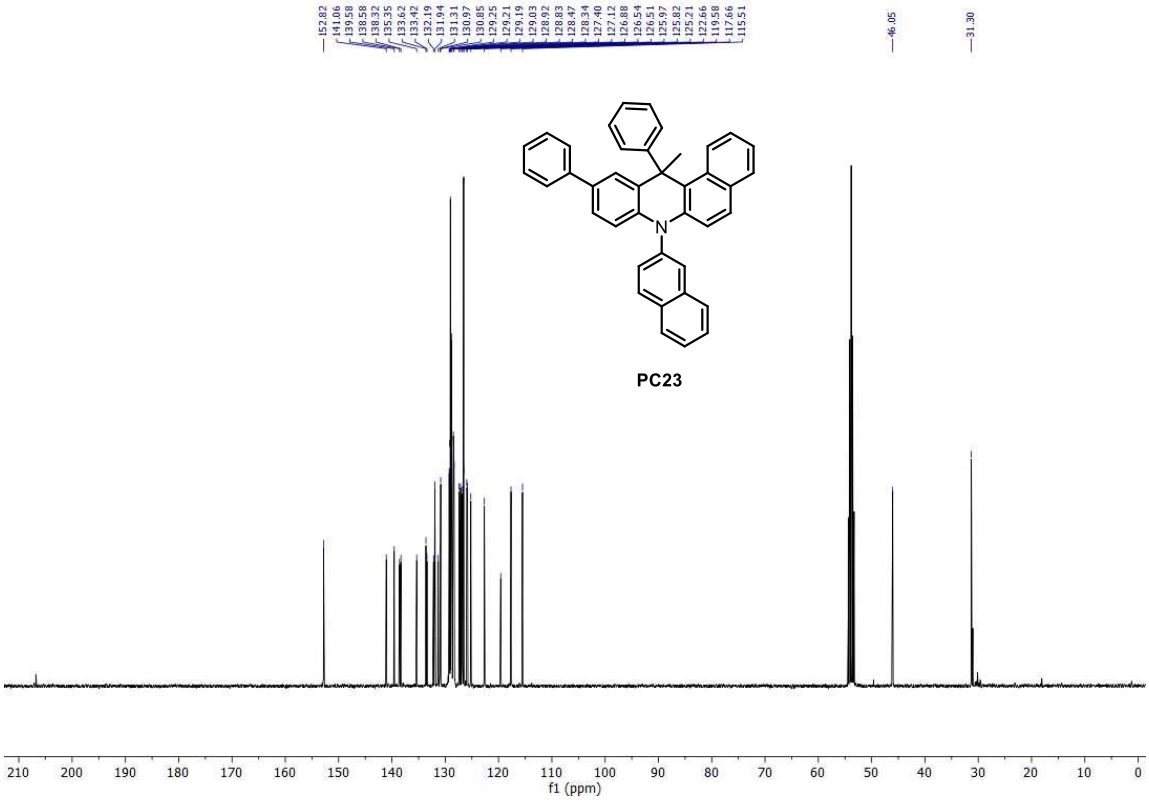

Figure S23. ^{13}C-NMR spectrum of PC23 in CD_2Cl_2.

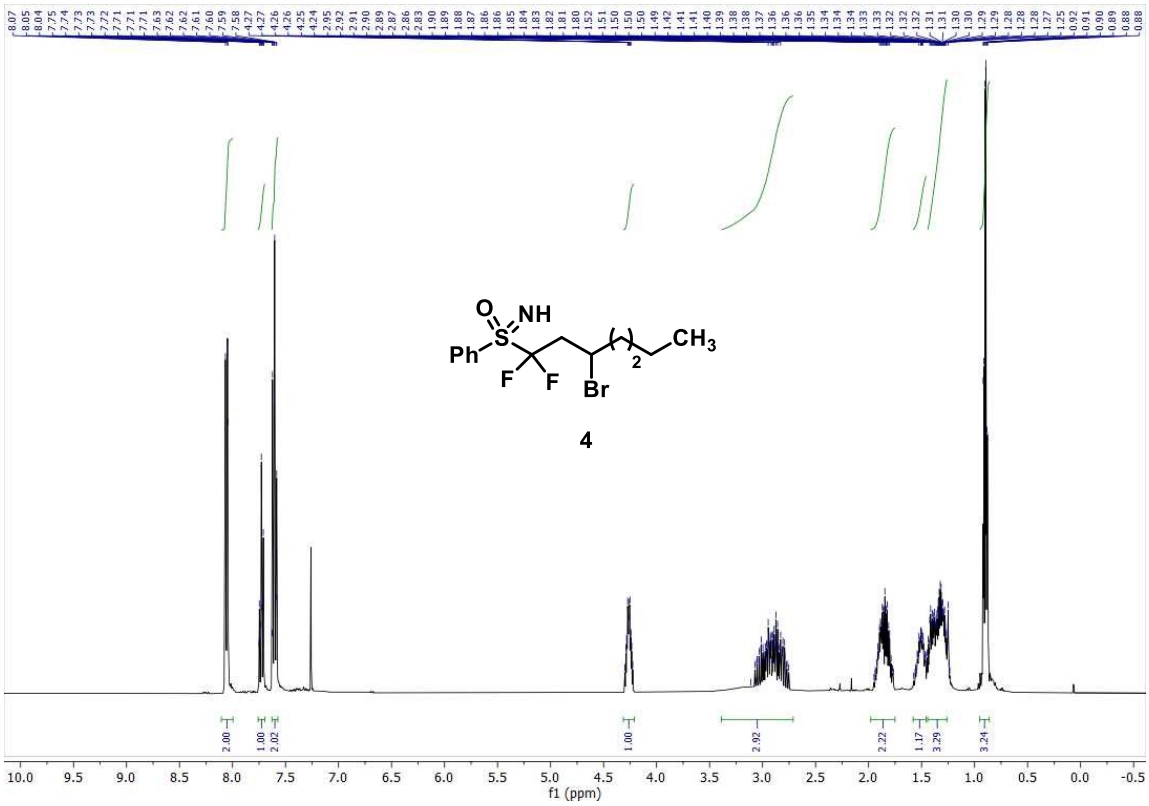

Figure S24. ^{1}H-NMR spectrum of 4 in $CDCl_3$.

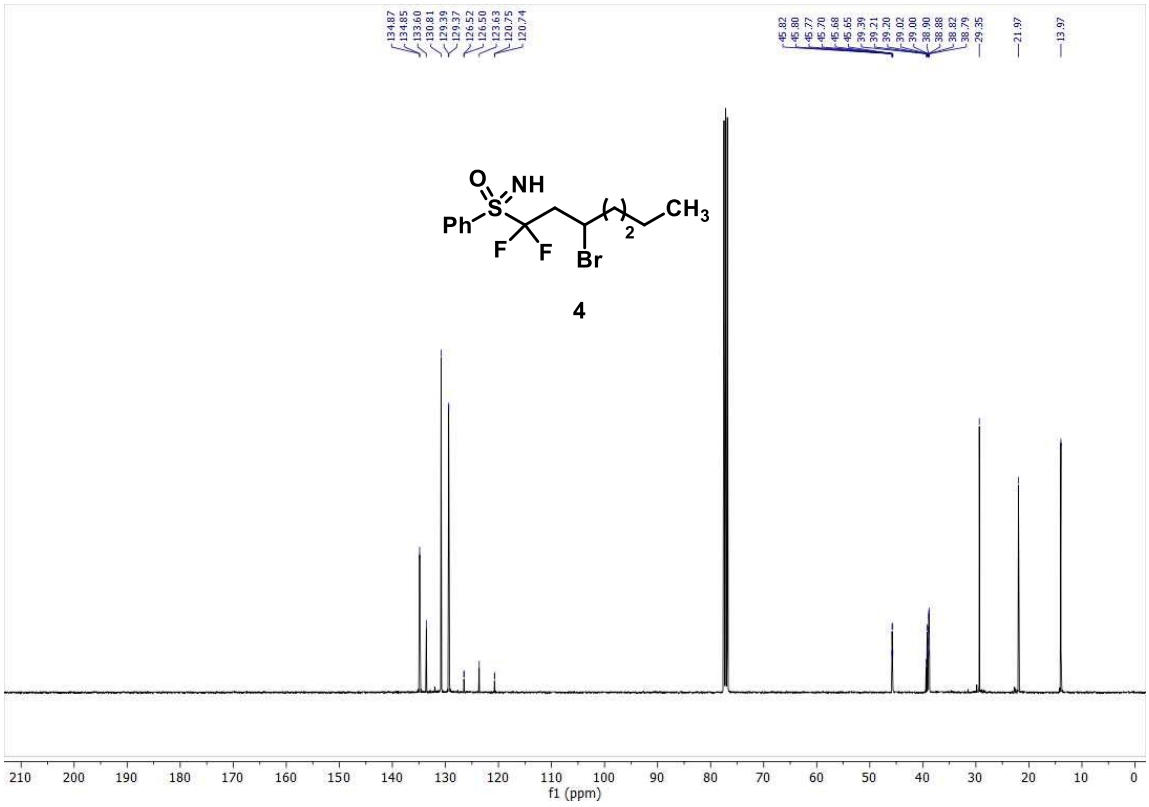

Figure S25. ^{13}C-NMR spectrum of 4 in $CDCl_3$.

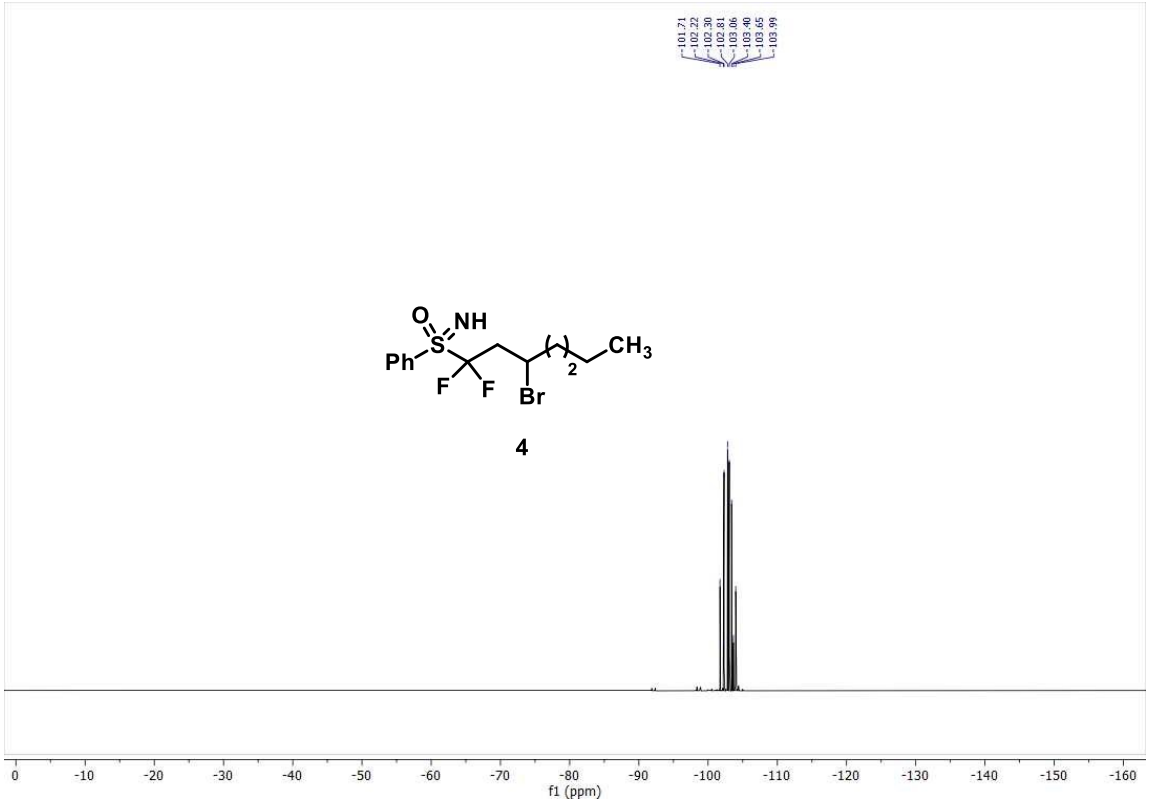

Figure S26. ^{19}F-NMR spectrum of 4 in $CDCl_3$.

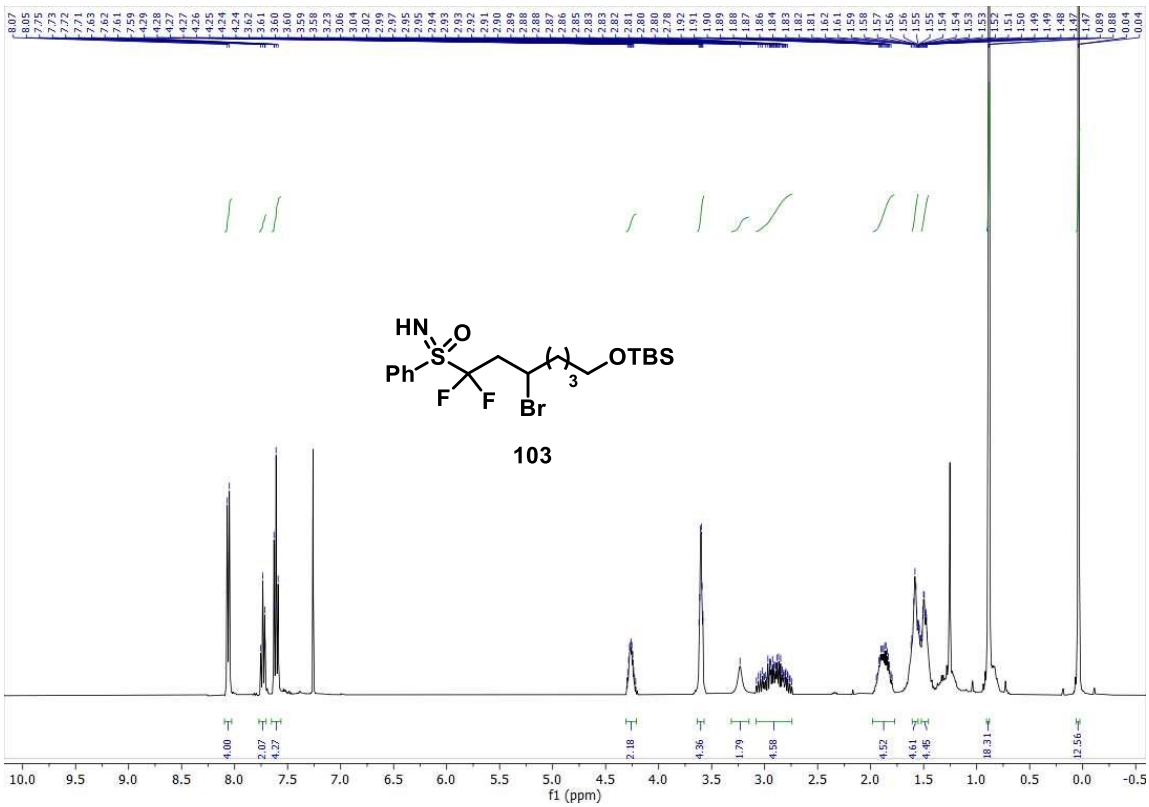

Figure S27. ^{1}H-NMR spectrum of 103 in $CDCl_3$.

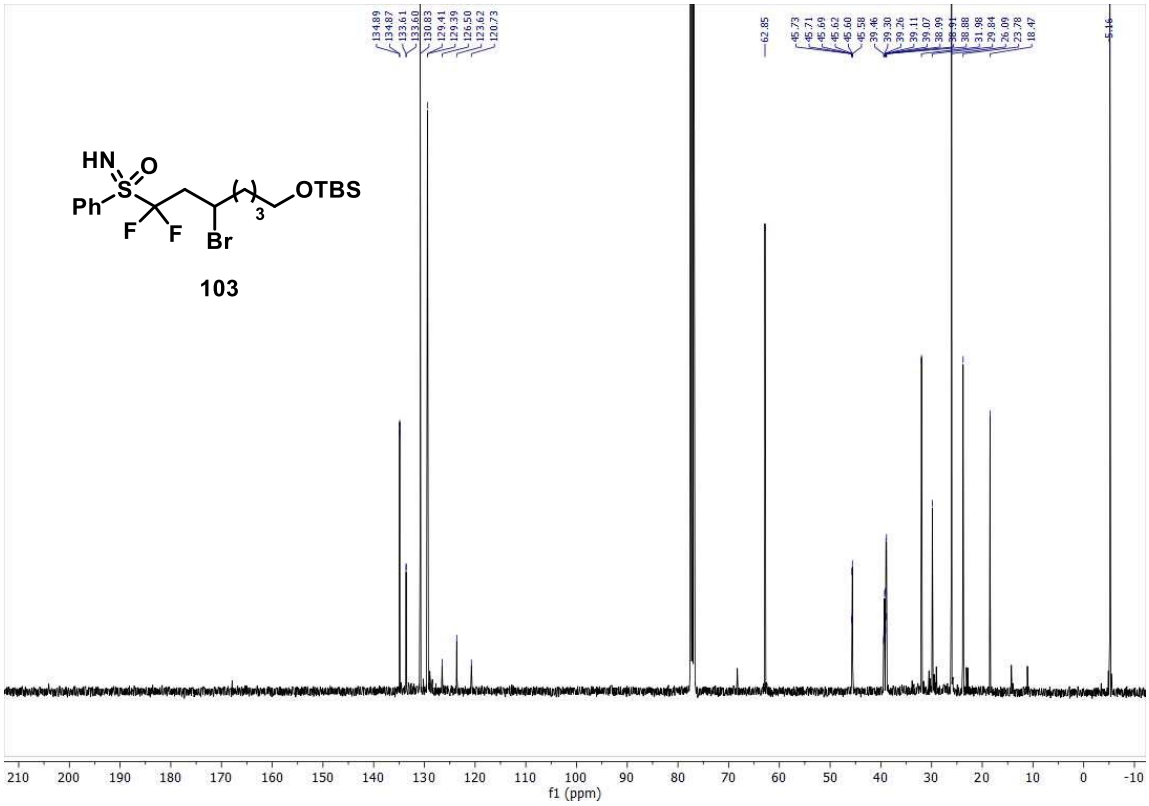

Figure S28. ^{13}C-NMR spectrum of 103 in $CDCl_3$.

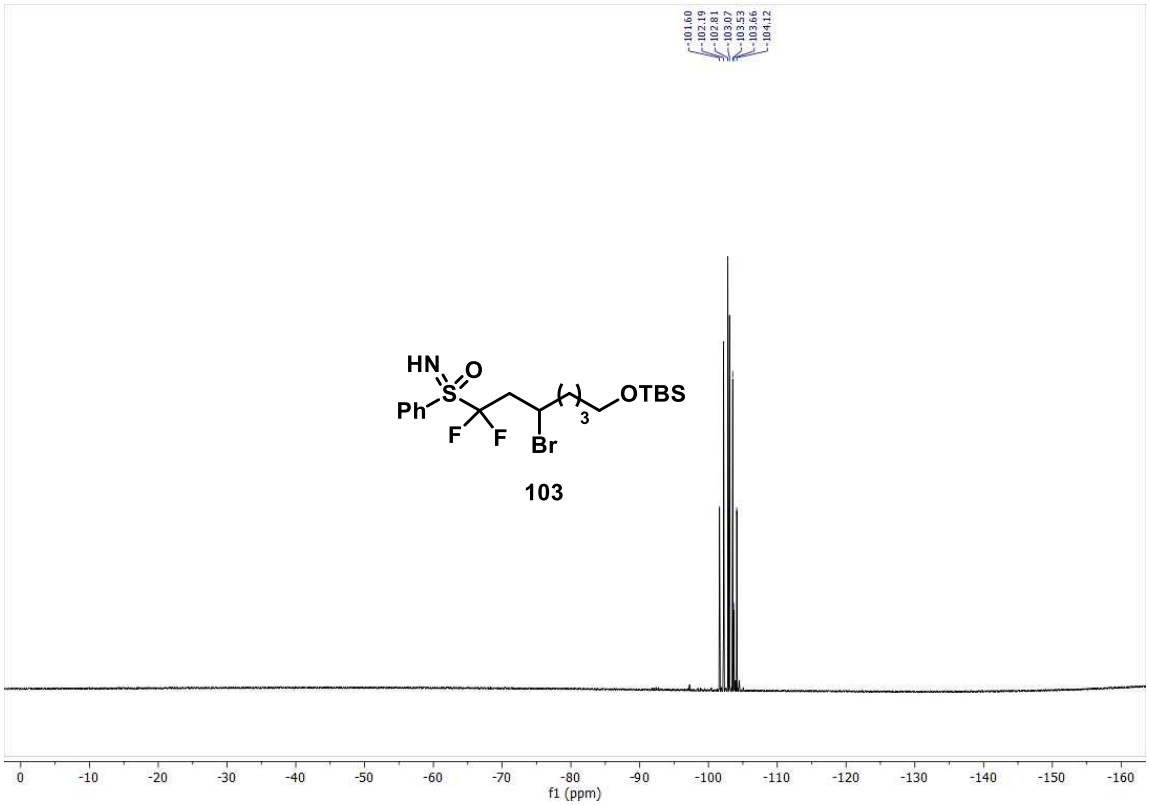

Figure S29. ^{19}F-NMR spectrum of 103 in $CDCl_3$.

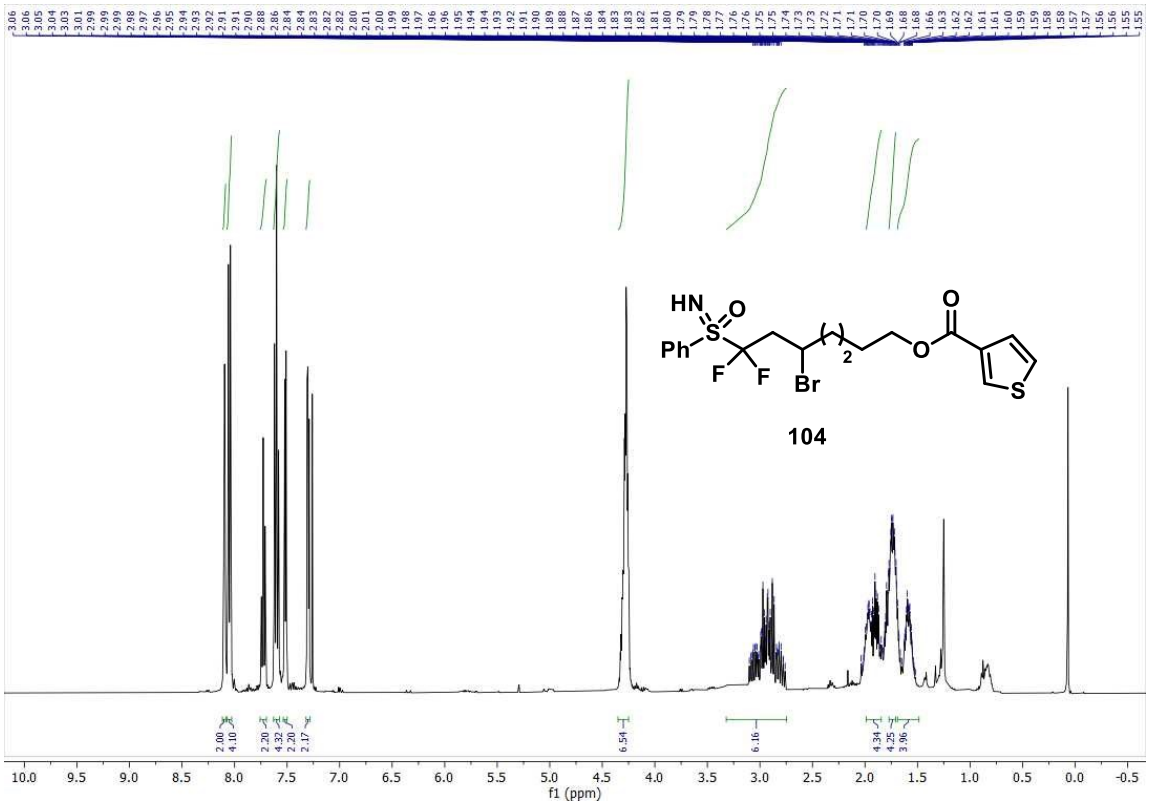

Figure S30. ^{1}H-NMR spectrum of 104 in $CDCl_3$.

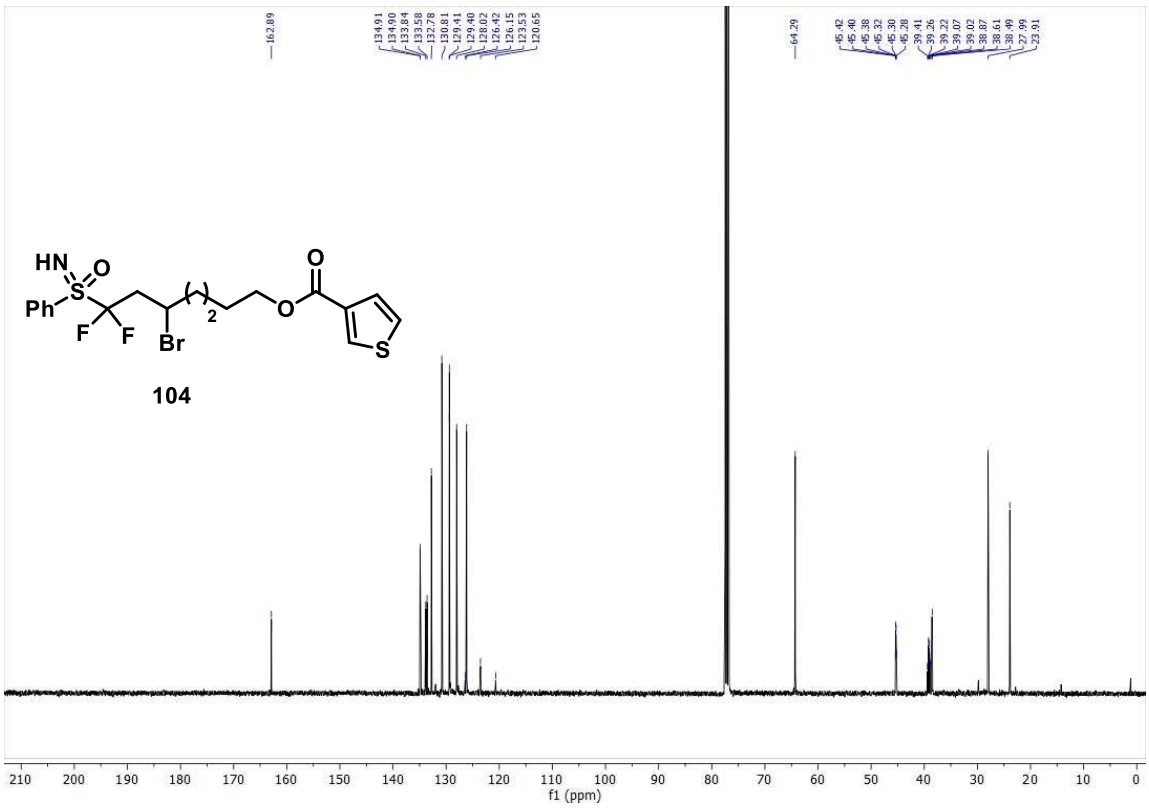

Figure S31. ^{13}C-NMR spectrum of 104 in $CDCl_3$.

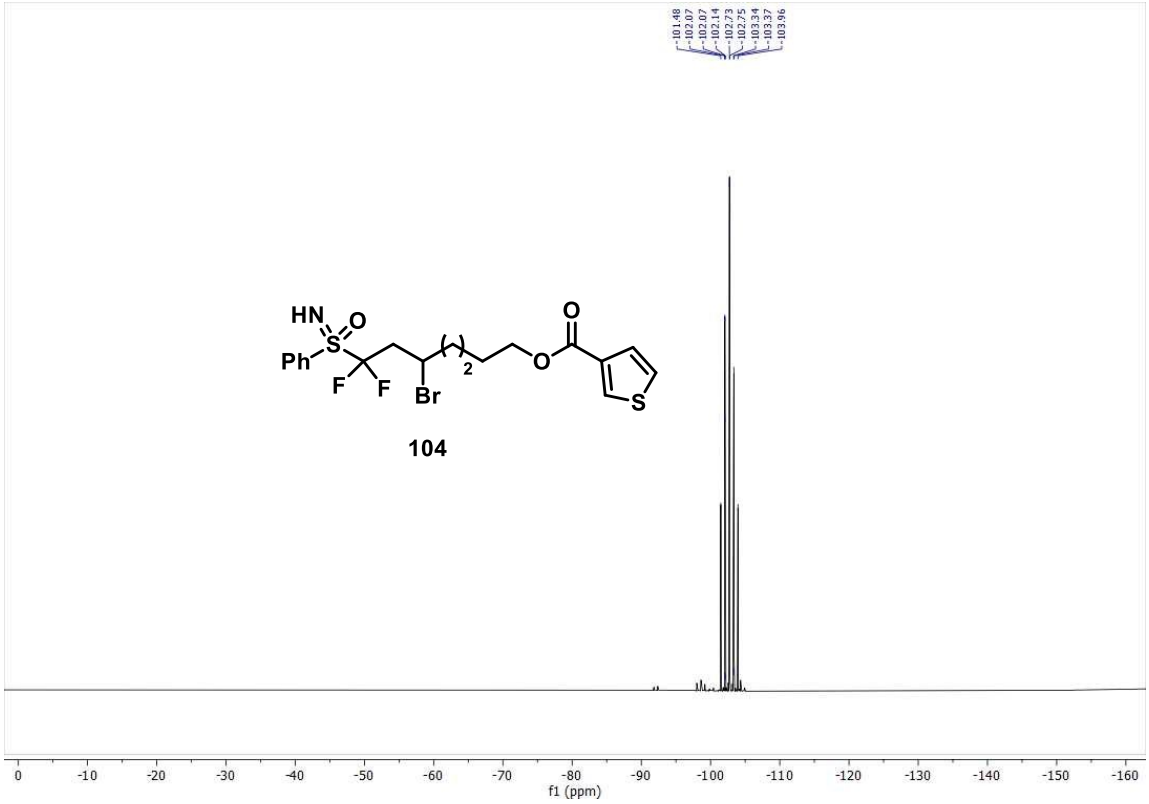

Figure S32. ^{19}F-NMR spectrum of 104 in $CDCl_3$.

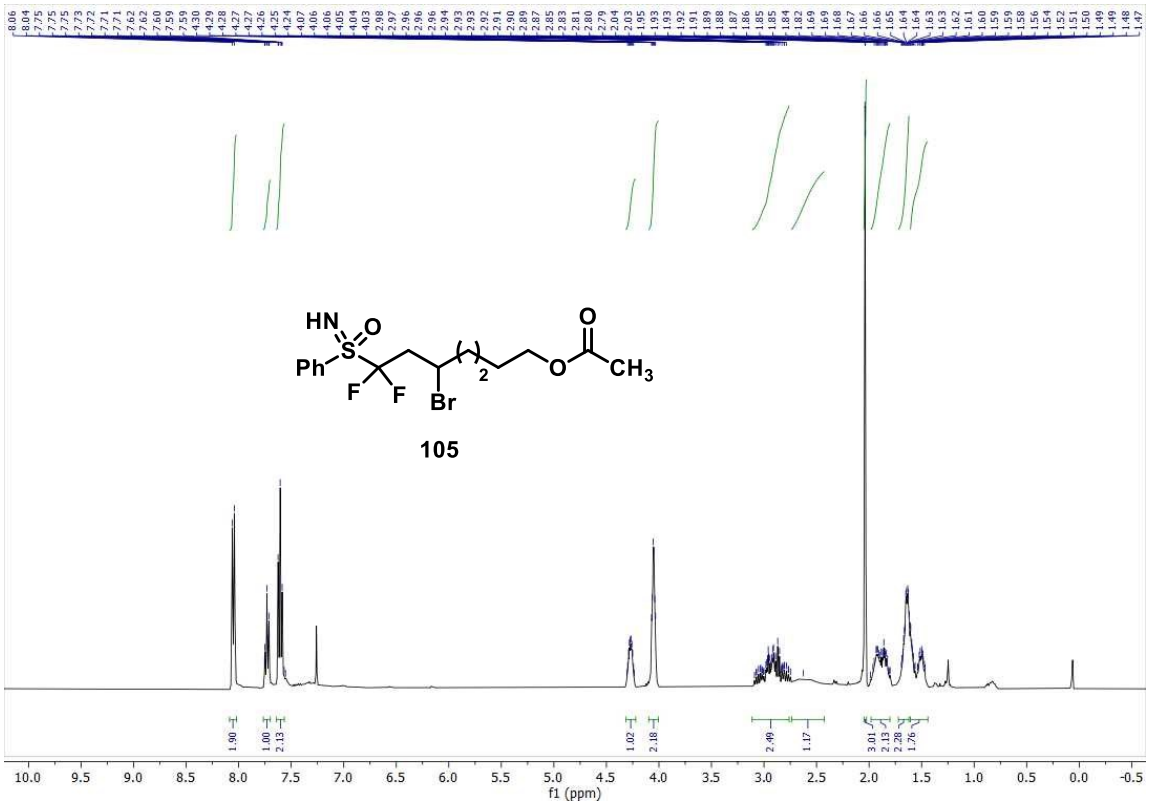

Figure S33. ^{1}H-NMR spectrum of 105 in $CDCl_3$.

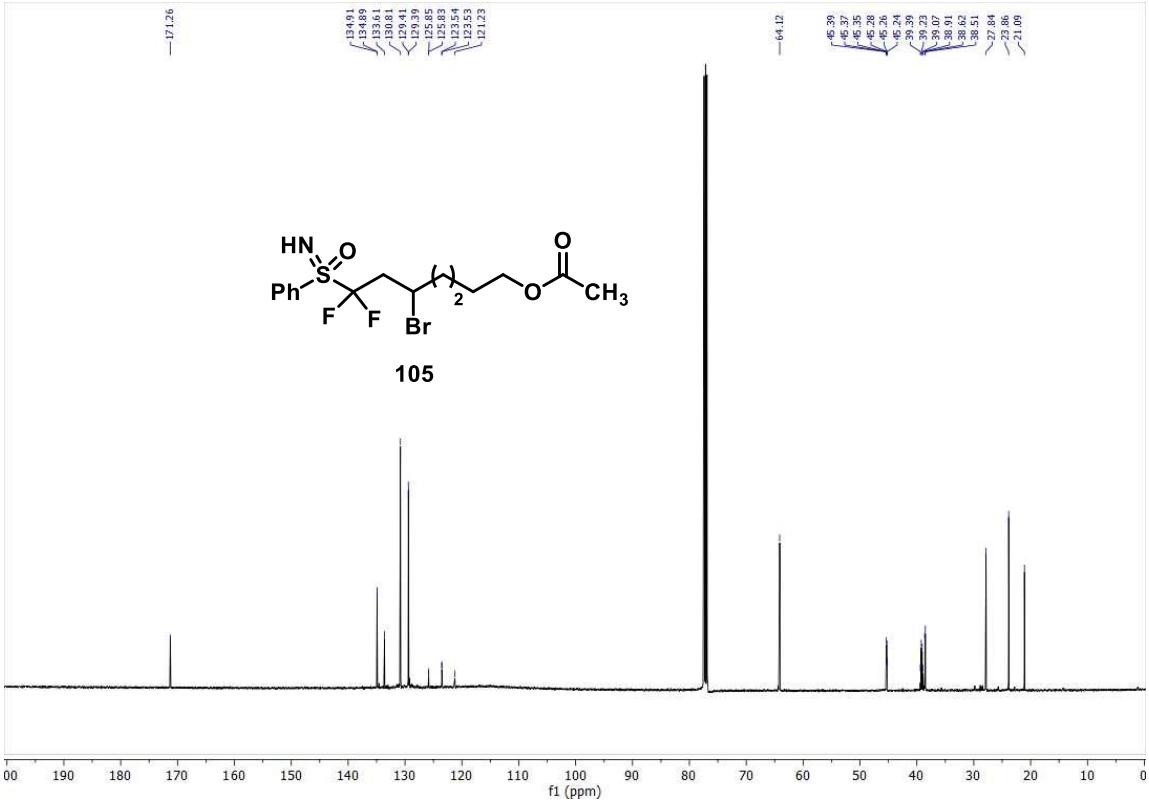

Figure S34. ^{13}C-NMR spectrum of 105 in $CDCl_3$.

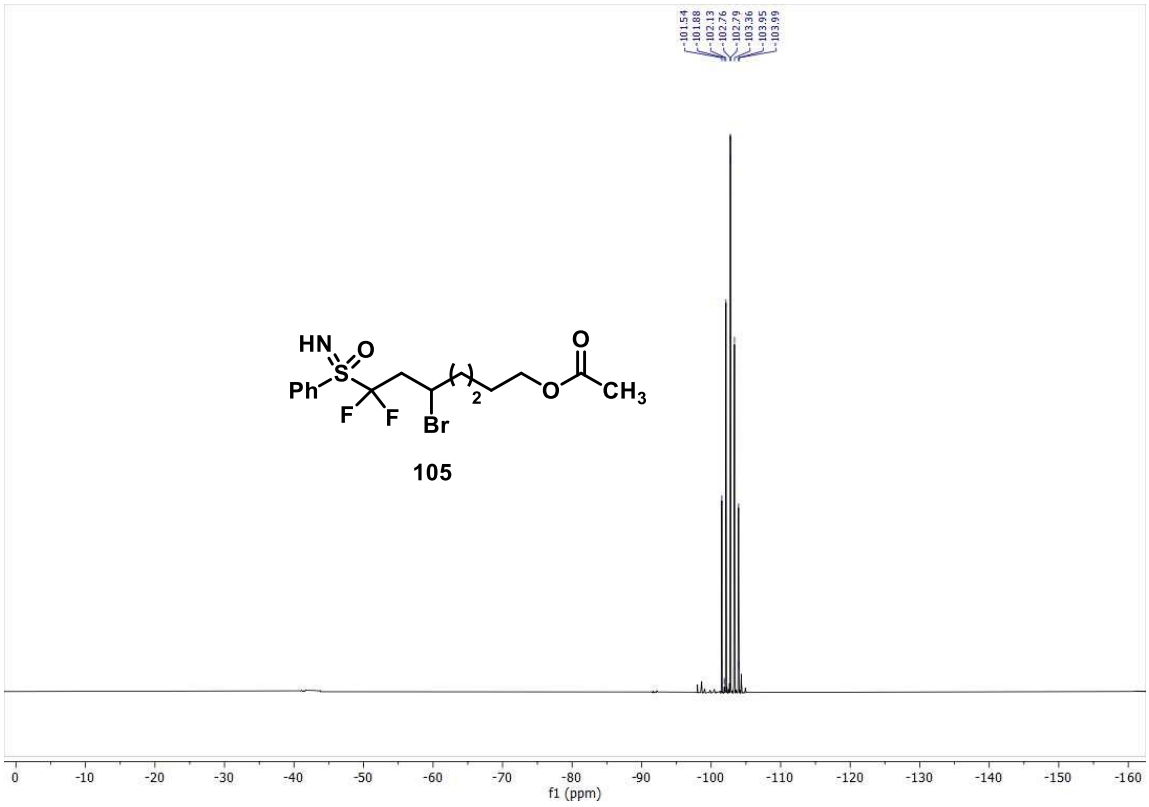

Figure S35. ^{19}F-NMR spectrum of 105 in $CDCl_3$.

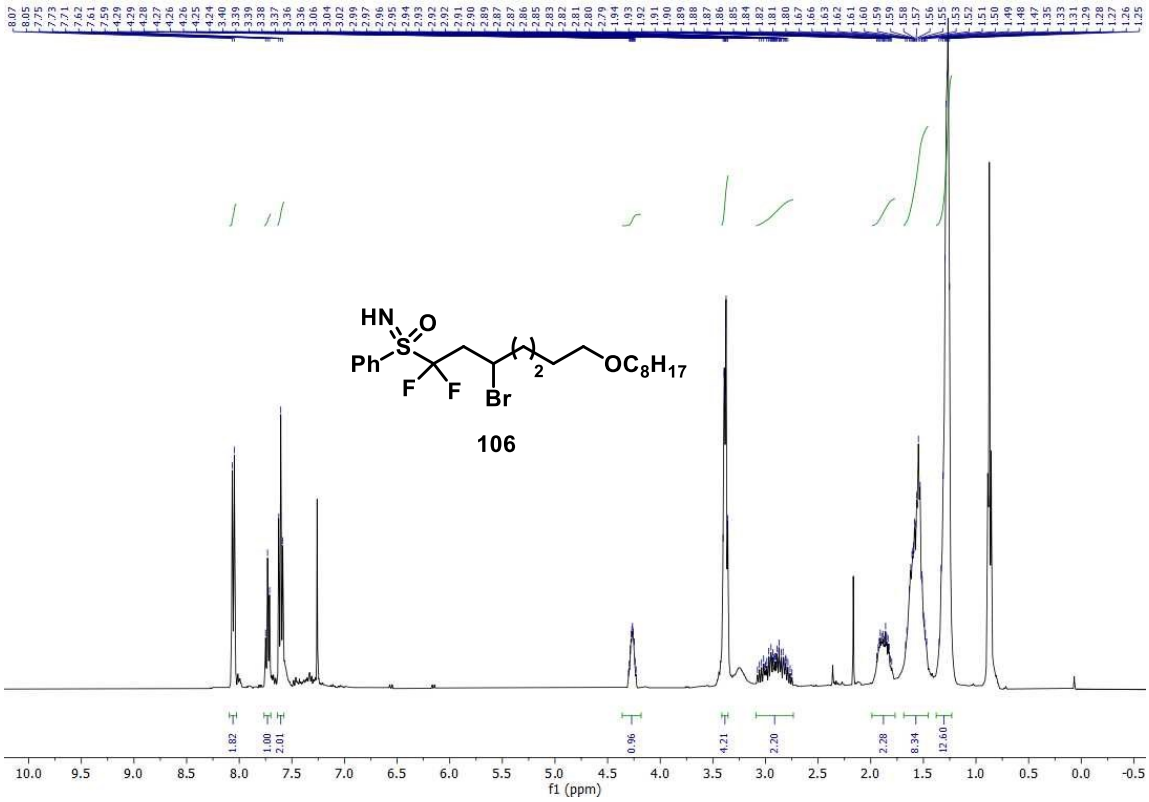

Figure S36. ^{1}H-NMR spectrum of 106 in $CDCl_3$.

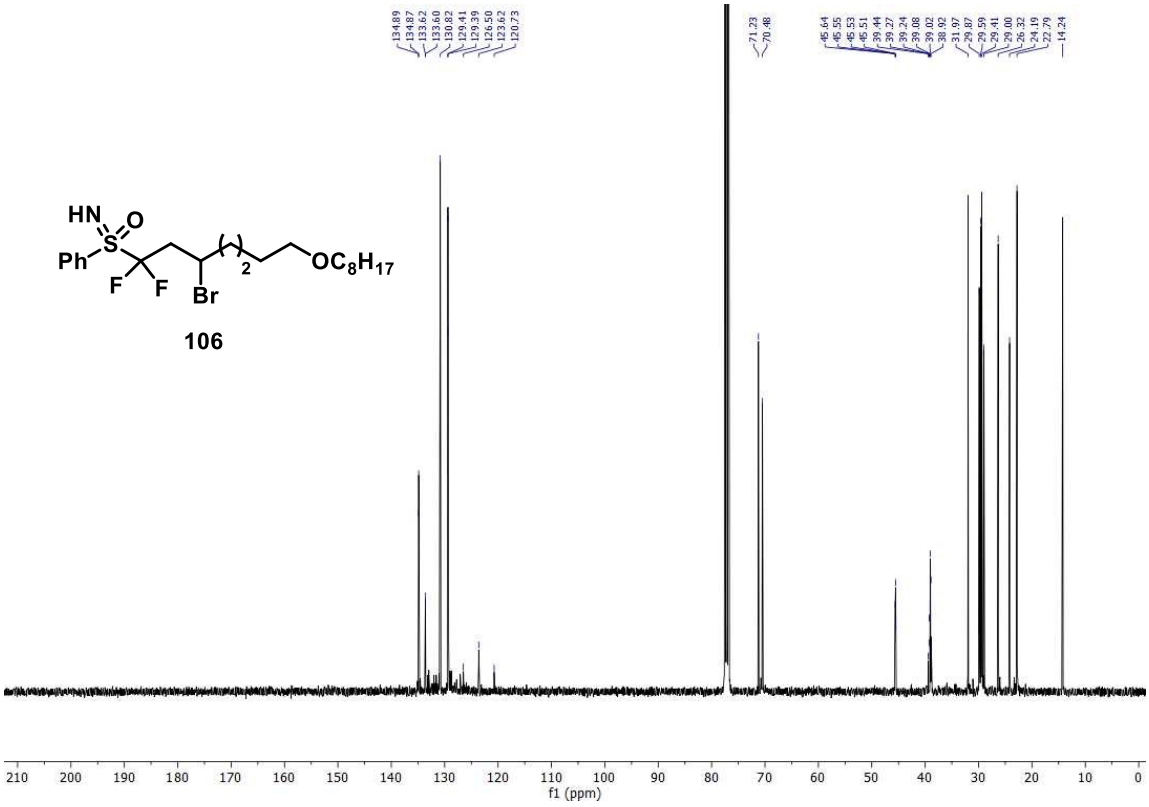

Figure S37. ^{13}C-NMR spectrum of 106 in $CDCl_3$.

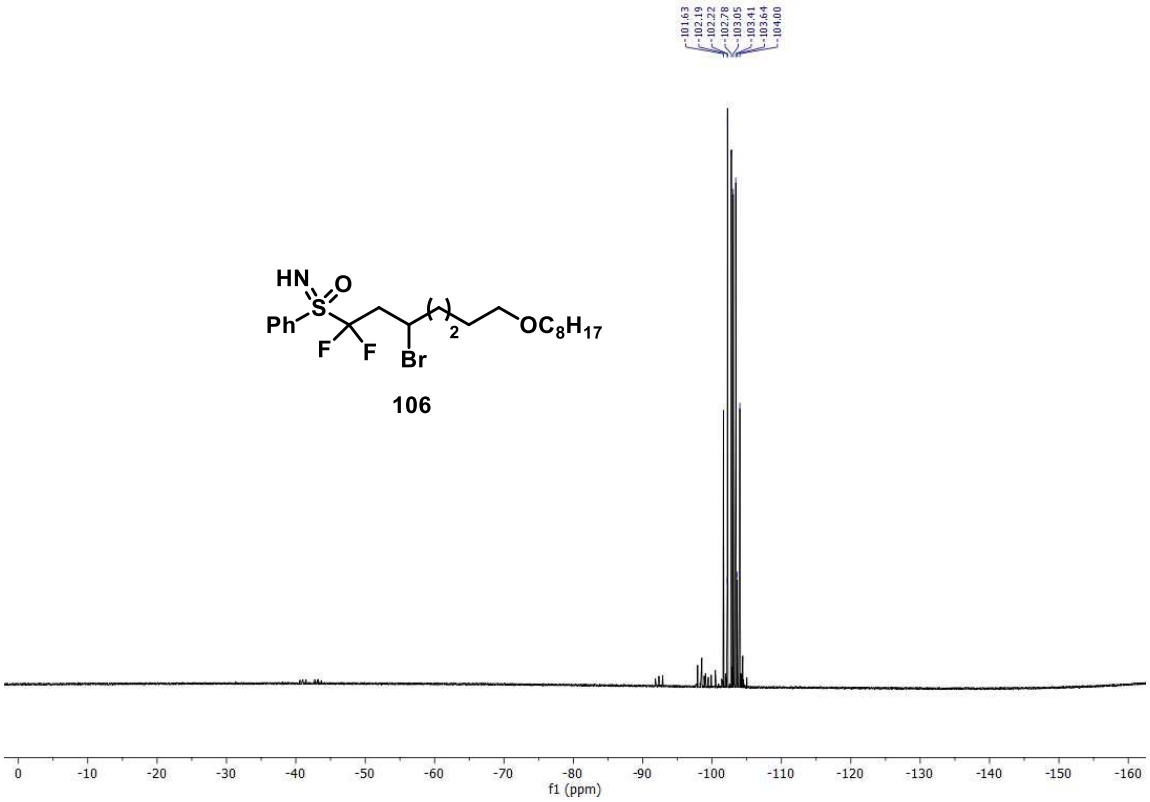

Figure S38. ^{19}F-NMR spectrum of 106 in $CDCl_3$.

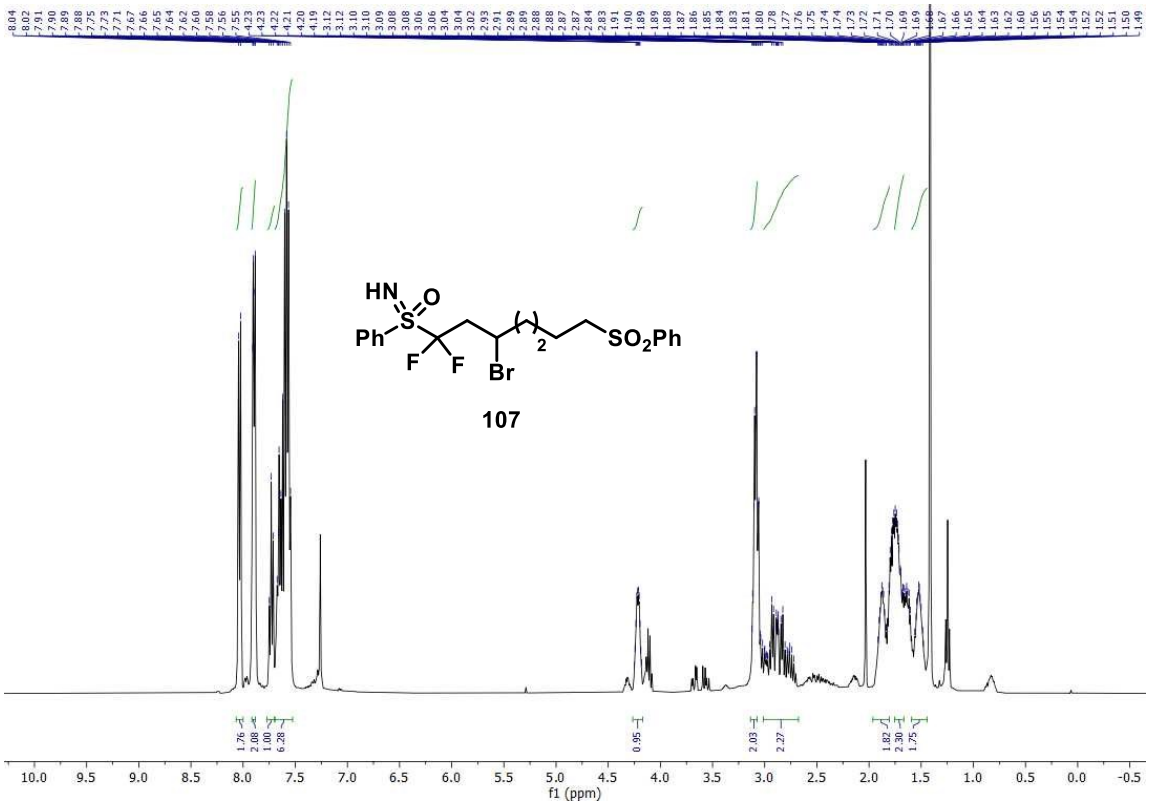

Figure S39. ^{1}H-NMR spectrum of 107 in $CDCl_3$.

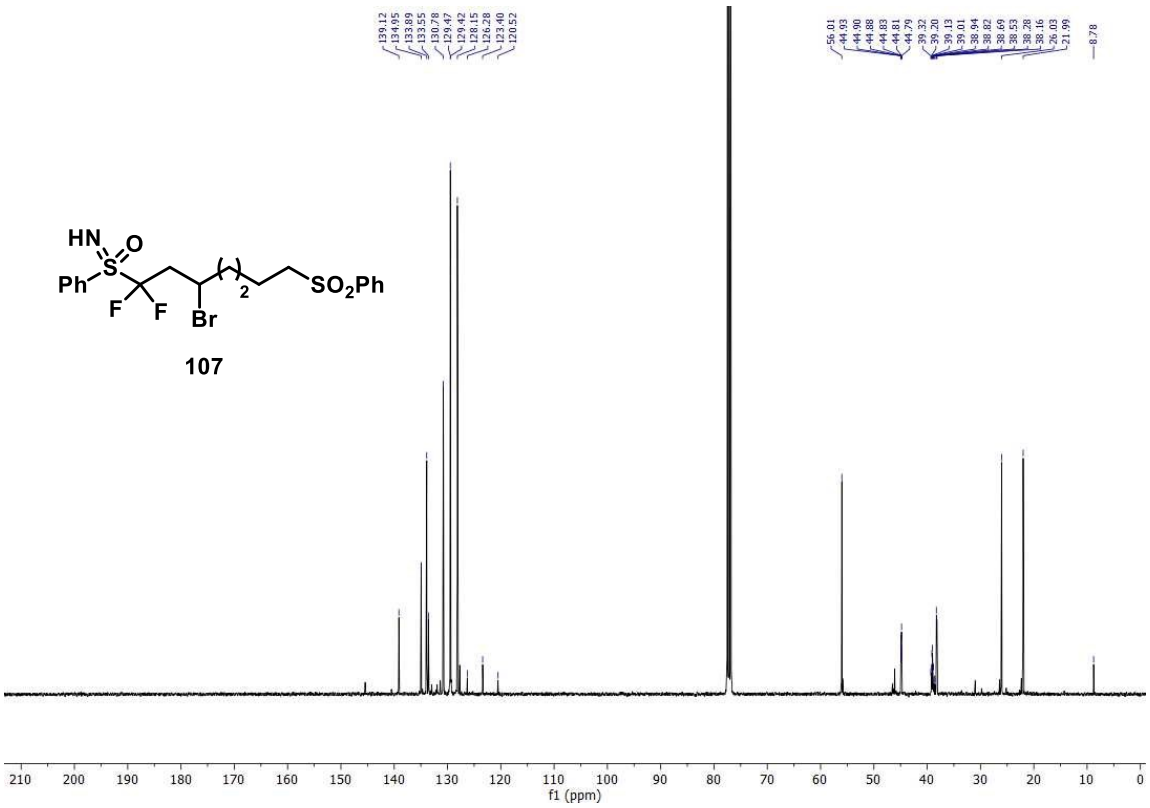

Figure S40. ^{13}C-NMR spectrum of 107 in $CDCl_3$.

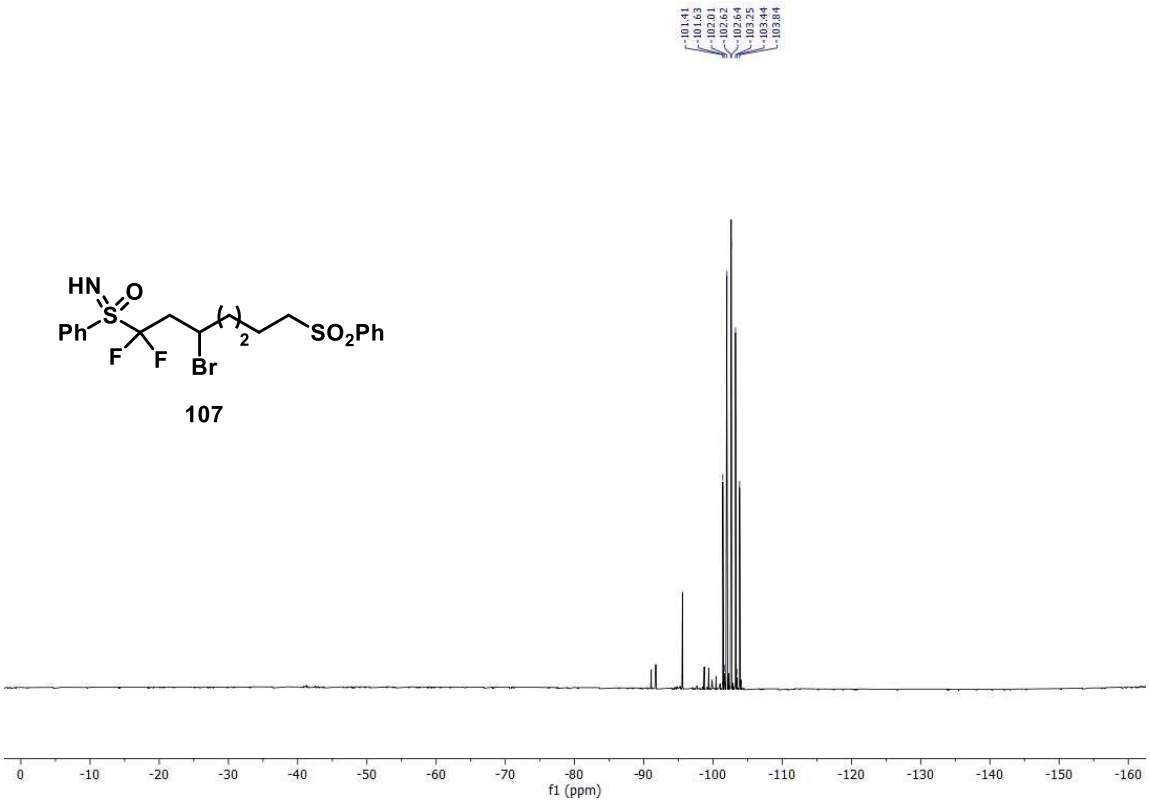

Figure S41. ^{19}F-NMR spectrum of 107 in $CDCl_3$.

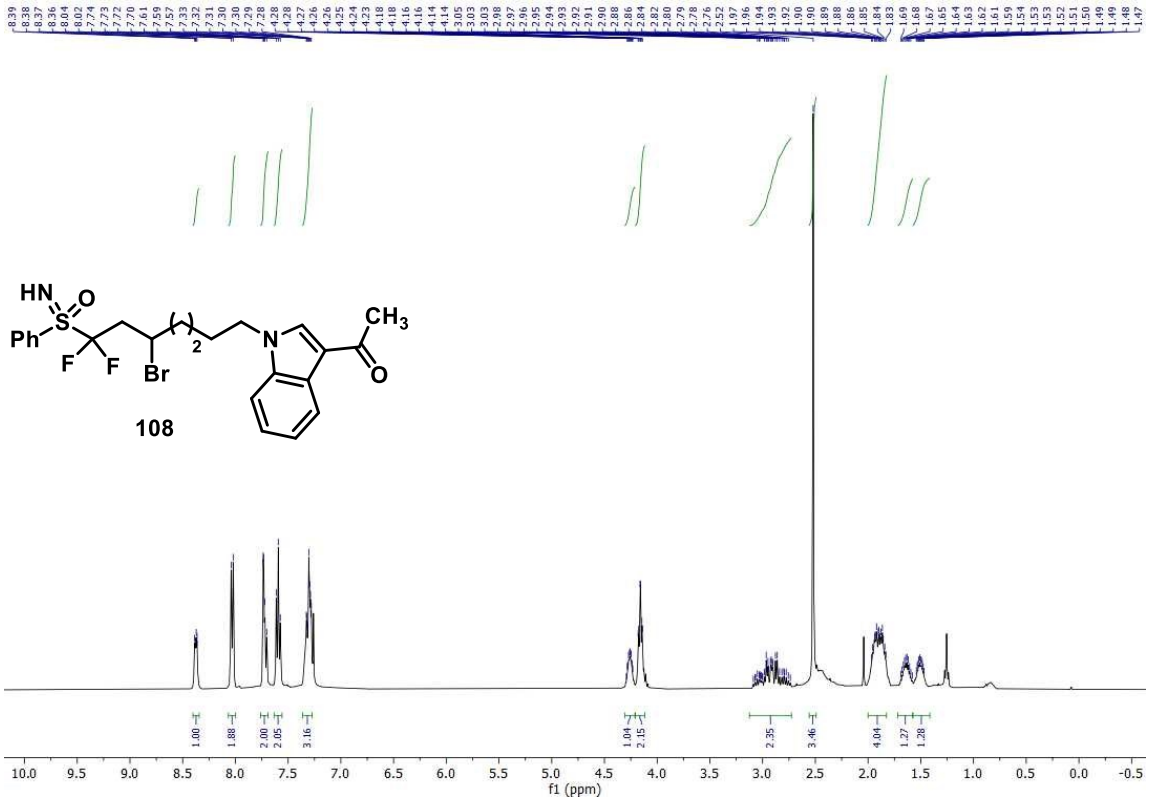

Figure S42. ^{1}H-NMR spectrum of 108 in $CDCl_3$.

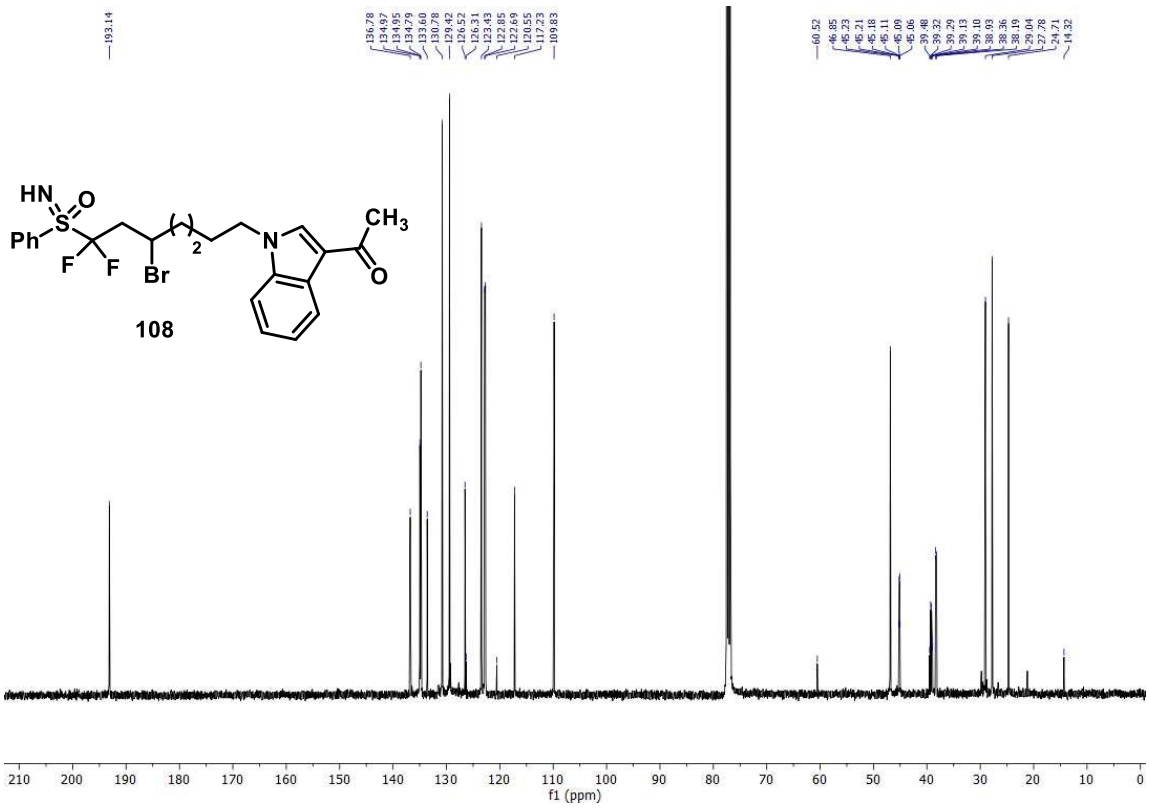

Figure S43. ^{13}C-NMR spectrum of 108 in $CDCl_3$.

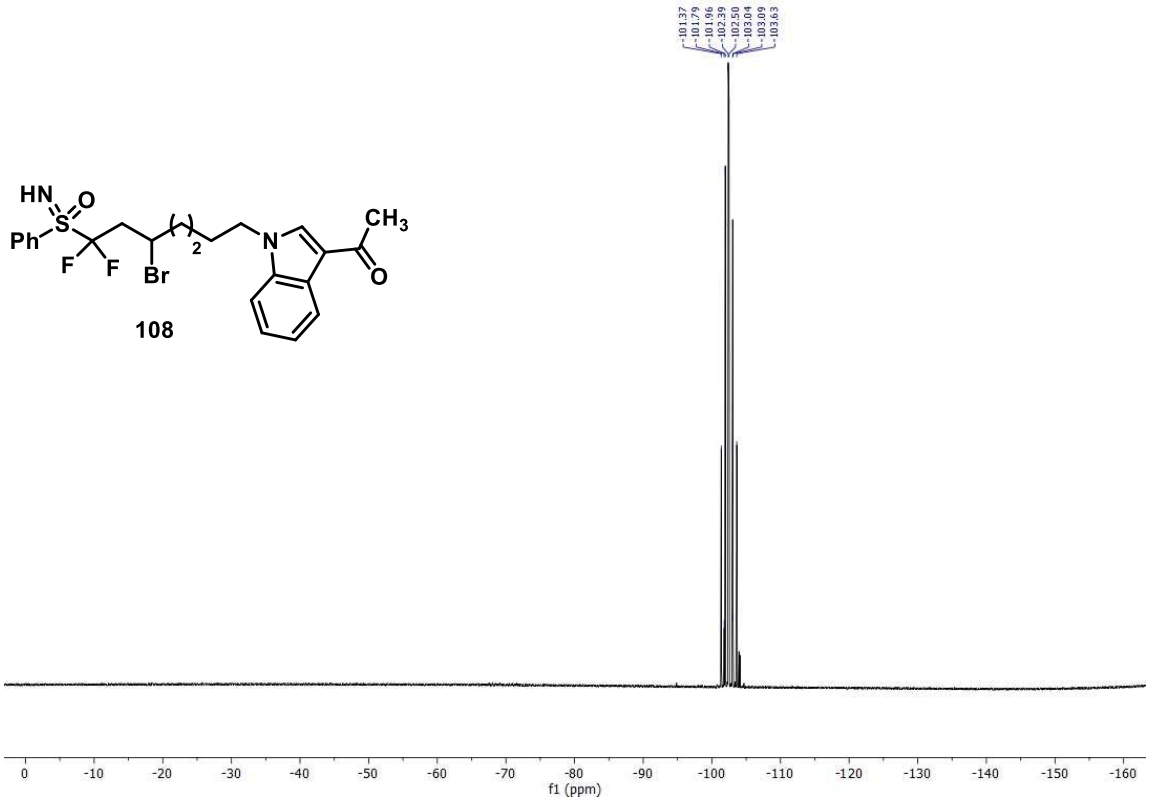

Figure S44. ^{19}F-NMR spectrum of 108 in $CDCl_3$.

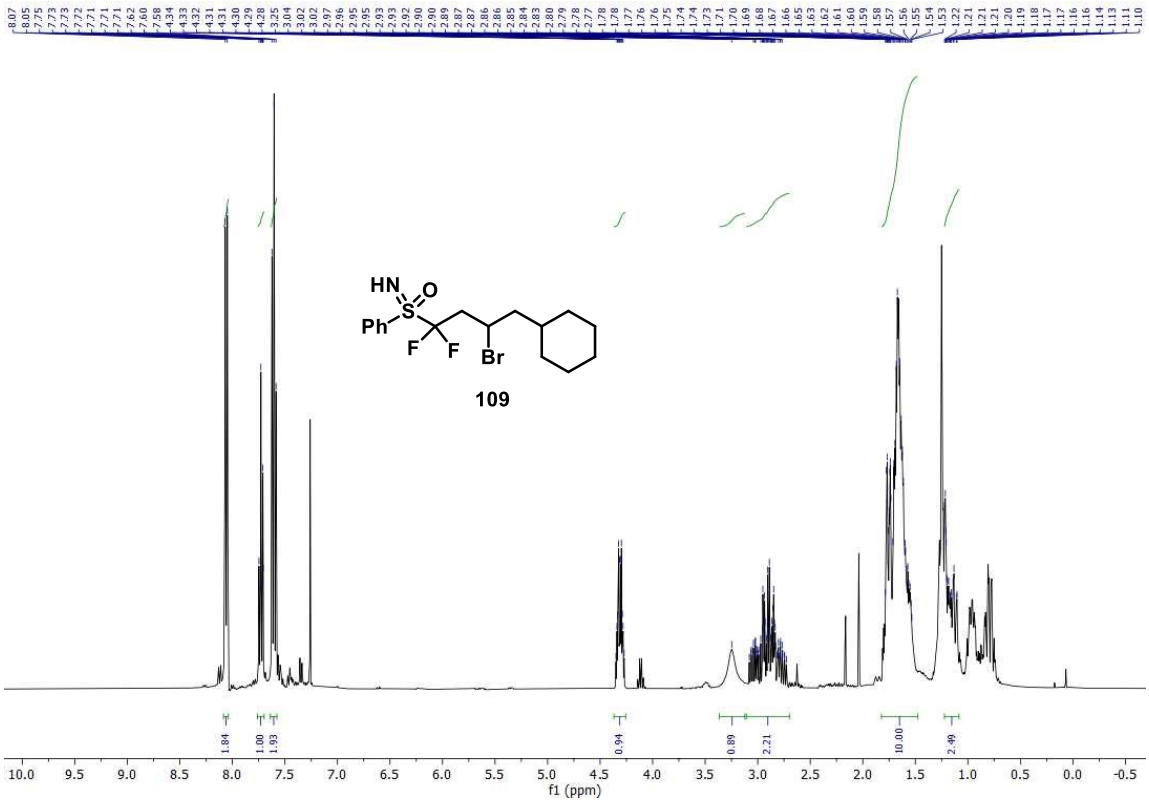

Figure S45. ^{1}H-NMR spectrum of 109 in $CDCl_3$.

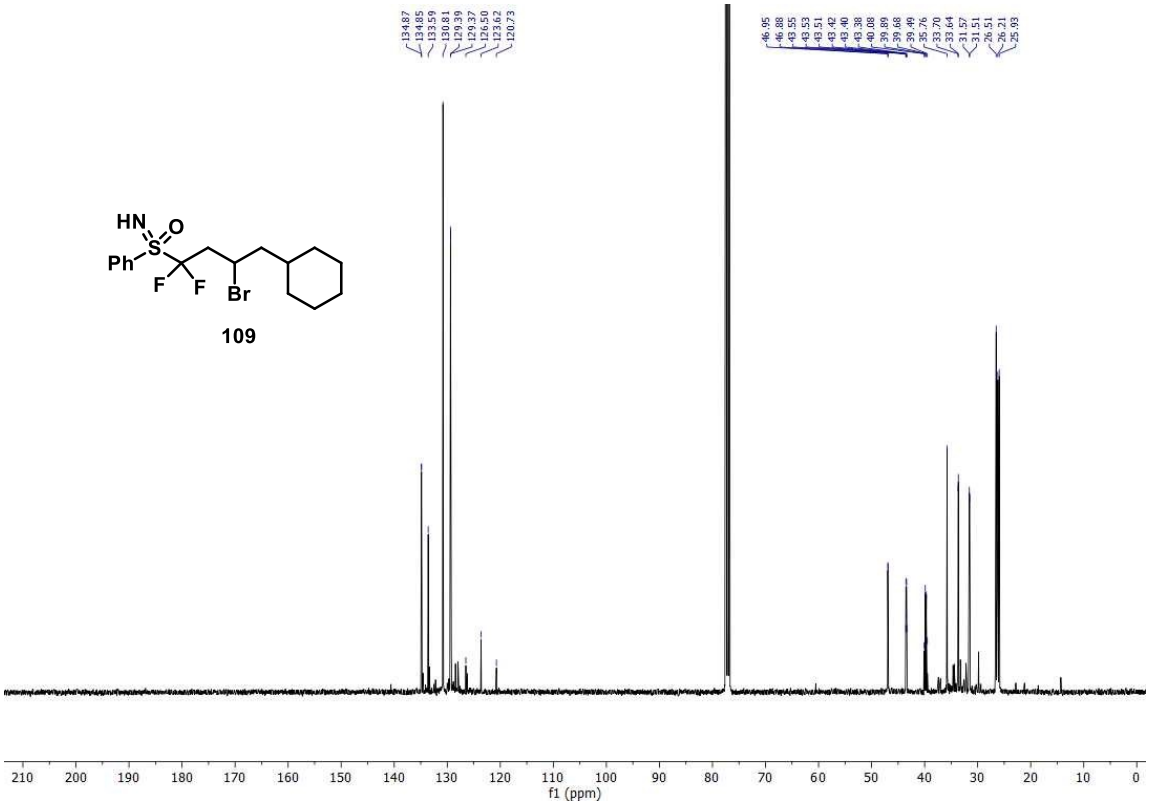

Figure S46. ^{13}C-NMR spectrum of 109 in $CDCl_3$.

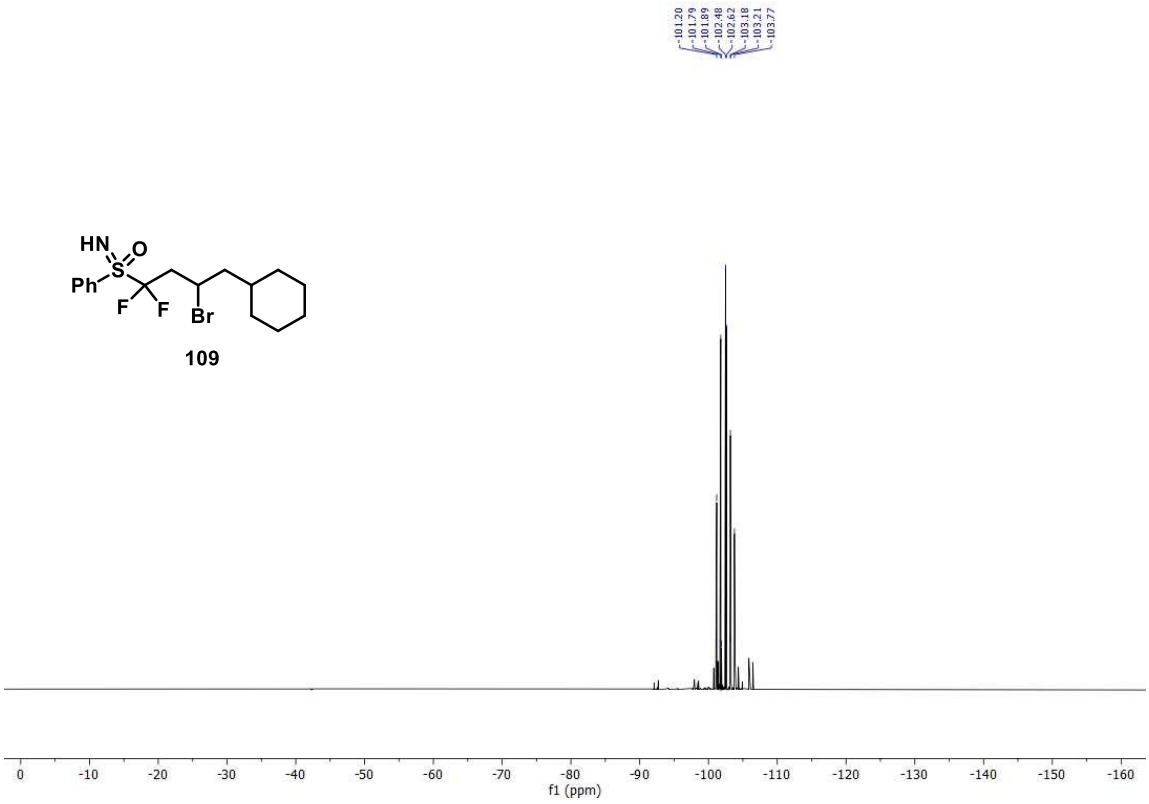

Figure S47. ^{19}F-NMR spectrum of 109 in $CDCl_3$.

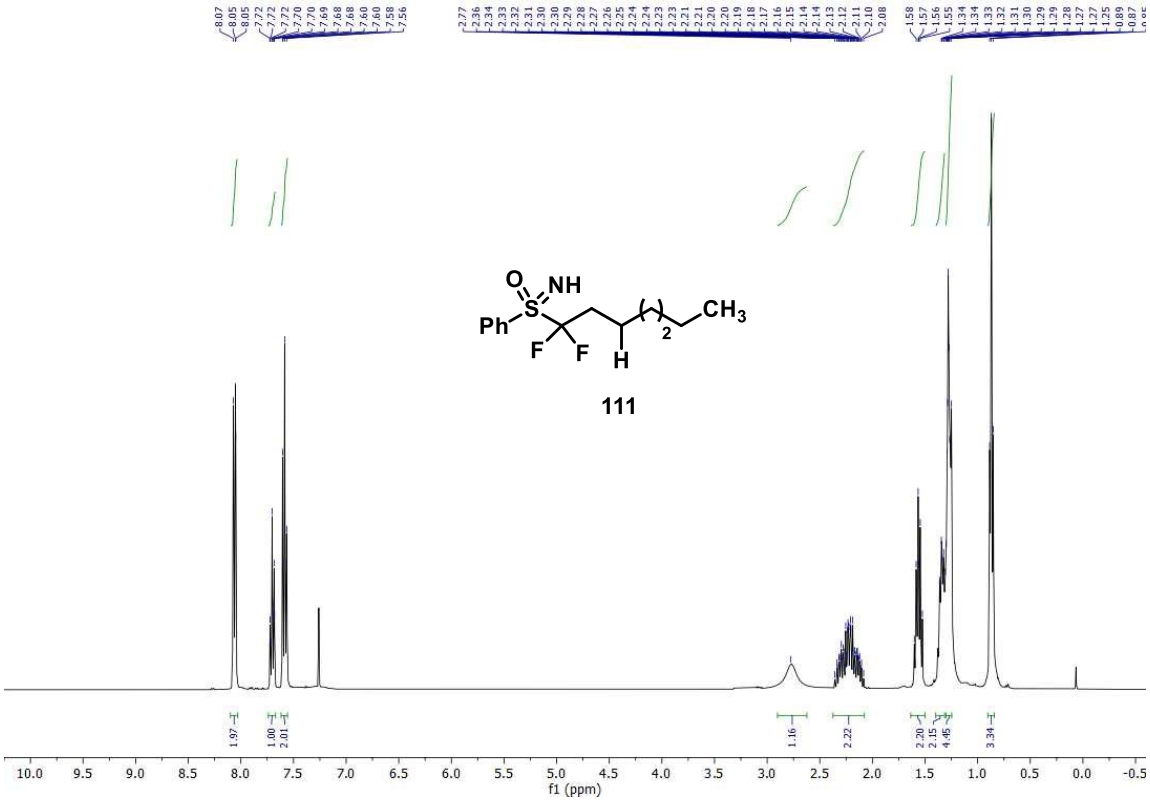

Figure S48. ^{1}H-NMR spectrum of 111 in $CDCl_3$.

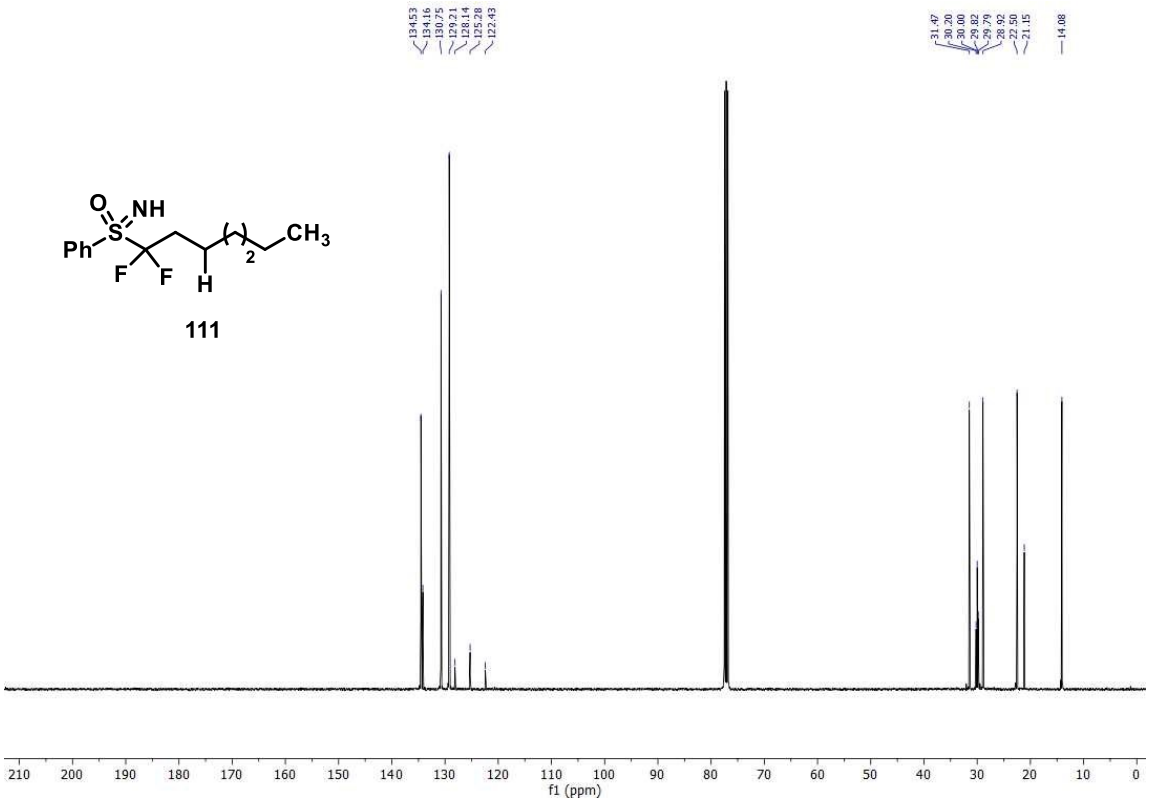

Figure S49. ^{13}C-NMR spectrum of 111 in $CDCl_3$.

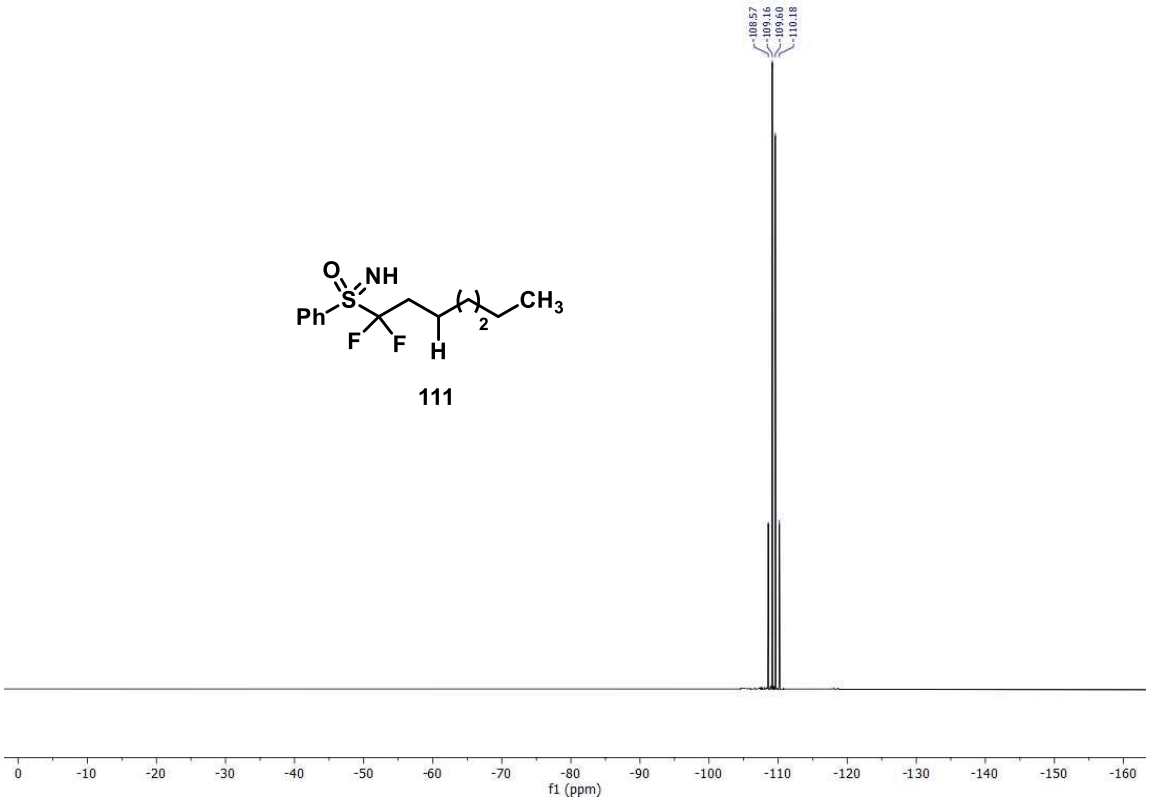

Figure S50. ^{19}F-NMR spectrum of 111 in $CDCl_3$.

5.9 Calculation of $E_{0,0}$

PC12

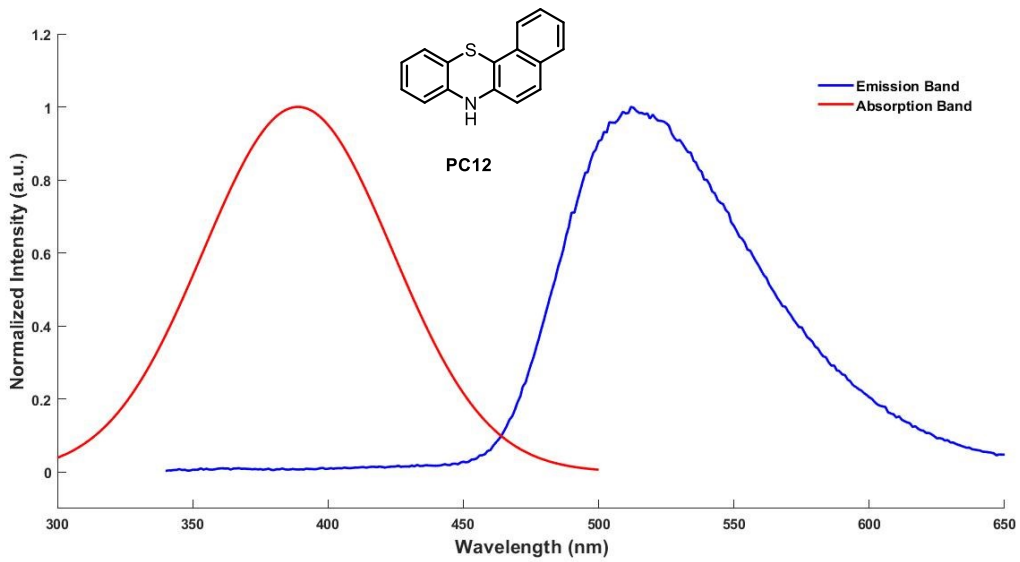

Figure S51. Calculation of the $E_{0,0}$ from the wavelength of the intersection (λ_{int}) between normalized absorbance and emission spectra. ***λ_{int} = 464 nm****.*

PC13

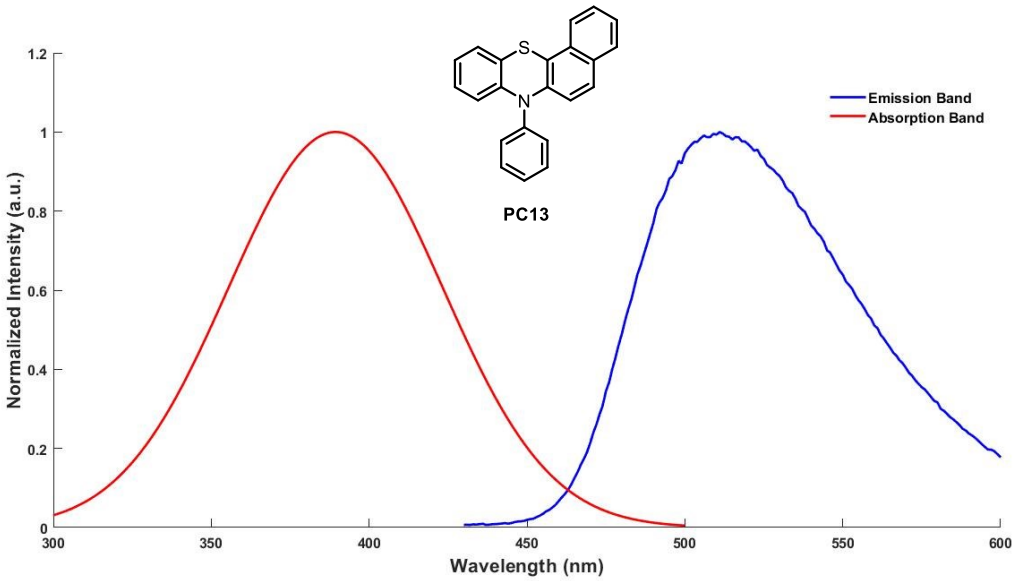

Figure S52. Calculation of the $E_{0,0}$ from the wavelength of the intersection (λ_{int}) between normalized absorbance and emission spectra. ***λ_{int} = 463 nm****.*

PC14

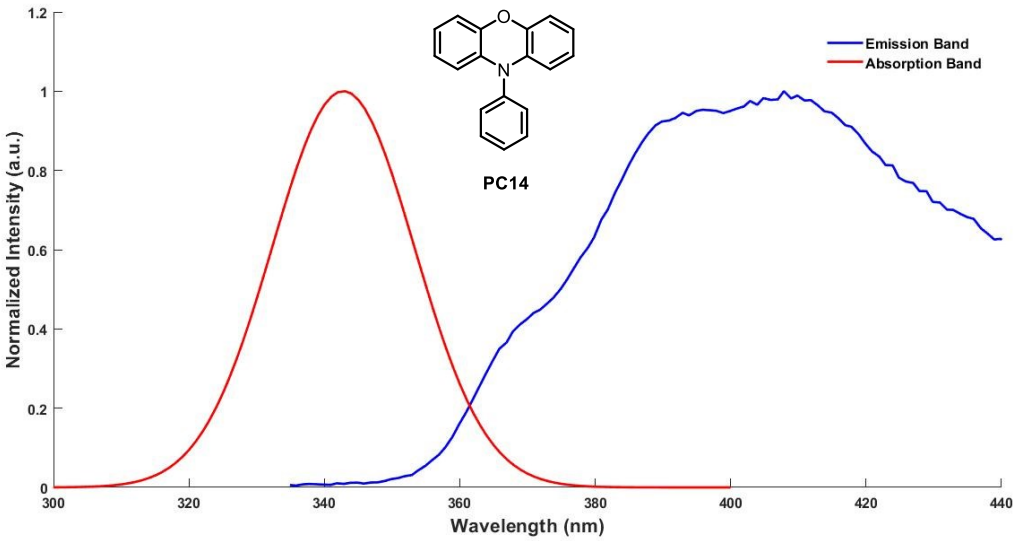

Figure S53. Calculation of the $E_{0,0}$ from the wavelength of the intersection (λ_{int}) between normalized absorbance and emission spectra. ***λ_{int} = 361 nm****.*

PC15

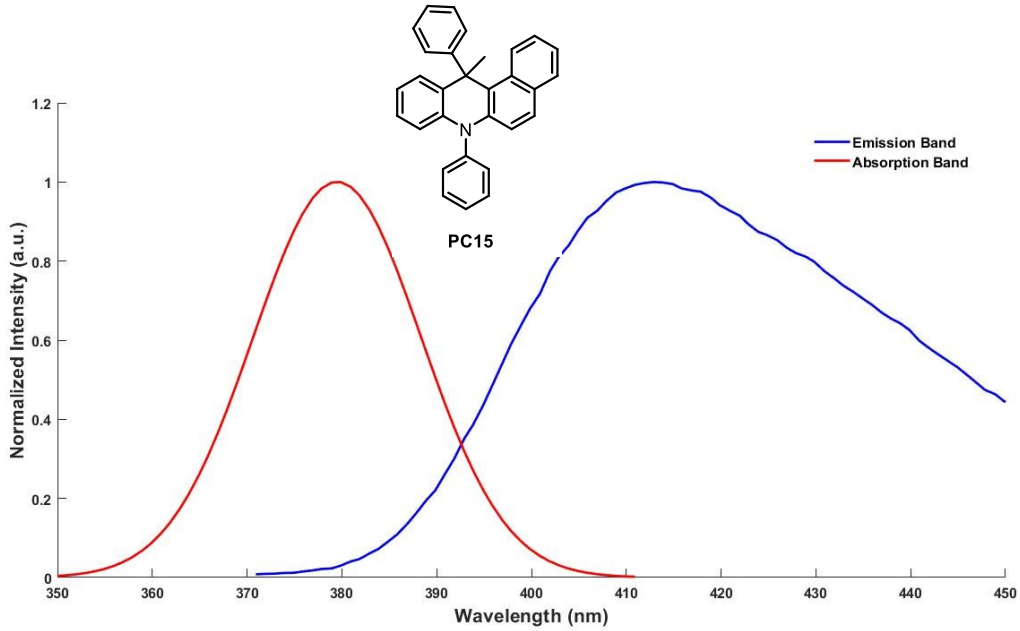

Figure S54. Calculation of the $E_{0,0}$ from the wavelength of the intersection (λ_{int}) between normalized absorbance and emission spectra. ***λ_{int} = 393 nm****.*

PC16

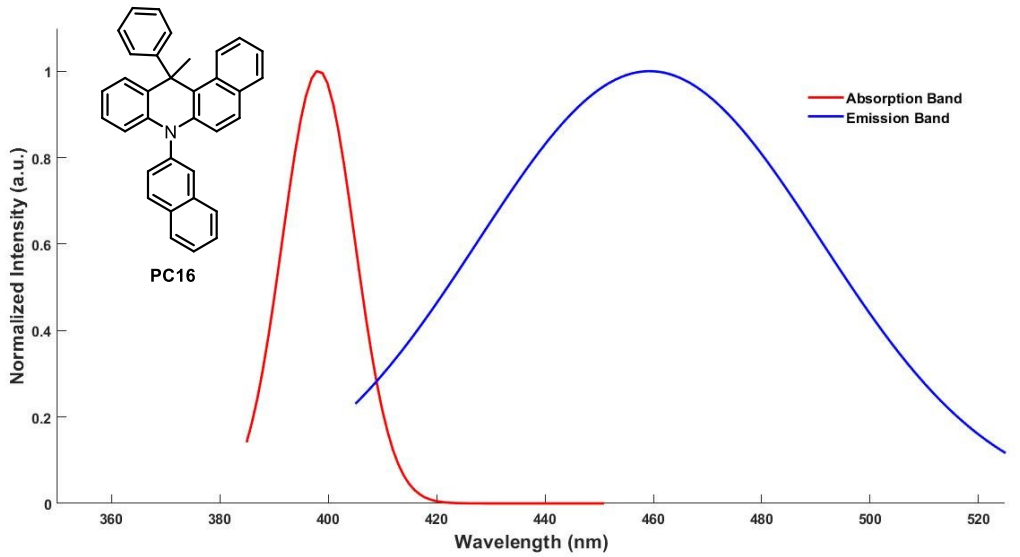

Figure S55. Calculation of the $E_{0,0}$ from the wavelength of the intersection (λ_{int}) between normalized absorbance and emission spectra. ***λ_{int} = 409 nm****.*

PC19

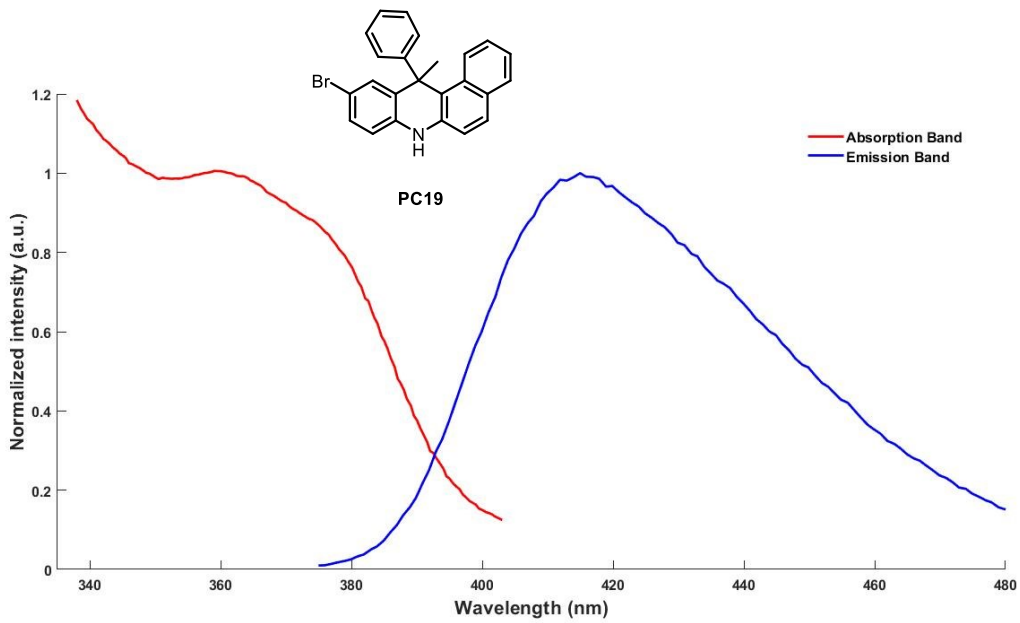

Figure S56. Calculation of the $E_{0,0}$ from the wavelength of the intersection (λ_{int}) between normalized absorbance and emission spectra. ***λ_{int} = 392 nm****.*

PC20

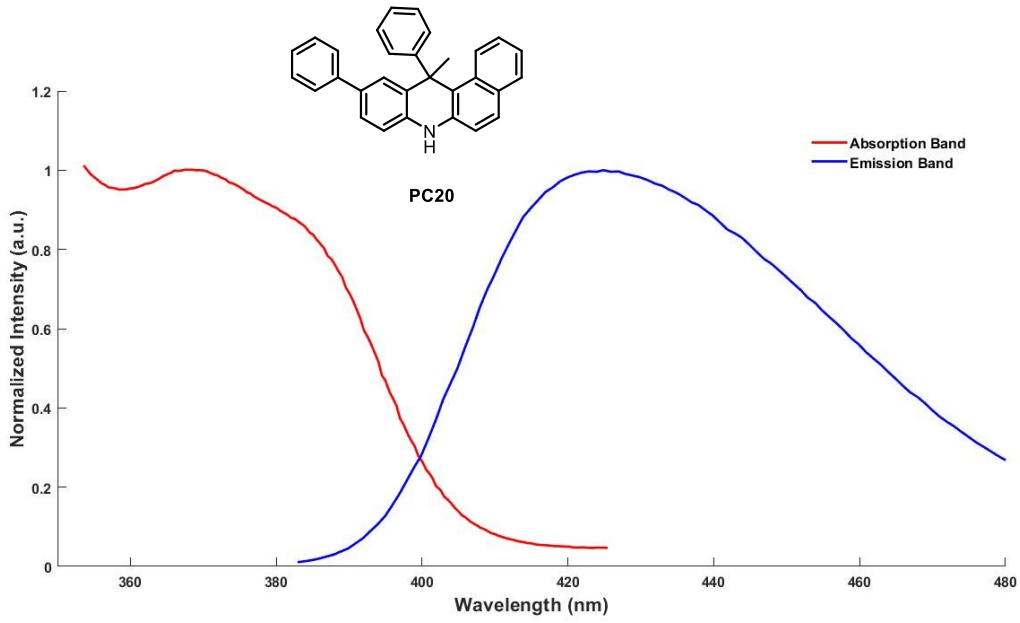

Figure S57. Calculation of the $E_{0,0}$ from the wavelength of the intersection (λ_{int}) between normalized absorbance and emission spectra. ***λ_{int} = 400 nm****.*

PC21

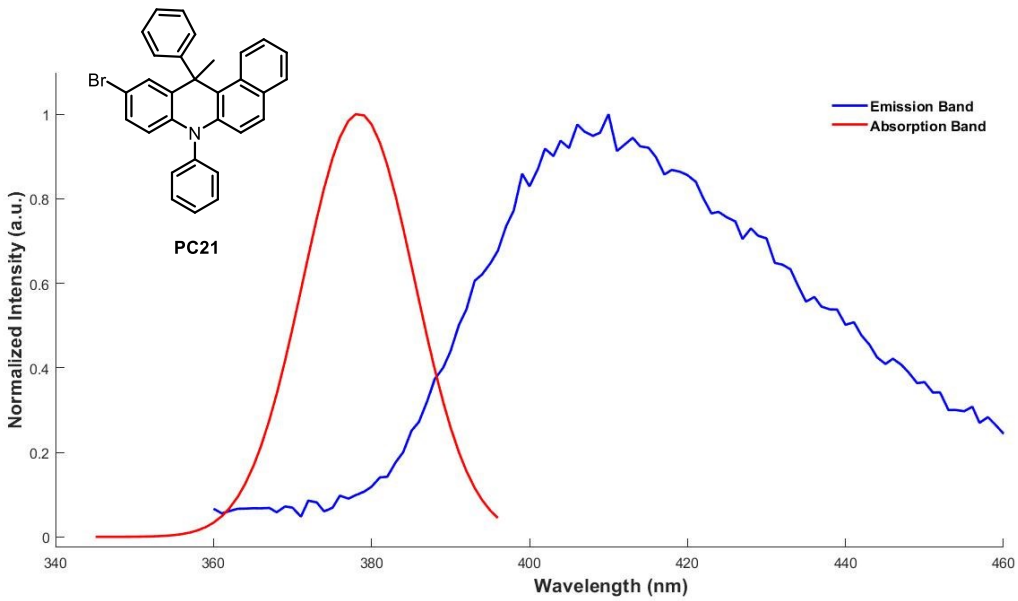

<u>Figure S58</u>. Calculation of the $E_{0,0}$ from the wavelength of the intersection (λ_{int}) between normalized absorbance and emission spectra. ***λ_{int} = 388 nm****.*

PC22

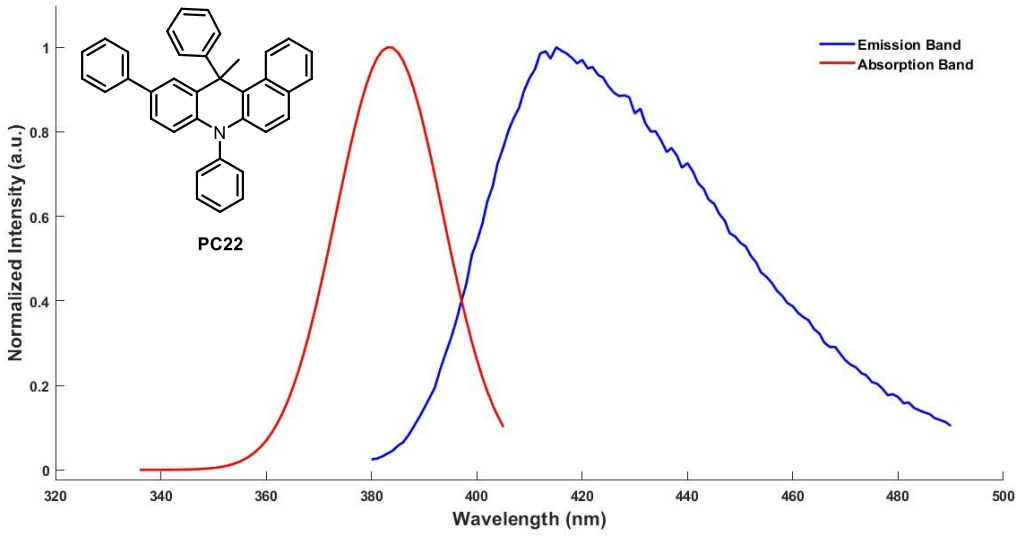

<u>Figure S59</u>. Calculation of the $E_{0,0}$ from the wavelength of the intersection (λ_{int}) between normalized absorbance and emission spectra. ***λ_{int} = 397 nm****.*

PC23

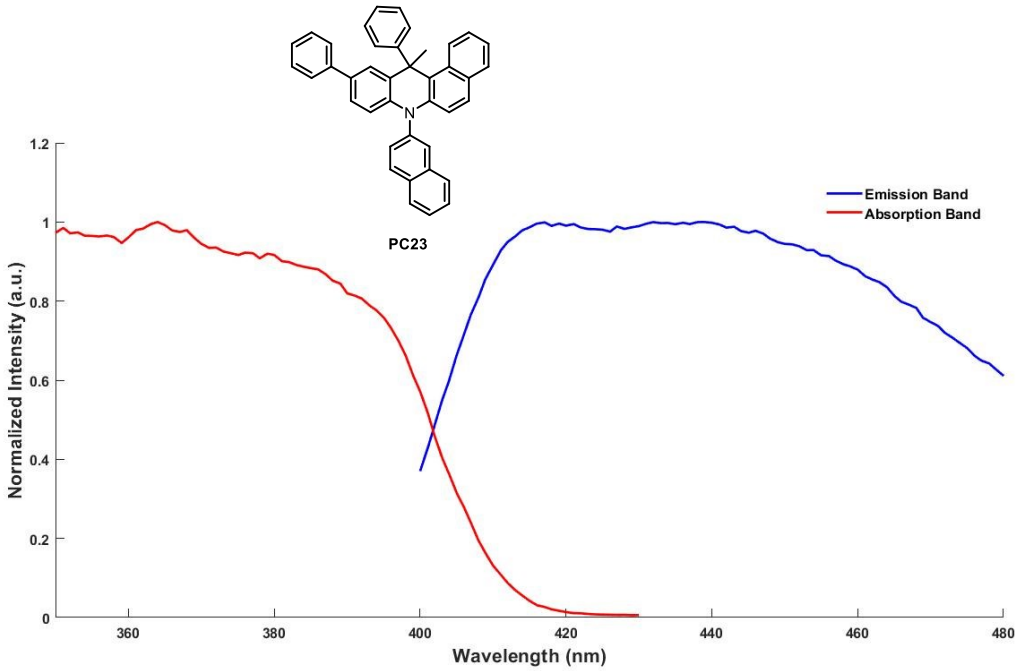

Figure S60. Calculation of the $E_{0,0}$ from the wavelength of the intersection (λ_{int}) between normalized absorbance and emission spectra. ***λ_{int} = 402 nm****.*

5.10 EDA complex formation analysis

PC1

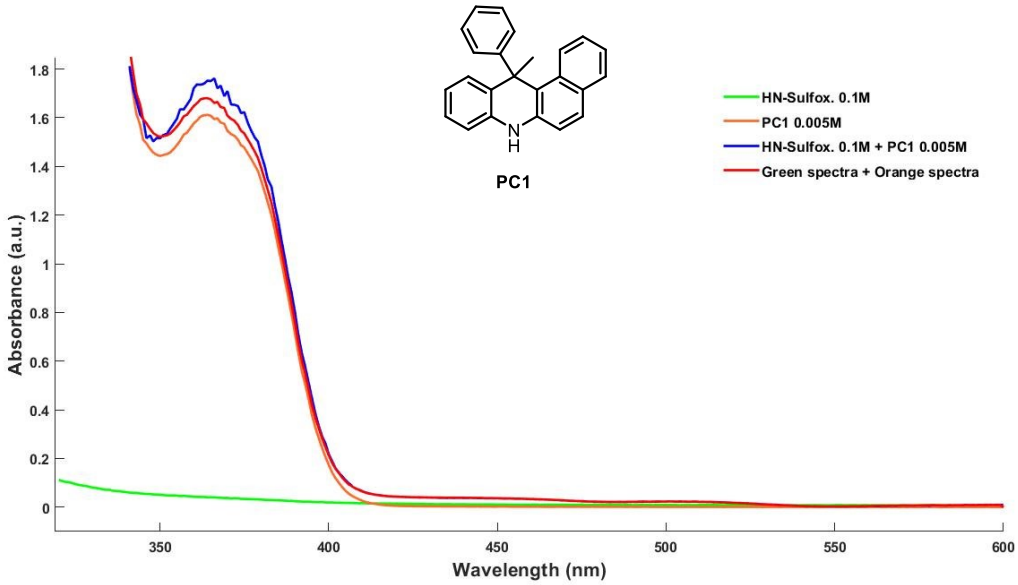

Figure S61. EDA complex formation analysis for ***PC1****. In the case of* ***PC1*** *there* ***IS NOT*** *the formation of an EDA complex.*

PC6

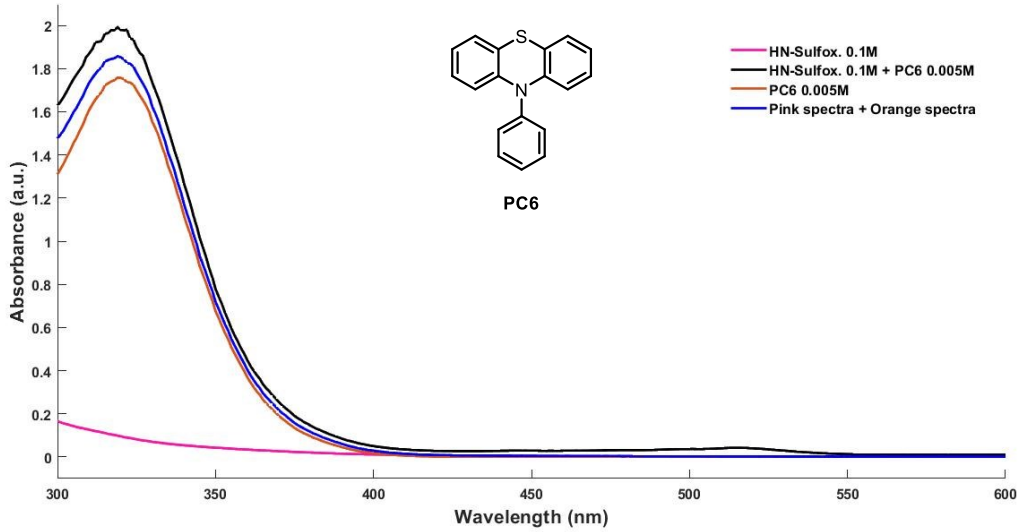

*Figure S62. EDA complex formation analysis for **PC6**. In the case of **PC6** there is the formation of an EDA complex.*

PC12

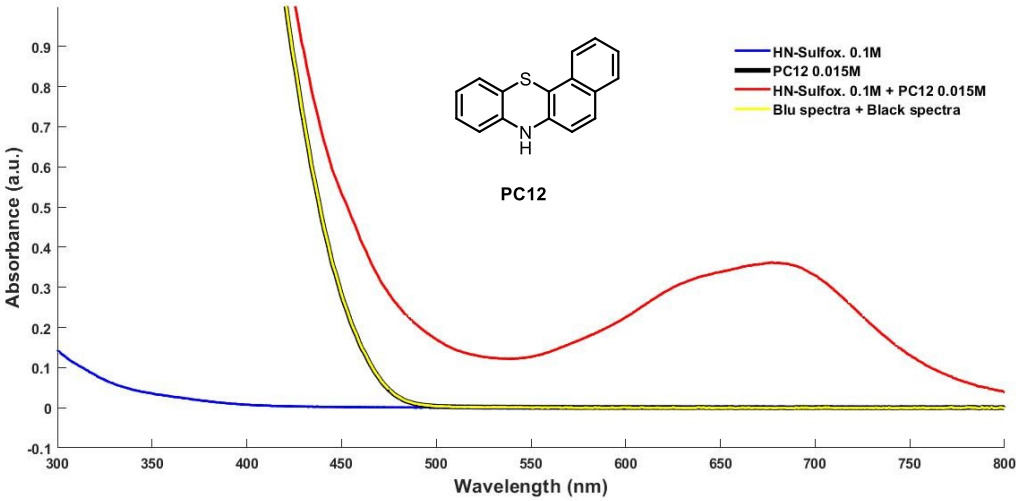

*Figure S63. EDA complex formation analysis for **PC12**. In the case of **PC12** there is the formation of an EDA complex.*

PC13

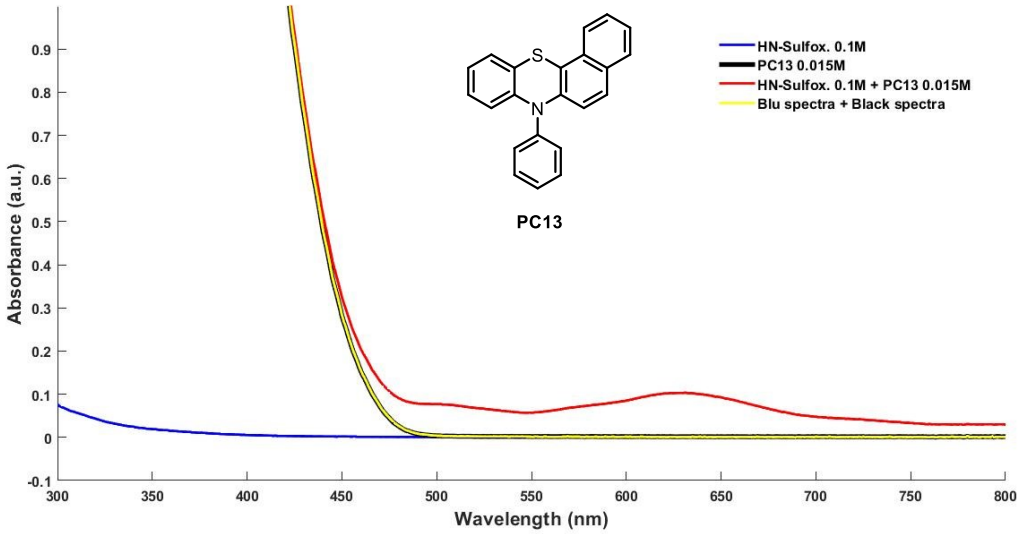

*Figure S64. EDA complex formation analysis for **PC13**. In the case of **PC13** there is the formation of an EDA complex.*

PC14

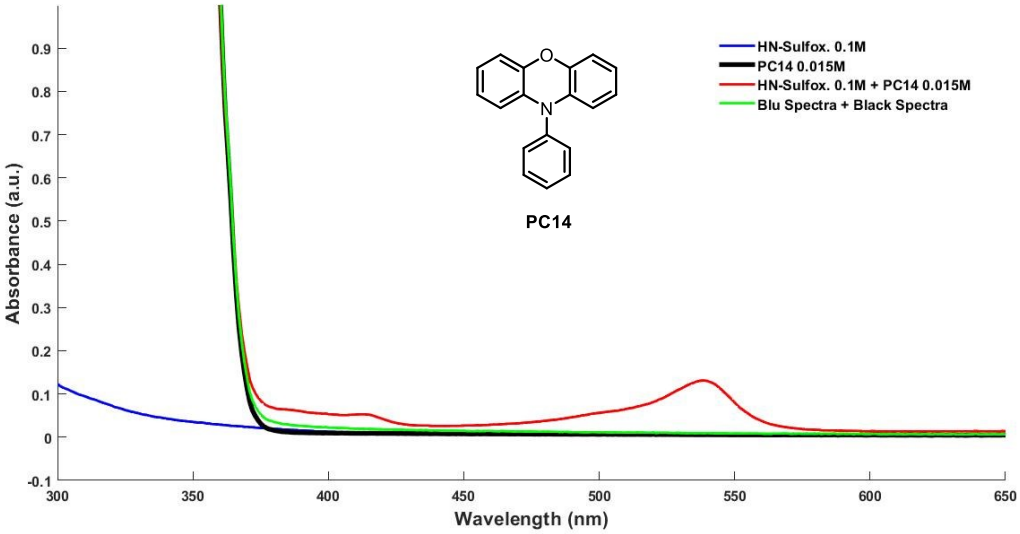

*Figure S65. EDA complex formation analysis for **PC14**. In the case of **PC14** there is the formation of an EDA complex.*

PC15

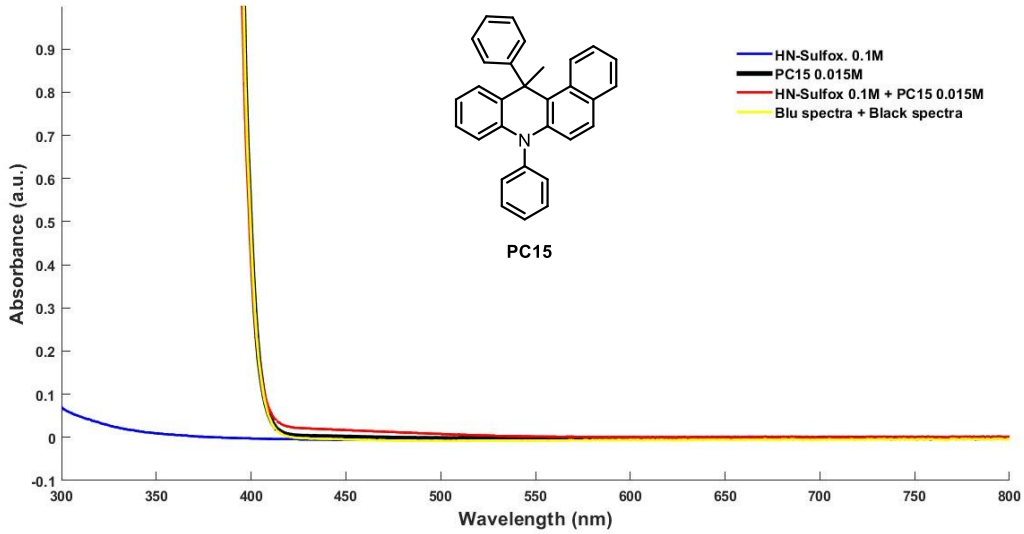

*Figure S66. EDA complex formation analysis for **PC15**. In the case of **PC15** there is the formation of an EDA complex.*

PC16

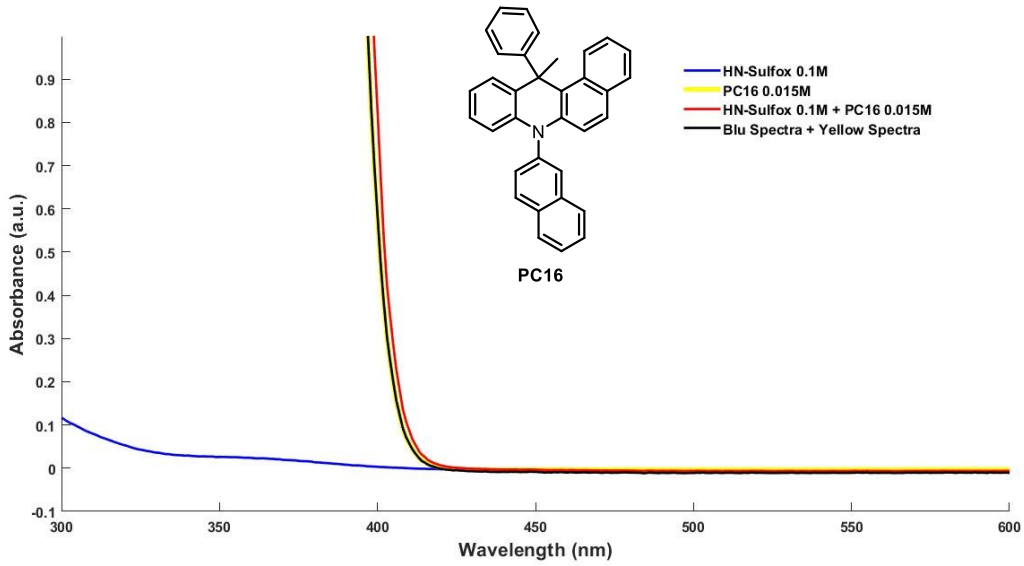

*Figure S67. EDA complex formation analysis for **PC16**. In the case of **PC16** there **IS NOT** the formation of an EDA complex.*

PC21

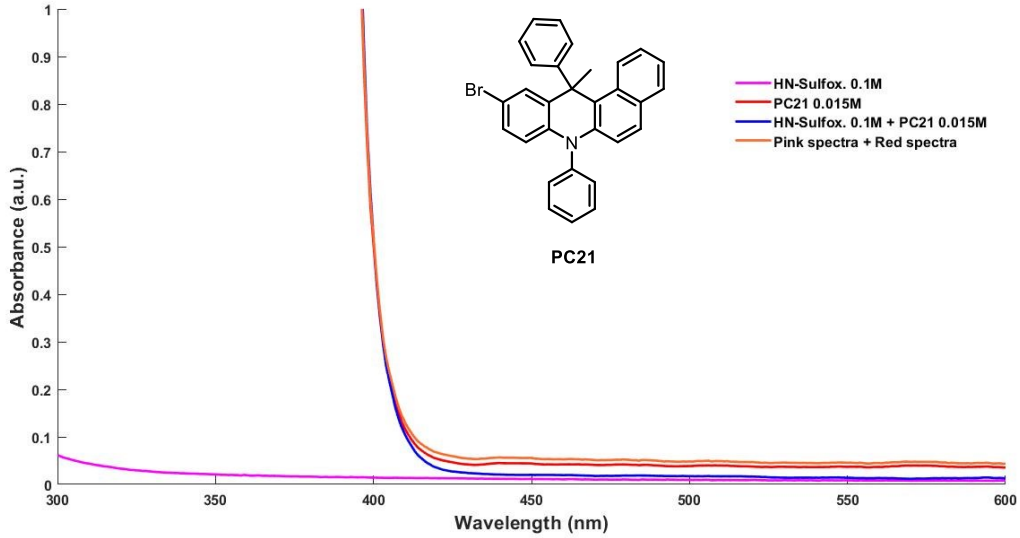

*<u>Figure S68</u>. EDA complex formation analysis for **PC21**. **NOTE**: Due to the insolubility of **PC21** under the conditions of analysis, a light scattering phenomenon is observed at the UV-Visible. This prevents the evaluation of the formation of an EDA complex.*

PC22

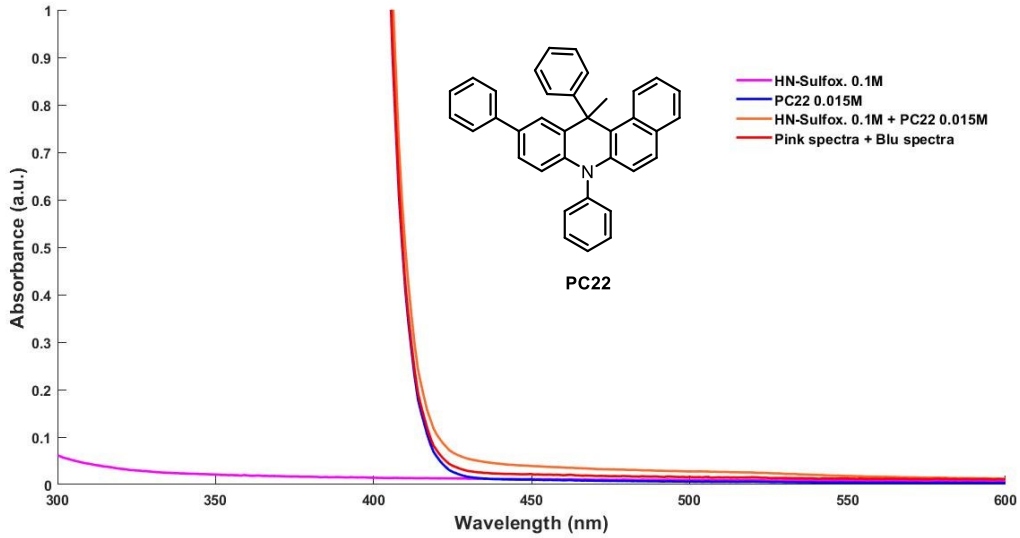

*<u>Figure S69</u>. EDA complex formation analysis for **PC22**. In the case of **PC22** there is the formation of an EDA complex.*

PC23

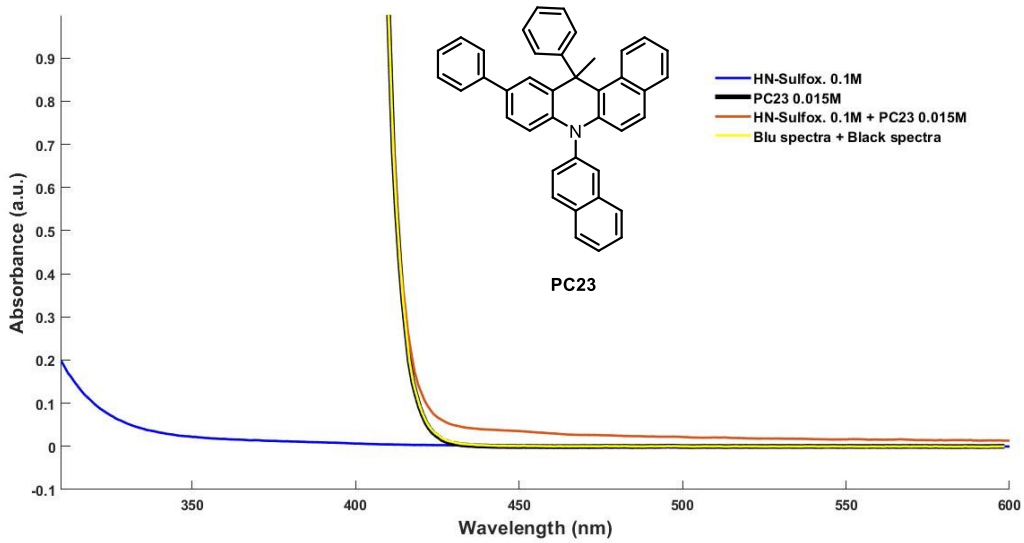

*<u>Figure S70</u>. EDA complex formation analysis for **PC23**. In the case of **PC23** there is the formation of an EDA complex.*

6. Bibliography

1. G. Ciamician, *The Photochemistry of the Future*, Science, **1912,** *36*, 385-394
2. G. Ciamician, *Sci. Am.* **1913**, *75*, 258–259
3. G. Ciamician, P. Silber, *Berichte der Dtsch. Chem. Gesellschaft,* **1908**, *41*, 1928–1935
4. T. Yoon et al., *Nature Chem*, **2010**, *2*, 527–532
5. H. E. Zimmerman, in *Pure and Applied Chemistry*, **2006**, *78*, 12, 2193–2203
6. S. Protti, M. Fagnoni, *Photochem. Photobiol. Sci.*, **2009**, *8*, 1499–1516
7. D. Ravelli, M. Fagnoni, A. Albini, *Chemical Society Reviews* **2013**, *42*, 97–113
8. M. H. Shaw, J. Twilton, D. W. C. MacMillan, *Journal of Organic Chemistry,* **2016**, *81*, 6898–6926.
9. D. Ravelli, S. Protti, A. Albini, *Molecules,* **2015**, *20*, 1527–1542
10. D. A. Dougherty, E. V. Anslyn, *Modern Physical Organic Chemistry*, University Science Book, **2006**
11. A. Albini, M. Fagnoni, *Handbook of Synthetic Photochemistry*, Wiley, **2009**
12. A. G. Griesbeck, J. Mattay, *Synthetic Organic Photochemistry*, CRC Press, **2004**
13. P. Muller, *Pure Appl. Chem.* **1994**, *66*, 1077–1184.
14. J. Clayden, N. Greeves, S. Warren, *Organic Chemistry*, Second edition, OUP Oxford, **2012**
15. P. Y. Bruice, *Organic Chemistry*, Eight edition, Pearson College Div., **2016**
16. K. J. Laidler, *Pure Appl. Chem.* **1981**, *53*, 753.
17. F. Strieth-Kalthoff et al., *Chem. Soc. Rev.* **2018**, *47*, 7190–7202
18. J.W. Verhoeven, *Pure and Applied Chemistry***, 1996***, 68*, 2223–2286
19. Q.-Q. Zhou et al., *Angew. Chem. Int. Ed*., **2019**, *58*, 1586–1604
20. *A. D. McNaught, A. Wilkinson, IUPAC. Compendium of Chemical Terminology (the "Gold Book"), Second edition, Blackwell Scientific Publications, Oxford, **1997**.*
21. D. M. Schultz, T. P. Yoon, *Science*, **2014**, *343*, 1239176.
22. T. Bortolato et al*., Chem. Commun*., **2022**, *58*, 1263-1283
23. M. Reckenthäler, A. G. Griesbeck, *Adv. Synth. Catal.* **2013**, *355*, 2727–2744
24. 24 R. A: Angnes et al., *Org. Biomol. Chem*., **2015**, *13*, 9152-9167
25. N. A. Romero, D. A. Nicewicz, *Chem. Rev*., **2016**, *116*, 10075−10166
26. C. K. Prier et al., *Chemical Reviews,* **2013**, *113*, 5322– 5363
27. A. Vega-Peñaloza et al., *Angew. Chem. Int. Ed*., **2021**, *60*, 1082–1097
28. P. Franceschi, *J. Org. Chem.*, **2023**, *88*, 10, 6454–6464
29. H. G. Yayla, R. R. Knowles, *Synlett* **2014**, *25*, 2819–2826
30. M. H. V. Huynh, T. J. Meyer, *Chem. Rev.,* **2007**, *107*, 11, 5004–5064
31. T. Bortolato et al., *J. Am. Chem. Soc.,* **2023**, *145*, 1835−1846
32. L. Capaldo, D. Ravelli, *Eur. J. Org. Chem.,* **2017**, 2056–2071
33. L. Capaldo, D. Ravelli, M. Fagnoni, Chem. Rev., **2022**, *122*, 1875−1924
34. C. R. J. Stephenson, T. P. Yoon D. W. C. MacMillan, *Visible Light Photocatalysis in Organic Chemistry,* First Edition, Wiley, **2018**
35. D. Bag et al., *Org. Biomol. Chem*., **2020**, *18*, 8278-8293
36. C.-J. Wallentin et al*., J. Am. Chem. Soc*. **2012**, *134*, 8875−8884
37. M. Frings et al., European Journal of Medicinal Chemistry, **2017**, *126*, 225-245
38. U. Lücking, Angew. Chem. Int. Ed. **2013**, *52*, 9399 – 9408
39. Y. Han et al., European Journal of Medicinal Chemistry, **2021**, *209*, 112885
40. M. Andresini et al., Chem. Eur. J. **2021**, *27*, 17293–17321
41. Gege et al., Sci. Transl. Med., **2021**, *13*

42. M. T. Reetz et al., Tetrahedron Lett. **2005**, *46*, 5643–5646;
43. A. Adrien et al., Org. Lett., **2007**, Vol. 9, No. 11
44. V. Bizet et al., Chem. Soc. Rev., **2015**, *44*, 3378
45. C. M. Rayner, Contemp. Org. Synth., **1995**, *2*, 409-440
46. J. Miao, Richards, et al., Chem. Commun., **2014**, *50*, 9687
47. J. A. Bull et al., Synlett **2017**; *28 (19*), 2525-2538
48. S. Superchi et al., Chirality, **2008**, *20*, 592–596
49. T. Uchida et al., Chem. Rec. **2014**, *14*, 117–129
50. X. Shen, J. Hu, Eur. J. Org. Chem. **2014**, 4437–4451
51. P. Ghosh et al., Asian J. Org. Chem. **2020**, *9*, 2035–2082
52. A. Wimmer; B. König, Org. Lett. **2019**, *21*, 8, 2740–2744
53. H. Lämmermann et al., Synlett **2018**, *29*, A–F
54. S. Pan et al., Adv. Synth. Catal. **2023**, *365*, 31 – 36
55. D. Zhang et al., Chem. Commun., **2018**, *54*, 5772
56. Langmuir, I., Journal ofthe American Chemical Society, **1919,** *41*,1543–1559
57. Nathan Brown; Bioisosteres in Medicinal Chemistry, **2012**, First Edition, Wiley-VCH
58. H. L. Friedman, Influence of isosteric replacements upon biological activity, NAS-NRS, **1951**, *206*, 295–358
59. C. W. Thornber, Chemical Society Reviews, **1979**, *8*, 563–580.
60. S. Cuadros et al., *Angew. Chem. Int. Ed.* **2023**, e202303585
61. N. A. Meanwell, J. Med. Chem. **2018**, *61*, 5822−5880
62. E. P. Gillis et al., J. Med. Chem., **2015**, *58*, 8315−8359
63. G. M. Dubowchik et al., Org. Lett., **2001**, *Vol. 3, No. 25*,
64. R. J. Gleave et al., Bioorg. Med. Chem. Lett., **2010**, *20*, 465–468
65. X. Shen; J. Hu, Eur. J. Org. Chem., **2014**, 4437–4451
66. V. Bizet et al., Chem. Soc. Rev., **2014**, *43*, 2426--2438
67. S. Chaabuoni et al., Chem. Eur. J., **2018**, *24*, 17006 – 17010
68. A. Prieto et al., Adv. Synth. Catal., **2019**, *361*, 436 –440
69. Q. Luo, X. Wang, J. Hu, Tetrahedron, **2022**, *113*, 132694
70. W. Zhang, W. Huang, J. Hu, Angew. Chem. **2009**, *121*, 10042 –10045
71. C. R. Johnson, E. R. Janiga, M. Haake, J. Am. Chem. Soc. **1968**, *90*, 14, 3890–3891
72. T. Koike, Chem. Rec. **2023**, e202300032
73. X. Shen et al., J. Am. Chem. Soc., **2019**, *141*, 26, 10566
74. Y. Macé et al., Tetrahedron, **2011**, *67*, 7575e7580
75. C. Rosso et al., *ACS Catal*., **2022**, *12*, 4290−4295
76. D.-G. Chen et al., Angew. Chem. Int. Ed., **2019**, *58*, 13297–13301. Supporting information
77. Y. Tian et al., Angew. Chem. Int. Ed., **2021**,60, 20259 –20263. Supporting information
78. R. M. Pearson, J. Am. Chem. Soc., **2016**, 138, 11399−11407
79. X.-L. Li et al., RSC Advances, 2013, 3, 12091
80. Current Patent Assignee: CHANGCHUN HAIPU RUNSI TECHNOLOGY CO LTD - CN111205272, 2020, A. Location in patent: Paragraph 0103-0105
81. K. Targos et al., J. Am. Chem. Soc., **2021**, *143*, 11, 4125–4132. Supporting information
82. G. Goti et al., Eur. J. Org. Chem., **2021**, 2655–2664
83. G. E. M: Crisenza et al., J. Am. Chem. Soc., **2020**, *142*, 5461−5476
84. K. Vandewal et al., Sustainable Energy Fuels, **2018**, *2*, 538-544
85. C. Katan et al., Phys. Chem. Chem. Phys., **2014**, *16*, 9064-9073

86. W. Xu et al., J. Phys. Chem. C, **2008**, *112*, 3, 874-880
87. Kavarnos, G. J. Energetics of photoinduced electron transfer. In Fundamentals of Photoinduced Electron Transfer; VCH: New-York, Weinheim, **1993**, pp 29–37.
88. E. H. Discekici et al., Chem. Commun., **2015**, *51*, 11705
89. Greene, T. W.; Wuts, P. G. Protective Groups In Organic Synthesis, 3rd ed.; John Wiley & Sons: New York, **2006**
90. G. S. Yedase, Asian J. Org. Chem., **2022**, *11*, e202200478
91. V. V. Pavlishchuk, A. W. Addison, Inorganica Chimica Acta, **2000**, *298*, 97-102
92. F. Dalla-Fenice et al., Angew. Chem. Int. Ed., **2021**, 60, 5693–5698. Supporting information
93. E. Vasilikogiannaki et al., Chem. Commun., **2015**, *51*, 2384–2387. Supporting information
94. C. Rosso et al., ChemPhotoChem, **2019**, *3*, 193–197. Supporting information
95. H. Yang et al., Org. Lett., **2010**, *12*, 3108–3111. Supporting information